DYNAMICS AND VIBRATION CONTROL OF ARTICULATING TRUSS STRUCTURES

Bernard A. Boutin

B. Eng. (The University of Manitoba), 1990

Department of Mechanical Engineering
McGill University
Montreal, Quebec

December 1995

A thesis submitted to the Faculty of Graduate Studies and Research
in partial fulfillment of the requirements of the degree of
Master of Engineering

Abstract

The dynamics of truss structures, articulated via a specific actuator arrangement, is examined in this thesis. The structure is treated as a flexible multi-body system, and sub-divided into numerous truss and actuator links. The resulting configuration becomes that of a crane-type manipulator. The prismatic actuator is modelled as a separate cylinder and piston-rod component, and considered rigid. Frame designations and kinematic expressions associated with each link-type, are established in order to evaluate the motion of the structure. Kinematic loops are introduced by the actuator installation, and the orientation angles of links dependent upon the loop are solved using the Newton-Raphson method. By virtue of the kinematic arrangement considered, only planar motion of truss cranes is examined in this thesis. The base of the structure is also considered to be fixed.

Initially, the equations of motion are formulated for the individual link with Lagrange's equations, and modal discretization is employed to model truss link flexibility. The finite element method is used to geometrically discretize the truss links, and only linear axial deformation of the members is modelled. The eigenvectors obtained from the eigenvalue problem of free vibration for each truss link, are employed in the modal discretization. The equations of motion for the entire structure are then assembled, and the non-working constraint forces between adjacent links are eliminated using the natural orthogonal complement of the velocity constraint matrix. As a result, a minimum set of dynamical equations are obtained in terms of the actuator extension and elastic (or modal) coordinate variables.

To address the active vibration control of truss crane manipulators, the singular

perturbation method is employed to establish a reduced-order model for the equations of motion. The resulting forms allow for the composite control design of the quasi-static motion and the modal coordinates. In this work, the robotic-based computed torque with PD control is applied to maintain the quasi-static motion, and an optimal LQR design of a specific configuration of the structure is considered for vibration control. Operation characteristics of the actuators are not modelled, and full state feedback of the vibration modes are assumed. These simplications allow for the initial assessment of this control approach, which was applied in a continuous manner.

The code GENMAN was developed to perform the dynamic and vibration control simulations for the planar motion of a N-link truss crane. Initially, inverse dynamics are executed using prescribed actuator extensions, in order to obtain the corresponding actuation forces. These values are then employed in the simulations of the forward dynamics to examine the resulting motion and structural vibrations. This thesis presents simulation results obtained for a space crane model of dimensions corresponding to that of a NASA concept.

Résumé

Cette thèse étudie le dynamique des structures en treillis flexibles qui sont articulés par une installation spécifique des actuateurs. La structure est composée de plusieurs corps classifiés comme treillis ou actuateur. L'actuateur, de type prismatique, se compose de deux membres; un cylindre et un piston qui sont considérés rigides.

Le mouvement de la structure est décrit en utilisant des repères cartésiens fixés sur chaque corps et par les expressions cinématiques attribuées à chaque type de corps. L'installation des actuateurs introduit des boucles cinématiques pour lesquelles, il faut obtenir les angles d'orientation de ces membres impliqués. Celles-ci sont résolues par la méthode de Newton-Raphson. Seul le mouvement planaire est considéré pour les structures en treillis étudiées dans cette thèse. En outre, le base est choisit fixe.

D'abord, les équations du mouvement sont formulées pour chaque corps individuel, en utilisant les équations d'Euler-Lagrange. Premièrement, la méthode des élément finis est employée pour la discrétisation spatiale des corps en treillis, et seule la déformation linéaire le long de ces membres de treillis est considerée. Ensuite, un certain nombre de vecteurs propres (eigenvectors), obtenues du problème des valeurs propres pour chaque corps en treillis, est employé pour la discrétisation modale. Les équations du mouvement du système en entier sont ensuites assemblées, et les forces et moments de contrainte passifs sont éliminés par l'application du complément orthogonal naturel. Le résultat est un système d'équations d'un ordre minimum, qui comporte les variables d'extensions des actuateurs et les variables modales.

Quant à l'amortissement actif des vibrations, la méthode de perturbations singulières est employée afin de réduire le degré des équations dynamiques. Le système

résultant permet l'application de commande individuelle pour la maneuvre de base et pour les variables modales. Dans cette étude, la méthode de contrôle "computed torque with PD feedback" utilisée pour les robots manipulateurs, est employée pour le mouvement de base. Le contrôle de "state feedback" est utilisé pour les modes vibratoires.

Le code GENMAN a été développé pour exécuter les simulations du mouvement planaire et pour contrôler les vibrations de structures en treillis comportant N corps. Premièrement, le problème de la "dynamique inverse" est résolu en utilisant des extensions d'actuateurs prescrites, afin d'obtenir les forces requises pour le mouvement rigide. Celles-ci sont alors employées en exécutant la "dynamique directe", afin d'observer le mouvement flexible et les vibrations résultantes. Des simulations d'une structure spatiale, conçue par la NASA, sont finalement présentées dans cette thèse.

Acknowledgments

First and foremost, I would like to thank my supervisor Prof. A.K. Misra for his guidance and support during the course of my work, and especially for the details required in the completion of this thesis.

I thank the people with whom I shared an office, laboratory, and computing facilities. I am gratefull to Jafar Sadigh and Mehdi Keshmiri for sharing their theoretical expertise and guidance during various discussions. Thanks to Eric Martin for his help regarding the Internet, and the grammar of the Résumé. I especially thank Ms. Barbara Whiston for her administrative expertise and friendliness.

I express my gratitude to NSERC (Natural Sciences and Engineering Research Council of Canada), for their financial assistance provided by the PGS-A Scholarship.

I thank my family for their support and concern.

Contents

Nomenclature

General Conventions

bold	bold variables designate a column vector or matrix
non-bold	an index or single value parameter
$\mathbf{0}_{33}$	3 by 3 zero matrix
$\mathbf{1}_{33}$	3 by 3 identity matrix
i	arbitrary link index under consideration
$i-1$	link preceeding link i per structure connectivity
$(\dot{})$	absolute time derivative of vector (w.r.t. inertial frame)
$(\circ)$	local time derivative of vector (w.r.t. rotating frame)
$(\tilde{})$	skew symmetric matrix of 3D vector
$()_{,(x)}$	X component of vector
$()_{,(y)}$	Y component of vector
$()_{,(z)}$	Z component of vector

Specific Symbols

$\mathbf{a}$	general 3D vector
$[\mathbf{a}_e^j]_j$	element j nodal displacement vector expressed w.r.t element j frame
$\mathbf{a}_e^j$	element j nodal displacement vector expressed w.r.t. link i frame
$\mathbf{a}_{e,1}^j$	element j dispacement vector of forward node (no. 1), w.r.t. link i frame
$\mathbf{a}_{e,2}^j$	element j dispacement vector of aft node (no. 2), w.r.t. link i frame
$\mathbf{a}_o^j$	element j nodal rigid position vector w.r.t. link i frame

$\mathbf{a}^j_{o,1}$	element j rigid position vector of forward node (no. 1), w.r.t. link i frame
$\mathbf{a}^j_{o,2}$	element j rigid position vector of aft node (no. 2), w.r.t link i frame
$\mathbf{a}_{e,k}$	node k nodal displacement vector, w.r.t. link i frame
$\mathbf{a}_{o,k}$	node k rigid position vector, w.r.t. link i frame
$\mathbf{a}_e$	assembled nodal displacement vector of link i
$\mathbf{A}$	system matrix of linear time-invariant state space form
A_i	cross-sectional area of cylinder or piston-rod link i
A^j	cross-sectional area of bar element j
$\mathbf{b}_i$	the vector of elastic(modal) coordinates for link i
$\mathbf{b}$	system vector containing all elastic coordinates
$\mathbf{B}$	control matrix of linear time-invariant state space form
$\mathbf{B}_i$	general representation of shape function matrix for flexible link i
$\mathbf{B}^j_i$	deflection shape functions of node j, on flexible truss link i
$\mathbf{c}_\mathbf{b}$	vector of nonlinear terms in the independent dynamical equations of motion, for elastic coordinate equations
$\mathbf{c}_\theta$	vector of nonlinear terms in the independent dynamical equations of motion, for independent joint coordinate equations
$\mathbf{C}_i$	rotation matrix from link i to $i-1$ frame, due to revolute angle θ_i about Z_i axis
d_i	extension of piston-rod link i
$\mathbf{D}^j_{i-1}$	rotation matrix from link j to $i-1$ frame, due to deformation slope at node j
E^j	Young's modulus of element j
E^*	complex modulus of elasticity
$\mathbf{f}$	elastic modal force vector for the system
$\bar{\mathbf{f}}$	quasi-static elastic modal force vector
$\mathbf{F}$	vibration control state feedback gain of reduced-order-model
$\mathbf{g}$	acceleration due to gravity vector

h^*	number of nodes per truss link
h	number of elements per truss link
$\mathbf{H}$	represents inverse of mass matrix in reduced-order-model derivations
$\mathbf{I}_i$	inertia matrix of link i, based on pose vector rate $\dot{\mathbf{q}}_i$
$\mathbf{K}$	assembled modal stiffness matrix of the total system
$\mathbf{K}_i^j$	element j stiffness matrix per link i element displacement $\mathbf{a}_e^j$
$\mathbf{K}_i^*$	full link stiffness matrix per nodal pose $\mathbf{q}_i^*$ components
$\mathbf{K}_i$	link modal stiffness matrix per flexible pose $\mathbf{q}_i$ components
$\mathbf{K}_{ee}^*$	sub-matrix of $\mathbf{K}_i^*$ for the $\mathbf{a}_e$ components
$\mathbf{K}_{ee}$	sub-matrix of $\mathbf{K}_i$ for the $\mathbf{b}_i$ components
$\mathbf{K}_P$	proportional gain matrix for actuator extensions
$\mathbf{K}_D$	derivative gain matrix for actuator extension rate
l	total number of kinematic loops
l'	total number of system independent and dependent coordinates
L^j	length of bar element j
L_i	length of cylinder or piston-rod link i
$\mathbf{L}_i$	transformation matrix from pose vector rate $\dot{\mathbf{q}}_i$, to twist vector $\mathbf{v}_i$
$\hat{\mathbf{L}}_i$	transformation matrix from euler parameter rate $\dot{\hat{\mathbf{q}}}_i$ to angular velocity $\boldsymbol{\omega}_i$
m_i	number of elastic (modal) coordinates modelled for flexible link i
m	total number of system elastic coordinates
M^j	mass of element j
M_i	mass of link i
$\mathbf{M}_i^j$	element j contribution to mass matrix $\mathbf{M}_i^*$
$\mathbf{M}_i^*$	link i mass matrix for nodal twist $\mathbf{v}_i^*$
$\mathbf{M}_i$	link i mass matrix for link flexible twist $\mathbf{v}_i$
$\mathbf{M}$	assembled system mass matrix for system twist vector $\mathbf{v}$
$\hat{\mathbf{M}}$	assembled system mass for independent coordinates $\boldsymbol{\psi}_I$
n	number of actuators (independent joint coordinates)

n'	total number of independent coordinates in the system
N	total number of links in the structure (system)
$\mathbf{N}$	natural orthogonal complement for the system
$\mathbf{N}_o^j$	element interpolation matrix for rigid position vector $\mathbf{a}_o^j$
$\mathbf{N}_e^j$	element interpolation matrix for displacement vector $[\mathbf{a}_e^j]_j$
p_i	dimension of link i pose vector $\mathbf{q}_i$
p'_i	dimension of link i twist vector $\mathbf{v}_i$
p'	total dimension of system twist vector $\mathbf{v}$
$\mathbf{p}_i$	inertial position of link i origin expressed in link i frame
$\mathbf{q}_i$	flexible (rigid) pose vector of flexible (rigid) link i
$\hat{\mathbf{q}}_i$	a 4 parameter Euler or linear invariant set
$\mathbf{Q}_i$	orientation matrix of link frame $X_iY_iZ_i$ w.r.t. inertial frame $X_oY_oZ_o$
$\mathbf{R}_i$	orientation matrix of link frame $X_iY_iZ_i$ w.r.t. preceeding link frame $X_{i-1}Y_{i-1}Z_{i-1}$
$\mathbf{R}_i^j$	orientation matrix of element j frame w.r.t. link frame $X_iY_iZ_i$
$\mathbf{r}_i$	local position of arbitrary point on link i
$\mathbf{r}_{e,i}$	elastic displacement component of $\mathbf{r}_i$
$\mathbf{r}_{o,i}$	rigid position component of $\mathbf{r}_i$
$\mathbf{s}_i$	inertial position of arbitrary point on link i, expressed in link i frame
t	time (sec)
$\tilde{t}$	fast time scale of the reduced-order-model
T_i^j	kinetic energy of element j
T_i	kinetic energy of link i
U_i^j	potential (strain) energy of element j
U_i	potential (strain) energy of link i
$\mathbf{v}_i^j$	flexible twist vector of element j nodes
$\mathbf{v}_i^*$	flexible twist vector of nodes of flexible link i
$\mathbf{v}_i$	flexible (rigid) twist vector of flexible (rigid) link i

$\mathbf{v}$	generalized twist vector of assembled system
$\forall$	volume
$\mathbf{w}_i$	Euler-Lagrange wrench vector
X_i	Cartesian X-axis of link i
$\mathbf{x}_i$	unit vector of X_i axis
Y_i	Cartesian Y-axis of link i
$\mathbf{y}_i$	unit vector of Y_i axis
Z_i	Cartesian Z-axis of link i
$\mathbf{z}_i$	unit vector of Z_i axis

Greek Symbols

ε	axial strain along a bar member
ϵ	perturbation parameter of reduced-order model in state space
$\delta_{i/i-1(z)}$	link $i-1$ deflection slope rotation about Z_{i-1} axis, at node i
κ	number of nodal DOF per element
κ'	number of nodal DOF per node
κ^*	total number of nodal DOF per link
$\boldsymbol{\Lambda}_i$	transformation matrix from twist vector $\mathbf{v}_i$ to pose vector rate $\dot{\mathbf{q}}_i$
$\widehat{\boldsymbol{\Lambda}}_i$	transformation matrix from angular velocity $\boldsymbol{\omega}_i$ to parameter rate $\dot{\hat{\mathbf{q}}}_i$
μ	perturbation parameter of reduced-order-model
ρ^j	material density of element j
ρ_i	material density of cylinder or piston-rod link i
$\boldsymbol{\phi}_i$	transformed Euler-Lagrange wrench vectors
$\boldsymbol{\Phi}^j$	element-node DOF association matrix
$\boldsymbol{\psi}$	total system vector of independent and dependent coordinates
$\boldsymbol{\psi}_i$	vector of independent and dependent coordinates for link i
$\boldsymbol{\psi}_I$	generalized (system) vector of independent coordinates
$\boldsymbol{\psi}_{I,i}$	vector of independent coordinates for link i

ψ_D	system vector of dependent coordinates
$\psi_{D,i}$	vector of dependent coordinates for link i
τ	actuator force (torque) of link joint i
ν	complex (Young's modulus) damping ratio
θ_i	rotation angle between axes X_{i-1} and X_i, measured about the positive Z_i axis
θ_I	system vector of all the n independent joint variables
ω_i	angular velocity vector of link i frame expressed in link i frame
ζ	conventional damping ratio of single DOF spring-dashpot mass system
ζ	constraint equation of kinematic loop

List of Figures

List of Tables

Chapter 1

INTRODUCTION

1.1 Background and Motivation

The concept of truss manipulators originates from two areas of aerospace research. The first involves the field of adaptive structures, in which a structural assembly is equipped with certain self-sensing-self-actuating devices embedded into the members or substituted for entire members. The installation of these elements transforms the structure into an active system, allowing for autonomous motion and vibration control, [Crawley et al.'87]. As a result, and with proper control design and implementation of the sensing/actuation systems, a structure obtains the capability to actively vary the geometry or mechanical properties of its members to yield a more acceptable configuration in terms of structural integrity or vibration suppression. Hence, as variable geometry truss (VGT) arrangements were proposed for the deployment masts of space antennaes, other manipulating truss configurations evolved, [Miura'93], [Chen et al.'90].

Truss cranes were also examined for the in-orbit construction of future spacecraft. The requirements associated with interplanetary missions suggested that the dimensions and mass of manned spacecraft vehicles will exceed the capabilities of any present day launch vehicle. Various examples include Lunar and Mars transfer vehicles that have masses on the order of 190,500 and 862,000 kg, respectively. Their representative dimensions are 15.2 m diameter/ 22.8 m length, and 33.5 m

diameter/ 51.8 m length, respectively, [Dorsey et al.'92]. More recent concepts of a Mars vehicle propose an arrangement with mass and dimensions of larger magnitudes, [Sherwood'94]. These figures far exceed the payload capabilities of the present day space shuttle, which is of the order of 19,500 kg, and the maximum allowable payload shroud size is 4.8 m diameter/18.3 m length, [Dorsey et al.'92]. Hence, it appears inevitable that the main assembly of future interplanetary and manned spacecraft will be performed on an in-space construction facility (ISCF) located in low-earth orbit, illustrated in Figure 1.1.

The deployment operations for orbiting structures and the future in-space construction of space vehicles, therefore imply that considerable manipulation capabilities will be needed. The ISCF facility would be equipped with various manipulator systems, in which three typical arrangements include:

- remote (telerobotic) manipulator systems (RMS),
- articulated truss space cranes, Figure 1.2, [Dorsey et al.'92], and
- variable-geometry truss (VGT) manipulators, also referred to as adaptive truss manipulators (ATM), Figure 1.3, [Chen et al.'90].

According to conventional terminology, the first two systems are anthropomorphic manipulators consisting of "multi-joint-multi-link" configurations, [Chen et al.'90]. The joint manipulation is generally independent of the adjacent links. The third system is denoted as an adaptive configuration in which a collection or module of members vary in unison to effect the overall joint function or geometry change of the structure. In general, the joint modules of these systems are typically of octahedral assemblies.

The kinematic, dynamic, and control simulation of serial robotic manipulator systems receives considerable attention by the research community. Largely employed for industrial applications of production and materials handling, these manipulators

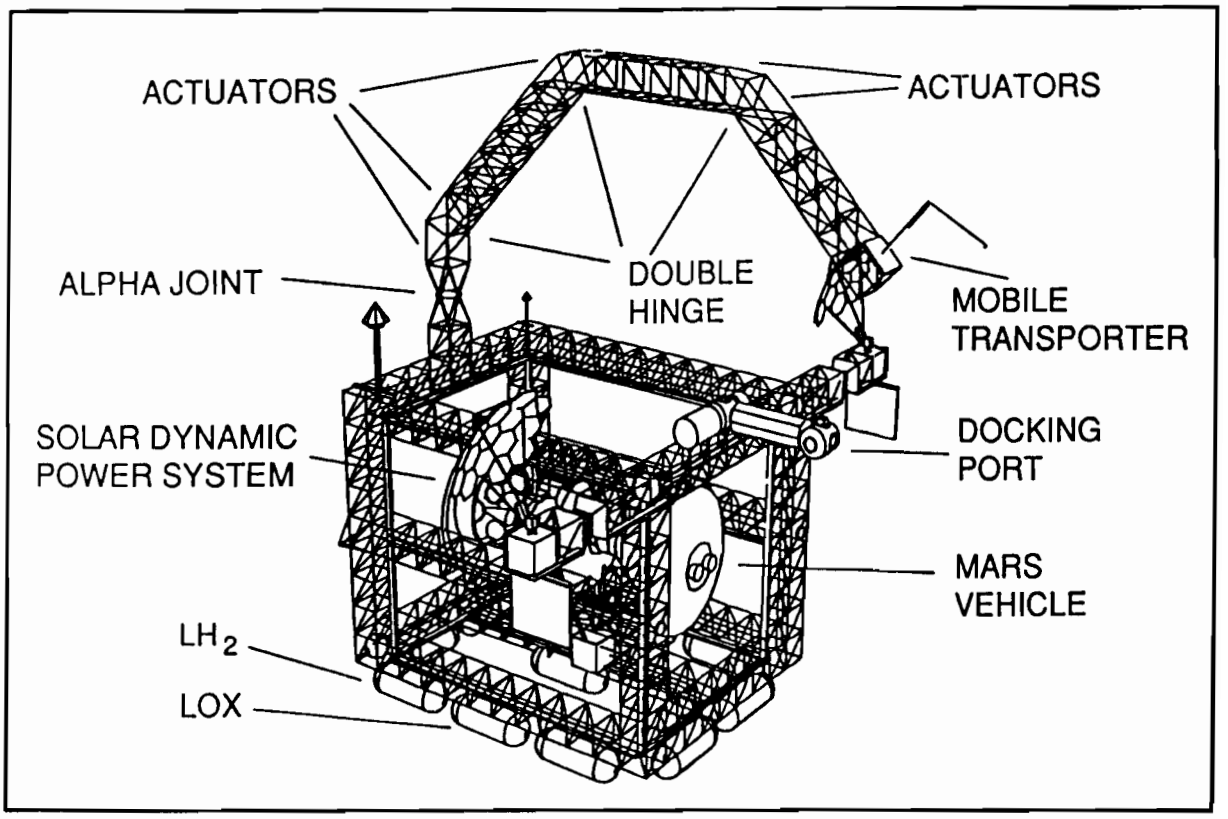

Figure 1.1: An in-space construction facility, [Chen et al.'90].

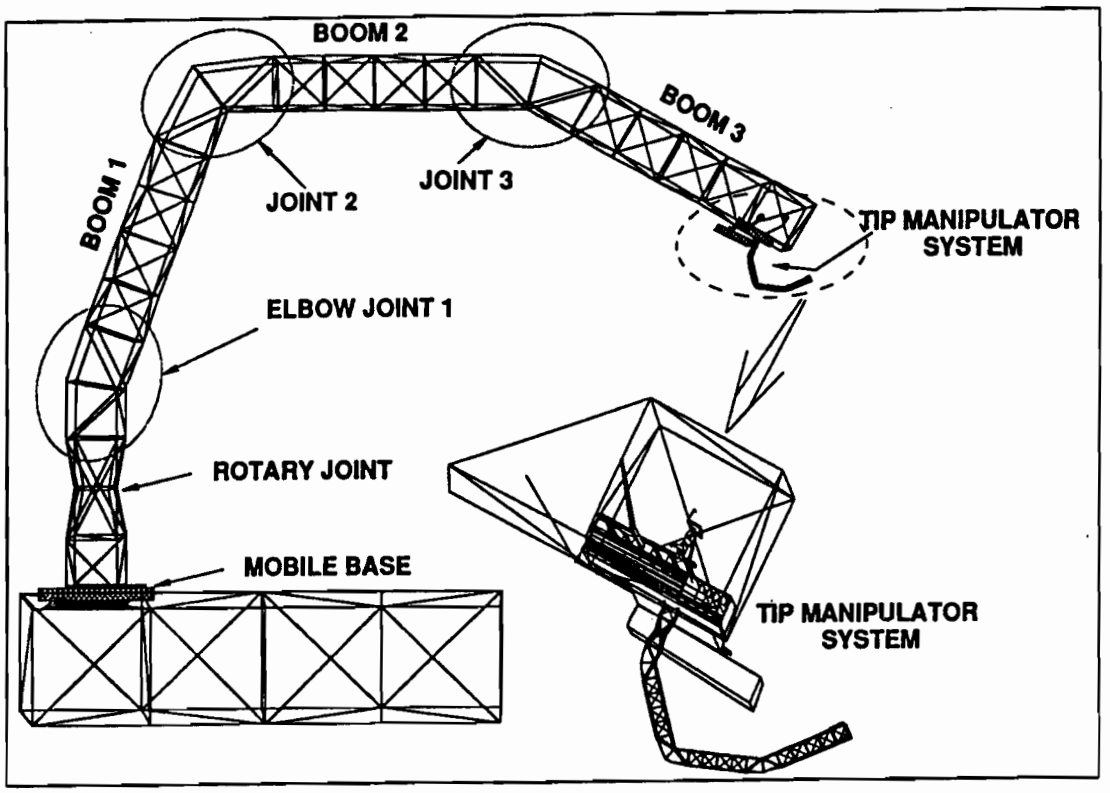

Figure 1.2: An articulating truss manipulator (crane), [Dorsey et al.'92].

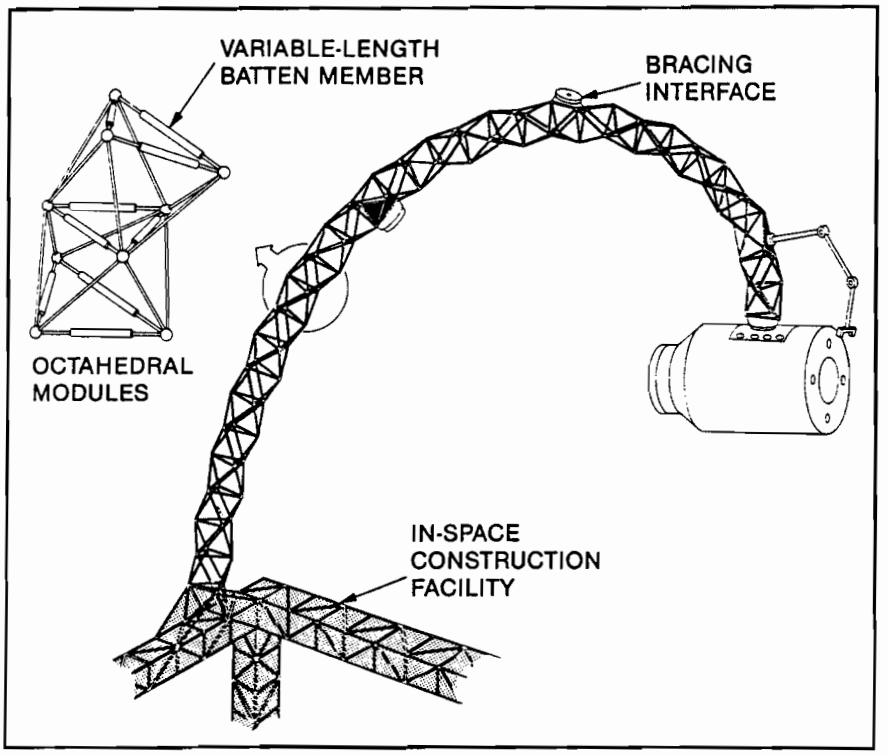

Figure 1.3: A variable geometry truss (VGT) manipulator, [Chen et al.'90].

operate ideally for reasonable dimensions of link members which usually possess a beam-type geometry. Present space applications of robotic manipulators include the renowned space shuttle's CANADARM and the proposed space station's remote manipulator system (SSRMS). Concepts and analyses of free-flying space robots are also under review.

During the development of adaptive structures, there has been considerable research in the field of VGT's. Efforts by the Japanese community are documented in [Miura et al.'85] and [Miura'93], and that of the United States stem from cooperative interests between NASA and other groups involved with adaptive structures (such as Jet Propulsion Labs, MIT, etc.), [Wada et al.'90]. Canadian involvement in this area includes the activities documented in [Hughes et al.'90].

In contrast, it appears that the dynamic modelling and vibration control of the truss crane arrangements per Fig. 1.2, has not been thoroughly addressed. These structures would contain truss-type booms to perform the gross manipulation of massive components or mobile transporter platforms. The truss geometry possesses a high stiffness-to-mass ratio, and provides both structural integrity and function dexterity. However, as the actuator and joint configurations become more complex, the kinematic dependencies between adjacent links in a truss crane require additional treatment when performing kinematic and dynamic analyses.

The focus of this thesis is to examine the dynamic simulation and vibration control of the planar motion for truss crane manipulators. A research survey regarding the modelling schemes and analyses thus far considered for various manipulating truss structures is initially provided in the subsequent section. The following sections presents a general discussion regarding the formulation methods for multi-body dynamics, and the vibration control schemes most applicable to truss-type configurations. This introductory chapter is then concluded with the main scope and organization of the thesis.

1.2 Manipulating Truss Structures

1.2.1 Articulating Truss Cranes

The development of the articulating truss crane concept in Fig. 1.2, has been motivated by NASA activities initiated in the late 1980's. Various joint arrangements are documented in [Vail et al.'91], [Sutter et al.'92], and [Wu et al.'92]. A summary of this work is provided in [Sutter et al.'90], which focuses upon the criteria used to characterize the joint configurations. These include the provisions for maintaining adequate structural stiffness with large joint rotations, and reasonable actuator stroke. Corresponding test results are also provided for a specific truss boom assembly, illustrating the rigid joint articulation, actuator load-deflection response, and the fundamental frequencies for specific configurations of the structure.

A form of the dynamical equations of motion for a truss crane were initially presented in [Das et al.'89], and derived using Hamilton's principle. The resulting equations are in terms of the angles between adjacent truss sections and in terms of the full elastic nodal deflections. A mass lumping scheme was also applied, but a displacement field (between the nodes of an element) was assumed that is inconsistent with the linear displacement field employed in the strain energy formulation. The dynamic simulations performed in this work, use prescribed link angle trajectories and integrate the equations of motion to obtain the resulting nodal deflections. Hence, the effect of the elastic motion upon the rigid body motion is essentially ignored. The corresponding actuation forces for this "flexible" motion are then computed. The structural configurations considered and simulation results provided, do not facilitate comparisons with a typical truss crane arrangement. In addition, with the flexible motion integrated from the prescribed rigid body motion, the high frequency vibration components associated with a true forward dynamics simulation are not obtained. As a subsequent activity to this work, an actuator compensation scheme that accounts for elastic deformations associated with a maneuver, is presented in [Das et al.'90a].

This procedure determines the actuator force correction needed (in addition to that calculated from the rigid body inverse dynamics) for tip point adjustment of the flexible structure. Again, these are essentially inverse dynamic simulations where the rigid body motion is specified and the corresponding elastic deflections are obtained from integrating the equations of motion for the nodes.

The trajectory planning of slow moving space cranes, for which inertial effects are neglected, is presented in [Ramesh et al.'91b] and [Utku et al.'91b]. Forward and inverse kinematic relations are derived to determine the corresponding actuation of specified members. The governing equations are established from the static response-excitation relations of truss structures presented in [Utku et al.'91a]. This Newtonian-based approach provides a linear set of equations which satisfy nodal and member force equilibrium, geometric compatibility between nodal deformations and member elongations, and the constitutive relation between the member force and elastic stiffness balance. The rearrangement of these expressions yields the member actuation needed to provide a specified trajectory of certain nodal degrees of freedom. A form of the Jacobian matrix relating the incremental change of end effector position due to incremental changes in the actuator lengths, is also obtained. The computational efficiency of the forward and inverse kinematic scheme is dependent upon the algorithm of [Ramesh et al.'91a] used to update the Jacobian matrix during the iteration of the trajectory solution. The justification given for neglecting the structure inertia, is that member actuation will occur over long durations of time. As a result, the forward kinematics would be ideally satisfied by the member actuation commanded. For this simplified scenario of negligible structural inertia, [Utku et al.'91b] also present an actuator compensation strategy to account for elastic deflections resulting from a payload.

Due to the highly nonlinear equations of motion and the changing vibration characteristics associated with articulating truss cranes, vibration control can be considered for final configurations of the maneuver, [Lu et al.'90]. This is achieved by intro-

ducing either passive or active members into the truss-links, which are intended for vibration suppression (and not gross manipulation). With the implementation of active members, the structure becomes adaptive. The governing equations of motion for the truss nodes are now linear and pertain to small deformations about the stationary configuration. Schemes developed for the vibration control of stationary truss structure are now applicable, as will be discussed in Section 1.4.1.

1.2.2 Adaptive Variable Geometry Trusses

Although VGT structures are not the topic of this thesis, the various research performed for this configuration is reviewed here for completion.

Two VGT concepts that correspond with the length dimension of the CANADARM manipulator, are presented in [Hughes et al.'90]. The resulting forms of the kinematic and rigid body dynamic equations of motion for the highly densed member topology are presented. Flexible body contributions are not modelled in the "articulation" dynamics, however, the modal characteristics of the structure are evaluated with NASTRAN for numerous configurations. The authors mention that a proportional-integral-derivative control model for each joint was established to effect the commanded trajectories. A laboratory model designated as the Trussarm (Mark I) structure was also introduced.

A general kinematic description for a typical variable geometry truss arrangement is presented in [Naccarato et al.'91], along with a classification of the various constraints associated with the highly densed configuration of members. These efforts focus upon the solution to the inverse kinematics problem of obtaining the required actuator lengths to yield the end-effector trajectory. The conventional scheme (applied to redundant robotic manipulators) of solving the pseudo-inverse of the differential kinematic Jacobian matrix, is used. In addition, the authors present a method which solves the required truss configuration conforming best to a reference curve of the desired shape of the structure. The scheme allows for the specification of certain

configuration constraints, such as for obstacle avoidance, and employs less complicated kinematic expressions. As a result, this reference curve inverse scheme is more computationally efficient, and hence quite promising to real-time applications.

The application of variable geometry trusses to the docking of a free floating structure is given by [Natori et al.'92a]. The inverse kinematics is based on the spatial description of the base planes of each module (or bay), and the dynamic equations of motion are formulated from principles of momentum conservation. The constraints governing the docking control equations are addressed, and an experimental demonstation of the docking operation is provided. Deployement and dexterity scenarios for a specific VGT structure are illustrated in [Chen et al.'90]. Many other activities regarding VGT arrangements are documented in [Miura'93].

1.3 Dynamical Formulation of Multibody Systems

The articulating truss manipulator of Fig.1.2 conforms to a consistent arrangement of the actuators and corresponding kinematic loops. For this thesis, the structure will be modelled as a collection of flexible links, driven by rigid actuated/extending members. Hence, it is ideal to select a formalism that facilitates this topology and establishes the governing dynamical expressions. Newton-Euler methods of deriving the equations of motion are convenient for serial configurations, in which the forces and moments transferred to adjacent bodies can be readily identified and treated as such. This is the case for serial robotic arrangements considered in [Hollerbach'80], but not necessarily for configurations involving kinematic loops. The flexible body problem also renders Newton-Euler derivations somewhat cumbersome.

Kane's method [Kane et al.'65], provides a very efficient formalism from which computer algebraic forms of the equations of motion have been developed, [Amirouche'92], [Singh et al.'85], [Huston'90]. Each body is modelled as part of the entire system, and with the method being an energy based approach, the inter-link constraint forces and moments do not appear in the final forms of the equations

of motion. As a result, a minimum set is obtained. This methology readily accommodates the consideration for structural flexibility, linearization of the equations of motion, and the simulation of constrained motion [Sadigh'95]. Although the features associated with Kane's method are most enviable, the Euler-Lagrange equations maintain extensive application throughout the various fields of dynamic simulation, [Chang et al.'91b], [Cyril et al.'91], [Chan et al.'90], and [Nagarajan et al.'90]. To account for structural flexibility, an assumed modes scheme is usually applied with the Euler-Lagrange equations. As a result, the partial differential equations of motion for the continous system are approximated by ordinary differential equations of a discretized system, [Meirovitch'90]. For a system of multibody chains, constraint forces and moments between adjacent bodies can either be included in the equations of motion with the use of Lagrange multipliers [Park et al.'90], or removed with an appropriate transformation of coordinates as obtained with the natural orthogonal complement method [Angeles et al.'88a]. The use of Lagrange multipliers introduces a larger system of equations to be simulated. Even though hybrid solution schemes exist to reduce simulation time [Park et al.'90], it is preferrable to obtain a minimum set of equations for (time integration) simplication.

The dynamic simulations of flexible manipulators and mechanisms employing the natural orthogonal complement, have been performed in [Cyril et al.'91], [Darcovitch'91], and [Fattah et al.'94]. The assumed modes method can be applied to model flexible beam-type members, and Lagrange's equations employed for the discretized system. The formulation initially derives the unconstrained equations of motion for each body or "link" in terms of the link origin velocity, frame angular velocity, and rates of the elastic coordinates. By appropriately introducing the natural orthogonal complement and the independent coordinates of the system, the non-working constraint forces are eliminated and the minimum set of dynamical equations of motion are obtained. The scheme additionally facilitates the general assembly and algorithmic treatment of consistent manipulator arrangements, provided that the

kinematic configuration is properly defined for the computation of the natural orthogonal complement of the velocity constraint matrix.

For structures consisting of numerous members, as is the case for the main truss booms of a truss crane, the flexible characteristics of each individual link can be readily obtained with finite element (FE) discretization. The application of the FE method to the dynamics of flexible mechanisms with complex geometries has been examined in [Sunada et al.'81]. The treament of planar-loop systems and the modelling of flexible members with FE modal discretization, is presented in [Fattah et al.'94]. The scheme employed in this latter work is most applicable to truss-type links, in which the system dimension of the dynamic equations is reduced with the consideration of only a few modes of vibration.

1.4 Vibration Control Methods

1.4.1 Vibration Suppression by Conventional Schemes

There is an extensive collection of research work regarding the vibration control of truss-type assemblies. For stationary applications, truss arrangements constitute the main support structures for the proposed space station platform, future spacecraft, space masts, optical interferometers, and the precision structures of reflectors and antennae used in space [Umland et al.'92], [Wada et al.'92], and [Voth et al.'94]. The majority of these arrangements consist a single truss, such that there is no articulation of adjacent segments. The governing equations of motion for these flexible structures are therefore linear differential equations expressed about the nominal configuration, obtained either through the finite element method or from the response-excitation relations presented in [Utku et al.'91a]. The equations may then be arranged in the linear state space form, in order to apply the schemes of independent modal space control [Meirovitch et al.'82], [Baruh et al.'92], or direct output feedback control [Meirovitch'90]. The equations of motion associated with the gross manipulation

of truss cranes are, however, nonlinear with time-varying inertial properties. Therefore, unless the equations can be linearized, or reduced into two separate systems consisting of the rigid body motion and linearized flexible body motion, the above control strategies are not applicable.

Damping augmentation or active local vibration control can be obtained by exploiting the truss geometry and introducing either passive and/or active struts. The implementation of these members into the main truss booms of a manipulating truss crane, would compensate for insufficient structural damping. The use of simultaneous sensing and actuation members would transform the structure into an adaptive or "intelligent" one. With the numerous members contained in truss structures, the effectiveness of the resulting vibration suppression is dictated by the actuator or damper placement. Considerable effort has already been focussed towards the determination of optimal actuator placement in stationary truss configurations and the criteria for assessing these. The application of optimal and linear control theory is usually employed for such analyses, and various optimal placement strategies have been addressed [Das et al.'90b], [Lu et al.'90], [Utku et al.'91a], [Maghami et al.'93], [Sener et al.'93], [Lammering et al.'94], and [Tongco et al.'94].

Experimental results of actively damping a truss structure are presented in [Preumont et al.'90]. A collocated piezoelectric actuator and force transducer is used to implement force feedback control. The work performed in [Dunn'92], established a control syntheses for different compensators. Details regarding the active and passive design methodologies, and implementation into a truss testbed typical of future space platforms are documented in [Voth et al.'94]. The active control is provided with the use of jet thrusters, hence, according to conventional terminology the structure is not adaptive. Viscoelastic struts are also installed for damping augmentation, and their placement is initially assessed using a modal strain energy method. It was demonstrated that proper integration of both active and passive control schemes allow for effective vibration suppression of truss arrangements.

1.4.2 Vibration Suppression by Actuated Motion

An initial study regarding the vibration control of the truss crane presented in Fig. 1.2, has been performed in [Reisenauer et al.'92]. The crane was allowed to rotate (out-of-plane) about its revolving base joint, and the resulting vibrations associated with several fixed orientations of the articulating booms were considered. A reduced-order FE model of the full structure was used, as obtained by modelling the three dimensional truss geometry by a Timoshenko beam. This simplified (beam) model reproduced the low frequency vibration characteristics of the full truss. By assuming small rotations at the base joint, and since the vibration characteristics of various fixed orientations of the truss were considered, then linear forms of the equations of motion were obtained. A linear quadratic regulator controller was initially examined to suppress the lower vibration modes, and destabilization of the unmodelled modes was observed. A compensator scheme using a series of residual mode filters, was then implemented and indicated good stabilization performance. The study demonstrated the complications involved when designing vibration control for such a complex 3D structure.

The open loop technique of pre-shaped command input can also be implemented for the vibration control of truss crane structures, [Dorsey et al.'92]. The maneuver actuation is applied so as to minimize the excitation of selected frequencies of vibration. Hence, the commanded extension rates of the actuators are modified to induce small residual motions while effecting the required maneuver. The advantages of this control scheme is that it is an open loop system, only the frequencies of vibration of the structure are required for its design, and for a specific operation bandwidth it can be designed to be insensitive to the physical system characteristics of vibration frequencies and damping, [Dorsey et al.'92].

The vibration control for in-plane motion of articulating trusses is addressed in this thesis. Since the theory regarding control of linear systems is well established,

it would be ideal to obtain the conventional linear state space form of the equations of motion. However, by virtue of the multibody system and the kinematic loop dependencies associated with the truss manipulators considered here, the governing dynamical equations are highly nonlinear. Linearization of the equations about an equilibrium state or trajectory, as performed in [Sadigh'95] with Kane's methodology, may become numerically unpractical for a specific formulation scheme. This is usually the case when the natural orthogonal complement is used to eliminate constraint forces of a Lagrangian formulation, and therefore other means of altering or reducing the order of the system must be sought.

One scheme that has been applied in the field of serial robotic manipulators is that of the singular perturbation method [Aoustin et al.'93], [Chedmail et al.'91], [Lewis et al.'93], [Siciliano et al.'88]. This procedure originates from the analytical theory of differential equations and boundary layer problems in fluid dynamics. In robotics, the technique establishes a quasi-static form of the equations of motion for a flexible structure, by exploiting the property that elastic vibration frequencies are usually greater than the frequency content of the rigid body motion trajectory. Hence, highly coupled differential equations of motion can be rearranged into two reduced-order systems, consisting of a "slow" (quasi-static) subsystem, and a "fast"(boundary layer) subsystem, for which the latter possesses a much faster time scale. A detailed explanation of the singular perturbation technique and its application in control systems modelling is provided in [Kokotovic'84], [Naidu'88] and [Suzuki'81]. The control scheme for each subsystem may then be addressed almost separately, to establish a composite control design. The resulting model of the flexible cooridinates becomes that of a linear time-varying system, and must be addressed accordingly. Therefore, the actuation forces and torques can be used to effect the maneuver while suppressing structural vibration. It is essential that the appropriate singular perturbation form ensures adequate separation in time scale between the two subsystems, which is fundamental when considering small but fast deviations about a nominal state of the

singular perturbation method. Then, as for every stable control system design, the assessment of controllability and the control strategy, must be addressed.

1.5 Scope and Organization of the Thesis

This work examines the simulation of the dynamic motion and vibration control of articulating truss cranes, confined to planar motion. The vectorial notation and derivations of the thesis are applicable to spatial (3D) motion, and the forms specific to in-plane motion will be distinguished. The equations of motion for each link are initially derived from application of modal discretization along with the Euler-Lagrange equations. The corresponding mode shapes of each truss links are obtained from finite element discretization. The natural orthogonal complement method is then employed to enforce the kinematic constraints between adjacent links, as detailed in [Cyril'88] for flexible serial manipulators. The resulting equations of motion are in terms of the independent coordinates for the system, which consist of the actuator extensions, and the flexible coordinates of the truss links. This scheme was selected over a Newton-Euler formulation or Kane's method, since it easily accommodates the computational assembly of the individual links defined per the structure topology used in the thesis. Hence, any articulating truss crane arrangement can be simulated, as long as the joint assembly between neighboring links corresponds with that used in constructing the natural orthogonal complement of the system. The actuator members are modelled as rigid bodies in this work, however, the formulation will allow for their flexibility considerations in future work.

The objectives of the dynamic simulations of truss manipulators, are those generally used for robotic manipulators. Firstly, the **inverse dynamics** problem is addressed, which involves the computation of actuator forces associated with the motion of the rigid system, obtained with prescribed actuator extension histories. These actuator forces are then used in the simulations of the **forward dynamics** of the rigid or flexible system, to examine whether the initial structure motion is obtained.

The forward dynamics is basically the time integration of the dynamical equations of motion, to yield the resulting actuator extension and flexible coordinates profiles. By modelling the desired number of flexible modes for each truss link, the resulting flexible body motion can be observed. The inverse kinematics problem of determining the required actuator extension histories to follow a certain end-effector path, is not addressed in this work.

A procedure for implementing vibration control of truss cranes, is also examined from the reduced-order models of the equations of motion, as obtained with the singular perturbation method. This scheme has been implemented for flexible manipulators in [Siciliano et al.'88], and individual control strategies can be designed for the main (quasi-static) maneuver and the vibration modes. For the quasi-static motion, the method of "computed torque" with proportional-derivative control (denoted as the feedforward control method in robotics) is used in this work. The control strategy selected for the flexible modes is that of full state feedback, which employs the optimal linear quadratic regulator (LQR) gains computed for only one specific orientation of the structure. Full state feedback will not usually be available in practice, therefore the implementation of state observers is recommended for future work. Vibration control simulations are performed here assuming ideal actuators with no limitations, however typical actuator characteristics should be modelled for subsequent activities.

The thesis is organized as follows:

- Chapter 2 introduces the structure configuration and topology for the truss manipulators considered in this work.

- Chapter 3 presents the kinematic description employed for arbitrary links.

- Chapter 4 provides the derivations of the dynamic properties associated with each link, namely the mass matrix from the kinetic energy expression, the truss stiffness from the potential strain energy, as well as the modal discretization and structural damping schemes applicable to the truss links.

- Chapter 5 presents the formulation of the equations of motion for each individual link, the assembly of the dynamical equations of motion for the entire system, and the details regarding the computations of the natural orthogonal complement.

- Chapter 6 presents the vibration control scheme, namely the reduced-order systems derived from the singular perturbation method, and the control strategies applied to the individual rigid and flexible systems.

- Chapter 7 explains the code GENMAN developed to perform the simulations of the dynamic motion and vibration control of truss cranes, and discusses its various features and capabilities.

- Chapter 8 introduces the truss crane model examined in this thesis for the simulation of the dynamic motion, and presents the corresponding results and discussion.

- Chapter 9 presents the conclusions established in the thesis and recommendations for future work.

- The Bibliography contains the various references.

- The Appendices include the more detailed formulations and simulation data.

Chapter 2

STRUCTURE DESCRIPTION

A manipulating truss structure contains certain length adjusting members to effect motion of the truss booms, as depicted in Fig. 2.1. The structure may be situated in a gravity environment such as for ground usage, or in micro-gravity when installed on an orbiting platform. For the work of this thesis, the base upon which the structure is attached is assumed to be stationary. However, if this is not the case, then a general model of the structure would assign specific generalized coordinates to the base frame to reference its orientation and location with respect to an inertial frame. For orbiting cases, if the base platform mass is either less than or of the same order of magnitude as the truss structure, then momentum principles must be applied to define the center of gravity of the entire system as the origin of the orbital frame.

For the configuration of Fig.2.1, the truss manipulator is modelled as a collection of substructures or links consisting of:

- statically determinate or indeterminate truss booms,
- prismatic actuators that act as length varying elements to effect the required geometry change of the overall structure, and
- possibly a remote manipulator as the end effector of the truss crane.

Each truss boom is treated as a separate body or link, and its flexibility is modelled using the finite element (FE) method, such that only axial deformation of its

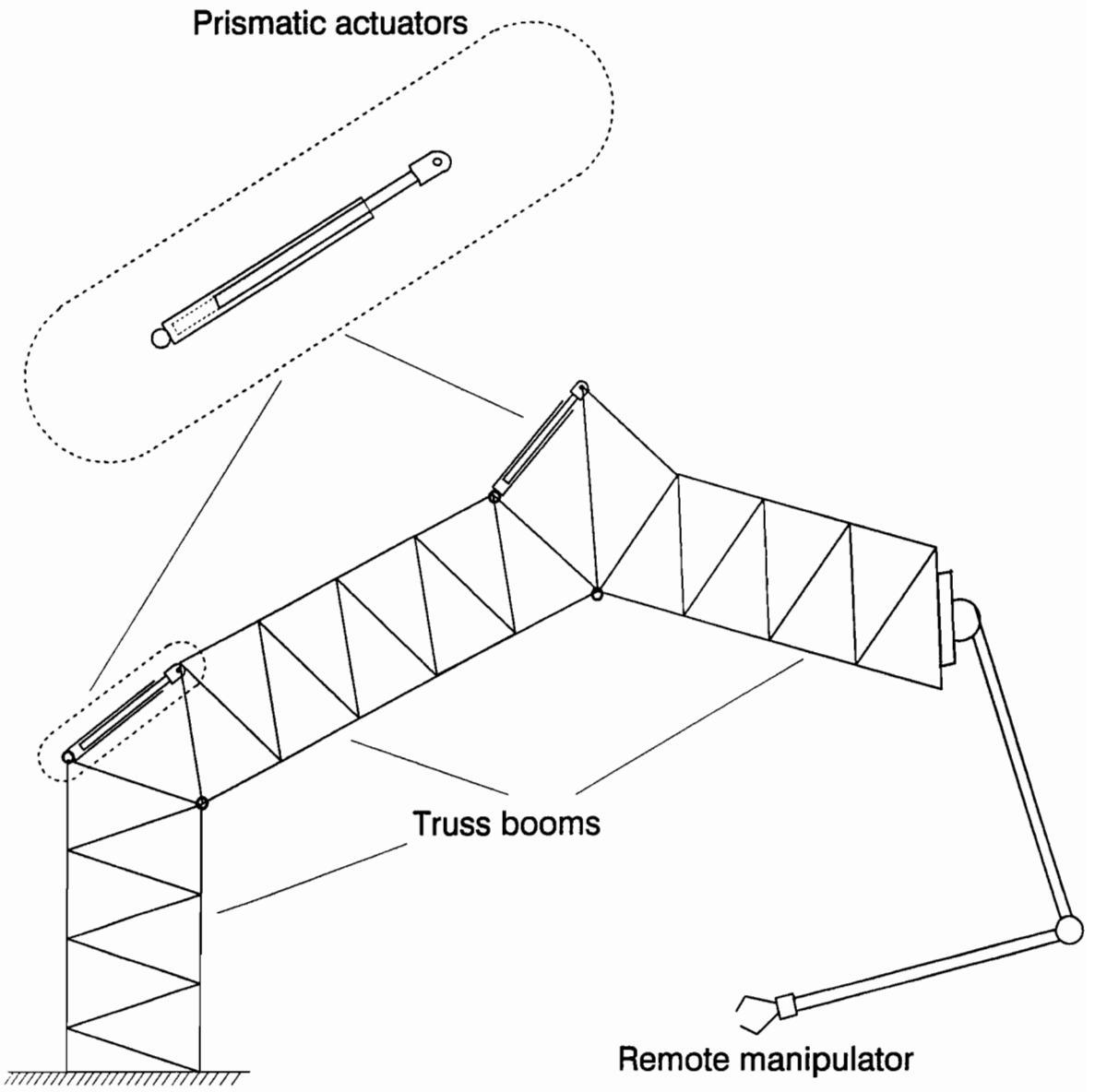

Figure 2.1: The member arrangements of a manipulating truss.

members is considered. The prismatic actuators are modelled as separate links, consisting of a cylinder component and an extending piston-rod, which is typical of the basic geometry of a hydraulic or servo cylinder actuator. As a result, the cylinder component contains inner and outer diameter dimensions, and it is assumed that the extending rod possesses the diameter of the inner dimension of the cylinder. In this thesis, the actuator members are considered as rigid elements, however their treatment as individual links in the formulations to follow will accommodate flexibility considerations for future work.

The following section presents the variables designating the generalized coordinates for an individual link i, and the recursive relations that express the link orientation and origin location of the assembled structure. Figure 2.2 illustrates the frame designation assigned to a typical seven link truss manipulator, and Table 2.1 presents the corresponding link definition and connectivity data. This information constitutes the topology of the structure, and fully describes the link arrangement. By virtue of the actuator installation of Fig.2.2, manipulating truss structures are not of a serial configuration, but rather contain multi-kinematic loops. The treatment of these loops and the dependent revolute angles associated with them, will also be addressd.

For the remainder of the thesis, variable N denotes the number of individual links contained in a truss manipulator, variable n represents the total number of actuated joints, and l is the total number of kinematic loops per the arrangement of Fig.2.2 . Many other variables will be defined during the course of the derivations.

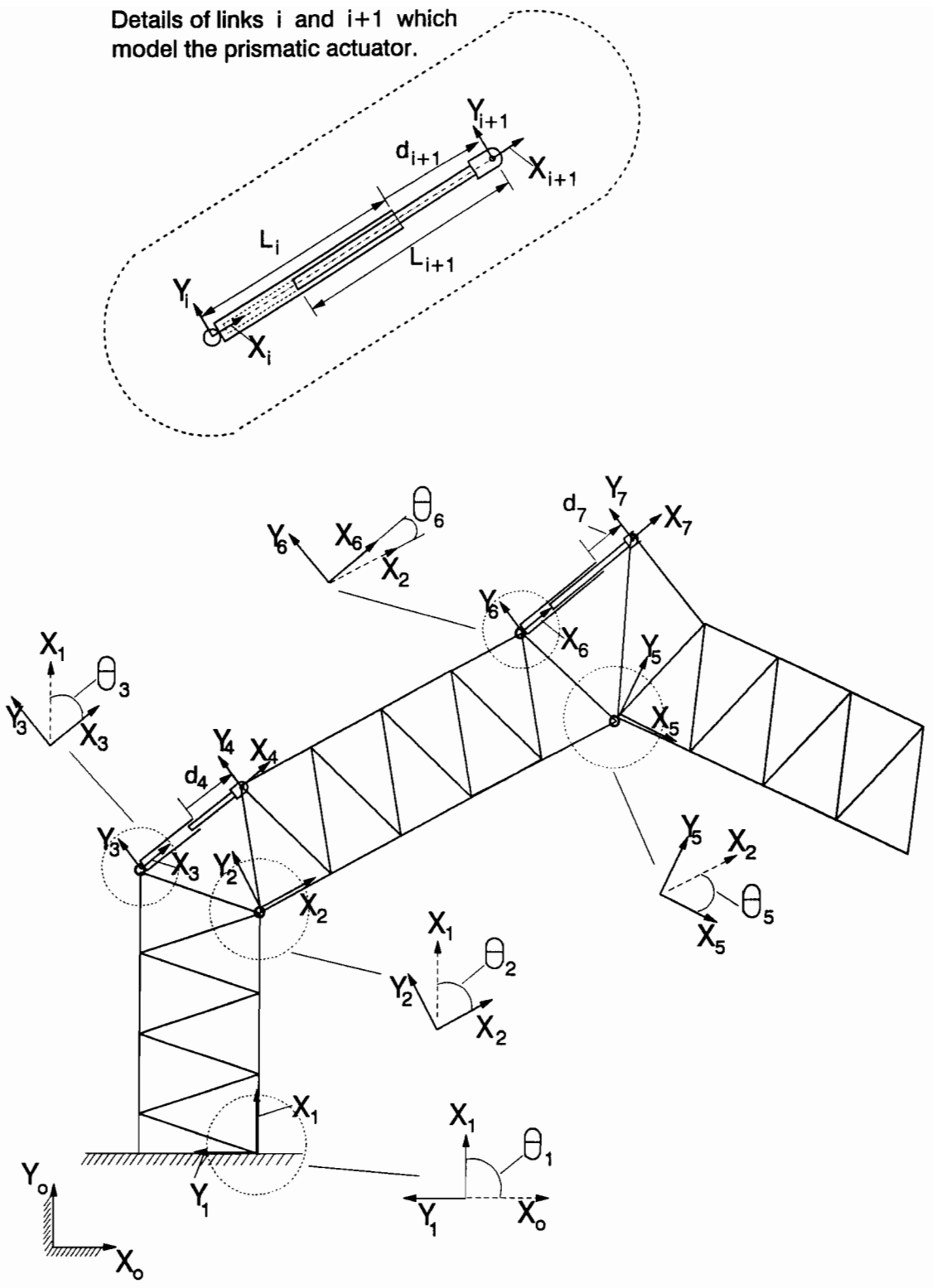

Figure 2.2: Link frames and structure topology of a seven link manipulating truss.

Table 2.1: The link connectivity/structure topology of the seven link truss manipulator.

$N = 7$ (Number of links)
$n = 2$ (Number of actuated joints)
$l = 2$ (Number of kinematic loops)

Link i	Link Type	Joint Type	**Preceeding** Link, $i-1$
1	truss	fixed	0
2	truss	dependent rev.	1
3	cylinder	dependent rev.	1
4	piston-rod	prismatic	3
5	truss	dependent rev.	2
6	cylinder	dependent rev.	2
7	piston-rod	prismatic	6

Chapter 3

SYSTEM KINEMATICS

The manipulating truss structures considered in this work are confined to planar (2D) motion by virtue of the joint and actuator arrangements considered. However, the vector notation and formulations presented in the following sections retain the general forms for spatial (3D) motion, unless explicitly noted. The allowance for spatial motion (of these structures) will require a more specific definition of the joint arrangement between adjacent links, such as to incorporate misalignments of the revolute axes. This will also be commented upon in the following section.

It is equally important to note that all vectors associated with a specific link will be expressed within its own frame. This choice provides some convenience during the formulation of the kinematic and dynamic equations of motion. In addition, in this thesis bold lower case letters represent a vectorial or array quantity, and bold upper case letters pertain to a matrix quantity. Variables which are of the standard (i.e. non-bold) type-face, generally represent a scalar quantity such as for a material or geometric property, or an index. All variables may contain superscripts and subscripts to clarify their representation, and will be defined upon presentation.

3.1 Kinematic Description of the Link Frame

The spatial position and orientation of an arbitrary link i with respect to an inertial reference system $X_oY_oZ_o$ is illustrated in Fig. 3.1. A body-fixed frame $X_iY_iZ_i$

is defined on each individual link and situated at its revolute base, and axis Z_i corresponds to that axis of rotation. Angle θ_i is used to represent the rotation about the positive Z_i axis, and is the angle from the X_{i-1} to the X_i axes. The index notation $i-1$ refers to the link **preceeding** a given link i per the structure topology, and does not necessarily represent the numeric assignment of the links, (see the final column of Table 2.1 and configuration of Fig. 2.2 as an example).

As denoted in Fig.3.1, vector $\mathbf{p}_i$ represents the position vector of the origin of link frame i from that of the inertial frame. In addition, the prismatic actuation of a piston-rod is defined to occur along the rod's X_i axis. This deviates from the modified Hartenberg-Denavit (HD) parameters used for serial manipulators in [Cyril'88], where actuation of a prismatic joint is along the link's Z_i axis. For future work regarding the spatial motion of truss cranes, it is foreseen that the links would require a similar HD parameter description, specifically when there are: individual robotic systems on the truss crane, angular misalignments between the revolute axes of adjacent links, or prismatic joints that incur out of plane motion.

The angular orientation of link frame i with respect to the inertial frame $X_oY_oZ_o$ is denoted by rotation matrix $\mathbf{Q}_i$, which contains the direction cosines of the frame i axes. Only three of the nine components in $\mathbf{Q}_i$ are independent, and the othogonality property of the rotation matrix $\mathbf{Q}_i^T\mathbf{Q}_i = \mathbf{1}_{33}$ provides six constraint equations. When using the Lagrangian method to derive the equations of motion, the angular orientation of frame i with respect to the inertial frame must be represented with generalized coordinates employing one of the following:

- three Euler angles of roll, yaw, and pitch,
- four dimensional vector of Euler parameters which represent the direction of the frame's local axis of rotation and corresponding angle of rotation, as discussed in [Cyril'88] and [Nikravesh et al.'85], or
- the four dimensional vector of a linear invariant set, discussed in [Cyril'88].

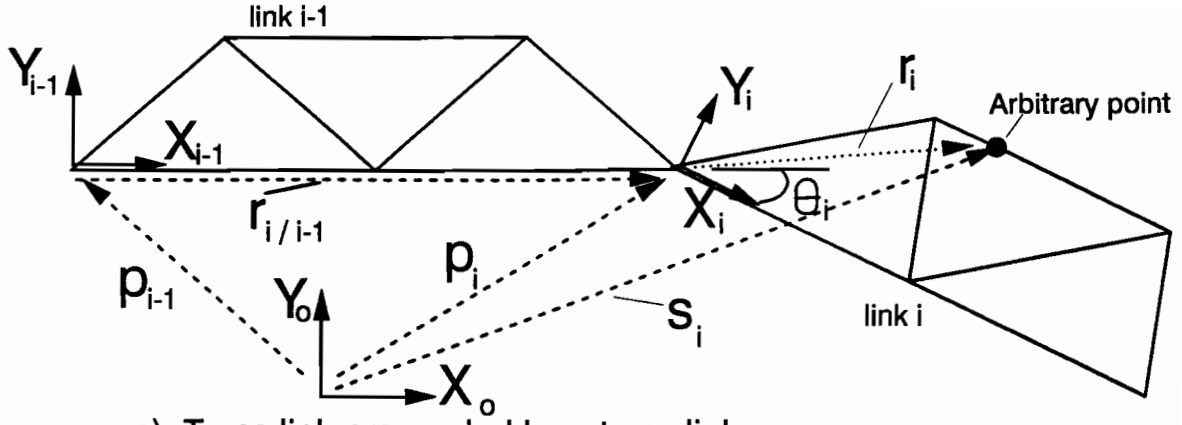

a) Truss link preceeded by a truss link.

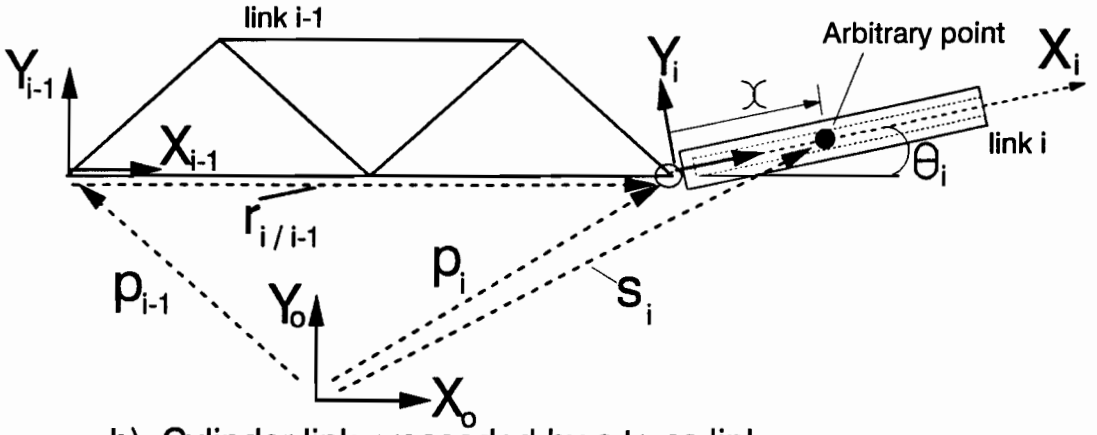

b) Cylinder link preceeded by a truss link.

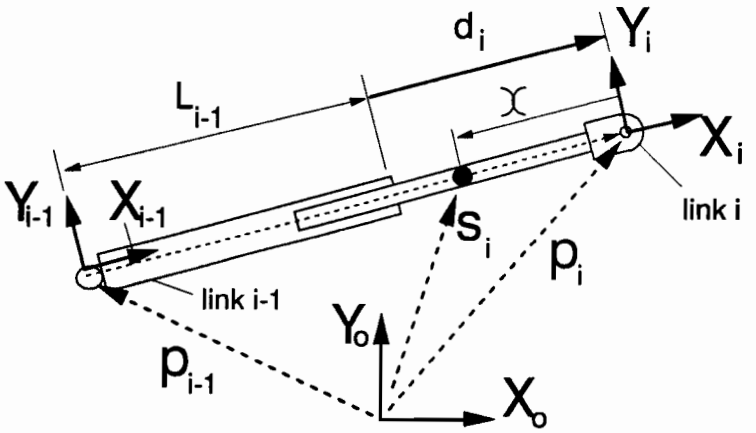

c) Piston-rod link preceeded by a cylinder link.

Figure 3.1: Kinematic descriptions of an arbitrary link.

The use of a four parameter set is preferred, and regardless of the set selected, this vector will not appear in the final form of the dynamical equations of motion. Denoting the chosen parameters for link frame i as $\hat{\mathbf{q}}_i$, it is shown in [Cyril'88] and [Nikravesh et al.'85] that the following identities between $\dot{\hat{\mathbf{q}}}_i$ and the link's 3-dimensional angular velocity vector $\boldsymbol{\omega}_i$ exist,

$$\boldsymbol{\omega}_i = \hat{\mathbf{L}}_i \dot{\hat{\mathbf{q}}}_i \tag{3.1}$$

$$\dot{\hat{\mathbf{q}}}_i = \hat{\boldsymbol{\Lambda}}_i \boldsymbol{\omega}_i \tag{3.2}$$

The algebraic constraint equation associated with the four parameter set is given as,

$$\hat{\mathbf{q}}_i^T \hat{\mathbf{q}}_i = 1 \tag{3.3}$$

Matrices $\hat{\mathbf{L}}_i$ and $\hat{\boldsymbol{\Lambda}}_i$ represent the transformations from $\dot{\hat{\mathbf{q}}}_i$ to $\boldsymbol{\omega}_i$ and vice versa, respectively, and their components are given in [Cyril'88]. Although these relations are employed in the derivations to follow, matrices $\hat{\mathbf{L}}_i$ and $\hat{\boldsymbol{\Lambda}}_i$ will not be present in the final form of the equations of motion.

3.2 Kinematic Description along the Link

The kinematics of an arbitrary point located on a link may be described using the link frame definitions presented in the previous section. As illustrated in Fig. 3.1, vector $\mathbf{s}_i$ denotes the inertial position of any point on link i, and given the local position $\mathbf{r}_i$ of the point with respect to the link origin we obtain,

$$\mathbf{s}_i = \mathbf{p}_i + \mathbf{r}_i \tag{3.4}$$

If the link is modelled as a flexible structure, then $\mathbf{r}_i$ can be represented in the **general form** of,

$$\mathbf{r}_i = \mathbf{r}_{o,i} + \mathbf{r}_{e,i} \tag{3.5}$$

where $\mathbf{r}_{o,i}$ is a 3-dimensional vector denoting the rigid body location of the point with respect to the link's origin, and $\mathbf{r}_{e,i}$ is the elastic deformation component. The

deformation may be discretized using a matrix of shape functions $\mathbf{B}_i$, and the corresponding m_i-dimensional vector of elastic or flexible coordinates $\mathbf{b}_i(t)$ denoted such as,

$$\mathbf{b}_i(t) = \langle\, b_{i,1}(t) \quad b_{i,2}(t) \quad \ldots \quad b_{i,m_i}(t) \,\rangle^T \tag{3.6}$$

where, the elastic deformation is expressed by,

$$\mathbf{r}_{e,i} = \mathbf{B}_i \mathbf{b}_i(t) \tag{3.7}$$

The shape functions contained in matrix $\mathbf{B}_i$ correspond to the deformation modes considered. For the case of beam type members of robotic manipulators, [Cyril'88] uses analytical mode shapes for lateral deflections of beams (to model the in- and out-of-plane deformations), and similarly for the torsional deformation about the longitudinal axis. In this thesis, a finite element (FE) discretization scheme is employed to model the in-plane deformation of each truss link. (Out-of-plane deformations would also result by virtue of dynamic coupling, and should be modelled in further extensions of this work.) The FE discretization scheme varies somewhat from the analytical discretization of [Cyril'88], therefore eq.(3.5) is not directly applicable. Initially, the structure is geometrically discretized and interpolation functions are used to express elemental deformations in terms of the nodal quantities. Then, subsequent to the assembly of the elemental mass and stiffness matrices for the link, the eigenvectors of the corresponding eigenvalue problem are obtained. Only a few of the lower eigenvectors are retained to represent the nodal deformations. Therefore, the local deformation of any given node j on link i can be denoted as $\mathbf{r}_{e,j/i}$, and expressed as,

$$\mathbf{r}_{e,j/i} = \mathbf{B}_i^j \mathbf{b}_i(t) \tag{3.8}$$

where now $\mathbf{B}_i^j$ is a 3 by m_i matrix containing the elements of the eigenvectors corresponding to node j. The exact details of FE discretization will be presented in the formulations of Section 4.1. The following section describes the flexible pose and twist vectors, as well as the generalized coordinates used in the Lagrangian formulation of the equations of motion for each link.

3.3 Kinematic and Generalized Coordinates

The kinematic state of each link may be described using the flexible pose vector $\mathbf{q}_i$, defined as,

$$\mathbf{q}_i = \langle \mathbf{p}_i{}^T \quad \hat{\mathbf{q}}_i^T \quad \mathbf{b}_i^T \rangle^T \tag{3.9}$$

and the flexible twist vector $\mathbf{v}_i$ containing,

$$\mathbf{v}_i = \langle \dot{\mathbf{p}}_i^T \quad \boldsymbol{\omega}_i{}^T \quad \dot{\mathbf{b}}_i^T \rangle^T \tag{3.10}$$

The dimension of $\mathbf{q}_i$ is denoted as p_i, and for general 3D motion is given as,

$$p_i = (3 + 4 + m_i) = (7 + m_i) \tag{3.11}$$

Similarly, p'_i is used to represent the dimension of the flexible twist $\mathbf{v}_i$, and is equal to,

$$p'_i = (3 + 3 + m_i) = (6 + m_i) \tag{3.12}$$

Recall that for **rigid links**, $m_i = 0$, and then the above vectors become more specifically the rigid pose and twist.

By using eq.'s (3.1) and (3.2), the following relations can be constructed,

$$\mathbf{v}_i = \mathbf{L}_i \dot{\mathbf{q}}_i \tag{3.13}$$

$$\dot{\mathbf{q}}_i = \boldsymbol{\Lambda}_i \mathbf{v}_i \tag{3.14}$$

where matrices $\mathbf{L}_i$ and $\boldsymbol{\Lambda}_i$ are of the form,

$$\mathbf{L}_i = \begin{bmatrix} \mathbf{1}_{33} & \mathbf{0}_{34} & \mathbf{0}_{3m_i} \\ \mathbf{0}_{33} & \widehat{\mathbf{L}}_i & \mathbf{0}_{3m_i} \\ \mathbf{0}_{m_i 3} & \mathbf{0}_{m_i 4} & \mathbf{1}_{m_i m_i} \end{bmatrix} \tag{3.15}$$

$$\boldsymbol{\Lambda}_i = \begin{bmatrix} \mathbf{1}_{33} & \mathbf{0}_{33} & \mathbf{0}_{3m_i} \\ \mathbf{0}_{43} & \widehat{\boldsymbol{\Lambda}}_i & \mathbf{0}_{4m_i} \\ \mathbf{0}_{m_i 3} & \mathbf{0}_{m_i 3} & \mathbf{1}_{m_i m_i} \end{bmatrix} \tag{3.16}$$

With the substitution of eq.(3.13) into eq.(3.14), we obtain,

$$\boldsymbol{\Lambda}_i \mathbf{L}_i = \mathbf{1}_{p_i p_i} \tag{3.17}$$

elastic coordinates used to model their flexibility. In addition, if a flexible manipulator arm is mounted on the structure and driven at its revolute joint by a torque, then the independent coordinates for the manipulator link would contain $\psi_{I,i} =< \theta_i \quad \mathbf{b}_i^T >^T$.

The generalized coordinates for the entire system consist of all the independent coordinates for each link. Hence, the generalized vector of independent coordinates is represented by ψ_I, and for a general structure arrangement is assembled as,

$$\psi_I = \langle \psi_{I,1}^T \quad \cdots \quad \psi_{I,i}^T \quad \cdots \quad \psi_{I,N}^T \rangle^T \tag{3.22}$$

Note that only links with independent coordinates $\psi_{I,i}$, contribute to the above. Therefore, both rigid truss links and cylinder links that are dependent upon a kinematic loop, have no contributions to ψ_I. The total number of elastic coordinates used to model the flexibility of the assembled manipulator will be denoted by variable m, and is given as the sum of the number of elastic coordinates modelled per link,

$$m = (m_1 + m_2 + \cdots + m_N) \tag{3.23}$$

Therefore, the dimension of ψ_I will be denoted by n', and is given as,

$$n' = (n + m) \tag{3.24}$$

Similarly, the total vector of dependent coordinates can be assembled and denoted by, ψ_D,

$$\psi_D = \langle \psi_{D,1}^T \quad \cdots \quad \psi_{D,i}^T \quad \cdots \quad \psi_{D,N}^T \rangle^T \tag{3.25}$$

and contains only those dependent angles associated with a kinematic loop. For the actuator arrangement in the truss manipulator of Fig. 2.2, there exists two dependencies per kinematic loop. Therefore, the dimension of ψ_D is $(2 \times l)$, where recalling from Chapter 2, l is the number of kinematic loops present in the truss manipulator.

In the treatment of the kinematic loops, a nonlinear 2-dimensional constraint equation is established, and can be expressed in the general form of,

$$\zeta(\psi_I, \psi_D) = \mathbf{0}_2 \tag{3.26}$$

from which the dependent angles θ_i for the truss link i, and θ_j for cylinder link j (associated with the loop under consideration), are obtained. The details of the kinematic loop and corresponding derivations are presented in Appendix D. In this work, the nonlinear eq.(3.26) is solved using the Newton-Raphson iterative scheme per [Nikravesh'88]. The corresponding angular rates are subsequently obtained by differentiating the the constraint equation ζ with respect to time, to yield linear equations that can be written in the general form of,

$$\dot{\psi}_D = \mathbf{N}_{DI}(\psi_I, \psi_D)\dot{\psi}_I \tag{3.27}$$

$$\ddot{\psi}_D = \dot{\mathbf{N}}_{DI}(\psi_I, \psi_D)\dot{\psi}_I + \mathbf{N}_{DI}(\psi_I, \psi_D)\ddot{\psi}_I \tag{3.28}$$

For the derivations of Appendix D, more specific forms of eq.'s (3.27) and (3.28) are presented in terms of twist vector components and some of the independent speed variables. These pertain to eq.'s (D.37) and (D.44). The construction of the natural orthogonal complement for the system will also employ these latter relations, as discussed in Section 5.3.

3.4 Recursive Relations

3.4.1 Frame Orientation Matrix

The orientation matrix $\mathbf{Q}_i$ of link frame i presented previously in Section 3.1, is obtained by the recursive relation of,

$$\mathbf{Q}_i = \mathbf{R}_1 \cdots \mathbf{R}_{i-1}\mathbf{R}_i \tag{3.29}$$

where again it is emphasized that the recursion is based upon the link connectivity defined for the structure, and notation $i-1$ refers to the link preceeding link i. In addition, the first rotation matrix $\mathbf{R}_1$ is that corresponding to the first truss link of the structure which is fixed, and will be constant for the arrangements considered here.

For link i being either a **truss** or a **cylinder**, and since only planar motion of truss manipulators is examined in this work, then $\mathbf{R}_i$ has the form of,

$$\mathbf{R}_i = \mathbf{D}^i_{i-1}\mathbf{C}_i \tag{3.30}$$

where matrix $\mathbf{C}_i$ accounts for rotation due to the revolute angle at joint i,

$$\mathbf{C}_i = \begin{bmatrix} cos(\theta_i) & -sin(\theta_i) & 0 \\ sin(\theta_i) & cos(\theta_i) & 0 \\ 0 & 0 & 1 \end{bmatrix} \tag{3.31}$$

If the truss $i-1$ is modelled as a rigid structure, then $\mathbf{D}^i_{i-1}$ is simply the identity matrix. On the other hand, if it is modelled as flexible, $\mathbf{D}^i_{i-1}$ is the rotation matrix to account for the deflection slope $\delta_{i/i-1(z)}$ at the connection node corresponding to joint i, and is given by the complete form of,

$$\mathbf{D}^i_{i-1} = \begin{bmatrix} cos(\delta_{i/i-1(z)}) & -sin(\delta_{i/i-1(z)}) & 0 \\ sin(\delta_{i/i-1(z)}) & cos(\delta_{i/i-1(z)}) & 0 \\ 0 & 0 & 1 \end{bmatrix} \tag{3.32}$$

Note from Fig. 3.2 that if the deflections are quite small compared to the length of the boom, then rotation $\delta_{i/i-1(z)}$ is approximately,

$$\delta_{i/i-1(z)} = \frac{\mathbf{r}_{e,i/i-1(y)}}{|\mathbf{r}_{o,i/i-1}|} = \mathbf{B}^{i*}_{i-1(y)}\mathbf{b}_{i-1}(t) \tag{3.33}$$

where,

$$\mathbf{B}^{i*}_{i-1(y)} = \frac{\mathbf{B}^i_{i-1(y)}}{a_{o,i/i-1}} \tag{3.34}$$

The one dimensional row matrix $\mathbf{B}^i_{i-1(y)}$ represents the Y-axis eigenvector components of the link $i-1$ evaluated at the node corresponding to joint i, and $a_{o,i/i-1}$ represents the rigid body length of joint i from $i-1$, given by the magnitude of its rigid body position vector $\mathbf{r}_{o,i/i-1}$,

$$a_{o,i/i-1} = |\mathbf{r}_{o,i/i-1}| \tag{3.35}$$

Therefore, by differentiating eq.(3.33) with respect to time, the rates associated with $\delta_{i/i-1(z)}$ are given simply as,

$$\mathring{\delta}_{i/i-1(z)} = \mathbf{B}^{i*}_{i-1(y)}\dot{\mathbf{b}}_{i-1}(t) \quad , \quad \mathring{\mathring{\delta}}_{i/i-1(z)} = \mathbf{B}^{i*}_{i-1(y)}\ddot{\mathbf{b}}_{i-1}(t) \tag{3.36}$$

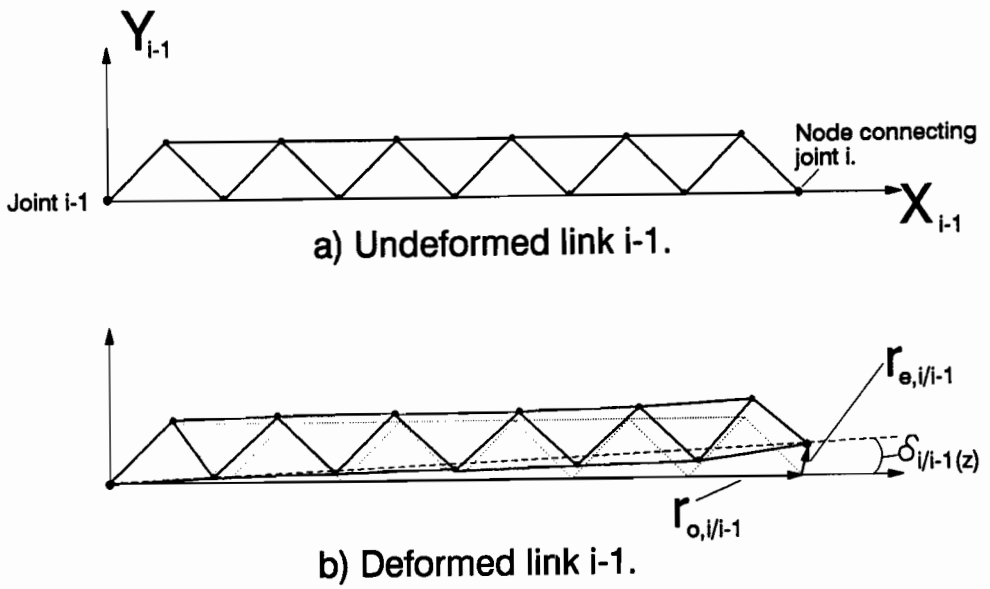

Figure 3.2: Deflection rotation defined for a flexible truss link.

So for the small deflection assumption, matrix $\mathbf{D}_{i-1}^{i}$ can be written as,

$$\mathbf{D}_{i-1}^{i} = \begin{bmatrix} 1 & -\delta_{i/i-1(z)} & 0 \\ \delta_{i/i-1(z)} & 1 & 0 \\ 0 & 0 & 1 \end{bmatrix} \tag{3.37}$$

Note that if there exists angular misalignments between the revolute axes of adjacent links, or out-of-plane deflection and bending to produce a rotation $\delta_{i/i-1(y)}$, and/or or torsional deformation that provides a rotation $\delta_{i/i-1(x)}$ of the link members, then these terms would have to be included in the computation of $\mathbf{R}_i$, as done in [Cyril'88] for flexible robotic manipulators.

For link i being a **piston-rod** and since the actuator components are modelled as

rigid members, we have simply,

$$\mathbf{R}_i = 1_{33} \tag{3.38}$$

3.4.2 Frame Origin and Rotational Vectors

The first link of a truss manipulator will be modelled as a fixed truss per Fig. 2.2. Therefore, the inertial position of the origin expressed in the link frame, is given by,

$$\mathbf{p}_1 = \mathbf{R}_1^T \mathbf{r}_{1/o} \tag{3.39}$$

where $\mathbf{r}_{1/o}$ represents the vector from the origin of the inertial frame to that of the first link frame, in terms of the inertial frame coordinates. Since the base of this truss link is fixed, then the velocity and acceleration vectors are simply,

$$\dot{\mathbf{p}}_1 = \mathbf{0}_3 \tag{3.40}$$

$$\ddot{\mathbf{p}}_1 = \mathbf{0}_3 \tag{3.41}$$

and the angular velocity and acceleration are similarly,

$$\boldsymbol{\omega}_1 = \mathbf{0}_3 \tag{3.42}$$

$$\dot{\boldsymbol{\omega}}_1 = \mathbf{0}_3 \tag{3.43}$$

Now proceeding along the structure, the inertial position of an arbitrary **truss** or **cylinder** link was illustrated previously in Figures 3.1a and 3.1b, and is given by the recursive relation,

$$\mathbf{p}_i = \mathbf{R}_i^T \left(\mathbf{p}_{i-1} + \mathbf{r}_{i/i-1} \right) \tag{3.44}$$

where, $\mathbf{p}_{i-1}$ is the inertial position vector of the origin of the preceeding link frame, and $\mathbf{r}_{i/i-1}$ is the local position vector of the end of link $i-1$, i.e., the position vector of joint i with respect to joint $i-1$. By differentiating eq.(3.44), the velocity of the origin of the i^{th} frame is,

$$\dot{\mathbf{p}}_i = \mathbf{R}_i^T \left(\dot{\mathbf{p}}_{i-1} + \boldsymbol{\omega}_{i-1} \times \mathbf{r}_{i/i-1} + \overset{\circ}{\mathbf{r}}_{i/i-1} \right) \tag{3.45}$$

where, $\overset{\circ}{\mathbf{r}}_{i/i-1}$ is the local velocity of the joint i relative to frame $i-1$. For link $i-1$ being a flexible truss, this is simply the local velocity of the node associated with joint i. Similarly, the acceleration of the origin of frame i is given as,

$$\begin{aligned}\ddot{\mathbf{p}}_i &= \mathbf{R}_i^T \Big[\ddot{\mathbf{p}}_{i-1} + \boldsymbol{\omega}_{i-1} \mathbf{x} (\boldsymbol{\omega}_{i-1} \mathbf{x} \mathbf{r}_{i/i-1}) \\ &\quad + \dot{\boldsymbol{\omega}}_{i-1} \mathbf{x} \mathbf{r}_{i/i-1} + 2\boldsymbol{\omega}_{i-1} \mathbf{x} \overset{\circ}{\mathbf{r}}_{i/i-1} + \overset{\circ\circ}{\mathbf{r}}_{i/i-1}\Big] \end{aligned} \tag{3.46}$$

Since only planar motion is considered for the truss manipulators of this work, then no transformations between the links are required for the angular velocity and accelerations of the frames. Hence, the angular velocity for the truss and cylinder links is given as,

$$\boldsymbol{\omega}_i = \boldsymbol{\omega}_{i-1} + \delta_{i/i-1(z)}\mathbf{z} + \dot{\theta}_i \mathbf{z} \tag{3.47}$$

which may also be written as,

$$\boldsymbol{\omega}_i = \omega_{i(z)}\mathbf{z} = (\omega_{i-1(z)} + \overset{\circ}{\delta}_{i/i-1(z)} + \dot{\theta}_i)\mathbf{z} \tag{3.48}$$

where $\overset{\circ}{\delta}_{i/i-1(z)}$ is given by eq.(3.36). Similarly, the angular acceleration is,

$$\dot{\boldsymbol{\omega}}_i = \dot{\boldsymbol{\omega}}_{i-1} + \overset{\circ\circ}{\delta}_{i/i-1(z)}\mathbf{z} + \ddot{\theta}_i \mathbf{z} \tag{3.49}$$

or,

$$\dot{\boldsymbol{\omega}}_i = \dot{\omega}_{i(z)}\mathbf{z} = (\dot{\omega}_{i-1(z)} + \overset{\circ\circ}{\delta}_{i/i-1(z)} + \ddot{\theta}_i)\mathbf{z} \tag{3.50}$$

Note that the unit vector $\mathbf{z}$ is common for all links, by virtue of planar motion of the truss manipulators considered here. However, as mentioned previously for the computation of the frame orientation, if there are misalignments between the revolute axes or if bending and torsion of the links are considered, then appropriate modifications must be undertaken in the above expressions.

The vectorial illustration for a **piston-rod** link was given previously in Fig. 3.1c. Since it is preceeded by the cylinder link and $\mathbf{R}_i = \mathbf{1}_{33}$, then the inertial position of the origin of its frame is expressed as,

$$\mathbf{p}_i = \mathbf{p}_{i-1} + (L_{i-1} + d_i)\mathbf{x}_i \tag{3.51}$$

where, $\mathbf{x}_i$ signifies the unit vector of the piston-rod's X axis, L_{i-1} is the length of the previous cylinder link, and d_i is the extended length of the piston rod. The velocity and acceleration of the origin of the piston-rod's frame are given by differentiating the above, and are respectively,

$$\dot{\mathbf{p}}_i = \dot{\mathbf{p}}_{i-1} + \boldsymbol{\omega}_{i-1} \times (L_{i-1} + d_i)\mathbf{x}_i + \dot{d}_i\mathbf{x}_i \tag{3.52}$$

$$\begin{aligned}\ddot{\mathbf{p}}_i = {} & \ddot{\mathbf{p}}_{i-1} + \boldsymbol{\omega}_{i-1} \times [\boldsymbol{\omega}_{i-1} \times (L_{i-1} + d_i)\mathbf{x}_i] \\ & + \dot{\boldsymbol{\omega}}_{i-1} \times (L_{i-1} + d_i)\mathbf{x}_i + 2\boldsymbol{\omega}_{i-1} \times \dot{d}_i\mathbf{x}_i + \ddot{d}_i\mathbf{x}_i\end{aligned} \tag{3.53}$$

Again, since the cylinder and piston-rod links are modelled as rigid members and there is no rotation between adjacent cylinder and piston-rod links, then the angular velocity and acceleration of the piston-rod frame is simply that of the previous cylinder link, i.e.,

$$\boldsymbol{\omega}_i = \boldsymbol{\omega}_{i-1} \tag{3.54}$$

$$\dot{\boldsymbol{\omega}}_i = \dot{\boldsymbol{\omega}}_{i-1} \tag{3.55}$$

Chapter 4

LINK DYNAMIC PROPERTIES

The following sections present the derivations of the kinetic and potential energy terms associated with the individual truss, cylinder, and piston-rod links. These quantities are required when deriving the dynamical equations of motion which will be presented in Chapter 5. The following formulations apply to general 3D motion, and the applicable 2D forms are obtained by simply retaining from the final 3D mass and stiffness matrices the components associated with; the X and Y dimensions for the origin displacements and elastic deformations, and the Z component of the rotational terms. The mathematical properties associated with vectors and their skew symmetric cross-product matrices will be used extensively, as presented in Appendix A.

4.1 Truss Links

4.1.1 Element Details

The bar members (or elements) of a truss link will be considered as slender, such that the diameter is much less than the length dimension, hence the cross-sectional contribution to the rotational inertia won't be significant (as is the case for a slender rod). To assist in the formulations that follow, several variables which designate the nodal and member dimension of a specific truss link will first be defined. Variable h^* is used to represent the number of nodes contained in a truss link, and h is the number

of elements. In addition to these, κ^* is the total number of nodal degrees of freedom (DOF) per link, κ is the number of nodal DOF per element, and κ' represents the number of DOF modelled per node. Therefore, κ^* is simply given by, $\kappa^* = \kappa' \times h^*$. These variables will be used to define the dimensions of the local truss vectors in the subsequent derivations.

Using the notation defined previously in eq.(3.4), the inertial position $\mathbf{s}_i$ of an arbitrary point located on element j of truss i, is expressed as,

$$\mathbf{s}_i = \mathbf{p}_i + \mathbf{r}_i \tag{4.1}$$

where $\mathbf{p}_i$ is the inertial position of the origin of the link frame, and $\mathbf{r}_i$ is the local position of the point with respect to the link's frame. Vector $\mathbf{r}_i$ may be expressed per eq.(3.5),

$$\mathbf{r}_i = \mathbf{r}_{o,i} + \mathbf{r}_{e,i} \tag{4.2}$$

where again vector $\mathbf{r}_{o,i}$ is the rigid body position vector, and the elastic deformation is represented with $\mathbf{r}_{e,i}$. Using the finite element method, the elastic deformation is expressed in terms of,

$$\mathbf{r}_{e,i} = \mathbf{R}_i^j \mathbf{N}_e^j [\mathbf{a}_e^j]_j \tag{4.3}$$

where $[\mathbf{a}_e^j]_j$ is the κ-dimensional element displacement vector expressed with respect to the frame of the j^{th} finite element, $\mathbf{N}_e^j$ is a matrix of interpolation functions representative of the displacement field, and $\mathbf{R}_i^j$ is the transformation matrix from the element frame to the link frame (hence contains the direction cosines of the element frame axis with respect to the link). If the element is within the plane of the link XY frame, and angle θ_i^j is defined as illustrated in Fig.4.1, then rotation matrix $\mathbf{R}_i^j$ is simply given by the form of eq.(3.31) with the substitution of θ_i by θ_i^j.

It is preferrable to express the element displacements with respect to the link frame, which will be denoted by $\mathbf{a}_e^j$. This is possible by performing a transformation given by,

$$[\mathbf{a}_e^j]_j = \overline{\mathbf{R}_i^j}^T \mathbf{a}_e^j \tag{4.4}$$

where $\overline{\mathbf{R}_i^j}$ will be defined shortly. Hence, eq.(4.3) becomes,

$$\mathbf{r}_{e,i} = \mathbf{R}_i^j \mathbf{N}_e^j \overline{\mathbf{R}_i^j}^T \mathbf{a}_e^j \tag{4.5}$$

and $\mathbf{a}_e^j$ is a κ-dimensional vector of the element DOF with respect to the link frame.

The rigid body position vector $\mathbf{r}_{o,i}$ can be similarly expressed per,

$$\mathbf{r}_{o,i} = \mathbf{N}_o^j \mathbf{a}_o^j \tag{4.6}$$

where matrix $\mathbf{N}_o^j$ contains linear functions for a truss geometry with non-curved members, and for the 3D description of a truss, $\mathbf{a}_o^j$ is a 6-dimensional vector containing,

$$\mathbf{a}_o^j = \langle \mathbf{a}_{o,1}^{j\,T} \quad \mathbf{a}_{o,2}^{j\,T} \rangle^T \tag{4.7}$$

Nodal vectors $\mathbf{a}_{o,1}^j$ and $\mathbf{a}_{o,2}^j$ are the rigid body position vectors of the first and second nodes of the element, respectively, given in the typical form of,

$$\mathbf{a}_{o,1}^j = \langle a_{o,1(x)}^j \quad a_{o,1(y)}^j \quad a_{o,1(z)}^j \rangle^T, \; \mathbf{a}_{o,2}^j = \langle a_{o,2(x)}^j \quad a_{o,2(y)}^j \quad a_{o,2(z)}^j \rangle^T \tag{4.8}$$

In this thesis, the members of the truss links are modelled as axially deformable elements, as illustrated in Fig. 4.1. Therefore matrix $\mathbf{N}_e^j$ is also of linear form and the displacement vector $\mathbf{a}_e^j$ is 6-dimensional, and contains simply the linear deformation components of the two nodes of the element,

$$\mathbf{a}_e^j = \langle \mathbf{a}_{e,1}^{j\,T} \quad \mathbf{a}_{e,2}^{j\,T} \rangle^T \tag{4.9}$$

where the respective nodal displacement vectors are given by,

$$\mathbf{a}_{e,1}^j = \langle a_{e,1(x)}^j \quad a_{e,1(y)}^j \quad a_{e,1(z)}^j \rangle^T, \; \mathbf{a}_{e,2}^j = \langle a_{e,2(x)}^j \quad a_{e,2(y)}^j \quad a_{e,2(z)}^j \rangle^T \tag{4.10}$$

Matrices $\mathbf{N}_o^j$ and $\mathbf{N}_e^j$ are therefore equivalent, and will be denoted henceforth by $\mathbf{N}^j$,

$$\mathbf{N}^j = \mathbf{N}_o^j = \mathbf{N}_e^j = \begin{bmatrix} N_1 & 0 & 0 & N_2 & 0 & 0 \\ 0 & N_1 & 0 & 0 & N_2 & 0 \\ 0 & 0 & N_1 & 0 & 0 & N_2 \end{bmatrix} \tag{4.11}$$

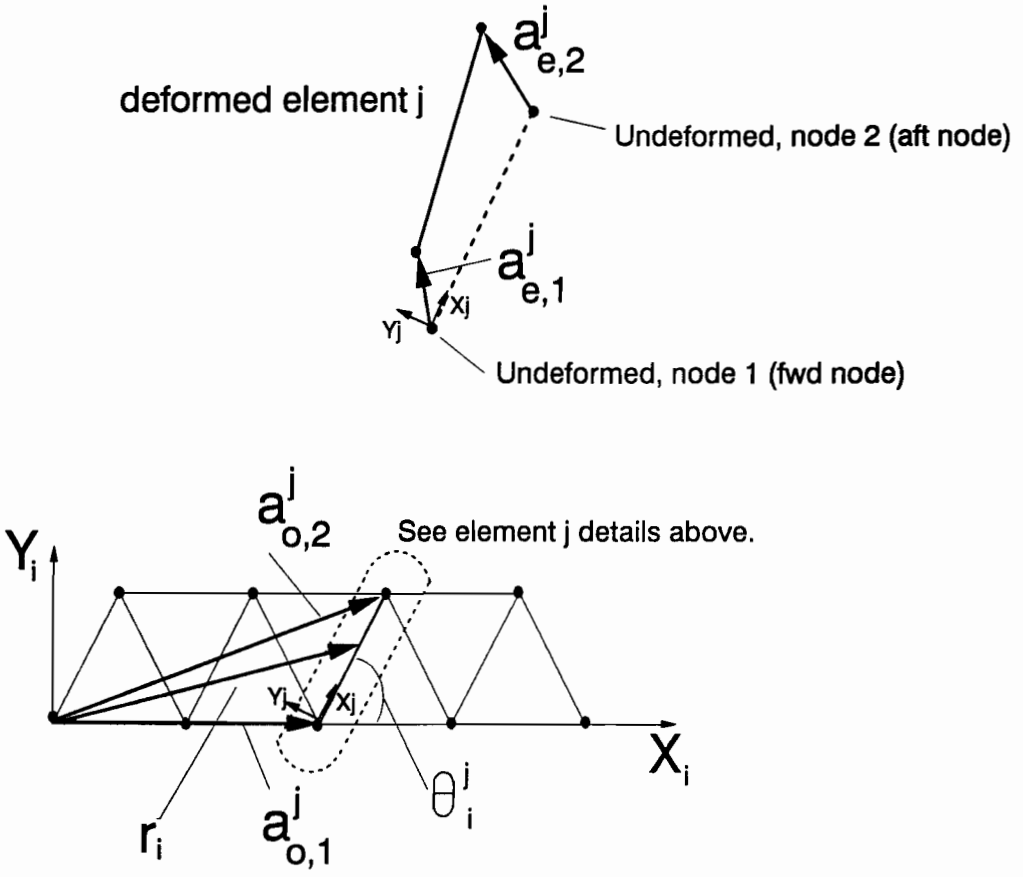

Figure 4.1: Element details of a flexible truss link.

where,

$$N_1 = 1 - \frac{x^j}{L^j}, \qquad N_2 = \frac{x^j}{L^j} \tag{4.12}$$

It should be noted that for space frames in which torsion and bending deformation modes of the elements are to be modelled, higher order functions would be required in matrix $\mathbf{N}_e^j$, such as that considered in [Necib et al.'89]. Other schemes that model the out-of-plane motion of truss frames are presented in [Berry et al.'84] and [Karpurapu et al.'93]. With the linear interpolation functions considered in eq.(4.11), the transformation matrix $\overline{\mathbf{R}_i^j}$ of eq.(4.4) takes the form of,

$$\overline{\mathbf{R}_i^j}^T = \begin{bmatrix} \mathbf{R}_i^j & \mathbf{0}_{33} \\ \mathbf{0}_{33} & \mathbf{R}_i^j \end{bmatrix}^T = \begin{bmatrix} \mathbf{R}_i^{jT} & \mathbf{0}_{33} \\ \mathbf{0}_{33} & \mathbf{R}_i^{jT} \end{bmatrix} \tag{4.13}$$

and the term $\mathbf{R}_i^j \mathbf{N}_e^j \overline{\mathbf{R}_i^j}^T$ in eq.(4.5) simplifies as follows,

$$\begin{aligned}
\mathbf{R}_i^j \mathbf{N}_e^j \overline{\mathbf{R}_i^j}^T &= \mathbf{R}_i^j \mathbf{N}^j \overline{\mathbf{R}_i^j}^T \\
&= \mathbf{R}_i^j \begin{bmatrix} N_1 & 0 & 0 & N_2 & 0 & 0 \\ 0 & N_1 & 0 & 0 & N_2 & 0 \\ 0 & 0 & N_1 & 0 & 0 & N_2 \end{bmatrix} \begin{bmatrix} \mathbf{R}_i^{jT} & \mathbf{0}_{33} \\ \mathbf{0}_{33} & \mathbf{R}_i^{jT} \end{bmatrix} \\
&= \mathbf{R}_i^j \begin{bmatrix} N_1 \mathbf{1}_{33} & N_2 \mathbf{1}_{33} \end{bmatrix} \begin{bmatrix} \mathbf{R}_i^{jT} & \mathbf{0}_{33} \\ \mathbf{0}_{33} & \mathbf{R}_i^{jT} \end{bmatrix} \\
&= \begin{bmatrix} N_1 \mathbf{R}_i^j \mathbf{R}_i^{jT} & N_2 \mathbf{R}_i^j \mathbf{R}_i^{jT} \end{bmatrix} \\
&= \begin{bmatrix} N_1 \mathbf{1}_{33} & N_2 \mathbf{1}_{33} \end{bmatrix} \qquad (4.14)
\end{aligned}$$

Therefore, with the linear interpolation functions we obtain,

$$\mathbf{R}_i^j \mathbf{N}_e^j \overline{\mathbf{R}_i^j}^T = \mathbf{N}^j \qquad (4.15)$$

which will provide considerable simplications in the calculations to follow, that would have not resulted with higher order interpolation functions for the element deformation model.

The velocity of the point on element j, is obtained by differentiating eq.(4.1) as,

$$\dot{\mathbf{s}}_i = \dot{\mathbf{p}}_i + (\boldsymbol{\omega}_i \mathbf{x} \mathbf{r}_i) + \mathring{\mathbf{r}}_i \qquad (4.16)$$

again, where $\boldsymbol{\omega}_i$ is the angular velocity of the link frame. By substituting the result of eq.(4.15) into eq.(4.5) , the local time derivative $\mathring{\mathbf{r}}_i$ is given by,

$$\mathring{\mathbf{r}}_i = \mathbf{N}^j \mathring{\mathbf{a}}_e^j \qquad (4.17)$$

Eq.(4.16) may also be expressed as,

$$\dot{\mathbf{s}}_i = \dot{\mathbf{p}}_i - \tilde{\mathbf{r}}_i \boldsymbol{\omega}_i + \mathring{\mathbf{r}}_i \qquad (4.18)$$

where $\tilde{\mathbf{r}}_i$ is the skew symmetric matrix associated with the local position vector $\mathbf{r}_i$, with its components arranged per eq.(A.2) of Appendix A,

$$\tilde{\mathbf{r}}_i = \begin{bmatrix} 0 & -z & y \\ z & 0 & -x \\ -y & x & 0 \end{bmatrix} \qquad (4.19)$$

To facilitate further derivations, eq.(4.16) will be expressed in the form of [Fattah et al.'94],

$$\dot{\mathbf{s}}_i = \mathbf{E}\mathbf{v}_i^j \tag{4.20}$$

where

$$\mathbf{E} = [\,\mathbf{1}_{33} \quad -\tilde{\mathbf{r}}_i \quad \mathbf{N}^j\,] \tag{4.21}$$

and the flexible twist vector $\mathbf{v}_i^j$ for element j is given by,

$$\mathbf{v}_i^j = \langle\, \dot{\mathbf{p}}_i{}^T \quad \boldsymbol{\omega}_i{}^T \quad \mathring{\mathbf{a}}_e^{j\,T} \,\rangle^T \tag{4.22}$$

With these definitions, the kinetic energy of the element and then of the assembled link can be established, as described in the following section.

4.1.2 Kinetic Energy

The kinetic energy T_i^j of element j is given by evaluating the expression,

$$\mathrm{T}_i^j = \frac{1}{2}\int_{\forall j} \dot{\mathbf{s}}_i^T \dot{\mathbf{s}}_i \rho^j d\forall = \frac{1}{2}\mathbf{v}_i^{j\,T}\mathbf{M}_i^j\mathbf{v}_i^j \tag{4.23}$$

where ρ^j and $\forall^j$ represents the material density and volume of the element, respectively, and the elemental mass matrix $\mathbf{M}_i^j$ is evaluated from,

$$\mathbf{M}_i^j = \int_{\forall j} \mathbf{E}^T\mathbf{E}\rho^j d\forall = \begin{bmatrix} \mathbf{M}_{dd}^j & \mathbf{M}_{dr}^j & \mathbf{M}_{de}^j \\ \mathbf{M}_{rd}^j & \mathbf{M}_{rr}^j & \mathbf{M}_{re}^j \\ \mathbf{M}_{ed}^j & \mathbf{M}_{er}^j & \mathbf{M}_{ee}^j \end{bmatrix} \tag{4.24}$$

Subscripts d, r and e represent the displacement of the origin of link frame i, rotation of the frame and elastic deformation, respectively. The mass matrix components are given by,

$$\mathbf{M}_{dd}^j = \rho^j \int_{\forall j} \mathbf{1}_{33} d\forall = M^j \mathbf{1}_{33} \tag{4.25}$$

$$\mathbf{M}_{dr}^j = -\rho^j \int_{\forall j} \tilde{\mathbf{r}}_i d\forall \tag{4.26}$$

$$\mathbf{M}_{de}^j = \rho^j \int_{\forall j} \mathbf{N}^j d\forall \tag{4.27}$$

$$\mathbf{M}_{rd}^j = -\rho^j \int_{\forall j} \tilde{\mathbf{r}}_i^T d\forall \qquad = (\mathbf{M}_{dr}^j)^T \tag{4.28}$$

$$\mathbf{M}^j_{rr} = \rho^j \int_{\forall j} \tilde{\mathbf{r}}_i^T \tilde{\mathbf{r}}_i d\forall \tag{4.29}$$

$$\mathbf{M}^j_{re} = -\rho^j \int_{\forall j} \tilde{\mathbf{r}}_i^T \mathbf{N}^j d\forall \tag{4.30}$$

$$\mathbf{M}^j_{ed} = \rho^j \int_{\forall j} \left(\mathbf{N}^j\right)^T d\forall \quad = (\mathbf{M}^j_{de})^T \tag{4.31}$$

$$\mathbf{M}^j_{er} = -\rho^j \int_{\forall j} \left(\mathbf{N}^j\right)^T \tilde{\mathbf{r}}_i d\forall = (\mathbf{M}^j_{re})^T \tag{4.32}$$

$$\mathbf{M}^j_{ee} = \rho^j \int_{\forall j} \left(\mathbf{N}^j\right)^T \mathbf{N}^j d\forall \tag{4.33}$$

where M^j is the total mass of the element. For simulation efficiency, it is desirable that the integrations involving the interpolation functions be expanded and performed explicitly off-line from the time integration of the dynamic motion. Fortunately, this is possible with the linear interpolation functions employed for the truss structures of this work. However, if bending of the truss elements is to be modelled for the case of space frames, then the integration terms of the mass matrix become quite complex and on-line integrations may be required. It is shown in Appendix B.1 that eq.'s (4.26) to (4.33), expand to the forms of,

$$\mathbf{M}^j_{dr} = -\rho^j \left[\left(Q^j_1 \tilde{\mathbf{a}}^j_{o,1} + Q^j_2 \tilde{\mathbf{a}}^j_{o,2}\right) + \left(Q^j_1 \tilde{\mathbf{a}}^j_{e,1} + Q^j_2 \tilde{\mathbf{a}}^j_{e,2}\right)\right] \tag{4.34}$$

$$\mathbf{M}^j_{de} = \rho^j \left[\, Q^j_1 \mathbf{1}_{33} \;,\; Q^j_2 \mathbf{1}_{33} \,\right] \tag{4.35}$$

$$\begin{aligned} \mathbf{M}^j_{rr} = -\rho^j \Big[& S^j_{11}(\tilde{\mathbf{a}}^j_{o,1} + \tilde{\mathbf{a}}^j_{e,1})^2 + S^j_{12}(\tilde{\mathbf{a}}^j_{o,1} + \tilde{\mathbf{a}}^j_{e,1})(\tilde{\mathbf{a}}^j_{o,2} + \tilde{\mathbf{a}}^j_{e,2}) \\ & + S^j_{12}(\tilde{\mathbf{a}}^j_{o,2} + \tilde{\mathbf{a}}^j_{e,2})(\tilde{\mathbf{a}}^j_{o,1} + \tilde{\mathbf{a}}^j_{e,1}) + S^j_{22}(\tilde{\mathbf{a}}^j_{o,2} + \tilde{\mathbf{a}}^j_{e,2})^2 \Big] \end{aligned} \tag{4.36}$$

$$\begin{aligned} \mathbf{M}^j_{re} = & \rho^j \left[\left(S^j_{11}\tilde{\mathbf{a}}^j_{o,1} + S^j_{12}\tilde{\mathbf{a}}^j_{o,2}\right), \;\; \left(S^j_{12}\tilde{\mathbf{a}}^j_{o,1} + S^j_{22}\tilde{\mathbf{a}}^j_{o,2}\right) \right] \\ & + \rho^j \left[\left(S^j_{11}\tilde{\mathbf{a}}^j_{e,1} + S^j_{12}\tilde{\mathbf{a}}^j_{e,2}\right), \;\; \left(S^j_{12}\tilde{\mathbf{a}}^j_{e,1} + S^j_{22}\tilde{\mathbf{a}}^j_{e,2}\right) \right] \end{aligned} \tag{4.37}$$

$$\mathbf{M}^j_{ee} = \rho^j \begin{bmatrix} S^j_{11}\mathbf{1}_{33}, & S^j_{12}\mathbf{1}_{33} \\ S^j_{12}\mathbf{1}_{33}, & S^j_{22}\mathbf{1}_{33} \end{bmatrix} \tag{4.38}$$

where the integrals of the interpolation functions are given by,

$$\begin{array}{rcccl} Q^j_1 & = & \int_{\forall j} N_1 d\forall & = & \int_{\forall j} \left(1 - x^j/L^j\right) d\forall \\ Q^j_2 & = & \int_{\forall j} N_2 d\forall & = & \int_{\forall j} \left(x^j/L^j\right) d\forall \end{array} \tag{4.39}$$

$$\begin{array}{rcccl} S^j_{11} & = & \int_{\forall j} (N_1)^2 d\forall & = & \int_{\forall j} \left(1 - x^j/L^j\right)^2 d\forall \\ S^j_{12} & = & \int_{\forall j} N_1 N_2 d\forall & = & \int_{\forall j} \left(1 - x^j/L^j\right)\left(x^j/L^j\right) d\forall \\ S^j_{22} & = & \int_{\forall j} (N_2)^2 d\forall & = & \int_{\forall j} \left(x^j/L^j\right)^2 d\forall \end{array} \tag{4.40}$$

It should be noted that the mass matrices in eq.'s(4.35) and (4.38) are constants, where as in eq.'s (4.34), (4.36) and (4.37), only matrix operations with the nodal vectors remain. By further expansion of the $\mathbf{M}^j_{rr}$ components, it is also possible to obtain explicit terms involving only the rigid nodal position vectors, and other terms involving the elastic deformation vectors (as is the case with $\mathbf{M}^j_{dr}$ and $\mathbf{M}^j_{re}$). Hence, the mass matrix components containing only the constant integral values and the rigid nodal vectors can be computed once prior to the dynamic simulation, and then added to those varying mass components involving the nodal displacement vectors (which must be re-computed throughout the flexible body simulation).

The mass matrix for the total truss link is obtained by assembling the elemental matrices, which can be represented using an element-node association matrix $\boldsymbol{\Phi}^j$, such that,

$$\mathbf{a}^j_e = \boldsymbol{\Phi}^j \mathbf{a}_e \tag{4.41}$$

where $\mathbf{a}_e$ is the total nodal deflection vector for the truss link, and is of dimension κ^*. The element-node association matrix $\boldsymbol{\Phi}^j$ consists of zeros and ones which properly associate the element j nodal DOF's to that of the total link nodal DOF vector, and is therefore of dimension (κ x κ^*). By substituting eq.(4.41) into eq.(4.22) we obtain the element twist vector in the form of,

$$\mathbf{v}^j_i = \langle\ \dot{\mathbf{p}}_i{}^T \quad \boldsymbol{\omega}_i{}^T \quad (\boldsymbol{\Phi}^j \mathring{\mathbf{a}}_e)^T\ \rangle^T \tag{4.42}$$

from which the link's nodal twist vector $\mathbf{v}^*_i$ can be extracted as,

$$\mathbf{v}^*_i = \langle\, \dot{\mathbf{p}}_i{}^T \quad \boldsymbol{\omega}_i{}^T \quad \mathring{\mathbf{a}}_e{}^T \rangle^T \tag{4.43}$$

Hence, the full kinetic energy of the link is obtained by summing the elemental energies of all h elements,

$$\mathrm{T}_i = \sum_{j=1}^{h} \mathrm{T}^j_i = \frac{1}{2} \mathbf{v}^{*T}_i \mathbf{M}^*_i \mathbf{v}^*_i \tag{4.44}$$

where the assembled mass matrix $\mathbf{M}_i^*$ for truss link i is given by,

$$\mathbf{M}_i^* = \sum_{j=1}^{h} \begin{bmatrix} \mathbf{M}_{dd}^j & \mathbf{M}_{dr}^j & \mathbf{M}_{de}^j \boldsymbol{\Phi}^j \\ \mathbf{M}_{dr}^{j\,T} & \mathbf{M}_{rr}^j & \mathbf{M}_{re}^j \boldsymbol{\Phi}^j \\ \left(\mathbf{M}_{de}^j \boldsymbol{\Phi}^j\right)^T & \left(\mathbf{M}_{re}^j \boldsymbol{\Phi}^j\right)^T & \boldsymbol{\Phi}^{jT} \mathbf{M}_{ee}^j \boldsymbol{\Phi}^j \end{bmatrix} = \begin{bmatrix} \mathbf{M}_{dd} & \mathbf{M}_{dr} & \mathbf{M}_{de}^* \\ \mathbf{M}_{dr}^T & \mathbf{M}_{rr} & \mathbf{M}_{re}^* \\ \mathbf{M}_{de}^{*\,T} & \mathbf{M}_{re}^{*\,T} & \mathbf{M}_{ee}^* \end{bmatrix} \tag{4.45}$$

It should be noted that this mass matrix is in terms of the full number of nodal DOF's. In addition to the mass of the elements, there may be concentrated nodal masses, which must also be included in the kinetic energy of the truss link. The consideration of these additional terms are addressed in Appendix B.2. Given that a truss link may consist of numerous nodal degrees of freedom, Section 4.1.4 will present the modal discretization operations in which only a few of the lower vibration modes of the truss link are used to represent the nodal deformation. By employing these, the order of the full mass matrix $\mathbf{M}_i^*$ above is reduced to obtain the modal discretized mass matrix $\mathbf{M}_i$ corresponding to the link flexible twist vector $\mathbf{v}_i$, defined previously by eq.(3.10). Prior to implementing the modal discretization scheme, the stiffness matrix for the link must be established, as presented next by considering the potential strain energy of the elements.

4.1.3 Potential Energy

The potental strain energy of truss links modelled with linear interpolation functions for the element displacement field, is given in [Cook'81]. The resulting strain energy of an element, U_i^j, is simply that due to the axial strain ε along the element,

$$\varepsilon = \frac{da_{e,(x)}^j}{dx} \tag{4.46}$$

where $a_{e,(x)}^j$ represents the deformation along the element's x^j axis. Therefore, the strain energy for element j is given by,

$$\mathrm{U}_i^j = \frac{1}{2}\int_{\forall j} E^j \varepsilon^2 d\forall = \frac{1}{2}[\mathbf{a}_e^j]_j^T \left(\int_{x=0}^{L^j} ([\boldsymbol{\partial}]\mathbf{N}^j)^T E^j A^j ([\boldsymbol{\partial}]\mathbf{N}^j) dx\right) [\mathbf{a}_e^j]_j \tag{4.47}$$

where E^j is the Young's modulus of the material, A^j is the cross-sectional area, and the matrix operator $[\partial]$ is of the form,

$$[\partial] = \begin{bmatrix} \frac{d}{dx} & 0 & 0 & \frac{d}{dx} & 0 & 0 \\ 0 & 0 & 0 & 0 & 0 & 0 \\ 0 & 0 & 0 & 0 & 0 & 0 \end{bmatrix} \tag{4.48}$$

Substituting in for the matrix $\mathbf{N}^j$ from eq.(4.11) yields,

$$\mathrm{U}_i^j = \frac{1}{2}[\mathbf{a}_e^j]_j^T \left(\frac{E^j}{(L^j)^2} \int_{x=0}^{L^j} A^j dx \right) \mathbf{S}[\mathbf{a}_e^j]_j \tag{4.49}$$

where,

$$\mathbf{S} = (L^j)^2([\partial]\mathbf{N}^j)^T([\partial]\mathbf{N}^j) = \begin{bmatrix} 1 & 0 & 0 & -1 & 0 & 0 \\ 0 & 0 & 0 & 0 & 0 & 0 \\ 0 & 0 & 0 & 0 & 0 & 0 \\ -1 & 0 & 0 & 1 & 0 & 0 \\ 0 & 0 & 0 & 0 & 0 & 0 \\ 0 & 0 & 0 & 0 & 0 & 0 \end{bmatrix} \tag{4.50}$$

By recalling eq.(4.4), the nodal displacements will be expressed with respect to link frame, and eq.(4.49) becomes

$$\mathrm{U}_i^j = \frac{1}{2}\mathbf{a}_e^{jT}\overline{\mathbf{R}_i^j} \left(\frac{E^j}{(L^j)^2} \int_{x=0}^{L^j} A^j dx \right) \mathbf{S}\, \overline{\mathbf{R}_i^j}^T \mathbf{a}_e^j = \frac{1}{2}\mathbf{a}_e^{jT}\mathbf{K}_i^j\mathbf{a}_e^j \tag{4.51}$$

where the element stiffness matrix $\mathbf{K}_i^j$ with respect to the link frame, is given by,

$$\mathbf{K}_i^j = \overline{\mathbf{R}_i^j} \left(\frac{E^j}{(L^j)^2} \int_{x=0}^{L^j} A^j dx \right) \mathbf{S}\, \overline{\mathbf{R}_i^j}^T \tag{4.52}$$

Now, the nodal pose vector $\mathbf{q}_i^*$ for link i consists of the total nodal DOF's, i.e.,

$$\mathbf{q}_i^* = \langle\, \mathbf{p}_i{}^T \quad \hat{\mathbf{q}}_i^T \quad \mathbf{a}_e{}^T \,\rangle^T \tag{4.53}$$

The quadratic form of the strain energy for link i, in terms of the nodal pose vector, is expressed as,

$$\mathrm{U}_i = \frac{1}{2}\mathbf{q}_i^{*T}\mathbf{K}_i^*\mathbf{q}_i^* \tag{4.54}$$

where the stiffness matrix $\mathbf{K}_i^*$ is in terms of the full nodal DOF and given by,

$$\mathbf{K}_i^* = \begin{bmatrix} \mathbf{0}_{33} & \mathbf{0}_{34} & \mathbf{0}_{3\kappa^*} \\ \mathbf{0}_{43} & \mathbf{0}_{44} & \mathbf{0}_{4\kappa^*} \\ \mathbf{0}_{\kappa^*3} & \mathbf{0}_{\kappa^*4} & \mathbf{K}_{ee}^* \end{bmatrix} \tag{4.55}$$

Recall that κ^* represents the total number of nodal DOF for truss link i. The elastic stiffness matrix $\mathbf{K}^*_{ee}$ is a square and symmetric matrix of dimension κ^*, and is assembled from eq.(4.52),

$$\mathbf{K}^*_{ee} = \sum_{j=1}^{h} (\boldsymbol{\Phi}^j)^T \mathbf{K}^j_i \boldsymbol{\Phi}^j \tag{4.56}$$

The following section will demonstrate that only a few of the vibration modes of the truss link will be employed to represent the nodal deflections. Hence, the full matrices $\mathbf{M}^*_i$ and $\mathbf{K}^*_i$ will be reduced to the link mass $\mathbf{M}_i$ and stiffness $\mathbf{K}_i$ matrices used in the final equations of motion.

4.1.4 Modal Discretization

To reduce the order of the truss mass matrices for the flexible body dynamic simulations, and hence the computation time, only a few lower vibration mode shapes of the truss link will be considered. These can be obtained by applying the appropriate boundary conditions to the eigenvalue problem for free vibration of the truss link, established from,

$$\mathbf{M}^*_{ee} \overset{oo}{\mathbf{a}}_e + \mathbf{K}^*_{ee} \mathbf{a}_e = \mathbf{0}_{\kappa^*} \tag{4.57}$$

By imposing nodal constraints that remove rigid body modes, and since the corresponding mass and stiffness matrices are symmetric, then real orthogonal eigenvectors will be obtained. Only those of the lowest m_i modes will be retained to establish a modal matrix $\mathbf{B}_i$, for which the r^{th} column contains the r^{th} eigenvector. Hence, $\mathbf{B}_i$ is of dimension κ^* by m_i. The corresponding modal or elastic coordinates are denoted by vector $\mathbf{b}_i(t)$, and the nodal deflections can be modelled by,

$$\mathbf{a}_e = \mathbf{B}_i \mathbf{b}_i(t) \tag{4.58}$$

The truss link mass matrix $\mathbf{M}_i$ to appear in the equations of motion, is now obtained by transforming eq.(4.45) in terms of the elastic coordinates $\mathbf{b}_i$,

$$\mathbf{M}_i = \begin{bmatrix} \mathbf{M}_{dd} & \mathbf{M}_{dr} & \mathbf{M}^*_{de}\mathbf{B}_i \\ \mathbf{M}_{dr}{}^T & \mathbf{M}_{rr} & \mathbf{M}^*_{re}\mathbf{B}_i \\ (\mathbf{M}^*_{de}\mathbf{B}_i)^T & (\mathbf{M}^*_{re}\mathbf{B}_i)^T & \mathbf{B}_i^T\mathbf{M}^*_{ee}\mathbf{B}_i \end{bmatrix} = \begin{bmatrix} \mathbf{M}_{dd} & \mathbf{M}_{dr} & \mathbf{M}_{de} \\ \mathbf{M}_{dr}{}^T & \mathbf{M}_{rr} & \mathbf{M}_{re} \\ \mathbf{M}_{de}{}^T & \mathbf{M}_{re}{}^T & \mathbf{M}_{ee} \end{bmatrix} \tag{4.59}$$

Similarly, the stiffness matrix corresponding to the quadratic form of the potential energy expressed in terms of the elastic coordinates, is given by,

$$\mathbf{K}_i = \begin{bmatrix} \mathbf{0}_{33} & \mathbf{0}_{34} & \mathbf{0}_{3m_i} \\ \mathbf{0}_{43} & \mathbf{0}_{44} & \mathbf{0}_{4m_i} \\ \mathbf{0}_{m_i3} & \mathbf{0}_{m_i4} & \mathbf{K}_{ee} \end{bmatrix} \tag{4.60}$$

where,

$$\mathbf{K}_{ee} = \mathbf{B}_i^T \mathbf{K}_{ee}^* \mathbf{B}_i \tag{4.61}$$

Since orthogonal eigenvectors are contained in the modal shape matrix $\mathbf{B}_i$, then the forms of $\mathbf{M}_{ee}$ and $\mathbf{K}_{ee}$ will be diagonal. Hence, the stiffness matrix $\mathbf{K}_{ee}$ for link i, can be written as,

$$\mathbf{K}_{ee} = diag\,[k_{i,1}, \quad k_{i,2}, \quad \ldots, \quad k_{i,m_i}] \tag{4.62}$$

This fact will be used in the vibration control scheme presented in Section 6.1. The methods by which to consider the structural damping of truss links, will now be addressed in the the following section.

4.1.5 Structural Damping

The structural damping associated with specific truss structures for space applications, has been experimentally evaluated in [Voth et al.'94] for NASA's space station test model, and in [Soucy et al.'84] for a typical space mast. In these activities, damping is expressed in terms of modal damping factors corresponding to FE computed modes. Since modal discretization is employed in this thesis, then the damping values observed in [Voth et al.'94] and [Soucy et al.'84] could be examined for the truss structures of this work, if a Rayleigh proportional damping model is implemented per [Bathe'82] or [Cook'81].

There exists yet a more simplified scheme to account for structural damping, and is that of the complex elastic modulus. As discussed in [Nashif et al.'85], structural damping results from the energy dissipation due to cyclic stress and strain, in which the latter lags the former during sinusoidal deformation. In addition,

[Kimball et al.'29] demonstrated that damping is proportional to the square of the strain amplitude, and is almost unaffected by the frequency of deformation. Therefore, the stress-strain lag may be modelled per [Jaar'93], by the complex modulus of elasticity E^*, expressed as,

$$E^* = E\left(1 + \nu\frac{\partial}{\partial t}\right) \tag{4.63}$$

where ν will be referred to hereafter as the complex damping ratio. The complex modulus of elasticity is substituted for the Young's modulus appearing in the resulting elastic force terms of the final equations of motion for the truss link (and not into the initial strain energy expression). In addition, if the elements are of different materials with different ν's, then the proper element summations of the elastic force are required to correctly apply the complex damping model.

If we recall the vibration equation of a single degree of freedom system modelled with mass m, viscous damping c, and stiffness k, the conventional damping ratio ζ is defined as,

$$\zeta = c/c_{cr} \tag{4.64}$$

where c_{cr} is the critical viscous damping given from $c_{cr} = 2(mk)^{1/2}$. It can be shown that the relationship between damping ratio ζ and the complex damping ratio ν, is approximately,

$$2\zeta\omega = \nu\omega^2 \tag{4.65}$$

where ω represents the natural frequency of vibration of the system. Given a complex damping ratio ν, the above expression can be used to establish a rough order of magnitude of the damping ratio ζ for the lowest frequency of vibration of a structure.

4.2 Actuator Links

As mentioned previously in Chapter 2, the prismatic actuators will be modelled as two separate links given by a cylinder component and an extending piston-rod. As assumed for the truss members, their cross-sectional diameters will be considered

much smaller than that of the length. In addition, the acuator components will be considered structurally rigid, hence, kinetic energy contributions will be that of the rigid body displacement and rotation, and there will be no potential energy terms (since material strain is not modelled). The treatment of the actuators as two separate links, will facilitate flexibility considerations, as well as detailled modelling of either hydraulic or servo actuator control, for future work. The following sections present the evaluation of the kinetic energy for each actuator component, and the corresponding link mass matrix.

4.2.1 Kinetic Energy of Cylinder

Inertial position $\mathbf{s}_i$ of an arbitrary point along the cylinder component of the actuator can be expressed as done for the truss in eq.(4.1), and is illustrated in Fig.3.1b. For this rigid member, the local vector $\mathbf{r}_i$ of the point is simply that given by,

$$\mathbf{r}_i = \mathbf{r}_{o,i} = x\mathbf{x}_i \tag{4.66}$$

where x represents the position along the unit $\mathbf{x}_i$ axis of the cylinder link. Hence, as done for the truss link, the velocity along the cylinder component may be written as,

$$\dot{\mathbf{s}}_i = \dot{\mathbf{p}}_i + (\boldsymbol{\omega}_i \times \mathbf{r}_i) = \dot{\mathbf{p}}_i - x\tilde{\mathbf{x}}_i\boldsymbol{\omega}_i \tag{4.67}$$

where, $\tilde{\mathbf{x}}_i$ is the skew symmetrix matrix of the unit vector $\mathbf{x}_i$. Eq.(4.67) may also be expressed in the form of eq.(4.20),

$$\dot{\mathbf{s}}_i = \mathbf{E}\mathbf{v}_i \tag{4.68}$$

where $\mathbf{v}_i$ is the rigid twist vector of the cylinder link,

$$\mathbf{v}_i = \langle\, \dot{\mathbf{p}}_i^T \quad \boldsymbol{\omega}_i{}^T \,\rangle^T \tag{4.69}$$

and matrix $\mathbf{E}$ contains,

$$\mathbf{E} = [\, \mathbf{1}_{33} \quad -x\tilde{\mathbf{x}}_i \,] \tag{4.70}$$

The resulting kinetic energy T_i of the cylinder link is therefore given by evaluating the expression,

$$\mathrm{T}_i = \frac{1}{2}\int_{\forall_i} \dot{\mathbf{s}}_i^T \dot{\mathbf{s}}_i \rho_i d\forall = \frac{1}{2}\mathbf{v}_i{}^T \mathbf{M}_i \mathbf{v}_i \tag{4.71}$$

where the link mass matrix $\mathbf{M}_i$ consists of,

$$\mathbf{M}_i = \int_{\forall_i} \mathbf{E}^T \mathbf{E} \rho_i d\forall = \begin{bmatrix} \mathbf{M}_{dd} & \mathbf{M}_{dr} \\ \mathbf{M}_{dr}{}^T & \mathbf{M}_{rr} \end{bmatrix} \tag{4.72}$$

and $\int_{\forall_i}$ represents integration over the cylinder volume and ρ_i the material density. More specifically, the $\mathbf{M}_i$ components can be evaluated as,

$$\mathbf{M}_{dd} = \rho_i \int_{\forall_i} \mathbf{1}_{33} d\forall = M_i \mathbf{1}_{33} \tag{4.73}$$

$$\mathbf{M}_{dr} = -\rho_i \int_{\forall_i} x \tilde{\mathbf{x}}_i d\forall \tag{4.74}$$

$$\mathbf{M}_{rr} = \rho_i \int_{\forall_i} x^2 \tilde{\mathbf{x}}_i^T \tilde{\mathbf{x}}_i d\forall = -\rho_i \int_{\forall_i} x^2 \tilde{\mathbf{x}}_i^2 d\forall \tag{4.75}$$

For a cylinder geometry with uniform inner and outer diameters, eq.'s(4.74) and (4.75) reduce to,

$$\mathbf{M}_{dr} = -\left(\frac{M_i L_i}{2}\right) \tilde{\mathbf{x}}_i \tag{4.76}$$

$$\mathbf{M}_{rr} = -\left(\frac{M_i L_i^2}{3}\right) \tilde{\mathbf{x}}_i^2 \tag{4.77}$$

where, M_i is the total mass of the cylinder link and L_i is the length. Comments regarding the derivations of the above, are presented in Appendix B.3.

4.2.2 Kinetic Energy of Piston-Rod

For the piston-rod component, the inertial position $\mathbf{s}_i$ of an arbitrary point along its length can be expressed as done previously for the cylinder. Hence, eq.'s (4.67) to (4.75) are applicable. The difference to be noted, is that the origin of the piston rod is situated at the aft end of its length. Hence, the integral for the kinetic energy expression must be evaluated from the negative of its full length to its origin, (such

as $\int_{x=-L_i}^{0}$). For a piston-rod with a uniform diameter, the final forms of the mass matrices become

$$\mathbf{M}_{dd} = M_i \mathbf{1}_{33} \tag{4.78}$$

$$\mathbf{M}_{dr} = +\left(\frac{M_i L_i}{2}\right) \tilde{\mathbf{x}}_i \tag{4.79}$$

$$\mathbf{M}_{rr} = -\left(\frac{M_i L_i^2}{3}\right) \tilde{\mathbf{x}}_i^2 \tag{4.80}$$

where, M_i is the total mass of the piston-rod link and L_i is the length. Appendix B.4 contains the derivation details, and also presents the additional terms for a concentrated mass located at the origin of the piston-rod. The following chapter now considers the equations of motion corresponding to a general link i, and the assembly procedure required to obtain the dynamical equations for the entire system.

Chapter 5

EQUATIONS OF MOTION

5.1 Individual Links

The dynamical equations of motion for an unconstrained link undergoing arbitrary spatial motion will now be derived. The procedure employed here for truss manipulators corresponds to that used in [Cyril'88] for robotic manipulators, and will be briefly described.

The equations of motions for an individual link i, can be obtained from the Euler-Lagrange's equation,

$$\frac{d}{dt}\left(\frac{\partial \mathrm{T}_i}{\partial \dot{\mathbf{q}}_i}\right) - \frac{\partial \mathrm{T}_i}{\partial \mathbf{q}_i} + \frac{\partial \mathrm{U}_i}{\partial \mathbf{q}_i} = \mathbf{w}_i \tag{5.1}$$

where $\mathbf{w}_i$ is the wrench vector accounting for non-conservative forces and moments, and represents the sum of the: externally applied components $\mathbf{w}_i^E$, algebraic constraint wrench $\mathbf{w}_i^A$, and inter-link kinematic constraint wrench $\mathbf{w}_i^K$. (Note that a damping term may also be included here and represented as $\mathbf{w}_i^D$. However, this component will not be carried throughout the following derivations.) The potential energy due to gravity will be treated in the manner of [Cyril'88], and as suggested by [Luh et al.'80], where the inertial frame is assigned an acceleration of $\ddot{\mathbf{p}}_o = -\mathbf{g}$, and $\mathbf{g}$ is the gravitional acceleration vector.

The kinetic energy expression for link i may be written in the quadratic form of,

$$\mathrm{T}_i = f(\mathbf{q}_i, \dot{\mathbf{q}}_i) = \frac{1}{2}\dot{\mathbf{q}}_i^T \mathbf{I}_i \dot{\mathbf{q}}_i \tag{5.2}$$

where $\mathbf{I}_i$ represents the inertia matrix for link i. However, if eq.(3.14) is substituted into the above, the kinetic energy may also be expressed in the form previously considered for each link,

$$\mathrm{T}_i = f(\mathbf{q}_i, \mathbf{v}_i) = \frac{1}{2}\mathbf{v}_i^T \mathbf{M}_i \mathbf{v}_i \tag{5.3}$$

where mass matrix $\mathbf{M}_i$ is that already derived in the previous chapter for each link type. By substituting eq.(3.14) into eq.(5.2), and comparing the result with eq.(5.3), yields the relationship,

$$\mathbf{M}_i = \boldsymbol{\Lambda}_i^T \mathbf{I}_i \boldsymbol{\Lambda}_i \tag{5.4}$$

From the derivations to follow, it will be mass matrix $\mathbf{M}_i$ that prevails in the final forms of the equations of motion for an individual link.

The first two terms of eq.(5.1) can be evaluated using eq.(5.2), as

$$\frac{d}{dt}\left(\frac{\partial \mathrm{T}_i}{\partial \dot{\mathbf{q}}_i}\right) = \mathbf{I}_i \ddot{\mathbf{q}}_i + \dot{\mathbf{I}}_i \dot{\mathbf{q}}_i \tag{5.5}$$

$$\frac{\partial \mathrm{T}_i}{\partial \mathbf{q}_i} = \frac{1}{2}\dot{\mathbf{q}}_i^T \frac{\partial \mathbf{I}_i}{\partial \mathbf{q}_i}\dot{\mathbf{q}}_i \tag{5.6}$$

Substituting these two expressions into eq.(5.1), the equations of motion for link i may be written in the form of,

$$\mathbf{I}_i \ddot{\mathbf{q}}_i = \mathbf{w}_i^S + \mathbf{w}_i^E + \mathbf{w}_i^A + \mathbf{w}_i^K \tag{5.7}$$

where the system wrench $\mathbf{w}_i^S$ contains the terms,

$$\mathbf{w}_i^S = -\dot{\mathbf{I}}_i \dot{\mathbf{q}}_i + \frac{1}{2}\dot{\mathbf{q}}_i^T \frac{\partial \mathbf{I}_i}{\partial \mathbf{q}_i}\dot{\mathbf{q}}_i - \frac{\partial \mathrm{U}_i}{\partial \mathbf{q}_i} \tag{5.8}$$

By recalling eq.(3.13) and differentiating it with respect to time gives,

$$\dot{\mathbf{v}}_i = \dot{\mathbf{L}}_i \dot{\mathbf{q}}_i + \mathbf{L}_i \ddot{\mathbf{q}}_i \tag{5.9}$$

Pre-multiplying the above expression by $\boldsymbol{\Lambda}_i$, rearranging terms, and employing eq.(3.17), yields,

$$\ddot{\mathbf{q}}_i = \boldsymbol{\Lambda}_i \left(\dot{\mathbf{v}}_i - \dot{\mathbf{L}}_i \dot{\mathbf{q}}_i\right) \tag{5.10}$$

Substituting this into eq.(5.7) provides the form,

$$\mathbf{I}_i \boldsymbol{\Lambda}_i \dot{\mathbf{v}}_i = \left(\mathbf{I}_i \boldsymbol{\Lambda}_i \dot{\mathbf{L}}_i \dot{\mathbf{q}}_i + \mathbf{w}_i^S \right) + \mathbf{w}_i^E + \mathbf{w}_i^A + \mathbf{w}_i^K \tag{5.11}$$

Now, as demonstrated [Cyril'88], the algebraic constraint wrench $\mathbf{w}_i^A$ may by eliminated by pre-multiplying the above by $\boldsymbol{\Lambda}_i^T$. Hence, performing this operation and using the relation of eq.(5.4), eq.(5.11) reduces to,

$$\mathbf{M}_i \dot{\mathbf{v}}_i = \boldsymbol{\phi}_i^S + \boldsymbol{\phi}_i^E + \boldsymbol{\phi}_i^K \tag{5.12}$$

where we now denote the transformed wrenches by,

$$\boldsymbol{\phi}_i^S = \mathbf{M}_i \dot{\mathbf{L}}_i \dot{\mathbf{q}}_i + \boldsymbol{\Lambda}_i^T \mathbf{w}_i^S \tag{5.13}$$

$$\boldsymbol{\phi}_i^E = \boldsymbol{\Lambda}_i^T \mathbf{w}_i^E \tag{5.14}$$

$$\boldsymbol{\phi}_i^K = \boldsymbol{\Lambda}_i^T \mathbf{w}_i^K \tag{5.15}$$

It is also shown in [Cyril'88] that eq.(5.13) can be written as,

$$\boldsymbol{\phi}_i^S = -\boldsymbol{\Lambda}_i^T \left(\frac{\partial \mathrm{U}_i}{\partial \mathbf{q}_i} \right) - 2\boldsymbol{\Lambda}_i^T \dot{\mathbf{L}}_i^T \mathbf{M}_i \mathbf{v}_i - \dot{\mathbf{M}}_i \mathbf{v}_i + \frac{1}{2} \boldsymbol{\Lambda}_i^T \left[\mathbf{v}_i^T \left(\frac{\partial \mathbf{M}_i}{\partial \mathbf{q}_i} \right) \mathbf{v}_i \right] \tag{5.16}$$

For mass matrix $\mathbf{M}_i$ of the form,

$$\mathbf{M}_i = \begin{bmatrix} \mathbf{M}_{dd} & \mathbf{M}_{dr} & \mathbf{M}_{de} \\ \mathbf{M}_{rd} & \mathbf{M}_{rr} & \mathbf{M}_{re} \\ \mathbf{M}_{ed} & \mathbf{M}_{er} & \mathbf{M}_{ee} \end{bmatrix} \tag{5.17}$$

the system wrench $\boldsymbol{\phi}_i^S$ be written more specifically as,

$$\boldsymbol{\phi}_{i,d}^S = -\left(\dot{\mathbf{M}}_{dd} \dot{\mathbf{p}}_i + \dot{\mathbf{M}}_{dr} \boldsymbol{\omega}_i + \dot{\mathbf{M}}_{de} \dot{\mathbf{b}}_i \right) \tag{5.18}$$

$$\begin{aligned} \boldsymbol{\phi}_{i,r}^S = & -2\hat{\boldsymbol{\Lambda}}_i^T \dot{\hat{\mathbf{L}}}_i^T \left(\mathbf{M}_{rd} \dot{\mathbf{p}}_i + \mathbf{M}_{rr} \boldsymbol{\omega}_i + \mathbf{M}_{re} \dot{\mathbf{b}}_i \right) \\ & - \left(\dot{\mathbf{M}}_{rd} \dot{\mathbf{p}}_i + \dot{\mathbf{M}}_{rr} \boldsymbol{\omega}_i + \dot{\mathbf{M}}_{re} \dot{\mathbf{b}}_i \right) \end{aligned} \tag{5.19}$$

$$\begin{aligned} \boldsymbol{\phi}_{i,e}^S = & -\frac{\partial \mathrm{U}_i}{\partial b_{i,k}} - \left(\dot{\mathbf{M}}_{ed} \dot{\mathbf{p}}_i + \dot{\mathbf{M}}_{er} \boldsymbol{\omega}_i + \dot{\mathbf{M}}_{ee} \dot{\mathbf{b}}_i \right) \\ & + \frac{1}{2} \boldsymbol{\omega}_i{}^T \frac{\partial \mathbf{M}_{rr}}{\partial b_{i,k}} \boldsymbol{\omega}_i + \dot{\mathbf{p}}_i^T \frac{\partial \mathbf{M}_{dr}}{\partial b_{i,k}} \boldsymbol{\omega}_i + \boldsymbol{\omega}_i{}^T \frac{\partial \mathbf{M}_{re}}{\partial b_{i,k}} \dot{\mathbf{b}}_i; \; k = 1, 2, ..., m_i \end{aligned} \tag{5.20}$$

The following relation is also derived in [Cyril'88],

$$2\widehat{\mathbf{\Lambda}}_i^T\dot{\widehat{\mathbf{L}}}_i^T = \widetilde{\boldsymbol{\omega}}_i = \begin{bmatrix} 0 & -\boldsymbol{\omega}_{i,(z)} & \boldsymbol{\omega}_{i,(y)} \\ \boldsymbol{\omega}_{i,(z)} & 0 & -\boldsymbol{\omega}_{i,(x)} \\ -\boldsymbol{\omega}_{i,(y)} & \boldsymbol{\omega}_{i,(x)} & 0 \end{bmatrix} \tag{5.21}$$

and if the motion is planar, we obtain

$$-2\widehat{\mathbf{\Lambda}}_i^T\dot{\widehat{\mathbf{L}}}_i^T\left(\mathbf{M}_{rd}\dot{\mathbf{p}}_i + \mathbf{M}_{rr}\boldsymbol{\omega}_i + \mathbf{M}_{re}\dot{\mathbf{b}}_i\right) = \mathbf{0}_3 \tag{5.22}$$

The mass rates $\dot{\mathbf{M}}_i$ required in the system wrench calculations of eq.'s(5.18) to (5.20), are derived in Appendix C. The assembly of the individual link equations of motion to obtain the full system equations of motion is now addressed in the following section.

5.2 Assembled System

The equations of motion for the entire system are given by the forms used in [Cyril'88] and [Jaar'93],

$$\mathbf{M}\dot{\mathbf{v}} = \boldsymbol{\phi}^S + \boldsymbol{\phi}^E + \boldsymbol{\phi}^K \tag{5.23}$$

where according to the definitions of [Cyril'88], the generalized extended mass matrix consists of,

$$\mathbf{M} = diag\left[\mathbf{M}_1, \quad \mathbf{M}_2, \quad ..., \quad \mathbf{M}_N\right] \tag{5.24}$$

and the generalized extended vectors of acceleration $\dot{\mathbf{v}}$, system wrench $\boldsymbol{\phi}^S$, external wrench $\boldsymbol{\phi}^E$,and kinematic constraint wrench $\boldsymbol{\phi}^K$, are assembled respectively as,

$$\dot{\mathbf{v}} = \begin{Bmatrix} \dot{\mathbf{v}}_1 \\ \dot{\mathbf{v}}_2 \\ \vdots \\ \dot{\mathbf{v}}_N \end{Bmatrix} \qquad \boldsymbol{\phi}^S = \begin{Bmatrix} \boldsymbol{\phi}_1^S \\ \boldsymbol{\phi}_2^S \\ \vdots \\ \boldsymbol{\phi}_N^S \end{Bmatrix} \qquad \boldsymbol{\phi}^E = \begin{Bmatrix} \boldsymbol{\phi}_1^E \\ \boldsymbol{\phi}_2^E \\ \vdots \\ \boldsymbol{\phi}_N^E \end{Bmatrix} \qquad \boldsymbol{\phi}^K = \begin{Bmatrix} \boldsymbol{\phi}_1^K \\ \boldsymbol{\phi}_2^K \\ \vdots \\ \boldsymbol{\phi}_N^K \end{Bmatrix} \tag{5.25}$$

These vectors are p'-dimensional, where p' is given by recalling eq.(3.12),

$$p' = (p'_1 + p'_2 + \cdots + p'_N) \tag{5.26}$$

Therefore, eq.(5.23) represents a system of p' equations, for which it is preferred to obtain a minimum set in terms of the generalized vector of independent coordinates

ψ_I. This is performed by establishing the natural orthogonal complement $\mathbf{N}$ of the velocity constraint matrix for the system. The relationship between the twist vector and independent coordinates of the system is given by,

$$\mathbf{v} = \mathbf{N}\dot{\psi}_I \tag{5.27}$$

It is demonstrated in [Cyril'88] that the kinematic constraint wrench is eliminated when it is premultiplied by the transpose of the natural orthogonal complement, i.e.,

$$\mathbf{N}^T\boldsymbol{\phi}^K = \mathbf{0}_{n'} \tag{5.28}$$

which signifies that the kinematic constraint wrench performs no work. Therefore, by premultiplying eq.(5.23) with $\mathbf{N}^T$, and substituting in eq.(5.27), yields the n' dynamical equations of motion,

$$\hat{\mathbf{M}}\ddot{\psi}_I = \boldsymbol{\tau} + \boldsymbol{\phi}_I^S \tag{5.29}$$

where the independent system inertia matrix is,

$$\hat{\mathbf{M}} = \mathbf{N}^T\mathbf{M}\mathbf{N} \tag{5.30}$$

The actuator forces associated with the prismatic joints (and the torques of actuated revolute joints) are contained in vector $\boldsymbol{\tau}$,

$$\boldsymbol{\tau} = \mathbf{N}^T\boldsymbol{\phi}^E \tag{5.31}$$

and the reduced system dynamics vector is,

$$\boldsymbol{\phi}_I^S = \mathbf{N}^T\left(\boldsymbol{\phi}^S - \mathbf{M}\dot{\mathbf{N}}\dot{\psi}_I\right) \tag{5.32}$$

Calculation schemes for the natural orthogonal complement $\mathbf{N}$ and the term $\dot{\mathbf{N}}\dot{\psi}_I$ are presented in the following section.

5.3 Orthogonal Complement Calculations

The natural orthogonal complement **N** associated with the manipulator systems considered here, can be computed by two methods. The scheme presented in [Darcovitch'91], establishes the natural orthogonal complement by individually computing the system twist vector obtained with the s^{th} independent speed coordinate activated with a value of 1.0, while the others are nulled. The resulting twist vector corresponds to the s^{th} column of the natural orthogonal complement matrix. This method is described by considering the contents of the natural orthogonal complement, presented in [Darcovitch'91] as,

$$\begin{Bmatrix} \mathbf{v}_1 \\ \vdots \\ \mathbf{v}_r \\ \vdots \\ \mathbf{v}_N \end{Bmatrix} = \begin{bmatrix} \mathbf{N}_{11} & \cdots & \mathbf{N}_{1s} & \cdots & \mathbf{N}_{1n'} \\ \vdots & & \vdots & & \vdots \\ \mathbf{N}_{r1} & \cdots & \mathbf{N}_{rs} & \cdots & \mathbf{N}_{rn'} \\ \vdots & & \vdots & & \vdots \\ \mathbf{N}_{N1} & \cdots & \mathbf{N}_{Ns} & \cdots & \mathbf{N}_{Nn'} \end{bmatrix} \begin{Bmatrix} \dot{\psi}_{I,1} \\ \vdots \\ \dot{\psi}_{I,s} \\ \vdots \\ \dot{\psi}_{I,n'} \end{Bmatrix} \tag{5.33}$$

where the non-bold $\dot{\psi}_{I,s}$ represents the s^{th} component of the independent speed vector $\dot{\boldsymbol{\psi}}_I$. Therefore, the twist vector of the r^{th} link $\mathbf{v}_r$, computed with the s^{th} independent speed component set to 1.0, yields the column components $\mathbf{N}_{rs}$ of the natural othogonal complement matrix **N**.

For systems consisting of numerous links and modelled with many flexible coordinates, the above procedure may be computationally demanding. A second method examined in this work, is that of initially constructing the expressions between the system twist vector and both the independent $\boldsymbol{\psi}_I$ and dependent $\boldsymbol{\psi}_D$ vectors, to yield matrix $\mathbf{N}_o$,

$$\mathbf{v} = \mathbf{N}_o \dot{\boldsymbol{\psi}} \tag{5.34}$$

Vector $\boldsymbol{\psi}$ is the assembly of all the individual link vectors $\boldsymbol{\psi}_i$ defined in eq.(3.18), and therefore contains both the independent and dependent coordinates of the system,

$$\boldsymbol{\psi} = \langle \boldsymbol{\psi}_1^T \quad \boldsymbol{\psi}_2^T \quad \cdots \quad \boldsymbol{\psi}_N^T \rangle^T \tag{5.35}$$

Matrix $\mathbf{N}_o$ is established from the recursive equations that provide the origin velocity and angular velocity of the link frame. The kinematic forms associated with planar motion of the truss arrangement of Fig. 2.2, will now be used to generate $\mathbf{N}_o$.

Initially, the matrix $\mathbf{N}_o$ is zeroed,

$$\mathbf{N}_o = \mathbf{0}_{p'l'} \tag{5.36}$$

where p' is the dimension of the system twist vector given in eq.(5.26), and l' it the dimension of the vector $\boldsymbol{\psi}$ obtained from,

$$l' = n' + (2 \times l) \tag{5.37}$$

Recall that l is the total number of kinematic loops in the truss, and there exists two dependent angles per loop for the actuator arrangement of Fig. 2.2.

By commencing with the first link attached to the base, which will be that of a truss, its origin is fixed,

$$\dot{\mathbf{p}}_1 = \mathbf{0}_2 \tag{5.38}$$

and the angular velocity is simply,

$$\omega_{1(z)} = 0 \tag{5.39}$$

Therefore, with the flexible twist vector for the first link denoted as,

$$\mathbf{v}_1 = \langle \dot{\mathbf{p}}_1^T \quad \omega_{1(z)} \quad \dot{\mathbf{b}}_1^T \rangle^T \tag{5.40}$$

the first entries corresponding to the link $i = 1$ in $\mathbf{N}_o$ consist of,

$$\left\{ \begin{Bmatrix} \dot{\mathbf{p}}_1 \\ \omega_{1(z)} \\ \dot{\mathbf{b}}_1 \end{Bmatrix} \right\} = \begin{bmatrix} \mathbf{0}_{2m_1} & \cdots & \cdots \\ \mathbf{0}_{1m_1} & \cdots & \cdots \\ \mathbf{1}_{m_1 m_1} & \cdots & \cdots \\ \vdots & \vdots & \vdots \end{bmatrix} \begin{Bmatrix} \{\dot{\mathbf{b}}_1\} \\ \vdots \\ \{\boldsymbol{\psi}_N\} \end{Bmatrix} \tag{5.41}$$

where, per eq.(3.18) $\dot{\boldsymbol{\psi}}_{i=1} = \dot{\boldsymbol{\psi}}_{I,i=1} = \dot{\mathbf{b}}_1$. We now proceed along the structure to consider the following links. For a link i that is either a truss or cylinder preceeded

by a flexible truss, eq.(3.45) is used to write the velocity of the frame's origin in the matrix form of,

$$\dot{\mathbf{p}}_i = [\,\mathbf{R}_i^T \quad \mathbf{R}_i^T \mathbf{G} \mathbf{r}_{i/i-1} \quad \mathbf{R}_i^T \mathbf{B}_{i-1}^i\,]\,\mathbf{v}_{i-1} \tag{5.42}$$

where, $\mathbf{v}_{i-1}$ is the flexible twist of the truss link $i-1$,

$$\mathbf{v}_{i-1} = \langle\, \dot{\mathbf{p}}_{i-1}^T \quad \omega_{i-1(z)} \quad \dot{\mathbf{b}}_{i-1}^T \,\rangle \tag{5.43}$$

Note that matrix $\mathbf{G}$ is used to maintain the cross product between the angular velocity and local position vector of eq.(3.45), such that,

$$\omega_{i-1(z)} \mathbf{z} \times \mathbf{r}_{i/i-1} = \mathbf{G} \mathbf{r}_{i/i-1} \omega_{i-1(z)} \tag{5.44}$$

where

$$\mathbf{G} = \begin{bmatrix} 0 & -1 \\ 1 & 0 \end{bmatrix} \tag{5.45}$$

For the angular velocity of link frame i, we rearrange eq.(3.48) in a similar fashion to obtain,

$$\omega_{i(z)} = [\,\mathbf{0}_{12} \quad 1 \quad \mathbf{B}_{i-1(y)}^{i*}\,]\,\mathbf{v}_{i-1} + \dot{\theta}_i \tag{5.46}$$

where the (kinematic loop dependent) rate $\dot{\theta}_i$ is the dependent component $\dot{\boldsymbol{\psi}}_{D,i}$ of coordinate vector $\dot{\boldsymbol{\psi}}_i$. Hence, the rows in matrix $\mathbf{N}_o$ corresponding to link i may now be furnished by the proper multiplication of the coefficient matrix of eq.'s(5.42) and (5.46), to the corresponding contents contained in the rows for vectors $\mathbf{v}_{i-1}$. For the $\dot{\theta}_i$ contribution in eq.(5.46) a value of 1.0 will be simply inserted into the respective row and column location of $\omega_{i(z)}$ and $\dot{\theta}_i$. If link i is a flexible truss, then the identity matrix $\mathbf{1}_{m_i m_i}$ is assigned to the rows and columns of $\mathbf{N}_o$ corresponding to the flexible twist and $\dot{\boldsymbol{\psi}}$ locations, respectively, for $\dot{\mathbf{b}}_i$.

If link i is a piston-rod, then we have after rearranging eq.(3.52),

$$\dot{\mathbf{p}}_i = [\,\mathbf{1}_{22} \quad \mathbf{G}\mathbf{x}_{i-1}(L_{i-1} + d_i)\,]\,\mathbf{v}_{i-1} + \mathbf{x}_i \dot{d}_i \tag{5.47}$$

and the piston-rod angular velocity is simply that from eq.(3.54),

$$\omega_{i(z)} = \omega_{i-1(z)} \tag{5.48}$$

Therefore, we update the rows of $\mathbf{N}_o$ corresponding to $\dot{\mathbf{p}}_i$, by multiplying the coefficient matrix of eq.(5.47) to the contents of the rows of $\mathbf{v}_{i-1}$. In addition, we insert a value of 1.0 into the $\mathbf{N}_o$ location corresponding to the X-axis row for $\dot{\mathbf{p}}_i$ and the column associated with the piston-rod extension rate contained in $\dot{\psi}$. The row corresponding to the angular velocity $\omega_{i(z)}$, is simply assigned the contents of $\omega_{i-1(z)}$.

After considering all the links to complete the construction of matrix $\mathbf{N}_o$, the natural orthogonal complement can now be established. Firstly, the reader should note that within the actual simulation code, vector index pointers are used to indicate the corresponding locations of the independent and dependent speed variables within matrix $\mathbf{N}_o$. Therefore, the matrix partitioning scheme of the following explanation is not exactly that implemented, but effectively describes the fundamental procedure used to remove the dependent speeds $\dot{\psi}_D$ from matrix $\mathbf{N}_o$. For symbolic representation and clarification, matrix $\mathbf{N}_o$ is partitioned according to,

$$\mathbf{N}_o = [\mathbf{N}_{VI,o}\ \mathbf{N}_{VD,o}] \tag{5.49}$$

such that eq.(5.34) takes the form of,

$$\mathbf{v} = \mathbf{N}_o\dot{\psi} = \mathbf{N}_{VI,o}\dot{\psi}_I + \mathbf{N}_{VD,o}\dot{\psi}_{D,o} \tag{5.50}$$

and vectors $\dot{\psi}_I$ and $\dot{\psi}_D$ each consist of only the independent and dependent coordinates, respectively, per,

$$\dot{\psi}_I = \left\langle \dot{\psi}_{I,1}^T \quad \cdots \quad \dot{\psi}_{I,N}^T \right\rangle^T \tag{5.51}$$

$$\dot{\psi}_D = \left\langle \dot{\psi}_{D,1}^T \quad \cdots \quad \dot{\psi}_{D,N}^T \right\rangle^T \tag{5.52}$$

The dependent coordinates associated with the first kinematic loop will be represented as $\dot{\psi}_{D,1}^*$, and can be expressed in terms of the flexible twist components preceeding it $\mathbf{v}_{,1}$, and the independent speed vector $\dot{\psi}_I$,

$$\dot{\psi}_{D,1}^* = \mathbf{N}_{DV,1}\mathbf{v}_{,1} + \mathbf{N}_{DI,1}\dot{\psi}_I \tag{5.53}$$

Matrix $\mathbf{N}_{DV,1}$ represents the dependence of vector $\dot{\psi}^{*}_{D,1}$ upon the preceeding flexible twist $\mathbf{v}_{,1}$ components (that are not dependent upon the first loop), and similarly $\mathbf{N}_{DI,1}$ contains the dependence of $\dot{\psi}^{*}_{D,1}$ upon the coordinates of $\dot{\psi}_I$ affecting the loop. The contents of $\mathbf{N}_{DV,1}$ and $\mathbf{N}_{DI,1}$, and the corresponding twist and independent speed components involved in the formulation of eq.(5.53) for a specific loop, are presented in eq.(D.37) of Appendix D. It is emphasized that the components of $\mathbf{v}_{,1}$ are not dependent upon the first loop or upon the subsequent components contained in $\dot{\psi}_D$, therefore we can extract from eq.(5.34),

$$\mathbf{v}_{,1} = \mathbf{N}_{VI,1}\dot{\psi}_I \tag{5.54}$$

where $\mathbf{N}_{VI,1}$ contains those rows of $\mathbf{N}_{VI,o}$ associated with the twist components contained in $\mathbf{v}_{,1}$. Substituting eq.(5.54) into eq.(5.53) yields,

$$\dot{\psi}^{*}_{D,1} = [\mathbf{N}_{DV,1}\mathbf{N}_{VI,1} + \mathbf{N}_{DI,1}]\,\dot{\psi}_I \tag{5.55}$$

By rearranging the last term in eq.(5.50), we obtain,

$$\mathbf{v} = \mathbf{N}_{VI,o}\dot{\psi}_I + \mathbf{N}_{VD,o1}\dot{\psi}^{*}_{D,1} + \mathbf{N}_{VD,1}\dot{\psi}_{D,1} \tag{5.56}$$

where vector $\dot{\psi}_{D,o}$ of eq.(5.34) contained the components,

$$\dot{\psi}_{D,o} = \left\{ \begin{array}{c} \dot{\psi}^{*}_{D,1} \\ \dot{\psi}_{D,1} \end{array} \right\} \tag{5.57}$$

and vector $\dot{\psi}_{D,1}$ corresponds to those dependent coordinates of subsequent kinematic loops yet to be removed. Substituting eq.(5.55) into (5.56), yields the system twist vector in the form of,

$$\mathbf{v} = \mathbf{N}_{VI,1}\dot{\psi}_I + \mathbf{N}_{VD,1}\dot{\psi}_{D,1} \tag{5.58}$$

where,

$$\mathbf{N}_{VI,1} = \mathbf{N}_{VI,o} + \mathbf{N}_{VD,o1}[\mathbf{N}_{DV,1}\mathbf{N}_{VI,1} + \mathbf{N}_{DI,1}] \tag{5.59}$$

Note that the subscript (,1) in eq.(5.58) corresponds to the system twist vector, after the removal of the dependent coordinates $\dot{\psi}^{*}_{D,1}$ associated with kinematic loop number

1, (i.e. the first kinematic loop from the base). Therefore, the above operations can be re-performed for the subsequent kinematic loops of the structure topology, hence the dependent coordinates of $\dot{\psi}_D$ can be removed from eq.(5.34) in a recursive procedure, to yield the natural orthogonal complement $\mathbf{N}$ given by,

$$\mathbf{N} = \sum_{k=1}^{l} \left[\mathbf{N}_{VI,(k-1)} + \mathbf{N}_{VD,(k-1)(k)} \mathbf{N}^{*}_{DI,(k)} \right] \tag{5.60}$$

where,

$$\mathbf{N}^{*}_{DI,(k)} = \mathbf{N}_{DV,(k)} \mathbf{N}_{VD,(k)} + \mathbf{N}_{DI,(k)} \tag{5.61}$$

and matrices $\mathbf{N}_{DV,(k)}$, $\mathbf{N}_{VD,(k)}$ and $\mathbf{N}_{DI,(k)}$ correspond to the k^{th} kinematic loop, and constructed per the scheme described above for the first kinematic loop. The reader is referred to eq.(D.37) of Appendix D for the expressions used to establish matrices $\mathbf{N}_{DV,(k)}$ and $\mathbf{N}_{DI,(k)}$, (previously defined in eq.(5.53) for the first loop of $k = 1$).

The procedure to compute the term $\dot{\mathbf{N}}\dot{\psi}_I$ required in eq.(5.32), will be that employed by [Cyril'88] and [Darcovitch'91]. If the relation $\mathbf{v} = \mathbf{N}\dot{\psi}_I$ is differentiated with respect to time, we obtain,

$$\dot{\mathbf{v}} = \dot{\mathbf{N}}\dot{\psi}_I + \mathbf{N}\ddot{\psi}_I \tag{5.62}$$

We note from the above equation that the system twist vector is comprised of two terms, one that's a function of $\dot{\psi}_I$ and the other a function of $\ddot{\psi}_I$. This can also be expressed as,

$$\dot{\mathbf{v}}(\dot{\psi}_I) = \dot{\mathbf{N}}\dot{\psi}_I \tag{5.63}$$

$$\dot{\mathbf{v}}(\ddot{\psi}_I) = \mathbf{N}\ddot{\psi}_I \tag{5.64}$$

Therefore, eq.(5.63) simply indicates that the term $\dot{\mathbf{N}}\dot{\psi}_I$ consists of the flexible twist vector for the system calculated with zero acceleration of the independent speed vector. Recalling the definitions of $\mathbf{v}_i$ and $\mathbf{v}$ given in eq.'s (3.10) and (5.25), respectively, we obtain,

$$\dot{\mathbf{N}}\dot{\psi}_I = \dot{\mathbf{v}}(\dot{\psi}_I) = \begin{Bmatrix} \dot{\mathbf{v}}_1(\dot{\psi}_I) \\ \dot{\mathbf{v}}_2(\dot{\psi}_I) \\ \vdots \\ \dot{\mathbf{v}}_N(\dot{\psi}_I) \end{Bmatrix} \tag{5.65}$$

Therefore, for a specific link i we require,

$$\dot{\mathbf{v}}_i(\dot{\boldsymbol{\psi}}_I) = \langle\, \ddot{\mathbf{p}}_i(\dot{\boldsymbol{\psi}}_I)^T \quad \dot{\boldsymbol{\omega}}_i(\dot{\boldsymbol{\psi}}_I)^T \quad \ddot{\mathbf{b}}_i(\dot{\boldsymbol{\psi}}_I)^T \,\rangle^T \tag{5.66}$$

For the first truss link being fixed, the corresponding twist term is simply,

$$\dot{\mathbf{v}}_1(\dot{\boldsymbol{\psi}}_I) = \mathbf{0}_{p'_1} \tag{5.67}$$

For the remaining **truss** and **cylinder** links, the kinematic equations of eq.'s(3.46) and (3.49) are employed with $\ddot{\boldsymbol{\psi}}_I = \mathbf{0}_{n'}$,

$$\begin{aligned} \ddot{\mathbf{p}}_i &= \mathbf{R}_i^T \Big[\ddot{\mathbf{p}}_{i-1}(\dot{\boldsymbol{\psi}}_I) + \boldsymbol{\omega}_{i-1}(\dot{\boldsymbol{\psi}}_I) \times \Big\{ \boldsymbol{\omega}_{i-1}(\dot{\boldsymbol{\psi}}_I) \times \mathbf{r}_{i/i-1} \Big\} \\ &\qquad + \boldsymbol{\omega}_{i-1}(\dot{\boldsymbol{\psi}}_I) \times \mathbf{r}_{i/i-1} + 2\boldsymbol{\omega}_{i-1}(\dot{\boldsymbol{\psi}}_I) \times \mathring{\mathbf{r}}_{i/i-1} \Big] \qquad (5.68) \\ \dot{\boldsymbol{\omega}}_i &= \dot{\boldsymbol{\omega}}_{i-1}(\dot{\boldsymbol{\psi}}_I) + \ddot{\theta}_i(\dot{\boldsymbol{\psi}}_I)\mathbf{z}_i \qquad (5.69) \end{aligned}$$

Note that the dependent angular rates, $\ddot{\theta}_i(\dot{\boldsymbol{\psi}}_I)$, will not be zero even if the terms for $\ddot{\boldsymbol{\psi}}_I = \mathbf{0}_{n'}$. This is by virtue of the kinematic loop dependencies as represented per eq.(3.28), and more specifically given in eq.(D.44) of Appendix D.

For the **piston-rod** link, eq.'s(3.53) and (3.55) are similarly used,

$$\begin{aligned} \ddot{\mathbf{p}}_i &= \ddot{\mathbf{p}}_{i-1}(\dot{\boldsymbol{\psi}}_I) + \boldsymbol{\omega}_{i-1}(\dot{\boldsymbol{\psi}}_I) \times \Big\{ \boldsymbol{\omega}_{i-1}(\dot{\boldsymbol{\psi}}_I) \times (L_{i-1} + d_i)\mathbf{x}_i \Big\} \\ &\qquad + \dot{\boldsymbol{\omega}}_{i-1}(\dot{\boldsymbol{\psi}}_I) \times (L_{i-1} + d_i)\mathbf{x}_i + 2\boldsymbol{\omega}_{i-1}(\dot{\boldsymbol{\psi}}_I) \times \dot{d}_i\mathbf{x}_i \qquad (5.70) \\ \dot{\boldsymbol{\omega}}_i &= \dot{\boldsymbol{\omega}}_{i-1}(\dot{\boldsymbol{\psi}}_I) \qquad (5.71) \end{aligned}$$

For all flexible truss links, since the elastic coordinates $\mathbf{b}_i$ are also generalized coordinates, then for the computation of $\dot{\mathbf{N}}\dot{\boldsymbol{\psi}}_I$ we set,

$$\ddot{\mathbf{b}}_i(\dot{\boldsymbol{\psi}}_I) = \mathbf{0}_{m_i} \tag{5.72}$$

The following chapter presents the control scheme examined for the vibration suppression of the elastic coordinates.

Chapter 6

VIBRATION CONTROL

The singular perturbation method for reducing the order of a system of equations, was introduced in Section 1.4.2. Its application to the general nonlinear equations of motion for truss manipulators is presented in the following section, and is similar to the scheme developed in [Siciliano et al.'88] for the dynamical equations of flexible serial manipulators. This method is applicable when the lowest frequency of vibration of all individual links is greater than the highest frequency content of the rigid body motion, (such as ≈ 10 times). It should be noted that this condition is not necessarily the case for spinning flexible spacecraft.

6.1 The Reduced-Order Model

For notational convenience, the independent speed vector for the system will be partitioned according to,

$$\psi_I = \begin{Bmatrix} \theta_I \\ \mathbf{b} \end{Bmatrix} \tag{6.1}$$

where, vector θ_I contains all the n independent joint variables in the structure (i.e. all the prismatic extensions, and independent revolute angles of serial manipulators), and $\mathbf{b}$ contains all the flexible coordinates and is of dimension m. Then, the equations of motion given by eq.(5.29), can be rearranged in the form of,

$$\mathbf{M}(\theta_I, \mathbf{b}) \begin{Bmatrix} \ddot{\theta}_I \\ \ddot{\mathbf{b}} \end{Bmatrix} + \begin{Bmatrix} \mathbf{c}_\theta(\theta_I, \dot{\theta}_I, \mathbf{b}, \dot{\mathbf{b}}) \\ \mathbf{c}_\mathbf{b}(\theta_I, \dot{\theta}_I, \mathbf{b}, \dot{\mathbf{b}}) \end{Bmatrix} + \begin{Bmatrix} \mathbf{0}_n \\ \mathbf{K}\mathbf{b} \end{Bmatrix} = \begin{Bmatrix} \tau \\ \mathbf{0}_m \end{Bmatrix} \tag{6.2}$$

where $\mathbf{c}_{\boldsymbol{\theta}}$ and $\mathbf{c}_{\mathbf{b}}$ represent the nonlinear terms of the dynamical equations of motion. Recall that by using orthogonal shape functions for discretizing the elastic deflections in Section 4.1.4, the link stiffness matrix $\mathbf{K}_{ee}$ would be diagonal per eq.(4.62). In addition, since the flexible coordinates $\mathbf{b}_i$ have no dependence upon other coordinates when constructing the natural orthogonal complement matrix in Section 5.3, then matrix $\mathbf{K}$ in eq.(6.2) will also be diagonal and written in the form of,

$$\mathbf{K} = diag\,[k_1, k_2, ..., k_m] \tag{6.3}$$

It should be noted that $\mathbf{K}$ contains the total number of m modal stiffness values modelled in the assembled system.

The mass matrix will be partitioned as,

$$\mathbf{M}(\boldsymbol{\theta}_I, \mathbf{b}) = \begin{bmatrix} \mathbf{M}_{\boldsymbol{\theta}\boldsymbol{\theta}}(\boldsymbol{\theta}_I, \mathbf{b}) & \mathbf{M}_{\boldsymbol{\theta}\mathbf{b}}(\boldsymbol{\theta}_I, \mathbf{b}) \\ \mathbf{M}_{\mathbf{b}\boldsymbol{\theta}}(\boldsymbol{\theta}_I, \mathbf{b}) & \mathbf{M}_{\mathbf{b}\mathbf{b}}(\boldsymbol{\theta}_I, \mathbf{b}) \end{bmatrix} \tag{6.4}$$

Since it is positive definite, the inverse of $\mathbf{M}(\boldsymbol{\theta}_I, \mathbf{b})$ exists, and for the derivations to follow will be represented as,

$$\mathbf{M}(\boldsymbol{\theta}_I, \mathbf{b})^{-1} = \mathbf{H}(\boldsymbol{\theta}_I, \mathbf{b}) = \begin{bmatrix} \mathbf{H}_{\boldsymbol{\theta}\boldsymbol{\theta}}(\boldsymbol{\theta}_I, \mathbf{b}) & \mathbf{H}_{\boldsymbol{\theta}\mathbf{b}}(\boldsymbol{\theta}_I, \mathbf{b}) \\ \mathbf{H}_{\mathbf{b}\boldsymbol{\theta}}(\boldsymbol{\theta}_I, \mathbf{b}) & \mathbf{H}_{\mathbf{b}\mathbf{b}}(\boldsymbol{\theta}_I, \mathbf{b}) \end{bmatrix} \tag{6.5}$$

where, $\mathbf{H}_{\boldsymbol{\theta}\boldsymbol{\theta}}$ is a square matrix of dimension n, $\mathbf{H}_{\boldsymbol{\theta}\mathbf{b}}$ of size n x m, $\mathbf{H}_{\mathbf{b}\boldsymbol{\theta}}$ of size m x n, and $\mathbf{H}_{\mathbf{b}\mathbf{b}}$ is a square matrix of dimension m. Now, eq.(6.2) can be re-written as

$$\begin{aligned} \ddot{\boldsymbol{\theta}}_I &= -\mathbf{H}_{\boldsymbol{\theta}\boldsymbol{\theta}}(\boldsymbol{\theta}_I, \mathbf{b})\mathbf{c}_{\boldsymbol{\theta}}(\boldsymbol{\theta}_I, \dot{\boldsymbol{\theta}}_I, \mathbf{b}, \dot{\mathbf{b}}) - \mathbf{H}_{\boldsymbol{\theta}\mathbf{b}}(\boldsymbol{\theta}_I, \mathbf{b})\mathbf{c}_{\mathbf{b}}(\boldsymbol{\theta}_I, \dot{\boldsymbol{\theta}}_I, \mathbf{b}, \dot{\mathbf{b}}) \\ &\quad -\mathbf{H}_{\boldsymbol{\theta}\mathbf{b}}(\boldsymbol{\theta}_I, \mathbf{b})\mathbf{K}\mathbf{b} + \mathbf{H}_{\boldsymbol{\theta}\boldsymbol{\theta}}(\boldsymbol{\theta}_I, \mathbf{b})\boldsymbol{\tau} \qquad (6.6) \\ \ddot{\mathbf{b}} &= -\mathbf{H}_{\mathbf{b}\boldsymbol{\theta}}(\boldsymbol{\theta}_I, \mathbf{b})\mathbf{c}_{\boldsymbol{\theta}}(\boldsymbol{\theta}_I, \dot{\boldsymbol{\theta}}_I, \mathbf{b}, \dot{\mathbf{b}}) - \mathbf{H}_{\mathbf{b}\mathbf{b}}(\boldsymbol{\theta}_I, \mathbf{b})\mathbf{c}_{\mathbf{b}}(\boldsymbol{\theta}_I, \dot{\boldsymbol{\theta}}_I, \mathbf{b}, \dot{\mathbf{b}}) \\ &\quad -\mathbf{H}_{\mathbf{b}\mathbf{b}}(\boldsymbol{\theta}_I, \mathbf{b})\mathbf{K}\mathbf{b} + \mathbf{H}_{\mathbf{b}\boldsymbol{\theta}}(\boldsymbol{\theta}_I, \mathbf{b})\boldsymbol{\tau} \qquad (6.7) \end{aligned}$$

It is required to obtain the standard singular perturbation form of [Kokotovic'84]. Provided that the modal stiffness components are roughly of the same order of magnitude, we define elastic modal forces per [Siciliano et al.'88],

$$\mathbf{f} = k\hat{\mathbf{K}}\mathbf{b} \tag{6.8}$$

where k is the smallest common modal stiffness of matrix $\mathbf{K}$, and

$$\hat{\mathbf{K}} = (1/k)\mathbf{K} \tag{6.9}$$

The perturbation parameter for the system is defined as,

$$\mu = 1/k \tag{6.10}$$

and premultiplying eq.(6.7) by $\hat{\mathbf{K}}$, the perturbation form is given by,

$$\begin{aligned}
\ddot{\boldsymbol{\theta}}_I &= -\mathbf{H}_{\boldsymbol{\theta}\boldsymbol{\theta}}(\boldsymbol{\theta}_I, \mu\mathbf{f})\mathbf{c}_{\boldsymbol{\theta}}(\boldsymbol{\theta}_I, \dot{\boldsymbol{\theta}}_I, \mu\mathbf{f}, \mu\dot{\mathbf{f}}) - \mathbf{H}_{\boldsymbol{\theta}\mathbf{b}}(\boldsymbol{\theta}_I, \mu\mathbf{f})\mathbf{c}_{\mathbf{b}}(\boldsymbol{\theta}_I, \dot{\boldsymbol{\theta}}_I, \mu\mathbf{f}, \mu\dot{\mathbf{f}}) \\
&\quad -\mathbf{H}_{\boldsymbol{\theta}\mathbf{b}}(\boldsymbol{\theta}_I, \mu\mathbf{f})\mathbf{f} + \mathbf{H}_{\boldsymbol{\theta}\boldsymbol{\theta}}(\boldsymbol{\theta}_I, \mu\mathbf{f})\boldsymbol{\tau} \qquad (6.11) \\
\mu\ddot{\mathbf{f}} &= -\mathbf{H}'_{\mathbf{b}\boldsymbol{\theta}}(\boldsymbol{\theta}_I, \mu\mathbf{f})\mathbf{c}_{\boldsymbol{\theta}}(\boldsymbol{\theta}_I, \dot{\boldsymbol{\theta}}_I, \mu\mathbf{f}, \mu\dot{\mathbf{f}}) - \mathbf{H}'_{\mathbf{b}\mathbf{b}}(\boldsymbol{\theta}_I, \mu\mathbf{f})\mathbf{c}_{\mathbf{b}}(\boldsymbol{\theta}_I, \dot{\boldsymbol{\theta}}_I, \mu\mathbf{f}, \mu\dot{\mathbf{f}}) \\
&\quad -\mathbf{H}'_{\mathbf{b}\mathbf{b}}(\boldsymbol{\theta}_I, \mu\mathbf{f})\mathbf{f} + \mathbf{H}'_{\mathbf{b}\boldsymbol{\theta}}(\boldsymbol{\theta}_I, \mu\mathbf{f})\boldsymbol{\tau} \qquad (6.12)
\end{aligned}$$

where,

$$\mathbf{H}'_{\mathbf{b}\boldsymbol{\theta}} = \hat{\mathbf{K}}\mathbf{H}_{\mathbf{b}\boldsymbol{\theta}} \quad , \quad \mathbf{H}'_{\mathbf{b}\mathbf{b}} = \hat{\mathbf{K}}\mathbf{H}_{\mathbf{b}\mathbf{b}} \tag{6.13}$$

As $\mu \rightarrow 0$ and assuming $\mathbf{f}$ is a bounded quantity, the system is converted to the reduced form, which will be represented with the use of overbars as follows,

$$\begin{aligned}
\ddot{\bar{\boldsymbol{\theta}}}_I &= -\mathbf{H}_{\boldsymbol{\theta}\boldsymbol{\theta}}(\bar{\boldsymbol{\theta}}_I, 0)\mathbf{c}_{\boldsymbol{\theta}}(\bar{\boldsymbol{\theta}}_I, \dot{\bar{\boldsymbol{\theta}}}_I, 0, 0) - \mathbf{H}_{\boldsymbol{\theta}\mathbf{b}}(\bar{\boldsymbol{\theta}}_I, 0)\mathbf{c}_{\mathbf{b}}(\bar{\boldsymbol{\theta}}_I, \dot{\bar{\boldsymbol{\theta}}}_I, 0, 0) \\
&\quad -\mathbf{H}_{\boldsymbol{\theta}\mathbf{b}}(\bar{\boldsymbol{\theta}}_I, 0)\bar{\mathbf{f}} + \mathbf{H}_{\boldsymbol{\theta}\boldsymbol{\theta}}(\bar{\boldsymbol{\theta}}_I, 0)\bar{\boldsymbol{\tau}} \qquad (6.14) \\
0_m &= -\mathbf{H}'_{\mathbf{b}\boldsymbol{\theta}}(\bar{\boldsymbol{\theta}}_I, 0)\mathbf{c}_{\boldsymbol{\theta}}(\bar{\boldsymbol{\theta}}_I, \dot{\bar{\boldsymbol{\theta}}}_I, 0, 0) - \mathbf{H}'_{\mathbf{b}\mathbf{b}}(\bar{\boldsymbol{\theta}}_I, 0)\mathbf{c}_{\mathbf{b}}(\bar{\boldsymbol{\theta}}_I, \dot{\bar{\boldsymbol{\theta}}}_I, 0, 0) \\
&\quad -\mathbf{H}'_{\mathbf{b}\mathbf{b}}(\bar{\boldsymbol{\theta}}_I, 0)\bar{\mathbf{f}} + \mathbf{H}'_{\mathbf{b}\boldsymbol{\theta}}(\bar{\boldsymbol{\theta}}_I, 0)\bar{\boldsymbol{\tau}} \qquad (6.15)
\end{aligned}$$

After rearranging eq.(6.15), the "quasi-static" elastic force $\bar{\mathbf{f}}$, is given by,

$$\begin{aligned}
\bar{\mathbf{f}} &= -\mathbf{H}^{-1}_{\mathbf{b}\mathbf{b}}(\bar{\boldsymbol{\theta}}_I, 0)\mathbf{H}_{\mathbf{b}\boldsymbol{\theta}}(\bar{\boldsymbol{\theta}}_I, 0)\mathbf{c}_{\boldsymbol{\theta}}(\bar{\boldsymbol{\theta}}_I, \dot{\bar{\boldsymbol{\theta}}}_I, 0, 0) - \mathbf{c}_{\mathbf{b}}(\bar{\boldsymbol{\theta}}_I, \dot{\bar{\boldsymbol{\theta}}}_I, 0, 0) \\
&\quad +\mathbf{H}^{-1}_{\mathbf{b}\mathbf{b}}(\bar{\boldsymbol{\theta}}_I, 0)\mathbf{H}_{\mathbf{b}\boldsymbol{\theta}}(\bar{\boldsymbol{\theta}}_I, 0)\bar{\boldsymbol{\tau}} \qquad (6.16)
\end{aligned}$$

To establish the two reduced subsystems, eq.(6.11) and (6.12) will be written in the state space form. The following state variables are defined per [Siciliano et al.'88],

$$\begin{Bmatrix} \mathbf{x}_1 \\ \mathbf{x}_2 \end{Bmatrix} = \begin{Bmatrix} \boldsymbol{\theta}_I \\ \dot{\boldsymbol{\theta}}_I \end{Bmatrix} \qquad \begin{Bmatrix} \mathbf{z}_1 \\ \mathbf{z}_2 \end{Bmatrix} = \begin{Bmatrix} \mathbf{f} \\ \epsilon\dot{\mathbf{f}} \end{Bmatrix} \tag{6.17}$$

where,

$$\epsilon = \sqrt{\mu} \tag{6.18}$$

With these forms, eq.'s (6.11) and (6.12) become,

$$\begin{aligned}
\dot{\mathbf{x}}_1 &= \mathbf{x}_2 \\
\dot{\mathbf{x}}_2 &= -\mathbf{H}_{\boldsymbol{\theta\theta}}(\mathbf{x}_1, \epsilon^2\mathbf{z}_1)\mathbf{c}_{\boldsymbol{\theta}}(\mathbf{x}_1, \mathbf{x}_2, \epsilon^2\mathbf{z}_1, \epsilon\mathbf{z}_2) - \mathbf{H}_{\boldsymbol{\theta}\mathbf{b}}(\mathbf{x}_1, \epsilon^2\mathbf{z}_1)\mathbf{c}_{\mathbf{b}}(\mathbf{x}_1, \mathbf{x}_2, \epsilon^2\mathbf{z}_1, \epsilon\mathbf{z}_2) \\
&\quad -\mathbf{H}_{\boldsymbol{\theta}\mathbf{b}}(\mathbf{x}_1, \epsilon^2\mathbf{z}_1)\mathbf{z}_1 + \mathbf{H}_{\boldsymbol{\theta\theta}}(\mathbf{x}_1, \epsilon^2\mathbf{z}_1)\boldsymbol{\tau} \qquad (6.19) \\
\epsilon\dot{\mathbf{z}}_1 &= \mathbf{z}_2 \\
\epsilon\dot{\mathbf{z}}_2 &= -\mathbf{H}'_{\mathbf{b}\boldsymbol{\theta}}(\mathbf{x}_1, \epsilon^2\mathbf{z}_1)\mathbf{c}_{\boldsymbol{\theta}}(\mathbf{x}_1, \mathbf{x}_2, \epsilon^2\mathbf{z}_1, \epsilon\mathbf{z}_2) - \mathbf{H}'_{\mathbf{bb}}(\mathbf{x}_1, \epsilon^2\mathbf{z}_1)\mathbf{c}_{\mathbf{b}}(\mathbf{x}_1, \mathbf{x}_2, \epsilon^2\mathbf{z}_1, \epsilon\mathbf{z}_2) \\
&\quad -\mathbf{H}'_{\mathbf{bb}}(\mathbf{x}_1, \epsilon^2\mathbf{z}_1)\mathbf{z}_1 + \mathbf{H}'_{\mathbf{b}\boldsymbol{\theta}}(\mathbf{x}_1, \epsilon^2\mathbf{z}_1)\boldsymbol{\tau} \qquad (6.20)
\end{aligned}$$

So as the perturbation $\epsilon \rightarrow 0$, we obtain the quasi-static or slow subsystem equations of motion given by,

$$\begin{aligned}
\dot{\bar{\mathbf{x}}}_1 &= \bar{\mathbf{x}}_2 \\
\dot{\bar{\mathbf{x}}}_2 &= -\mathbf{H}_{\boldsymbol{\theta\theta}}(\bar{\mathbf{x}}_1, \mathbf{0})\mathbf{c}_{\boldsymbol{\theta}}(\bar{\mathbf{x}}_1, \bar{\mathbf{x}}_2, \mathbf{0}, \mathbf{0}) - \mathbf{H}_{\boldsymbol{\theta}\mathbf{b}}(\bar{\mathbf{x}}_1, \mathbf{0})\mathbf{c}_{\mathbf{b}}(\bar{\mathbf{x}}_1, \bar{\mathbf{x}}_2, \mathbf{0}, \mathbf{0}) \\
&\quad -\mathbf{H}_{\boldsymbol{\theta}\mathbf{b}}(\bar{\mathbf{x}}_1, \mathbf{0})\bar{\mathbf{z}}_1 + \mathbf{H}_{\boldsymbol{\theta\theta}}(\bar{\mathbf{x}}_1, \mathbf{0})\bar{\boldsymbol{\tau}} \qquad (6.21)
\end{aligned}$$

where,

$$\begin{aligned}
\bar{\mathbf{z}}_1 &= -\mathbf{H}_{\mathbf{bb}}^{-1}\mathbf{H}_{\mathbf{b}\boldsymbol{\theta}}(\bar{\mathbf{x}}_1, \mathbf{0})\mathbf{c}_{\boldsymbol{\theta}}(\bar{\mathbf{x}}_1, \bar{\mathbf{x}}_2, \mathbf{0}, \mathbf{0}) - \mathbf{c}_{\mathbf{b}}(\bar{\mathbf{x}}_1, \bar{\mathbf{x}}_2, \mathbf{0}, \mathbf{0}) \\
&\quad +\mathbf{H}_{\mathbf{bb}}^{-1}\mathbf{H}_{\mathbf{b}\boldsymbol{\theta}}(\bar{\mathbf{x}}_1, \mathbf{0})\bar{\boldsymbol{\tau}} \qquad (6.22)
\end{aligned}$$

For the fast subsystem, a new time scale $\tilde{t}$ is defined,

$$\tilde{t} = t/\epsilon \tag{6.23}$$

and implemented into eq.'s (6.19) and (6.20), to obtain,

$$\begin{aligned}
\frac{d\mathbf{x}_1}{d\tilde{t}} &= \epsilon\mathbf{x}_2 \\
\frac{d\mathbf{x}_2}{d\tilde{t}} &= \epsilon\Big[-\mathbf{H}_{\boldsymbol{\theta\theta}}(\mathbf{x}_1, \epsilon^2\mathbf{z}_1)\mathbf{c}_{\boldsymbol{\theta}}(\mathbf{x}_1, \mathbf{x}_2, \epsilon^2\mathbf{z}_1, \epsilon\mathbf{z}_2) - \mathbf{H}_{\boldsymbol{\theta}\mathbf{b}}(\mathbf{x}_1, \epsilon^2\mathbf{z}_1)\mathbf{c}_{\mathbf{b}}(\mathbf{x}_1, \mathbf{x}_2, \epsilon^2\mathbf{z}_1, \epsilon\mathbf{z}_2)
\end{aligned}$$

$$-\mathbf{H}_{\boldsymbol{\theta}\mathbf{b}}(\mathbf{x}_1, \epsilon^2\mathbf{z}_1)\mathbf{z}_1 + \mathbf{H}_{\boldsymbol{\theta}\boldsymbol{\theta}}(\mathbf{x}_1, \epsilon^2\mathbf{z}_1)\boldsymbol{\tau}\Big] \tag{6.24}$$

$$\begin{aligned}
\frac{d\mathbf{z}_1}{d\tilde{t}} &= \mathbf{z}_2 \\
\frac{d\mathbf{z}_2}{d\tilde{t}} &= -\mathbf{H}'_{\mathbf{b}\boldsymbol{\theta}}(\mathbf{x}_1, \epsilon^2\mathbf{z}_1)\mathbf{c}_{\boldsymbol{\theta}}(\mathbf{x}_1, \mathbf{x}_2, \epsilon^2\mathbf{z}_1, \epsilon\mathbf{z}_2) - \mathbf{H}'_{\mathbf{bb}}(\mathbf{x}_1, \epsilon^2\mathbf{z}_1)\mathbf{c}_{\mathbf{b}}(\mathbf{x}_1, \mathbf{x}_2, \epsilon^2\mathbf{z}_1, \epsilon\mathbf{z}_2) \\
&\quad -\mathbf{H}'_{\mathbf{bb}}(\mathbf{x}_1, \epsilon^2\mathbf{z}_1)\mathbf{z}_1 + \mathbf{H}'_{\mathbf{b}\boldsymbol{\theta}}(\mathbf{x}_1, \epsilon^2\mathbf{z}_1)\boldsymbol{\tau}
\end{aligned} \tag{6.25}$$

Now as $\epsilon \rightarrow 0$, only eq.(6.25) remains, and by defining new variables per [Siciliano et al.'88],

$$\boldsymbol{\eta}_1 = \mathbf{z}_1 - \bar{\mathbf{z}}_1, \qquad \boldsymbol{\eta}_2 = \mathbf{z}_2 \tag{6.26}$$

the fast or boundary layer subsystem is described by,

$$\begin{aligned}
\frac{d\boldsymbol{\eta}_1}{d\tilde{t}} &= \boldsymbol{\eta}_2 \\
\frac{d\boldsymbol{\eta}_2}{d\tilde{t}} &= -\mathbf{H}'_{\mathbf{b}\boldsymbol{\theta}}(\bar{\mathbf{x}}_1, \mathbf{0})\mathbf{c}_{\boldsymbol{\theta}}(\bar{\mathbf{x}}_1, \bar{\mathbf{x}}_2, \mathbf{0}, \mathbf{0}) - \mathbf{H}'_{\mathbf{bb}}(\bar{\mathbf{x}}_1, \mathbf{0})\mathbf{c}_{\mathbf{b}}(\bar{\mathbf{x}}_1, \bar{\mathbf{x}}_2, \mathbf{0}, \mathbf{0}) \\
&\quad -\mathbf{H}'_{\mathbf{bb}}(\bar{\mathbf{x}}_1, \mathbf{0})(\boldsymbol{\eta}_1 + \bar{\mathbf{z}}_1) + \mathbf{H}'_{\mathbf{b}\boldsymbol{\theta}}(\bar{\mathbf{x}}_1, \mathbf{0})\boldsymbol{\tau}
\end{aligned} \tag{6.27}$$

where, for differentiations with respect to the fast time scale, the quasi-static force varies slowly,

$$\frac{d\bar{\mathbf{z}}_1}{d\tilde{t}} \approx \mathbf{0}_m \tag{6.28}$$

If we substitute $\bar{\mathbf{z}}_1$ from eq.(6.22) into eq.(6.27), the fast subsystem simplifies to the linear state space form of,

$$\begin{aligned}
\frac{d\boldsymbol{\eta}_1}{d\tilde{t}} &= \boldsymbol{\eta}_2 \\
\frac{d\boldsymbol{\eta}_2}{d\tilde{t}} &= -\mathbf{H}'_{\mathbf{bb}}(\bar{\mathbf{x}}_1, \mathbf{0})\boldsymbol{\eta}_1 + \mathbf{H}'_{\mathbf{b}\boldsymbol{\theta}}(\bar{\mathbf{x}}_1, \mathbf{0})\boldsymbol{\tau}_f
\end{aligned} \tag{6.29}$$

where the control input for the fast subsystem is given by,

$$\boldsymbol{\tau}_f = \boldsymbol{\tau} - \bar{\boldsymbol{\tau}} \tag{6.30}$$

Hence, using eq.(6.29) we can establish the control scheme for suppressing the vibration coordinates. The overall composite control strategy for the slow and fast subsystems, is now addressed in the following section.

6.2 A Composite Control Strategy

The gross maneuver (i.e. quasi-static motion) of the articulating truss may be controlled using the conventional robotic computed torque schemes [Paul'81],[Craig'86]. If we consider actuators forces $\bar{\tau}_o$ for a specific maneuver, initially computed from the rigid body inverse dynamics (performed off-line from the forward dynamic simulations), then the actuation of the gross maneuver may be commanded according to the simple proportional-derivative (PD) scheme of,

$$\bar{\tau} = \bar{\tau}_o + \mathbf{K}_P(\boldsymbol{\theta}_{I,d} - \boldsymbol{\theta}_I) + \mathbf{K}_D(\dot{\boldsymbol{\theta}}_{I,d} - \dot{\boldsymbol{\theta}}_I) \tag{6.31}$$

where $\boldsymbol{\theta}_{I,d}$ and $\dot{\boldsymbol{\theta}}_{I,d}$ are the desired prismatic joint extensions and extension rates (or angular values for independent revolute joints), while $\boldsymbol{\theta}_I$ and $\dot{\boldsymbol{\theta}}_I$ are the actual measured values. $\mathbf{K}_P$ and $\mathbf{K}_D$ are the corresponding gain matrices, and when of diagonal form decouples the control between joints.

Implementing vibration control based on the fast subsystem of eq.(6.29), implies that either full state feedback is available or a state observer model be employed to provide estimates of the unmeasured states. Of course, both schemes require the installation of high performance measurement systems to detect the modal states of concern. Assuming these capabilities exist for our simulations, then the selection of a control scheme for the linear time-varying system of eq.(6.29) can be addressed.

In this thesis, vibration control will be applied using the gains computed for a **specific orientation** of the manipulator, hence, the system is treated as linear and time-invariant. It will be assumed that measurements for all modes of interest are available. In addition, actuator characteristics of sensitivity and response are not modelled, therefore no limitations are imposed on their operation. These ideal conditions are intended for the initial examination of vibration control obtained with the reduced-order model scheme. (In actuality, however, high operation bandwidths of the actuators would be required to suppress the high frequency flexible modes. Their operation characteristics must therefore be modelled for a complete assess-

ment of the stability and performance of the control system in question.) For the specific orientation considered, either the conventional pole placement or the linear quadratic regulator (LQR) design methods can be applied to the resulting linear time-invariant form of eq.(6.29). Therefore, the standard state space representation of [Takahashi et al.'70] will be employed per the following,

$$\dot{\boldsymbol{\eta}} = \mathbf{A}\boldsymbol{\eta} + \mathbf{B}\boldsymbol{\tau}_f \tag{6.32}$$

where, $\boldsymbol{\eta} = \langle \boldsymbol{\eta}_1^T \quad \boldsymbol{\eta}_2^T \rangle^T$, and is of dimension m^*, where $m^* = 2 \times m$. The system and control matrices are given by,

$$\mathbf{A} = \begin{bmatrix} \mathbf{0}_{mm} & \mathbf{1}_{mm} \\ -\mathbf{H}'_{\mathbf{bb}} & \mathbf{0}_{mm} \end{bmatrix} \qquad \mathbf{B} = \begin{bmatrix} \mathbf{0}_{mn} \\ \mathbf{H}'_{\mathbf{b}\theta} \end{bmatrix} \tag{6.33}$$

and matrix $\mathbf{B}$ must assure controllability of the states. If this is satisfied per the conditions of [Takahashi et al.'70], then with a state feedback control law given by $\boldsymbol{\tau}_f = -\mathbf{F}\boldsymbol{\eta}$, the closed-loop system and LQR performance index are given by,

$$\begin{aligned} \dot{\boldsymbol{\eta}} &= (\mathbf{A} - \mathbf{B}\mathbf{F})\boldsymbol{\eta} \\ J &= \int_0^\infty \boldsymbol{\eta}^T \left(\mathbf{Q} + \mathbf{F}^T\mathbf{R}\mathbf{F}\right)\boldsymbol{\eta} \quad dt \end{aligned} \tag{6.34}$$

where weighting matrices $\mathbf{Q}$ and $\mathbf{R}$ are symmetric, and $\mathbf{Q} \geq \mathbf{0}_{m^*m^*}$, $\mathbf{R} > \mathbf{0}_{m^*m^*}$. The optimal stabilizing gain $\mathbf{F}$ that minimizes the performance index J, is given per [Takahashi et al.'70],

$$\mathbf{F} = \mathbf{R}^{-1}\mathbf{B}^T\mathbf{P} \tag{6.35}$$

where matrix $\mathbf{P}$ is the solution to the matrix Ricatti equation,

$$\mathbf{A}^T\mathbf{P} + \mathbf{P}\mathbf{A} - \mathbf{P}\mathbf{B}\mathbf{R}^{-1}\mathbf{B}^T\mathbf{P} + \mathbf{Q} = \mathbf{0}_{m^*m^*} \tag{6.36}$$

This optimal LQR scheme will be applied in the following control simulations to compute the modal control gains $\mathbf{F}$ for the specific orientation of the truss manipulator. Figure 6.1 represents the continuous-time, composite-control approach presented. Note that the inner loop corresponds to vibration control of the flexible coordinates, and the outer loop is that of the computed torque scheme with PD feedback (for control of the gross maneuver).

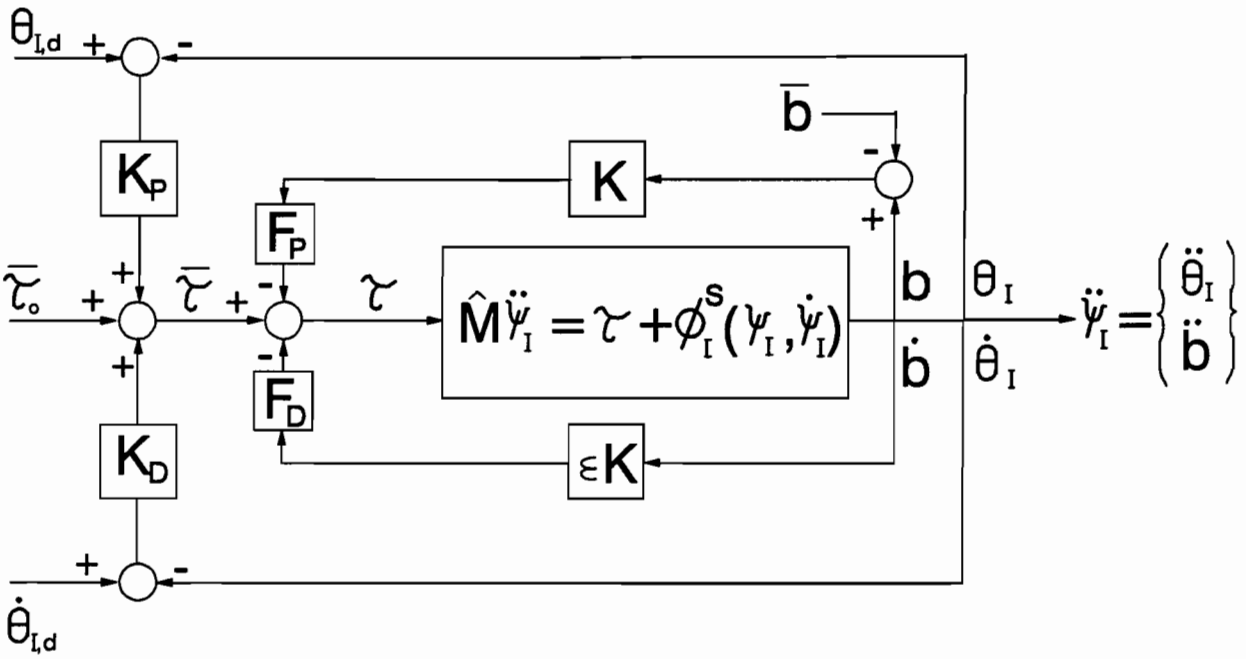

Figure 6.1: Block schematic of the composite control scheme.

Chapter 7

SIMULATION CODE DESCRIPTION

The simulation code developed to perform the kinematic and dynamic calculations for planar truss manipulators was written in the FORTRAN77 standard language. The resulting execution code was designated as **GENMAN** (for general manipulator), because in addition to the truss, cylinder and piston-rod links, the corresponding dynamic terms for flexible beam type members of serial robotic manipulators were also included. The main motive for implementing the beam type links was to assist in verifying the simulation scheme used in GENMAN, since numerous simulation results are available for serial robotic configurations. The mass and stiffness matrix derivations for beam links are contained in [Cyril'88], and will not be provided in this thesis.

The main operation flow of GENMAN is illustrated in Fig.7.1, and the corresponding simulation sequence of the inverse and forward dynamics is presented in Figures 7.2 and 7.3, respectively. It should be noted that the same "SYSTEM DYNAMICS" block is used for both simulations, and hence, its contents are presented only in Fig.7.2.

Since four different link types are modelled in GENMAN, the code contains numerous identifier arrays to indicate not only the link type, but also the joint type. The various joint types consist of independent revolute or prismatic joints, and de-

pendent revolute joints associated with the kinematic loop considered in this work. The forward kinematic computations employ these identifier arrays exensively to distinguish the appropriate recursive relations for the link under consideration, and the instance when a kinematic loop has to be evaluated. Within the routine of the kinematic loop, the Newton-Raphson iterative scheme is employed to solve the nonlinear equations that provide the dependent angles, and to perform the linear computations of the corresponding dependent angular rates (per eq.'s(D.14), (D.37) and (D.44) of Appendix D). The inverse and forward dynamic simulations both require that the kinematic calculations be performed, since the twist vector components are required to evaluate the wrench vector per eq.'s(5.18) to (5.20).

In addition to the identifier arrays discussed above, vector index pointers are also established for the flexible twist, independent and dependent speed vectors. These are constructed automatically by the code (prior to commencing the iterative computations of the simulations), for the structure arrangement defined per the input file requirements. The vector index pointers are used for the assembly of the global mass matrix, dynamic vectors, and in the computations associated with the natural orthogonal complement.

Other features of the code include:

- The manipulator structure is defined and simulation specifications assigned via a user prepared input file. The corresponding joint trajectories of the actuators, needed for simulations of the inverse dynamics or gross manuever control, are also provided by a user supplied subroutine. If simulations of the forward dynamics are to be performed, then the user must provide either the corresponding data file or subroutine of the actuator force trajectory.

- **Prior** to the simulations of the equations of motion, the finite element solution to the eigenvalues and eigenvectors of each truss link are performed. After assembly of the nodal mass and stiffness matrices, the eigenvalue problem is

solved using routines of the EISPACK library of FORTRAN routines. The requested number of modes to be used in the simulation are retained, and the correponding eigenvectors ortho-normalized. The nodal mass ($\mathbf{M}^*_{ee}$) and stiffness ($\mathbf{K}^*_{ee}$) matrices are then reduced to that of the modal mass ($\mathbf{M}_{ee}$) and stiffness ($\mathbf{K}_{ee}$) matrices, respectively.

- Integration of the equations of motion can be performed using either the GEAR routine originating from the IMSL library, Adams method, or fourth order Runga Kutta.

- The solution of the matrix Ricatti equation given in eq.(6.36), and of the optimal LQR control gain $\mathbf{F}$, are obtained through calls to a routine of the CASCADE linear control systems FORTRAN library. The operations of CASCADE also rely upon the LINPACK linear algebra and EISPACK eigenvalue systems libraries.

As discussed in the first item above, the input file is used to define the articulating truss or robotic manipulator structure, and also specifies the type of simulation to perform; i.e. forward kinematics, inverse dynamics, or forward dynamics (with or without control). If control is to be performed, then the corresponding maneuver gains $K_{p,i}$ and $K_{d,i}$ can be specified for each prismatic joint. If vibration control is also examined, then either the time(s) at which to perform the vibration control gain calculations, or specified values of $\mathbf{F}$ can be assigned. Simulation output is stored in ASCII data files, and the results consist of:

- finite element eigenvalues and eigenvectors for each truss link,
- the trajectories of the inertial position and orientation (and corresponding rates) of the link frames,
- joint states,
- actuator states,
- total system energy and work calculations,

- modal coordinate or local deformation states, and
- the LQR gains calculated for the time(s) specified in the input data.

Simulations performed with GENMAN were executed on 486DX personal computers. The code was confirmed with the dynamic simulations of planar serial robotic configurations from [Cyril'88], and the vibration control simulations of [Siciliano et al.'88]. The solution of the eigenvalue problem for the truss links were verified with other independent codes. The following chapter presents various simulations performed for a truss crane based on a NASA concept. Calculation checks and observations of the results are discussed.

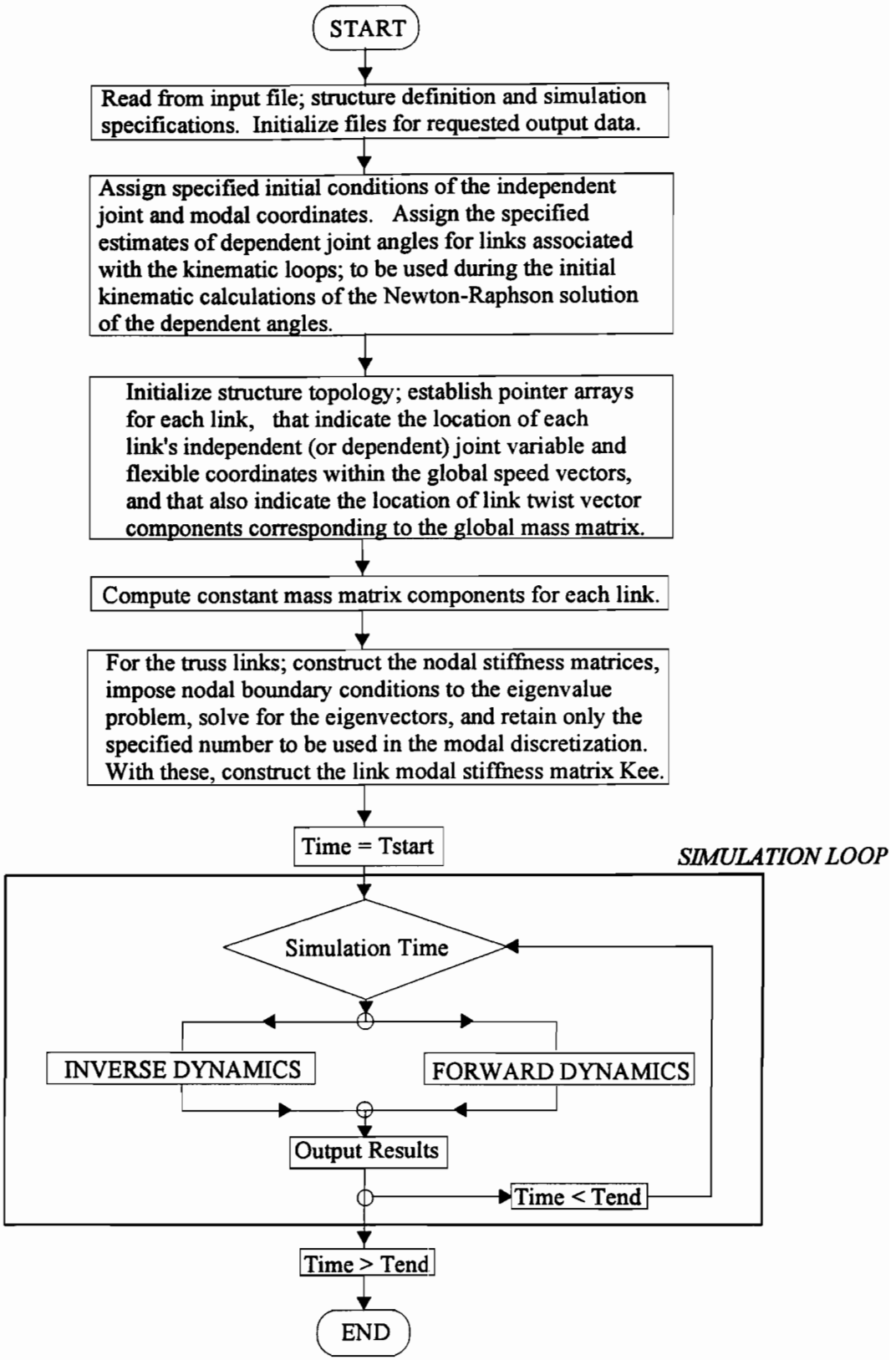

Figure 7.1: Main simulation flowchart for GENMAN.

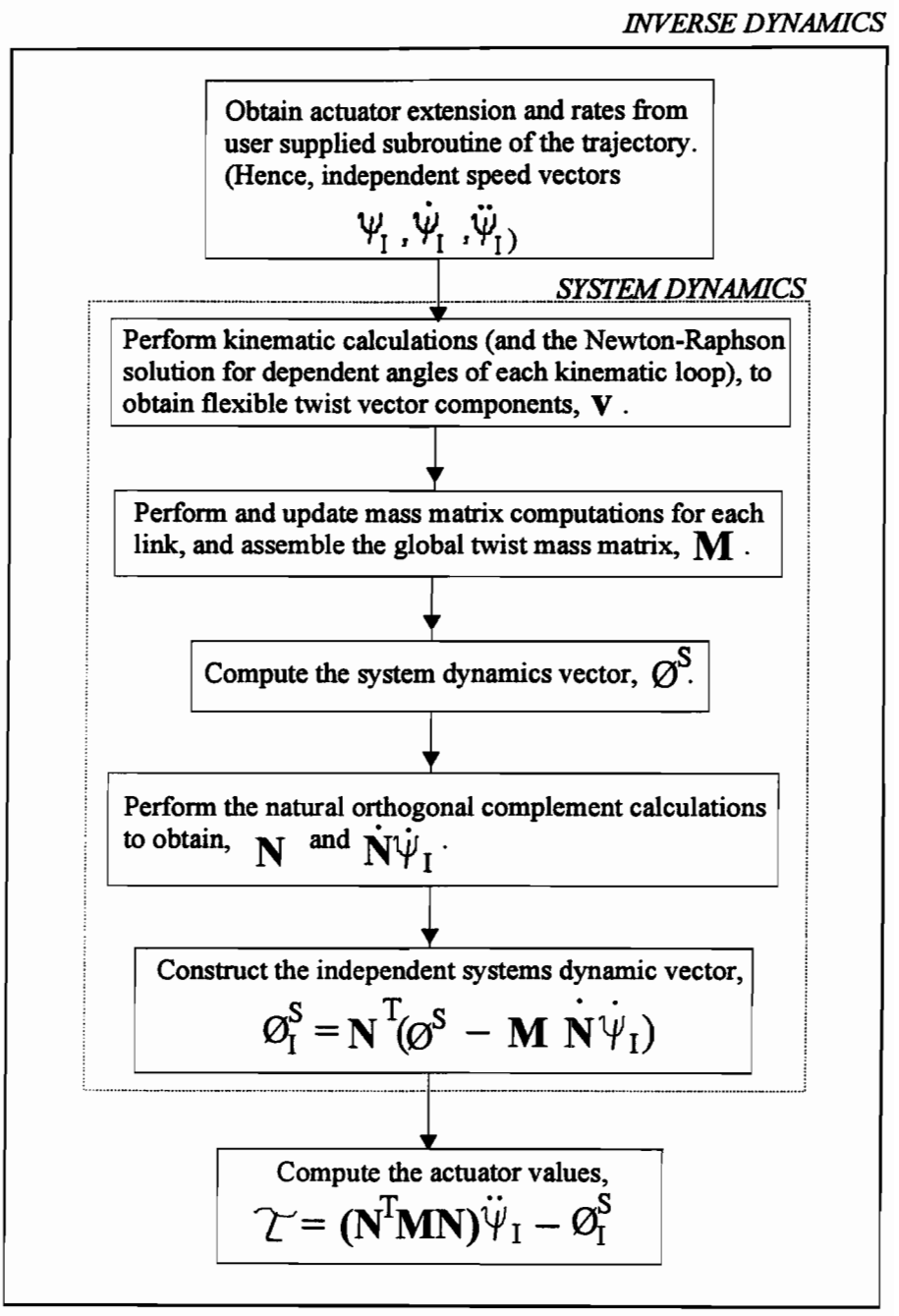

Figure 7.2: Rigid body inverse dynamics flowchart.

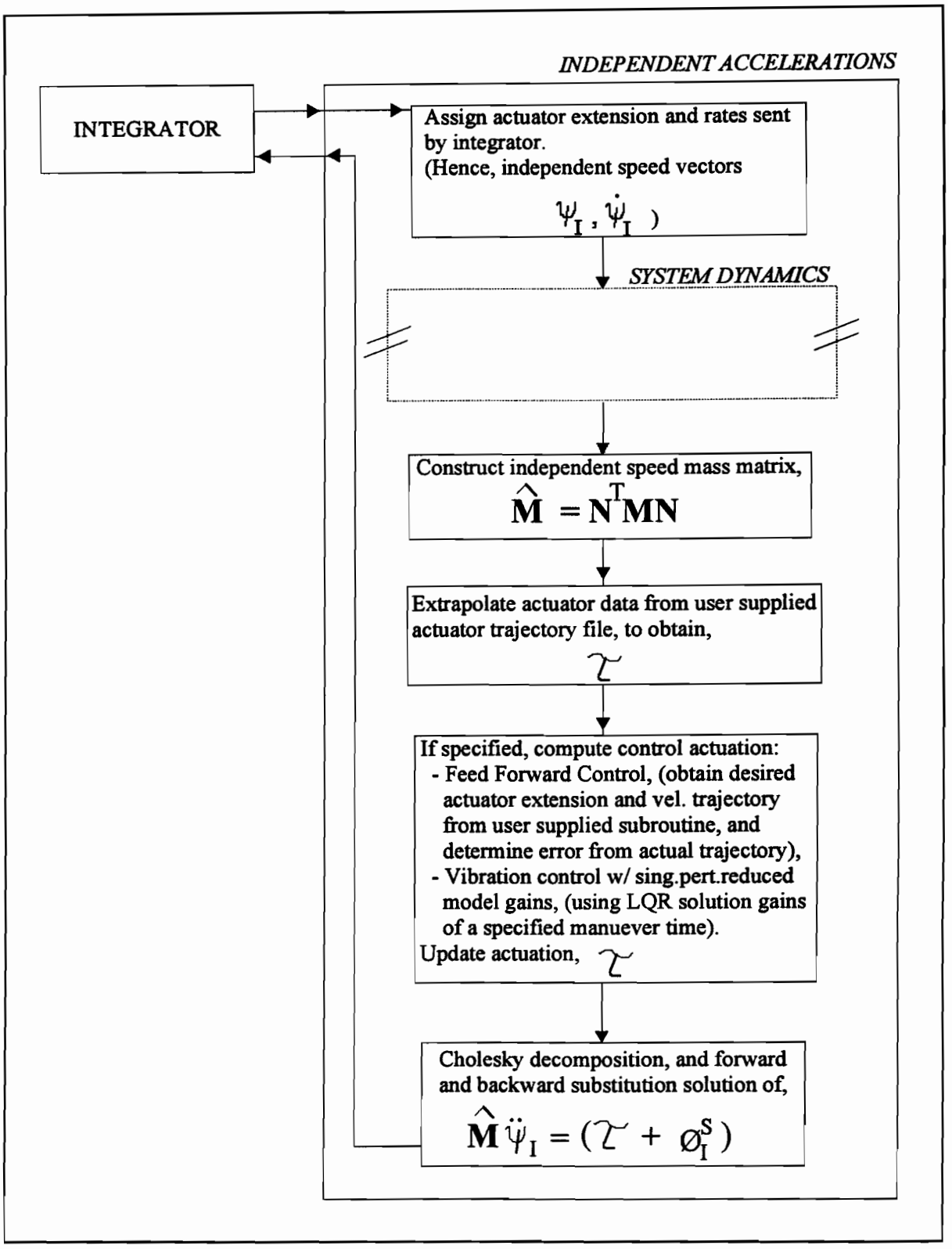

Figure 7.3: Forward dynamics flowchart.

Chapter 8

SIMULATIONS AND RESULTS

Simulations have been performed for the planar truss structure of Fig.8.1, situated in a **zero-gravity environment** and attached to a **fixed base**. This configuration originates from the 3D space crane concept of [Mikulas et al.'88b] and [Wu et al.'92], and employs material density and modulus of elasticity properties to reflect the 3D structure mass and stiffness. The extended length of the structure is 95 meters, and the width is 5 meters. The total mass of the structure is 1106 kg, which includes 300 kg of additional mass (as a platform and additional hardware) situated along the end batten. Such a structure could be intended to manipulate payloads on the order of 10^5 kg, which was not modelled in the simulations presented here.

The crane consists of three articulating truss booms, which are actuated via the joint configuration shown in Fig.8.1. This arrangement allows for a robust 90 degree planar articulation of each boom, by virtue of the two actuators per joint. The 3-member truss section located between the actuators of each joint, varies somewhat from that of [Mikulas et al.'88b]. The joint was defined here as such, since the work of [Wu et al.'92] considered three various arrangements which would require more detailed modelling. Appendix E contains the member properties used to model the flexibility effects, and the following sections discuss the simulation and calculation checks performed, along with the observations.

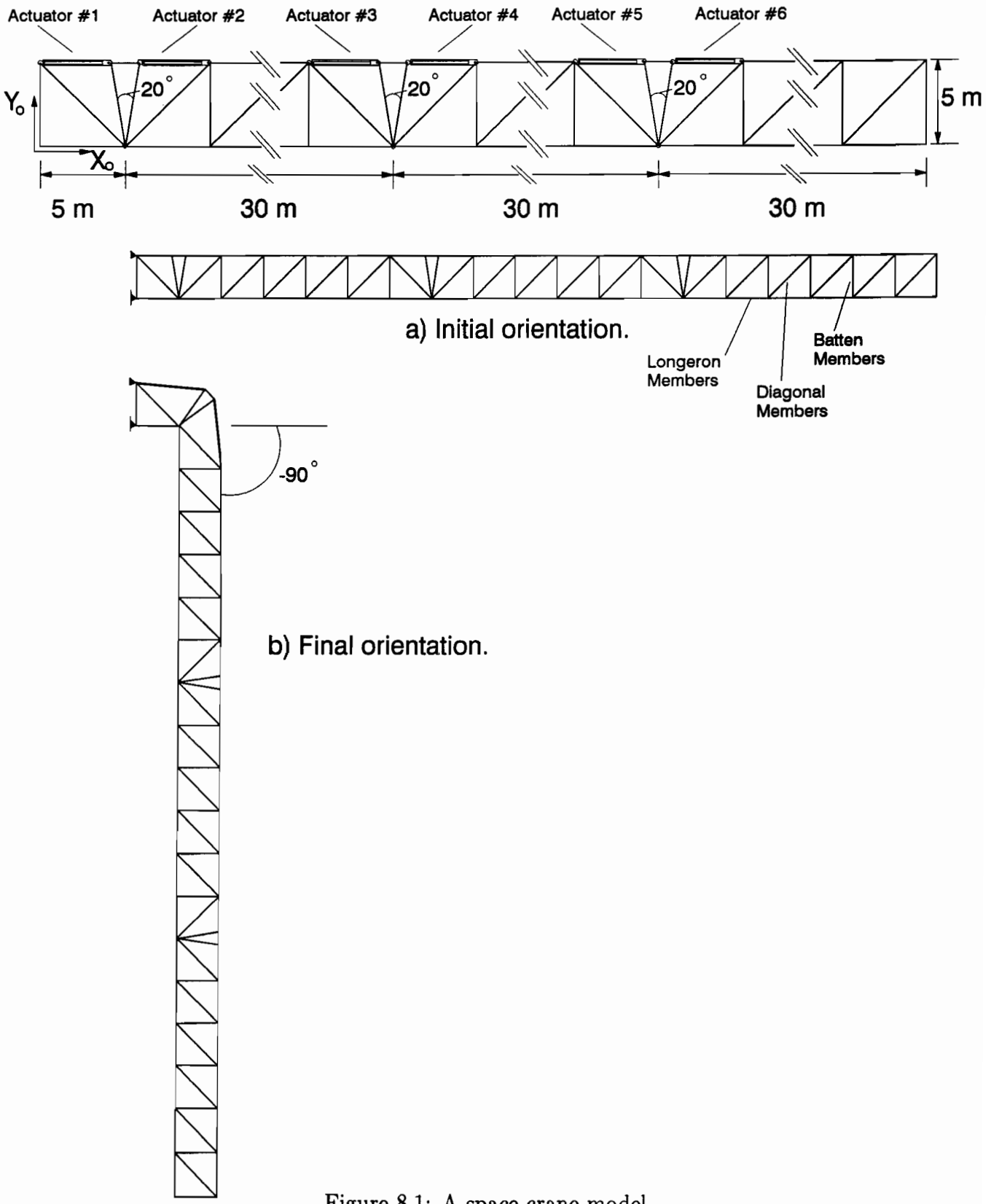

Figure 8.1: A space crane model.
(For more details, refer to Figure E.1a of Appendix E)

8.1 Fully Articulated Crane

Inverse dynamics were performed for the structure of Fig. 8.1, to examine the actuation forces associated with a 20 second maneuver from the extended orientation to the final configuration shown in Fig. 8.1b. Such a fast maneuver would not be recommended for a structure of such dimensions (especially with a massive payload at the end), and is only used here to examine the resulting dynamic behaviour. All six actuators were activated, hence each attributed a degree of freedom to the motion. The resulting dynamic model consists of 19 individual links; 7 trusses, 6 cylinders and 6 piston-rods. Initially, each actuator piston-rods have zero extension, however, to effect the motion of Fig. 8.1b, the **first two actuators** are commanded to extend during the 20 second maneuver per the following trajectories,

$$\begin{aligned} d(t) &= \frac{\Delta d}{T}\left[t - \frac{T}{2\pi}\sin\left(\frac{2\pi}{T}t\right)\right] \\ \dot{d}(t) &= \frac{\Delta d}{T}\left[1 - \cos\left(\frac{2\pi}{T}t\right)\right] \\ \ddot{d}(t) &= \frac{\Delta d}{T}\left[\frac{2\pi}{T}\sin\left(\frac{2\pi}{T}t\right)\right] \end{aligned} \tag{8.1}$$

where, $T = 20$ seconds, and $\Delta d = 3.832$ meters. The remaining four actuators are commanded to have zero extension throughout the maneuver. For times greater than 20 seconds, actuators 1 and 2 maintain the extended position of $d = 3.832$ meters. It should be noted from the trajectories in eq.(8.1), that actuators 1 and 2 are specified to yield zero velocity and acceleration at the initial and final maneuver times. However, based on the acceleration trajectory, a jerk will be imparted to the structure at $t = 20$ seconds. The final actuator extension of 3.832 meters was simply pre-computed based upon the joint geometry of Fig. 8.1, corresponding to the final orientation.

Figure 8.2 illustrates the extension trajectories commanded for actuators 1 and 2. The resulting history of the main truss angle is presented in Fig. 8.3, as computed when performing the kinematic computations of the rigid body inverse dynamics.

These were confirmed by simply considering the basic geometry relations of (the triangles formed by) the joint configurations, and then computing the angular rates obtained with the extension length and rates of the actuator. The actuator forces associated with the maneuver and as obtained from the inverse dynamics, are given in Fig. 8.4. For the joint configuration modelled in this space crane, the magnitude of the force between adjacent actuators will be similar, namely by virtue of the symmetry of their placement and of the small inertia contribution of the three member truss links interfacing the actuator pairs. This result is noted in Fig. 8.4 for all actuator pairs, i.e. 1 and 2, 3 and 4, and 5 and 6. The force values of actuator 6 were also confirmed by performing a manual computation of the free-body dynamic force balance with the final truss link.

The actuator force profiles of Fig. 8.4 would be used to perform the simulations of the forward dynamics. However, in an attempt to reduce the computation time anticipated with the flexible body forward dynamics, actuators 3 to 6 were replaced by non-active members, and assigned values of Young's modulus equivalent to that of the longeron truss members. The simulations corresponding to this model, are presented in the following section.

8.2 Reduced Articulated Crane

For the truss configuration of the previous section, actuators 3 to 6 are substituted with static members, to reduce the rigid degrees of freedom of the full truss crane from 6 to 2. The simulations of the rigid body inverse dynamics were re-performed using the same extension trajectories of actuators 1 and 2, given previously in eq.(8.1) and Fig. 8.2. As expected, the computed actuator forces agreed exactly with those of Fig.8.4, since the same mass properties were used. The simulations of the forward dynamics can now be performed by using this inverse dynamic actuator data, provided in an ASCII file ("look-up table") at a given storage rate, and interpolating linearly between the two stored data points (that bound the time of interest). The following sections

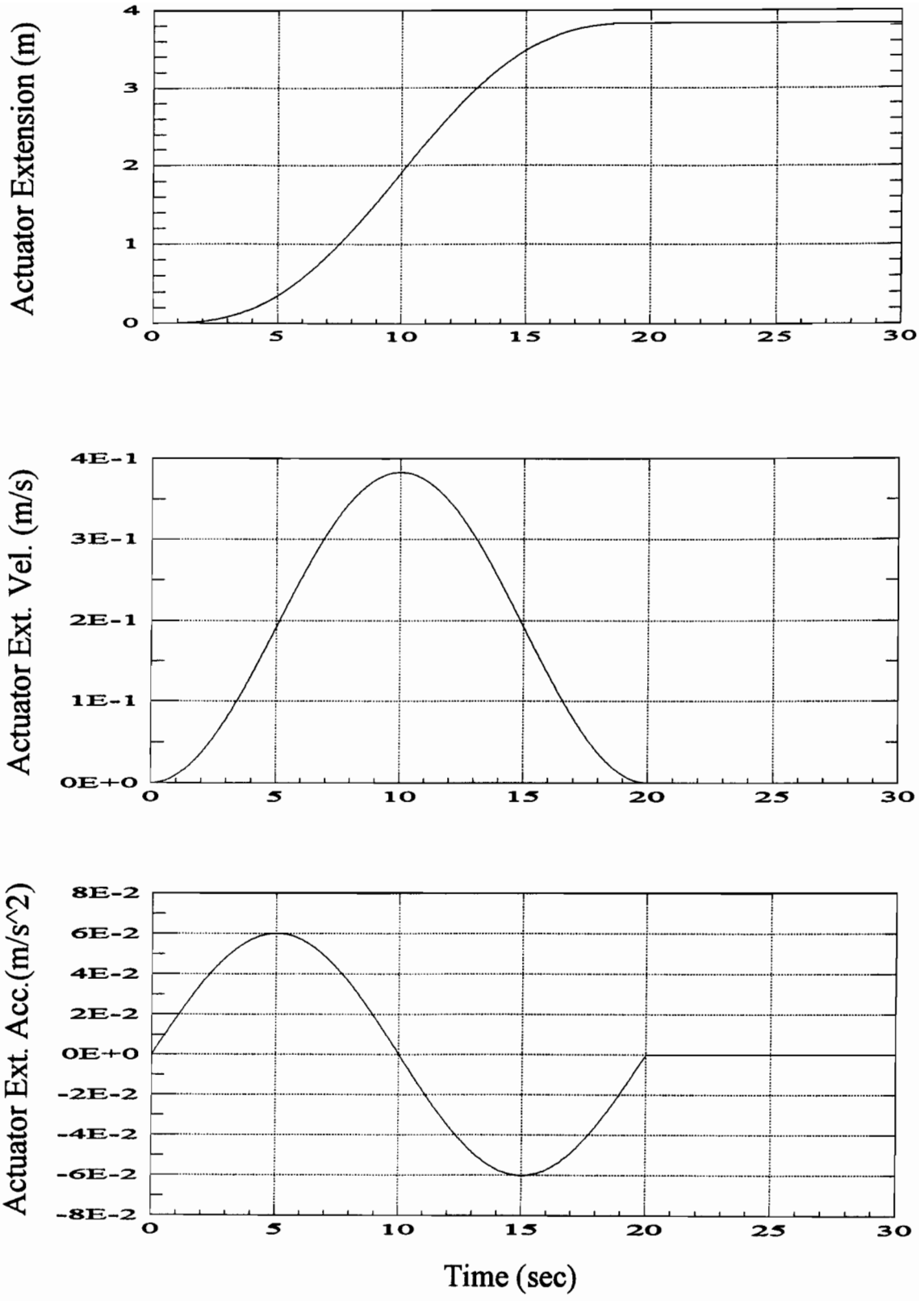

Figure 8.2: Prescribed extension trajectory of actuators 1 and 2.

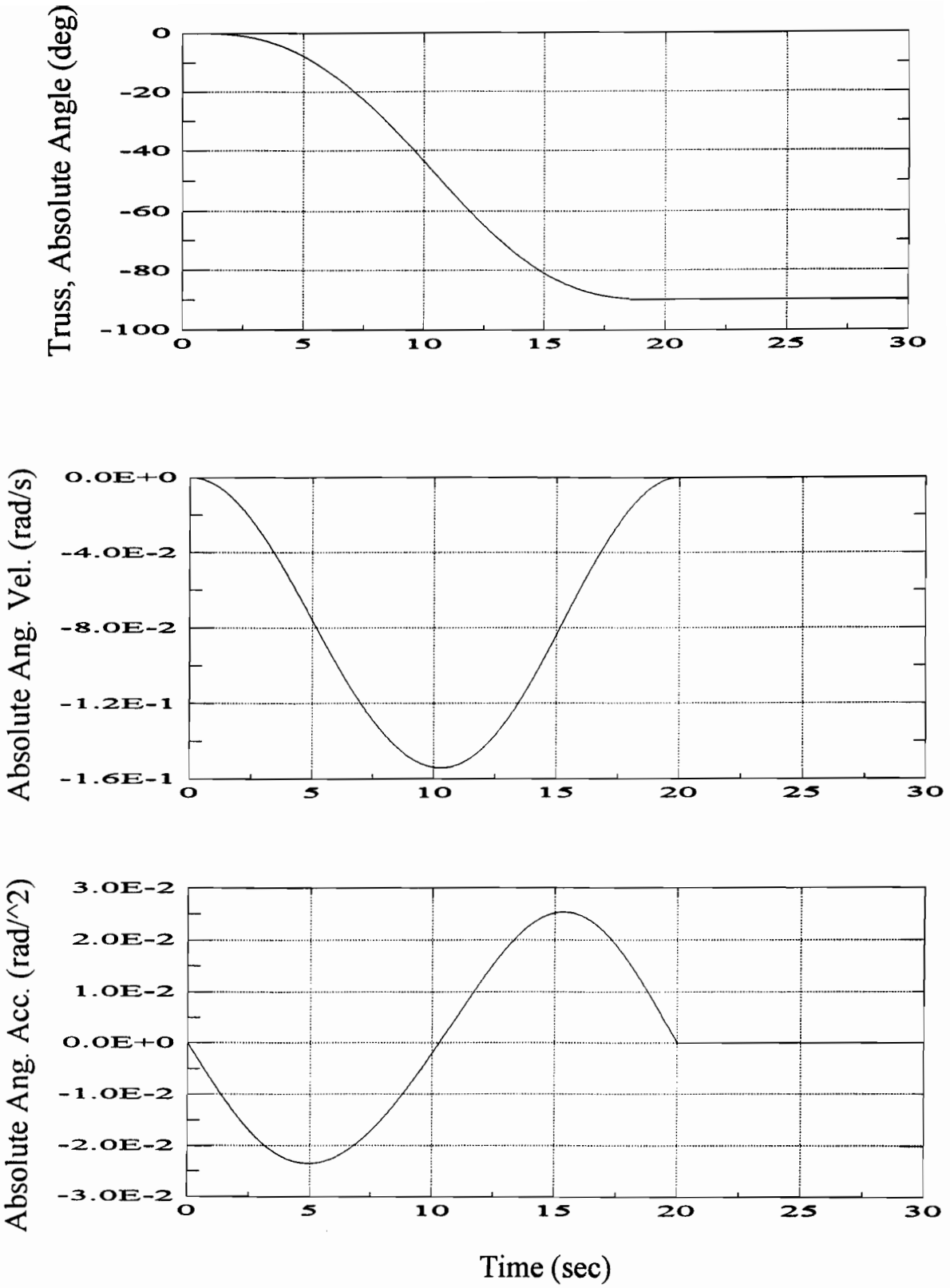

Figure 8.3: Absolute angular kinematic trajectory of the truss boom.

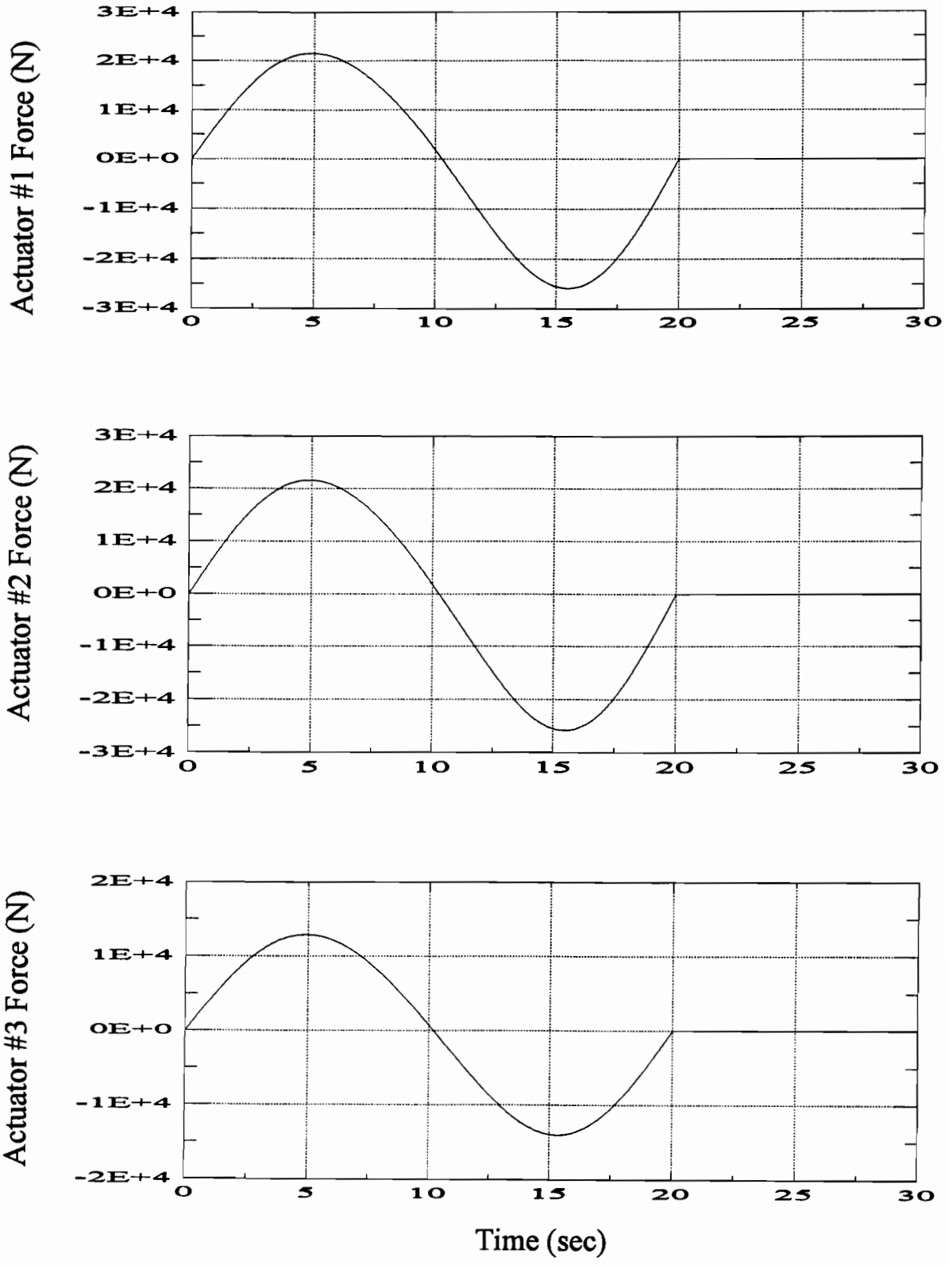

Figure 8.4: Actuator forces computed from inverse dynamics.

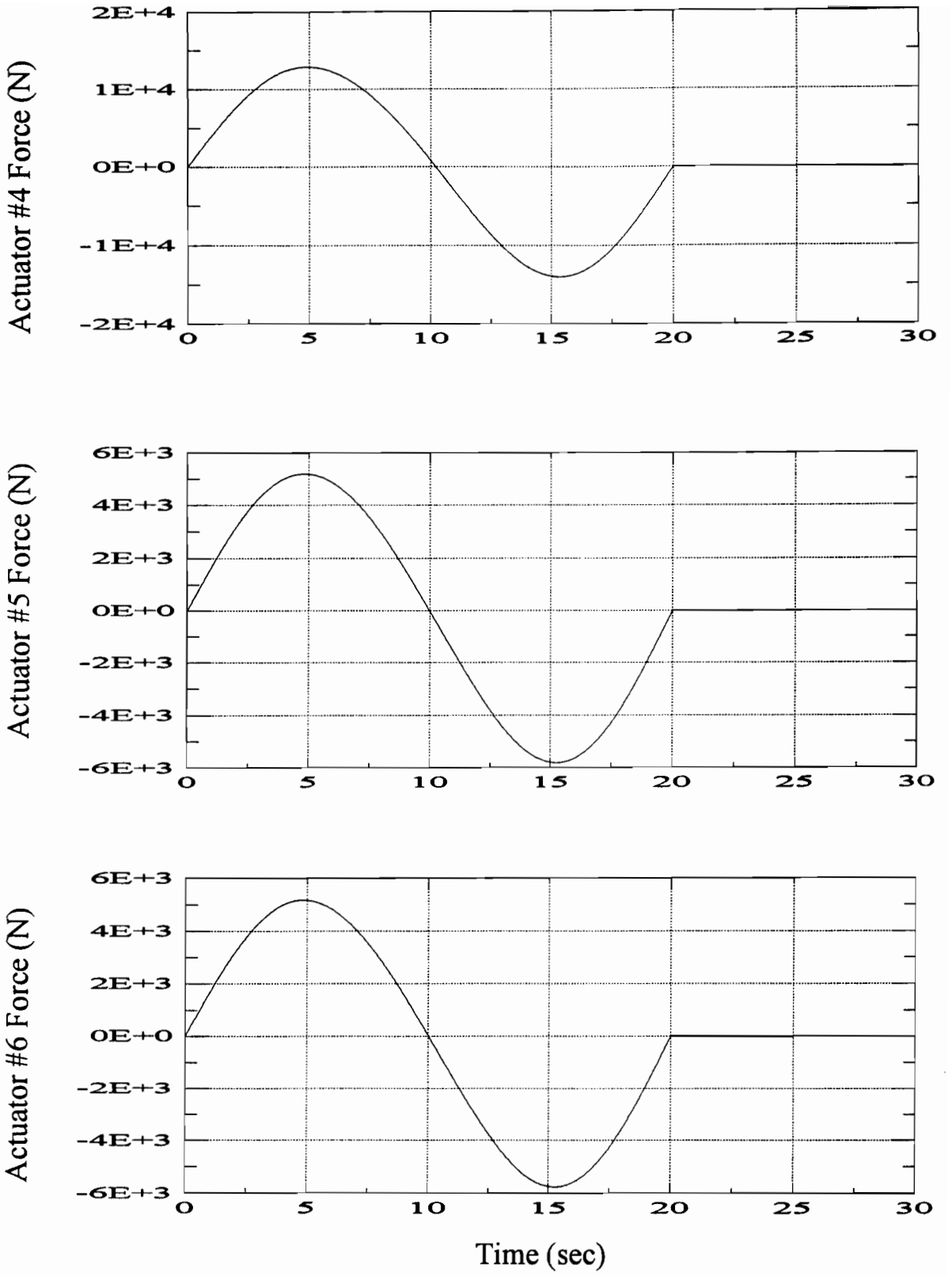

Figure 8.4: Actuator forces computed from inverse dynamics. (cont.)

describe the forward dynamics for both a rigid and flexible structure, respectively.

8.2.1 Initial Simulation Validations

As mentioned previously in Chapter 7, simulations of the rigid and flexible body dynamics for serial robotic manipulators were used to initially verify the operations of GENMAN. Hence, the simulation results presented for the planar configurations in [Cyril'88], were duplicated by GENMAN. Vibration control simulations using the reduced-order models and as performed by GENMAN, were also validated with those presented for the serial manipulator considered in [Siciliano et al.'88]. Free-body dynamic force balances were manually computed to verify the inverse dynamics actuation of the multi-loop truss crane arrangements (as described previously in Section 8.1 for actuator number 6). Other validations performed specifically for truss crane structures are addressed in the simulation results of the following sections.

8.2.2 Rigid Body Simulations

As mentioned, the rigid body forward dynamics are performed by the linear interpolation (between two data points that bound the specific time of interest) of the pre-computed inverse dynamic data file. When this was initially attempted, it was observed that the simulations of the forward dynamics became unstable depending upon the frequency at which the inverse dynamic force data was previously stored in the ASCII file. This instability is illustrated with the extension velocity of the actuators, given in Fig. 8.5. The dotted curve is the forward dynamics using actuator data of the inverse dynamics that was stored in an ASCII file every 0.1 seconds. Similarly, the dashed line is the forward dynamics using actuator data that was stored in an ASCII file every 0.01 seconds. From these curves, we note they diverge in opposite directions from the original prescribed trajectory of the solid line.

To investigate these behaviours, the energy characteristics the simulations were examined. Figure 8.6a presents the total kinetic energy associated with the rigid

body inverse dynamics. The energy discrepancy due to the numerical calculations, is illustrated by the solid line of Fig. 8.6b, which represents the difference between the kinetic energy and the work done on the system, divided by the maximum kinetic energy. This energy discrepancy increases gradually during the computations of the inverse dynamics (as would be expected), and is only of the order of 10^{-4}. The energy discrepancies associated with the two unstable simulations of the forward dynamics, are given by the dotted and dashed lines in Fig. 8.6b. These correspond with that of the inverse dynamics, up until their respective instance of divergence.

In an attempt to identify the source of these instabilities, numerous aspects of the simulation procedure and code were investigated. Firstly, the occurrence of the instability was observed to be very sensitive not only to the frequency rate at which the pre-computed inverse dynamic actuator values were saved to the data file, but also to the precision of the data retained. For the simulations presented here, 16 digits were used. The implementation of the Adams and Runga-Kutta integrators (instead of Gear's integrator) were also attempted, and experienced the same simulation instability. The computation of the natural othogonal complement using the scheme given per eq.(5.33) was also performed. The same instability behaviour resulted at approximately the same instances, and hence no improvement was obtained. The numerical instabilities can also result with a simpler manipulator configuration, but do take longer to appear. Therefore, the simulations of inverse dynamics provide the required actuator values for a specified maneuver, with an additional small numerical error of non-zero mean. This error is larger for more complex systems, and when the computed actuator values are integrated in the simulations of the forward dynamics, the non-zero mean term produces an unbounded response, and hence the instabilities as observed in this work.

In an attempt to stabilize the simulations of the rigid body forward dynamics (for this truss crane arrangement), the computed torque with PD feedback control, was implemented. Feedback gains which provide successful execution of the rigid body

forward dynamics, consist of $K_p = K_d = 5000$ for both actuators. Figure 8.7 contains the resulting additional actuation forces, which are only on the order of 10^{-6} of the nominal forces of the inverse dynamics presented previously in Fig. 8.4. The actuator extension trajectories of the original prescribed values were re-duplicated, therefore the maneuver control scheme effectively stabilized the integration.

8.2.3 Flexible Body Simulations

The flexible body simulations performed for this truss configuration employ the ortho-normalized eigenvectors of the main truss boom, presented in Table 8.1. These were computed from the FE eigenvalue problem discussed in Section 4.1.4, using the boundary conditions illustrated in Fig.8.8. For these nodal constraints, the first and second vibration frequencies are 0.531 and 3.893 Hz, respectively. As a matter of comparison, a 3D space crane model presented in [Sutter et al.'90] that includes specific joint details (such as that of a revolving base joint), indicated a fundamental frequency of 0.135 Hz. Therefore, the truss crane model considered in this work is considerably stiffer than the detailed model of [Sutter et al.'90]. In addition, the frequency of the maneuver examined in these simulations is 0.05 Hz, as obtained from eq.(8.1). Therefore, the fundamental frequency of the crane simulated here is over 10 times that of the nominal rigid body maneuver, as recommended with the application of the singular perturbation method for vibration control. Conversely, the structure of [Sutter et al.'90] does not satisfy this requirement. But again, the fast maneuver examined here is only for simulation demonstration, and not recommended in actual practice.

The simulations of the flexible body dynamics presented here, were performed with the same PD feedback gains used for controlling the maneuver of the previous rigid body simulations, and no structural damping was modelled. The resulting actuator extension profiles are illustrated in Fig.'s 8.9 and 8.10, and the corresponding trajectories of flexible modes 1 and 2 are presented in Fig. 8.11. It is observed from

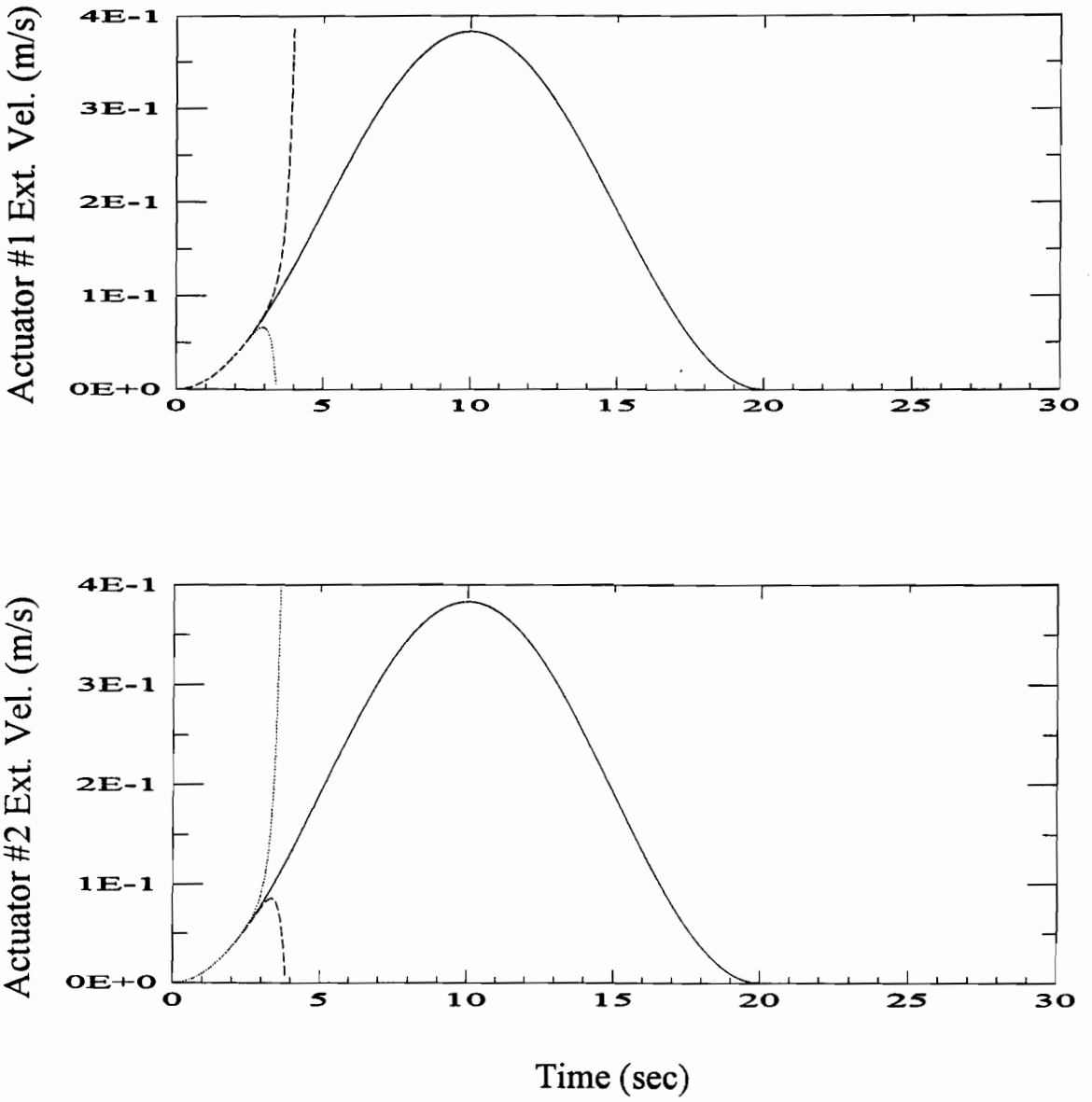

Figure 8.5: Simulation instabilities of the rigid body forward dynamics when interpolating from the inverse dynamic actuator forces contained in a data file.
(———Inv.dyn, · · · · · Fwd.dyn w/ inv.dyn actuator data file rate of 0.1 sec,
– – –Fwd.dyn w/ inv.dyn actuator data file rate of 0.01 sec.)

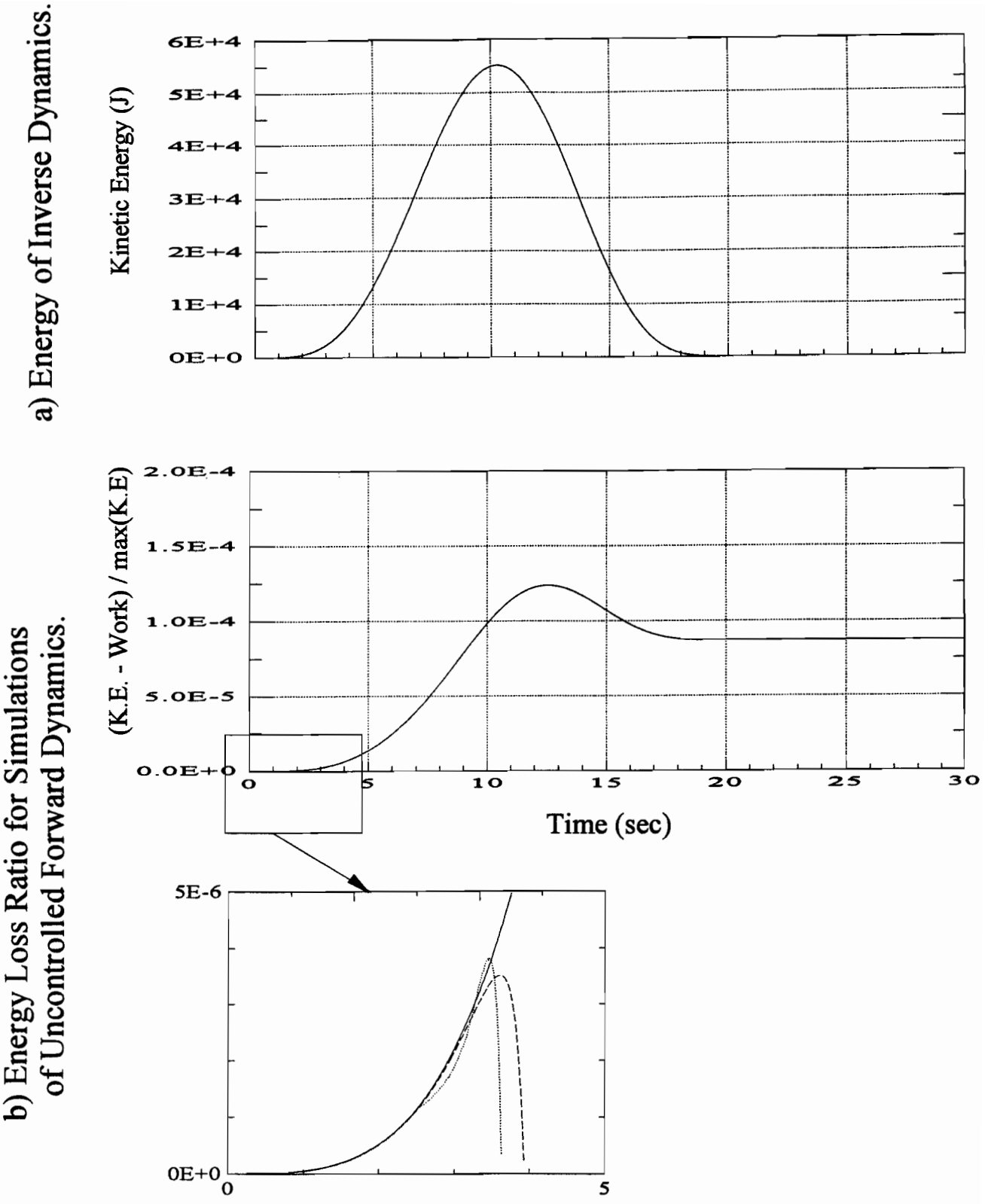

Figure 8.6: Energy comparison of the rigid body forward dynamics when interpolating from the inverse dynamic actuator forces contained in a data file.
(——Inv.dyn, ····· Fwd.dyn w/ inv.dyn actuator data file rate of 0.1 sec,
– – –Fwd.dyn w/ inv.dyn actuator data file rate of 0.01 sec.)

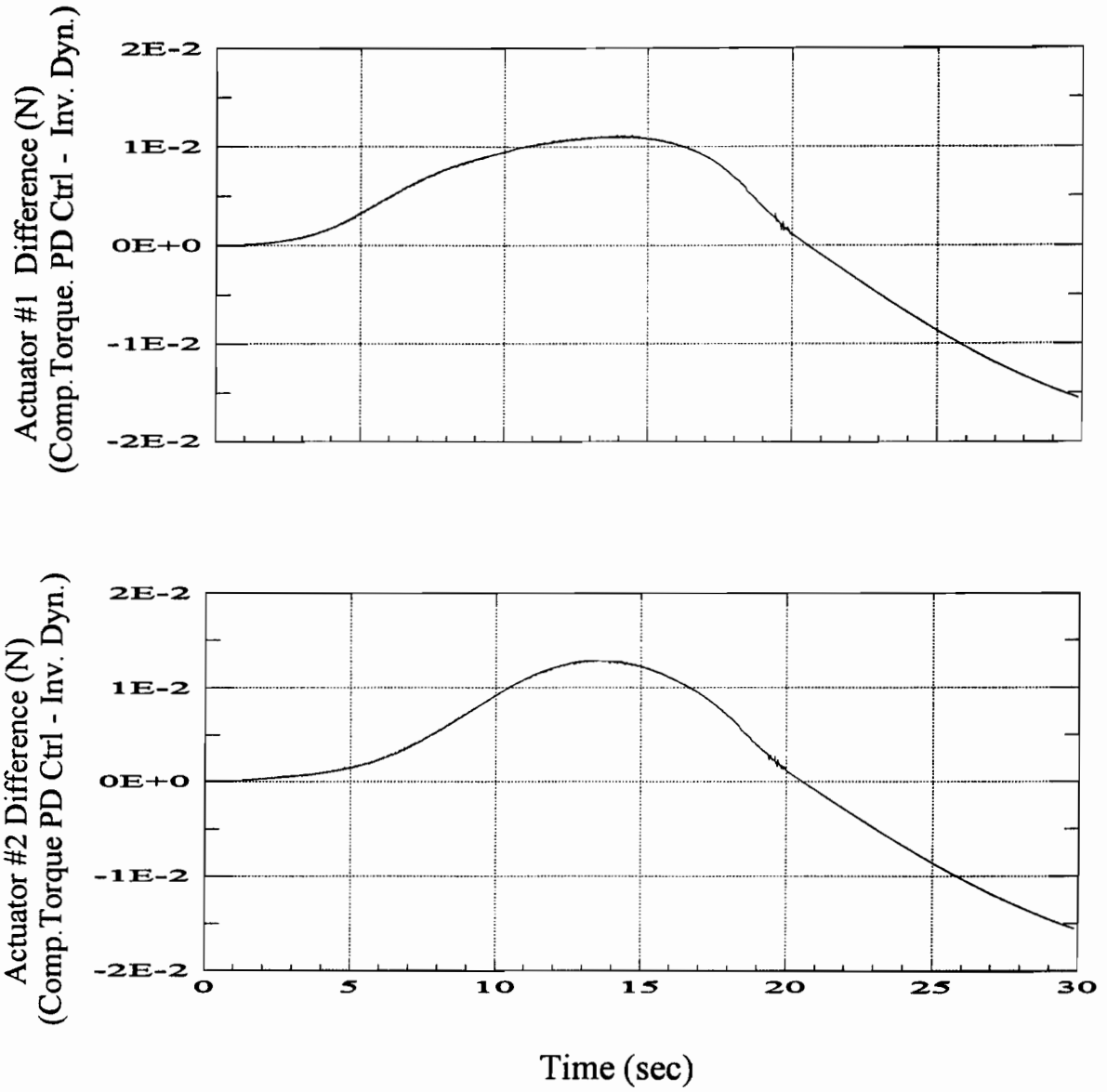

Figure 8.7: Additional actuation force required to stabilize the simulations of the rigid body forward dynamics.

this latter figure that the vibration modes are obviously damped, by noting their attenuation and the disappearance of the higher vibration frequency components which are initially visible at 0 and 20 sec (when maneuver jerks excite the system).

This damping is attributed to the PD feedback gains employed to stabilize the rigid body simulations. This was confirmed by performing flexible body simulations for the truss boom of Fig. 8.8, modelled to rotate simply about its origin (i.e. node 1) at the same angular rate of the truss crane, and driven by a torque. (Recall, as mentioned previously in Section 8.2.2, for simpler manipulator configurations the simulation instabilities of the forward dynamics take longer appear, and hence the use of simulation control is not immediately necessary.) Figure 8.12 illustrates these results. Fig. 8.12a corresponds to the flexible body simulations of the pivotting truss boom without control action, and Fig. 8.12b demonstrates the damping provided with the use of computed torque PD control on the driving torque. It should be noted that the high frequency components are maintained throughout the maneuver in Fig. 8.12a without the use of control. The simulations of the pivotting truss boom also confirmed the magnitudes of the vibration modes for the truss crane.

To additionally verify the modal magnitudes of the simulations of Fig. 8.11, a quasi-static loading analysis was performed by fixing the truss boom of Fig. 8.8 at its base nodes 1 and 2. Hence, for given maneuver time, the inertial loading distribution associated with the angular rotation of the boom was properly assigned to each node as a force vector (i.e. the net acceleration vector of each node was computed and multiplied by an equivalent lumped mass at the node). The corresponding nodal deflections of nodes 38 and 39, obtained from a FE static loading analysis, were observed to agree perfectly with that of the flexible body dynamics. As an example, for the time of 5 seconds, the magnitudes of modal coordinates 1 and 2 are 4.25 and -0.01 meters, respectively (as can be observed from Fig. 8.11). Using the eigenvector elements of node 39 from Table 8.1, this results in a nodal deflection of -0.0072 and 0.1912 meters in the X and Y directions, respectively. The corresponding quasi-static

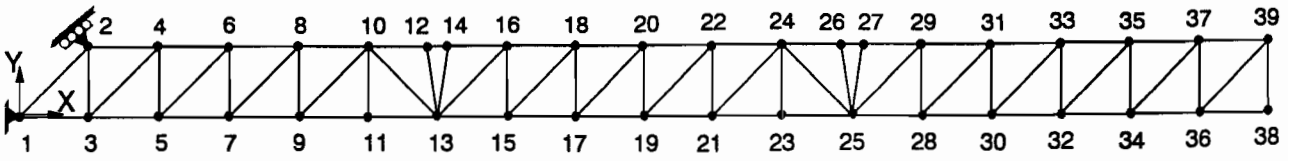

Figure 8.8: Boundary conditions for the main truss boom.

deflection for the angular rates at this time, suggested deflections for node 39 of -0.0073 and 0.1917 meters, respectively.

8.2.4 Vibration Control Simulations

The use of the vibration control gains **F** computed from the LQR solution of the reduced-order model for the modal coordinates, are now examined. For the final orientation (at the maneuver time of 20 sec), the corresponding gains are given in Table 8.2. It is noted from these values that actuator 1 has negligible authority. When this control is activated at 20 seconds, the resulting vibration suppression can be observed from the flexible mode rates of Fig. 8.13a. The solid line represents the controlled vibration and the dotted line corresponds to the original flexible body simulations of Fig. 8.11. The control scheme appears to be reasonably effective for vibration suppression. The additional control actuation was observed to be quite insignificant, as discussed in Section 8.3 for another truss configuration. In addition, Fig. 8.13b examines possible control spillover onto the higher modes 3 and 4, which is noted to be small. However, more uncontrolled modes should be examined, and recall that the presence of the PD feedback control required to stabilize the simulations, also provides damping (as observed initially in Section 8.2.3).

Now, the same flexible control gains were employed to examine the effect of activating this control immediately at 0 sec. The corresponding results are provided

Table 8.1: Ortho-normalized eigenvectors for the truss boom.

Mode 1: Eigenvalue = 11.139, Freq. = 3.338 rad/s = 0.531 Hz.
Mode 2: Eigenvalue = 598.182,Freq. = 24.458 rad/s = 3.893 Hz.

Node	Mode #1		Mode #2	
#	X	Y	X	Y
1	0.000E+00	0.000E+00	0.000E+00	0.000E+00
2	-1.499E-04	-1.499E-04	-6.986E-04	-6.986E-04
3	2.277E-04	-1.395E-04	1.364E-03	-4.201E-04
4	-3.777E-04	5.104E-04	-2.104E-03	4.228E-03
5	4.397E-04	5.208E-04	2.309E-03	4.505E-03
6	-5.897E-04	1.595E-03	-3.091E-03	1.107E-02
7	6.360E-04	1.605E-03	2.842E-03	1.134E-02
8	-7.860E-04	3.071E-03	-3.665E-03	1.897E-02
9	8.167E-04	3.082E-03	2.975E-03	1.923E-02
10	-9.667E-04	4.909E-03	-3.839E-03	2.711E-02
11	9.817E-04	4.909E-03	2.733E-03	2.711E-02
12	-9.810E-04	6.691E-03	-3.788E-03	3.328E-02
13	1.147E-03	7.066E-03	2.490E-03	3.437E-02
14	-1.034E-03	7.451E-03	-3.599E-03	3.547E-02
15	1.281E-03	9.314E-03	1.647E-03	4.132E-02
16	-1.048E-03	9.304E-03	-3.548E-03	4.116E-02
17	1.401E-03	1.183E-02	6.010E-04	4.639E-02
18	-1.182E-03	1.182E-02	-2.738E-03	4.627E-02
19	1.505E-03	1.458E-02	-5.912E-04	4.921E-02
20	-1.302E-03	1.457E-02	-1.724E-03	4.913E-02
21	1.596E-03	1.755E-02	-1.870E-03	4.946E-02
22	-1.407E-03	1.754E-02	-5.637E-04	4.942E-02
23	1.672E-03	2.068E-02	-3.173E-03	4.700E-02
24	-1.497E-03	2.068E-02	6.840E-04	4.698E-02
25	1.749E-03	2.396E-02	-4.476E-03	4.169E-02
26	-1.503E-03	2.339E-02	8.017E-04	4.265E-02
27	-1.526E-03	2.454E-02	1.233E-03	4.071E-02
28	1.800E-03	2.729E-02	-5.604E-03	3.540E-02
29	-1.532E-03	2.728E-02	1.350E-03	3.551E-02
30	1.839E-03	3.071E-02	-6.548E-03	2.670E-02
31	-1.582E-03	3.070E-02	2.450E-03	2.684E-02
32	1.867E-03	3.421E-02	-7.276E-03	1.603E-02
33	-1.621E-03	3.420E-02	3.368E-03	1.618E-02
34	1.884E-03	3.776E-02	-7.766E-03	3.869E-03
35	-1.649E-03	3.775E-02	4.072E-03	4.026E-03
36	1.893E-03	4.134E-02	-8.016E-03	-9.267E-03
37	-1.667E-03	4.133E-02	4.541E-03	-9.111E-03
38	1.893E-03	4.494E-02	-8.035E-03	-2.277E-02
39	-1.675E-03	4.493E-02	4.771E-03	-2.269E-02

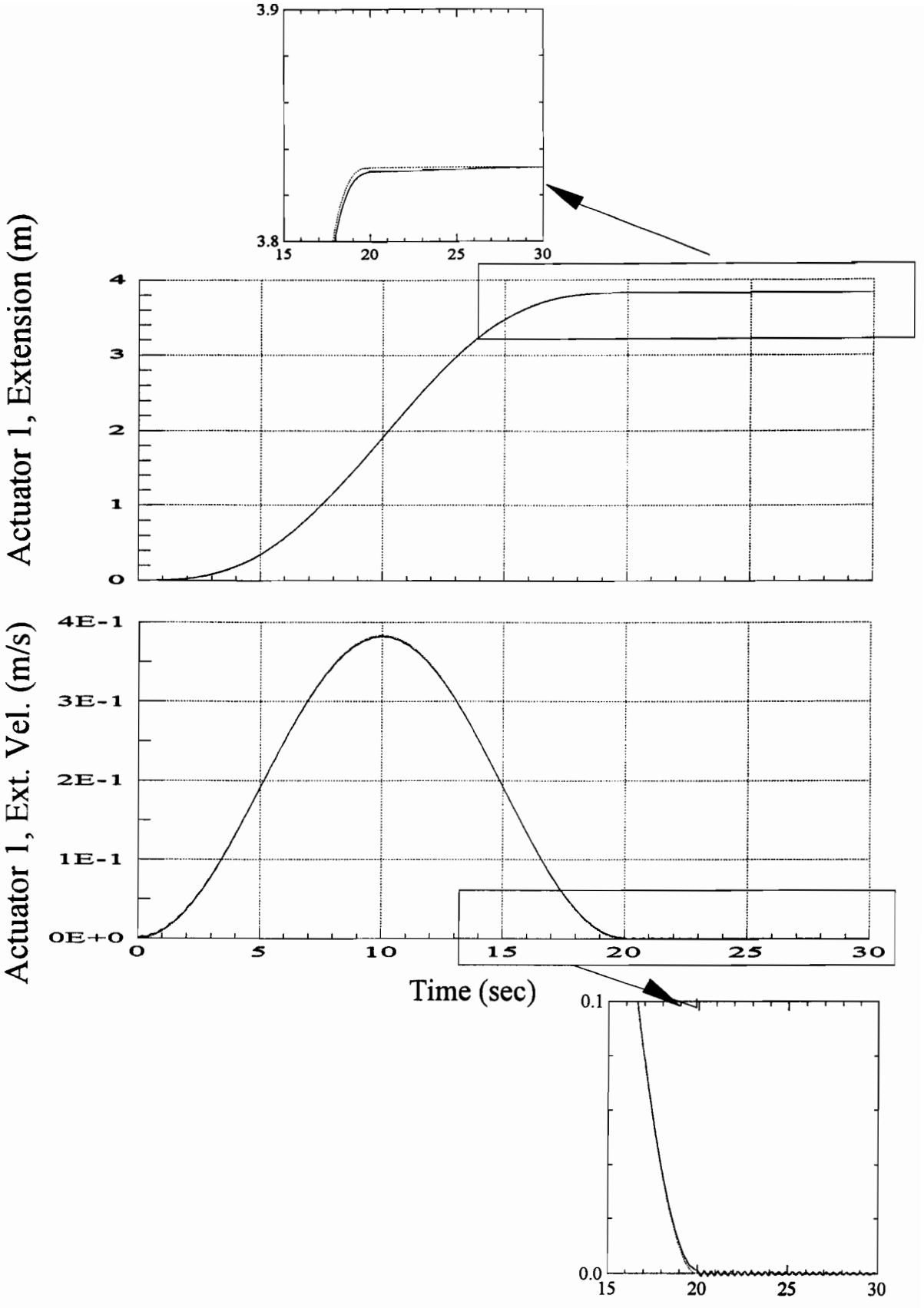

Figure 8.9: Actuator 1, flexible body forward dynamics extension trajectory.
(· · · · · · Prescribed trajectory of inverse dynamics, ——— Forward dynamics.)

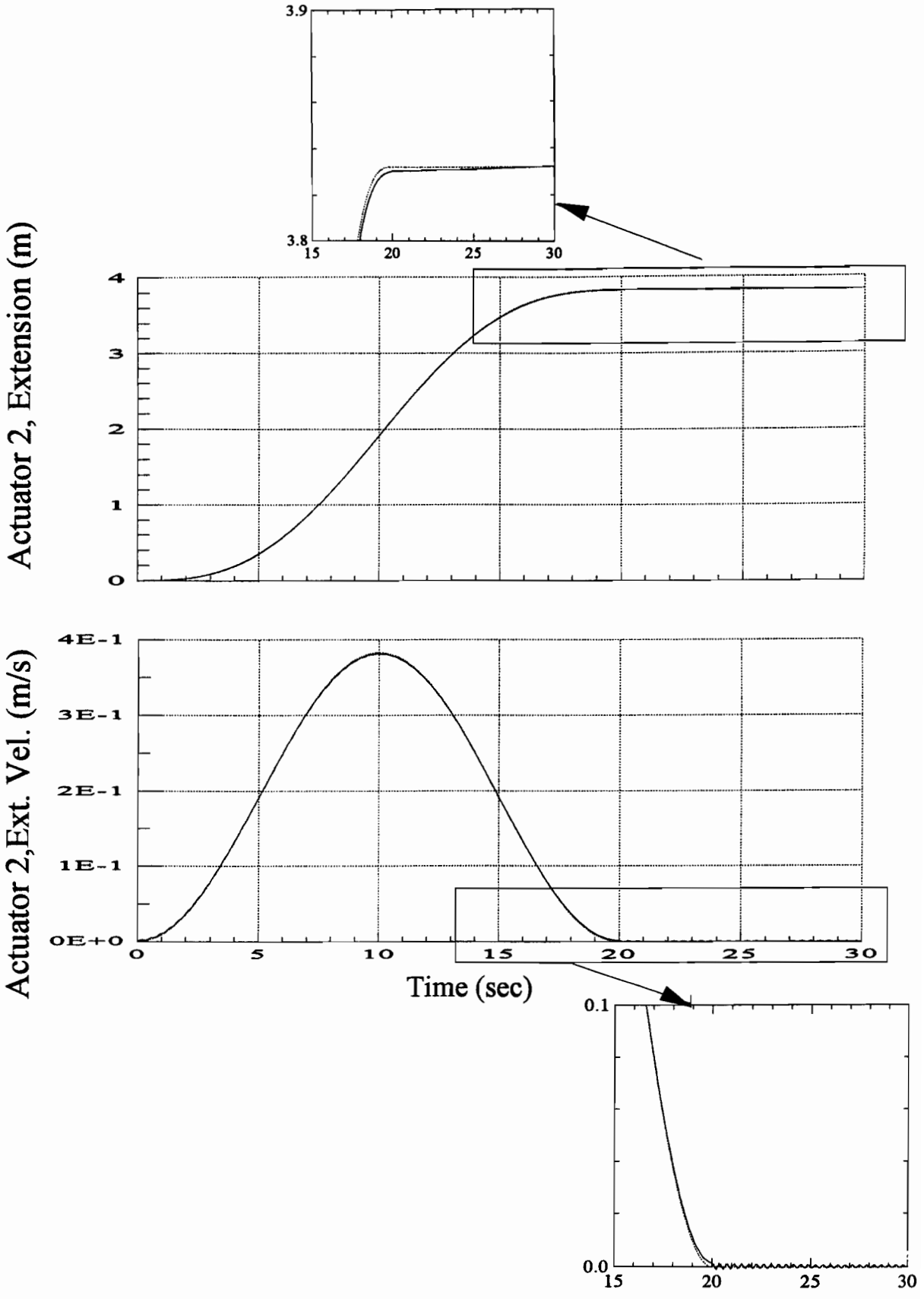

Figure 8.10: Actuator 2, flexible body forward dynamics extension trajectory. (· · · · · · Prescribed trajectory of inverse dynamics, ——Forward dynamics.)

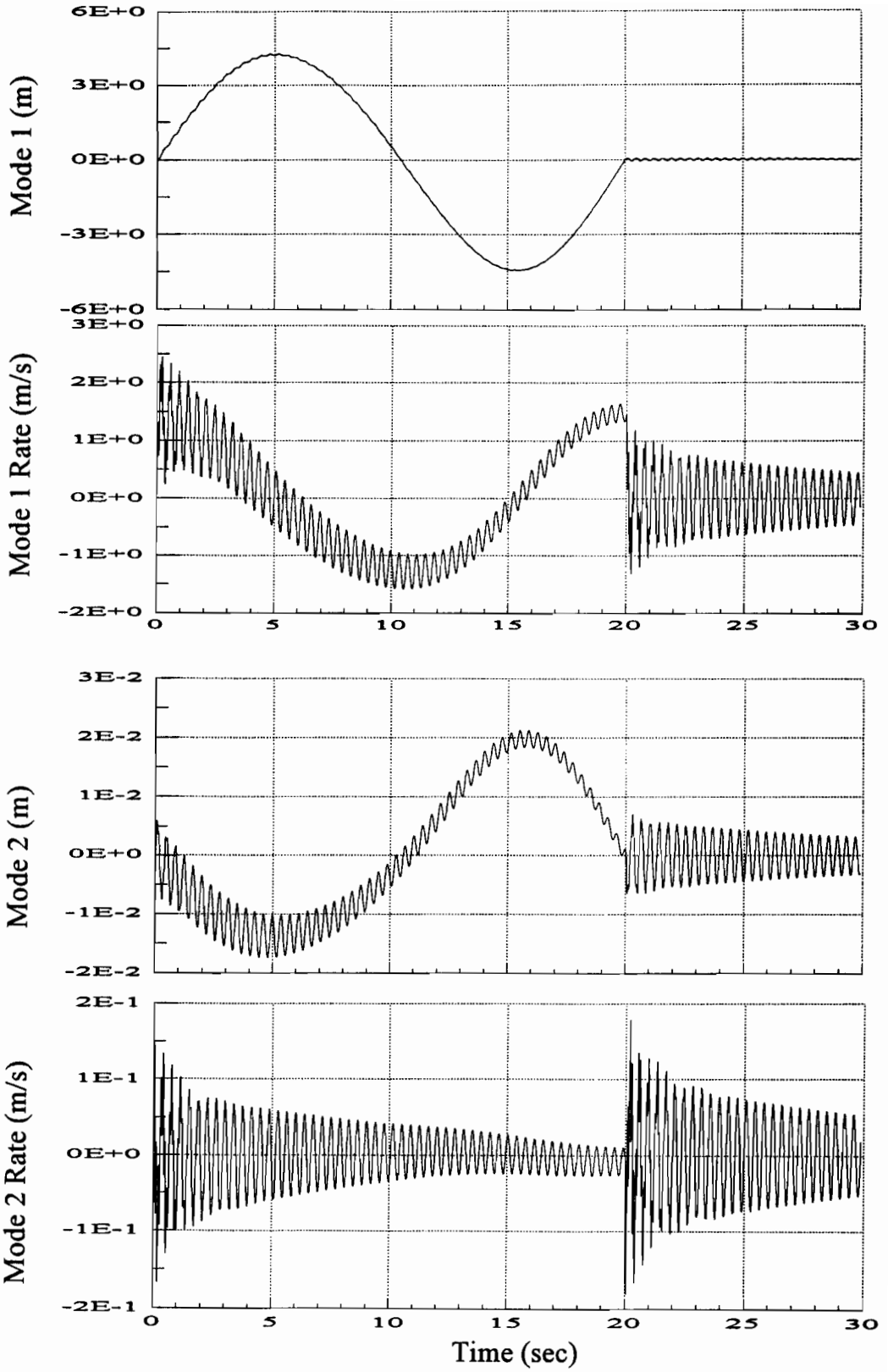

Figure 8.11: Vibration states of flexible body forward dynamics.

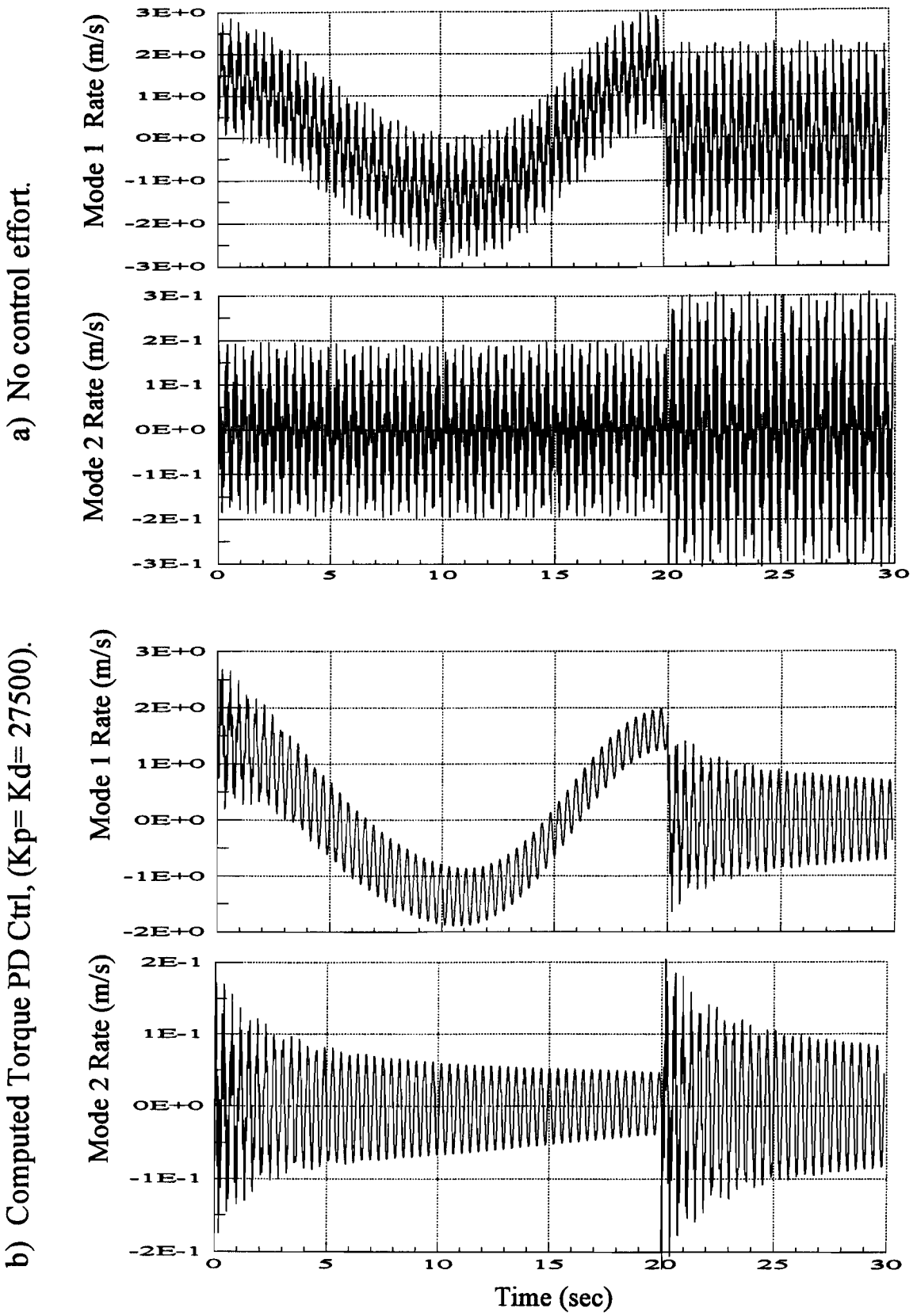

Figure 8.12: Vibration of a rotating truss beam.
(a) Without control. (b) With computed torque PD control.

in Fig. 8.14, and illustrate acceptable vibration control. However, it is cautioned that this may not always occur, since the controllability and the reduced-order model gains of the flexible modes varies with the orientation, as discussed in Section 6.2.

Simulation results for the truss motion considered later in Section 8.3 will more clearly demonstrate the vibration suppression of the reduced-order model vibration control, in which the computed torque PD control is not needed to stabilize the simulations of the forward dynamics. The following section considers the forward dynamics performed in a different manner.

Table 8.2: Vibration LQR control gains of the singular perturbation reduced model for the truss crane, computed at the final orientation (for maneuver time of 20 seconds).

Actuator	Mode #1		Mode #2	
	F_p	F_d	F_p	F_d
1	-2.2952E-9	-1.7665E-7	-8.8149E-9	-3.2608E-9
2	9.5991E-2	7.3881E0	3.6867E-1	1.3638E-1

8.2.5 Simulations with Prescribed Extension

As a matter of interest, the simulations of the flexible body forward dynamics were performed using **prescribed** actuator extension trajectories, and integrating the equations of motion to obtain the corresponding flexible modes. This in effect, assumes that the rigid body motion is not influenced by the flexible system. The corresponding flexible body actuation forces were also computed, and are provided in Fig. 8.15. The resulting vibrations obtained with the prescribed actuator extensions, are given in Fig. 8.16. It is noted that the vibrations persist after the maneuver, as is expected without structural damping or control. In addition, the observed vibration frequencies do not correspond to those of the true simulations of the forward dynamics performed previously, but are basically those of the eigenvalues presented in Table 8.1. This reflects the significance of the coupling between the rigid body and flexible body modes, and indicates the influence the former has upon the resulting flexible structure dynamics.

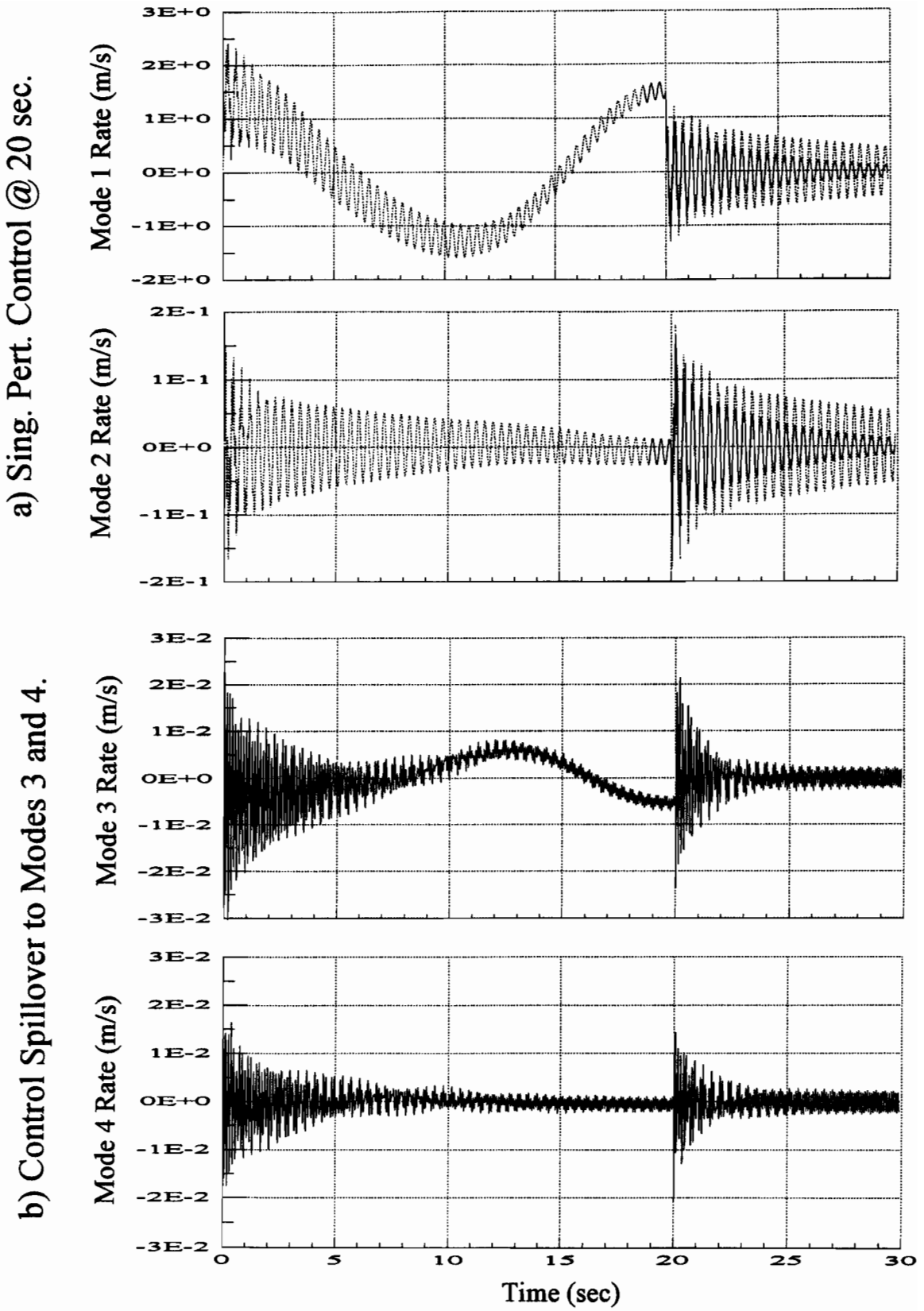

Figure 8.13: Singular perturbation control applied at 20 seconds.
(——With sing.pert.control, ····· Without sing.pert.control.)

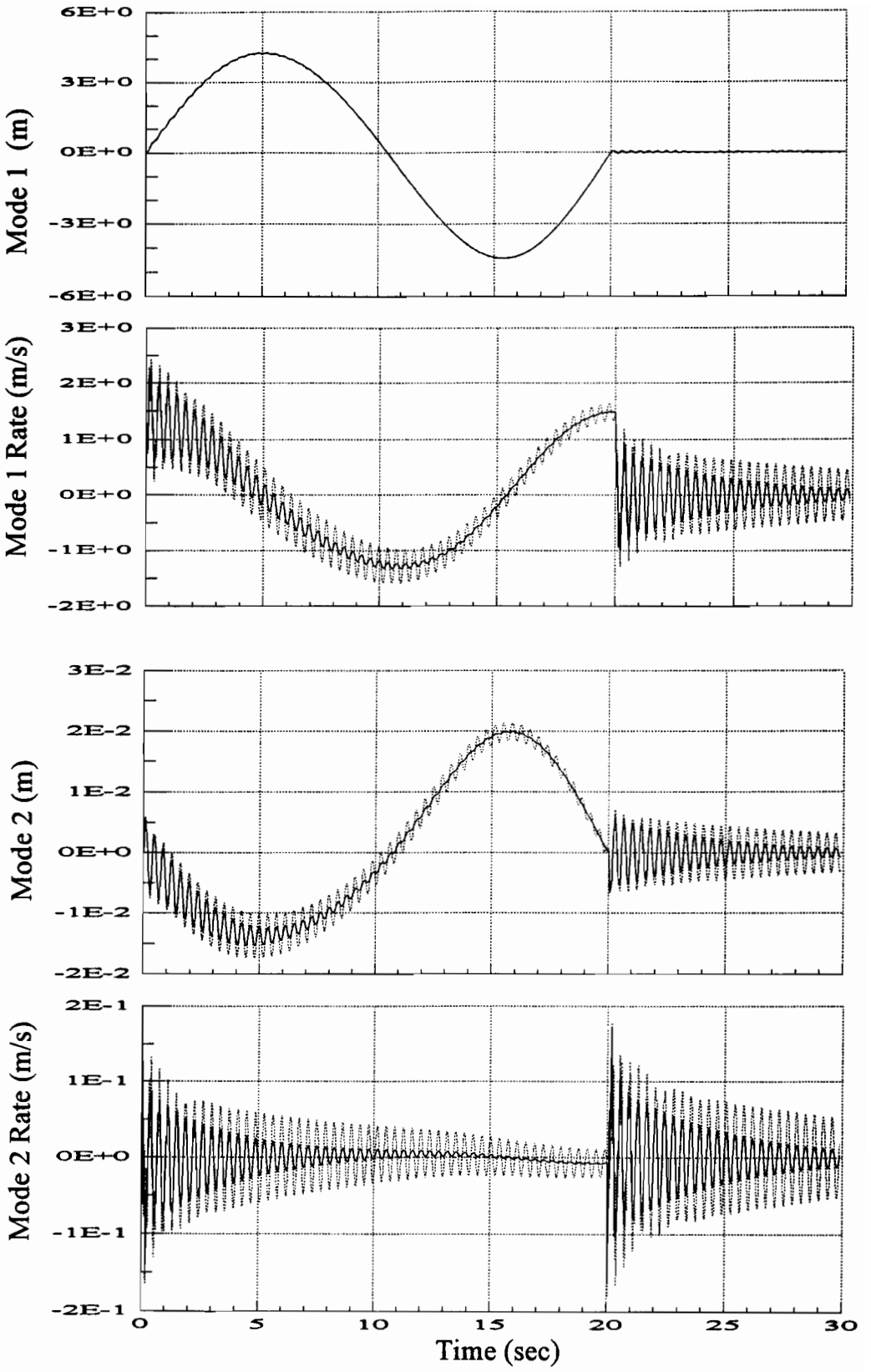

Figure 8.14: Singular perturbation control gains of 20 sec, applied at 0 sec. (———Sing.pert.control applied at 0 sec, · · · · · Without sing.pert.control.)

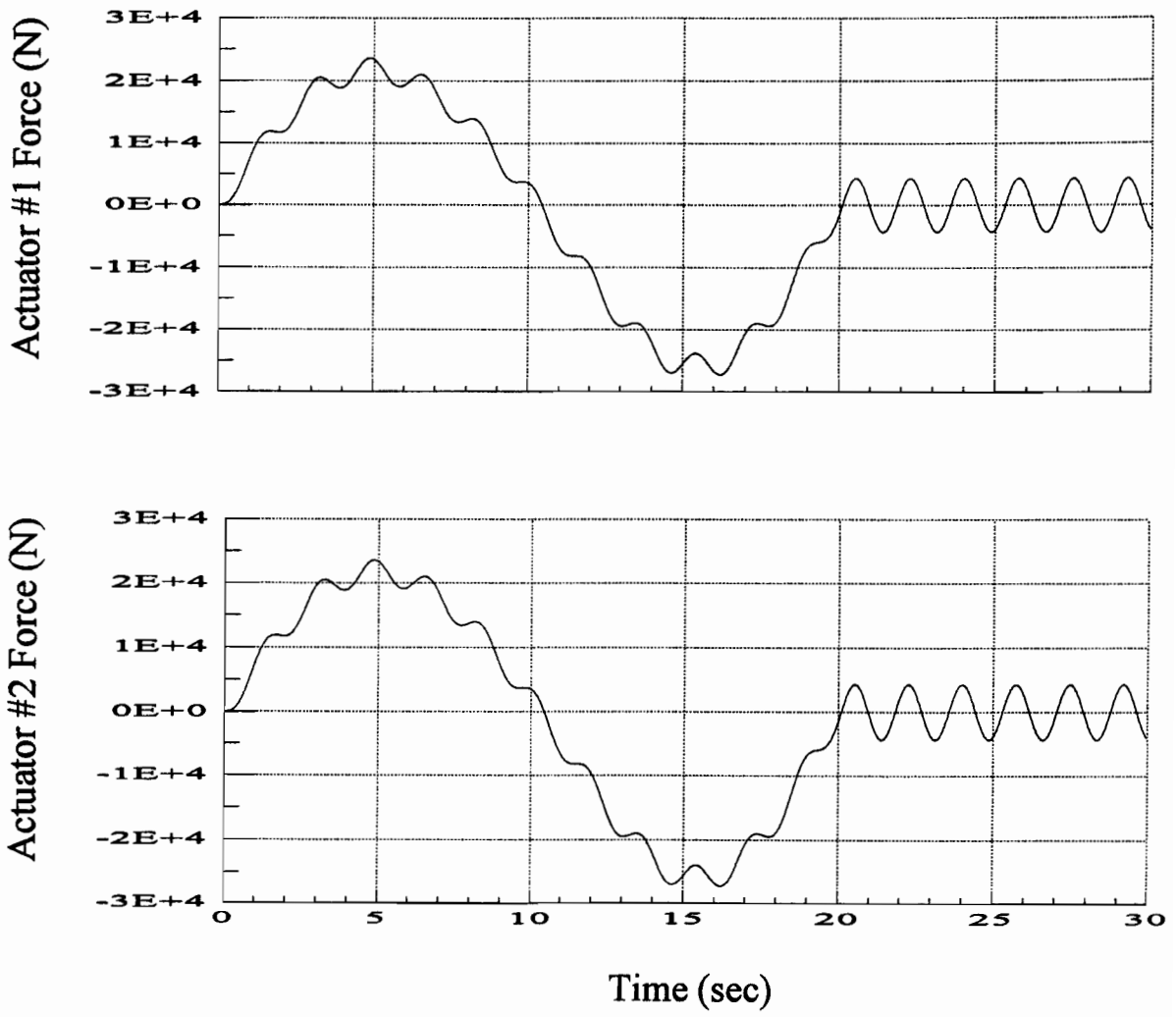

Figure 8.15: Actuator forces calculated by integrating only the flexible modes and using the prescribed actuator extension.

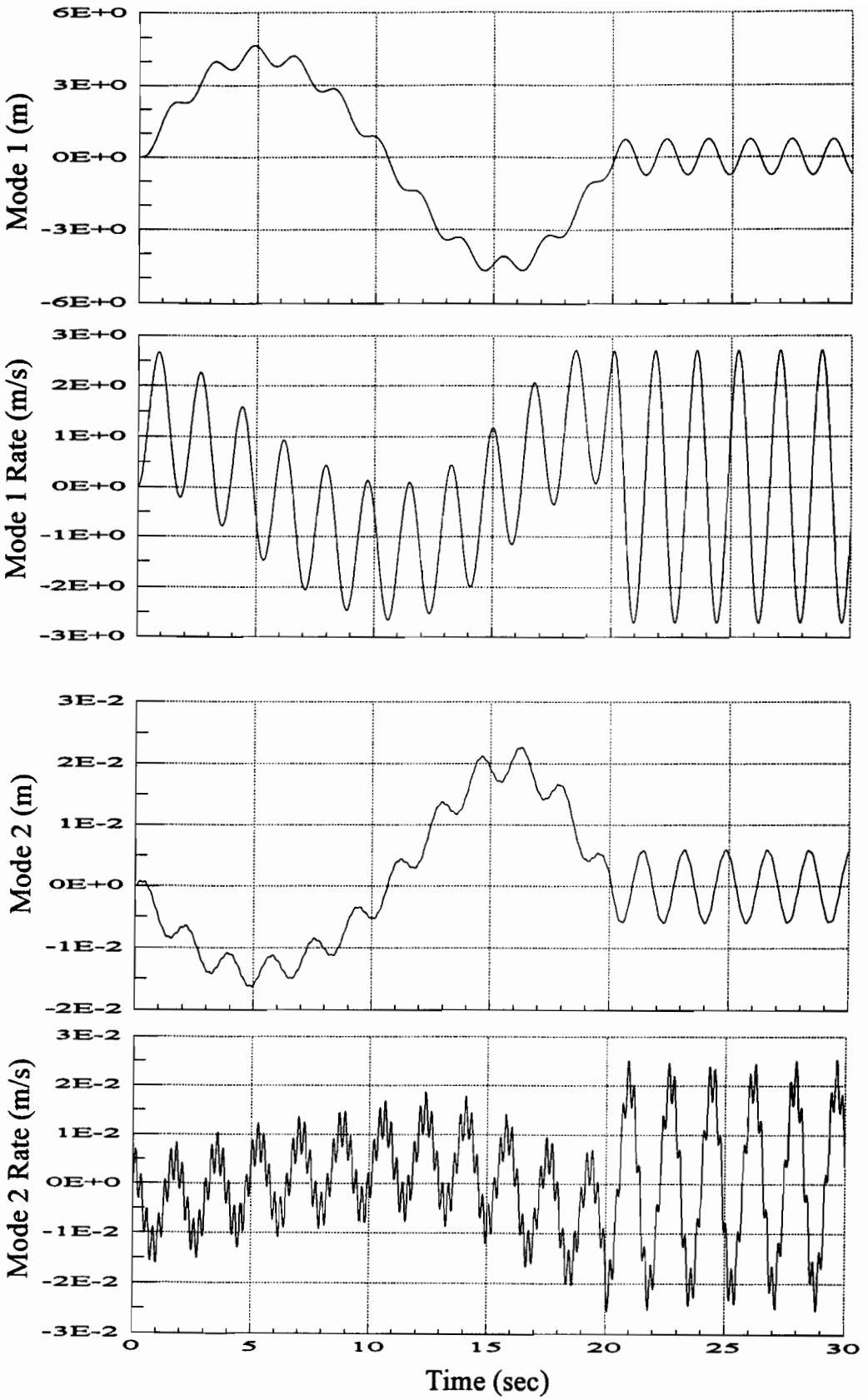

Figure 8.16: Vibration states when integrating only the flexible modes and using the prescribed actuator extension.

8.3 Single Actuated Maneuver

To demonstrate a truss crane arrangement for which simulation instabilities were not observed, and hence the forward dynamics are performed without computed torque PD control, only actuator 2 was activated per eq.(8.1) and Fig. 8.2, and actuator 1 was treated as a static (non-active) member. Therefore, the resulting structure has only one kinematic loop, and the configuration of Fig. 8.1a slews only 45 degrees clockwise. In addition, only half the angular acceleration and loading of the original crane is obtained (since actuator 1 is now inactive). The force of actuator 2 obtained from the inverse dynamics, is presented in Fig. 8.17a and was stored in an ASCII file at a rate of 0.01 seconds for the forward dynamics extrapolation. The simulations of the forward dynamics were observed to be stable for this case of the single kinematic loop, and hence no control of the maneuver was required. The simulation results of the flexible body dynamics are presented in the following section.

8.3.1 Flexible Body Simulations

Figure 8.18 presents the actuator extension of the flexible body forward dynamics, in which the slewing truss boom is again modelled by 2 modes, as contained previously in Table 8.1. The resulting vibration is illustrated in Fig. 8.19, in which no damping is observed, the high frequencies prevail, and the vibration persists as there is no control. Note that since the actuation magnitude of Fig.8.17a is approximately one half that of the previous Section 8.2.3, the vibration magnitudes are approximately one half those of Fig. 8.11.

8.3.2 Vibration Control Simulations

The vibration control simulations were again performed at the final maneuver time of 20 seconds. The corresponding LQR control gains for the flexible modes, are presented in Table 8.3. Since actuator 1 was given little control authority in the previous crane arrangement, it was expected that the control gains for actuator 2

should be similar to those of Table 8.2, as can be observed. Figure 8.17b presents the additional control force associated with this scheme, which is quite small compared to the magnitude of the nominal actuation force of the maneuver of Fig. 8.17a. The effectiveness of vibration suppression is illustrated in Fig. 8.20a for the rates of modes 1 and 2. As an initial control spillover check, Fig. 8.20b presents the rates for the uncontrolled modes 3 and 4. These are again suppressed, and destabilizing spillover is not observed.

The use of the vibration control gains (of the 20 second configuration) immediately at the start of the simulation, is examined in Fig. 8.21a. The corresponding actuation force is presented in Fig. 8.17c, which is again quite small in comparison to the magnitude of the nominal actuation force of the maneuver. However, it should be noted that the fast rates and small magnitude of the control force, imply fast response and very sensitive actuation. Hence, this vibration suppression scheme proves to be very effective, assuming ideal actuators with no operation limitations.

To examine the resulting vibrations obtained when introducing the computed torque PD control, which was needed to stabilize the simulations in Section 8.2, PD feedback gains of $K_p = K_d = 5000$ were implemented for actuator 2. Figure 8.21b presents these results, and confirms the vibration suppressing previously observed in Fig. 8.11 with this basic control scheme.

Table 8.3: Vibration LQR control gains of the singular perturbation reduced model for the truss crane with only actuator 2 active, computed at the final orientation (for maneuver time of 20 seconds).

Actuator	Mode #1		Mode #2	
	F_p	F_d	F_p	F_d
2	9.6015E-2	7.3882E0	3.6861E-1	1.3637E-1

8.3.3 Structurally Damped Vibrations

The effect of structural damping was examined by selecting a complex damping ratio ν as defined in Section 4.1.5. From Fig. 8.19, the lowest vibration frequency is noted to be approximately 2.725 Hz (17.12 rad/s). For damping ratios of the order $\zeta = 0.002$ and 0.01 (per that observed in the space truss structures of [Voth et al.'94] and [Soucy et al.'84]), the corresponding complex damping ratios are $\nu = 0.00024$ and 0.0012, as computed using eq.(4.65). Figure 8.22 illustrates the vibration suppression obtained with these two structural damping values. It is apparent from these results that inherent damping of these magnitudes are very desirable, and additional vibration control may not be necessary.

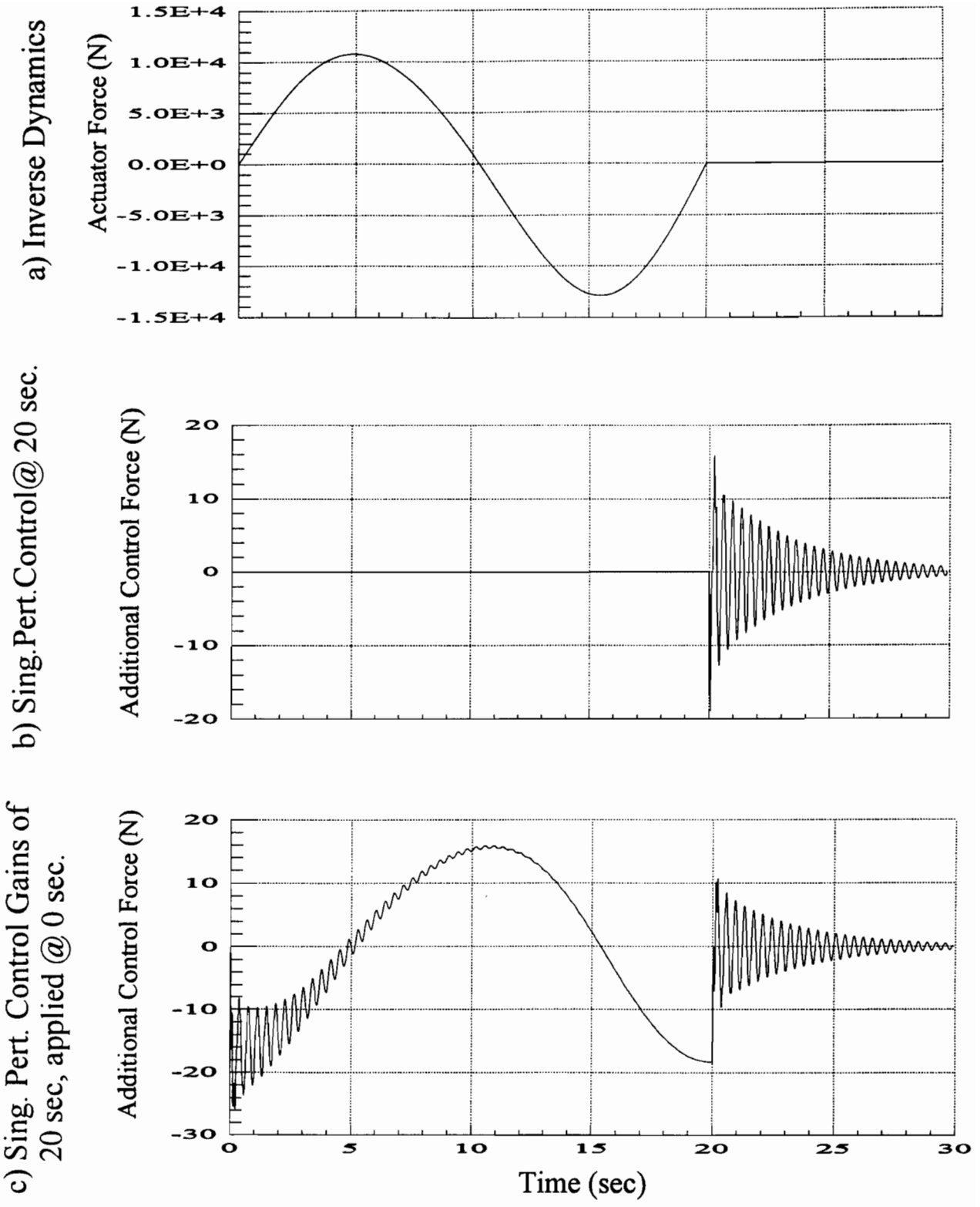

Figure 8.17: Actuator force trajectories of single acting actuator.
(a) Force of rigid body inv.dynamics. (b) Sing.pert.control force applied at 20 sec.
(c) Sing.pert.control force, using gains of 20 sec, applied at 0 sec.

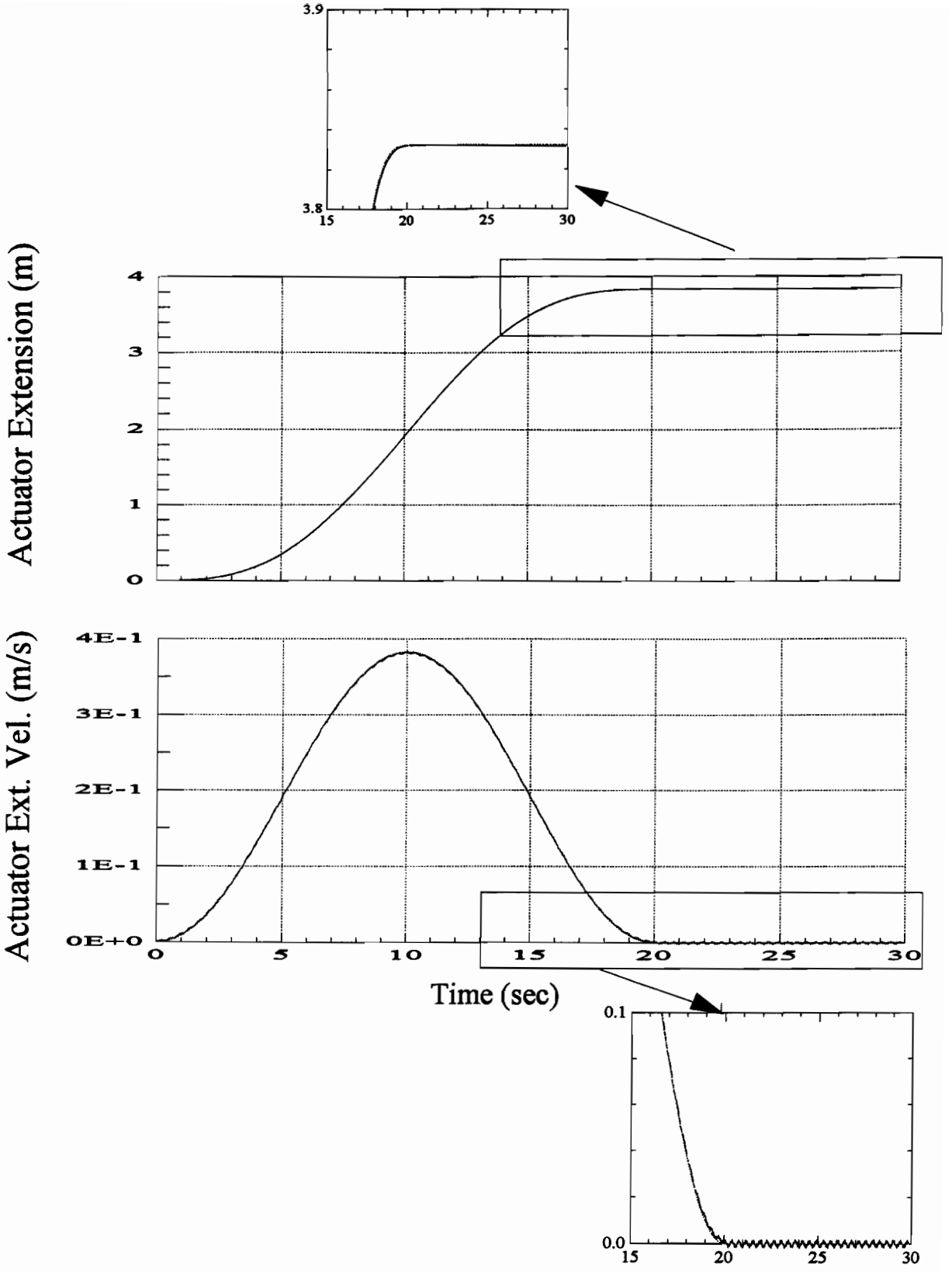

Figure 8.18: Extension trajectory for single acting actuator.
(· · · · · · Inv.dyn prescribed trajectory, ——Flexible body fwd.dyn.)

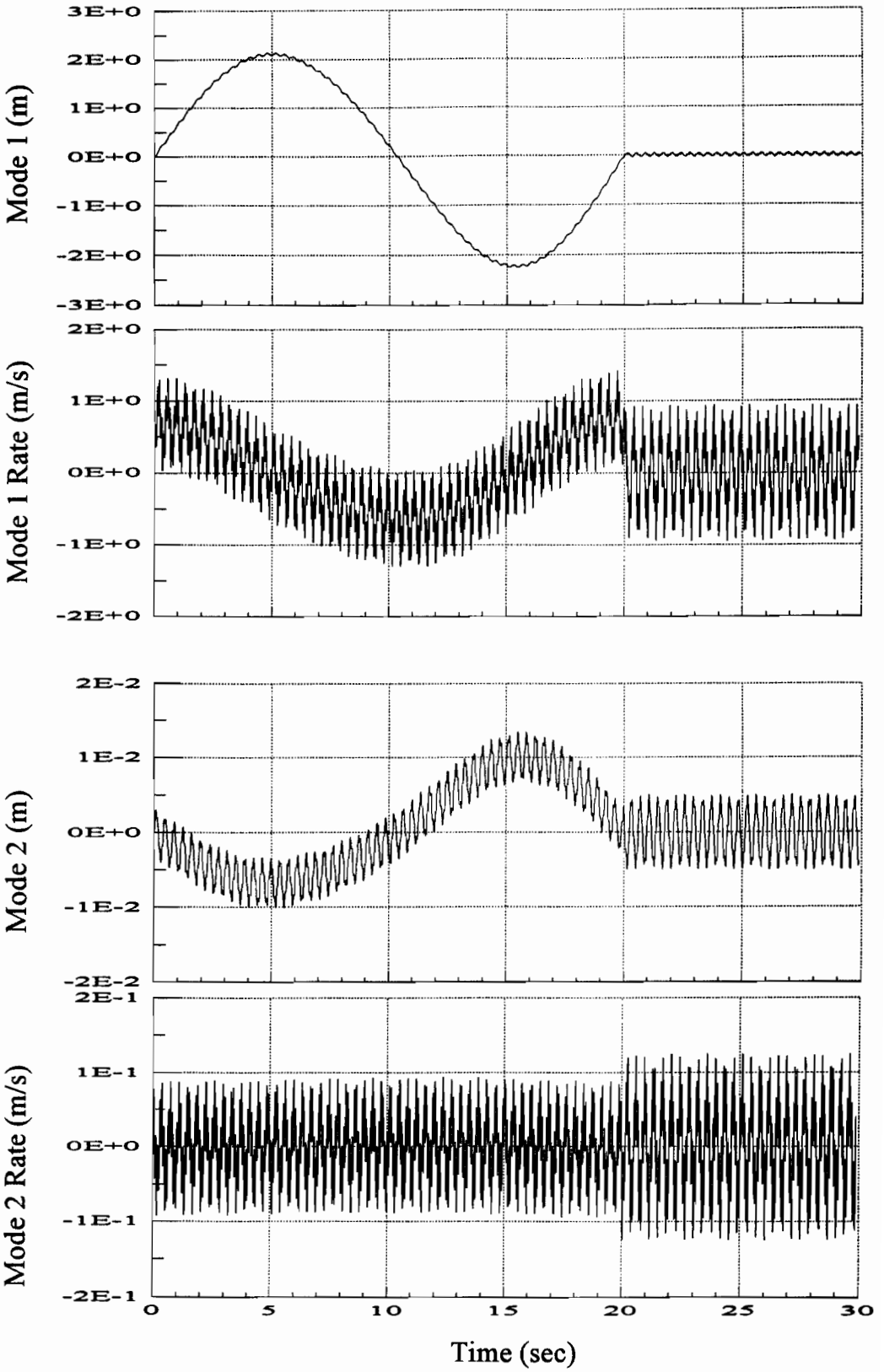

Figure 8.19: Vibration states for single acting actuator.

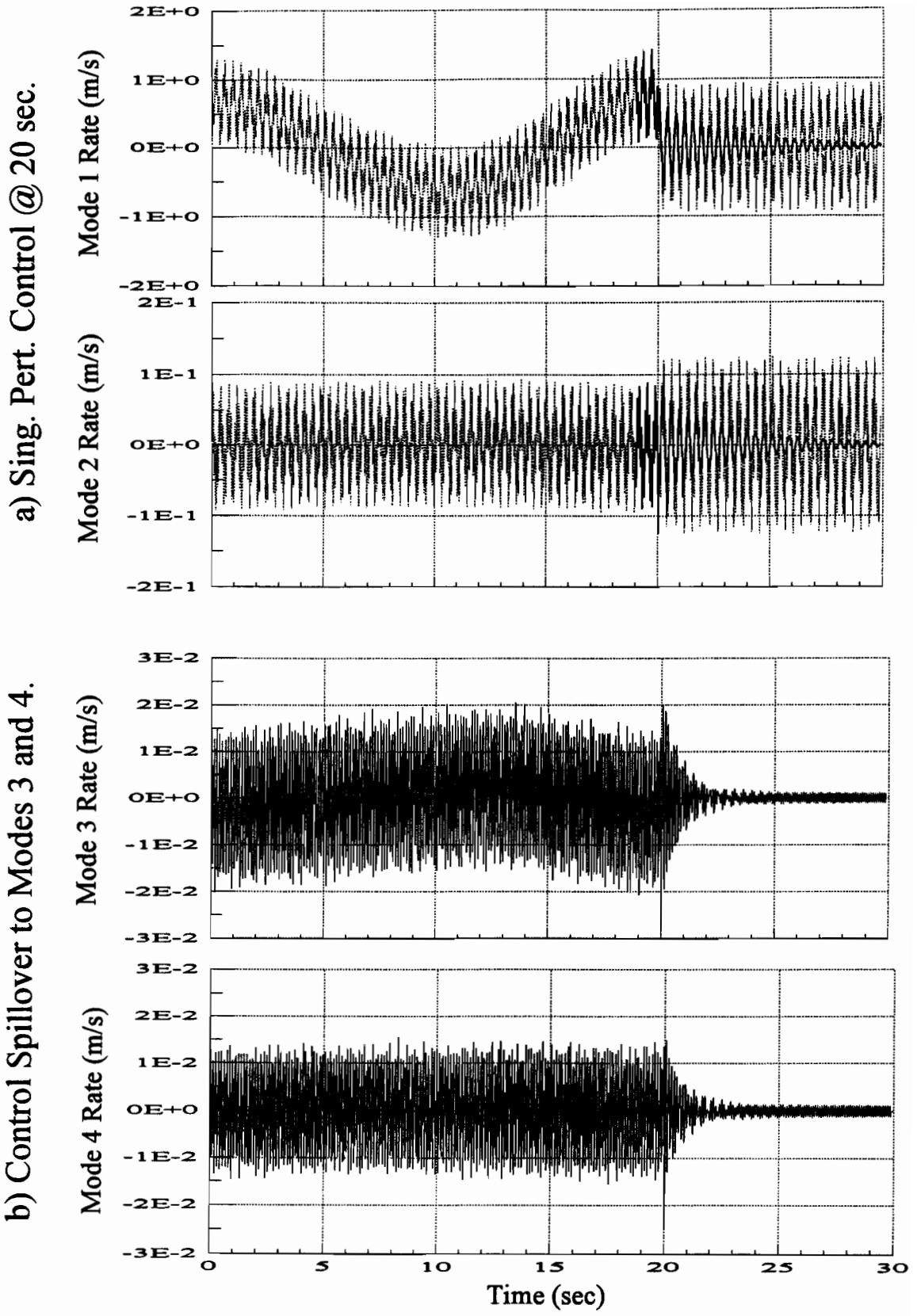

Figure 8.20: Singular pert. control applied at 20 sec for single acting actuator. (——With sing.pert.control, ····· Without sing.pert.control.)

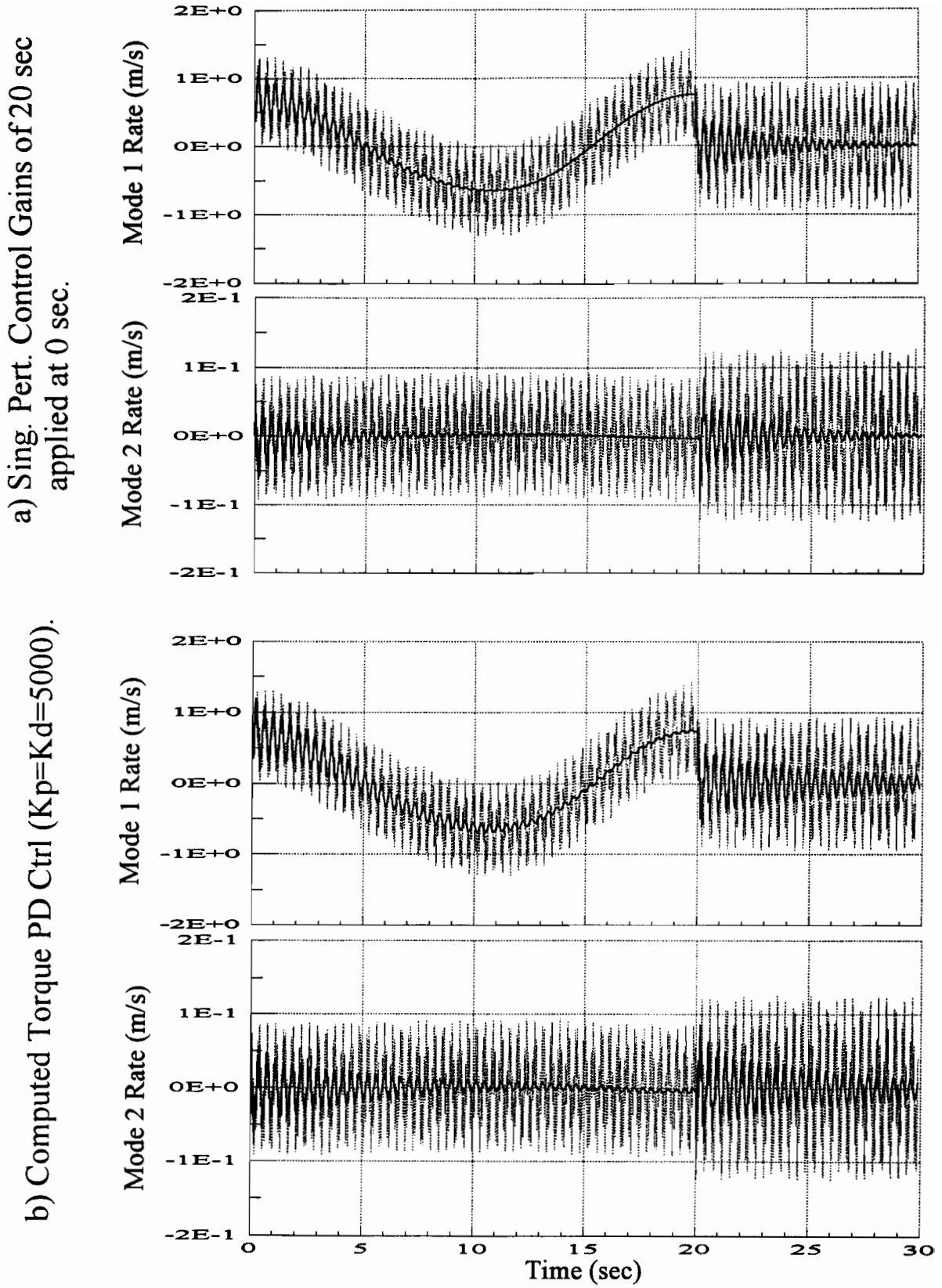

Figure 8.21: Vibration suppression with other control schemes.
(——With corresponding control, ····· Without control.)

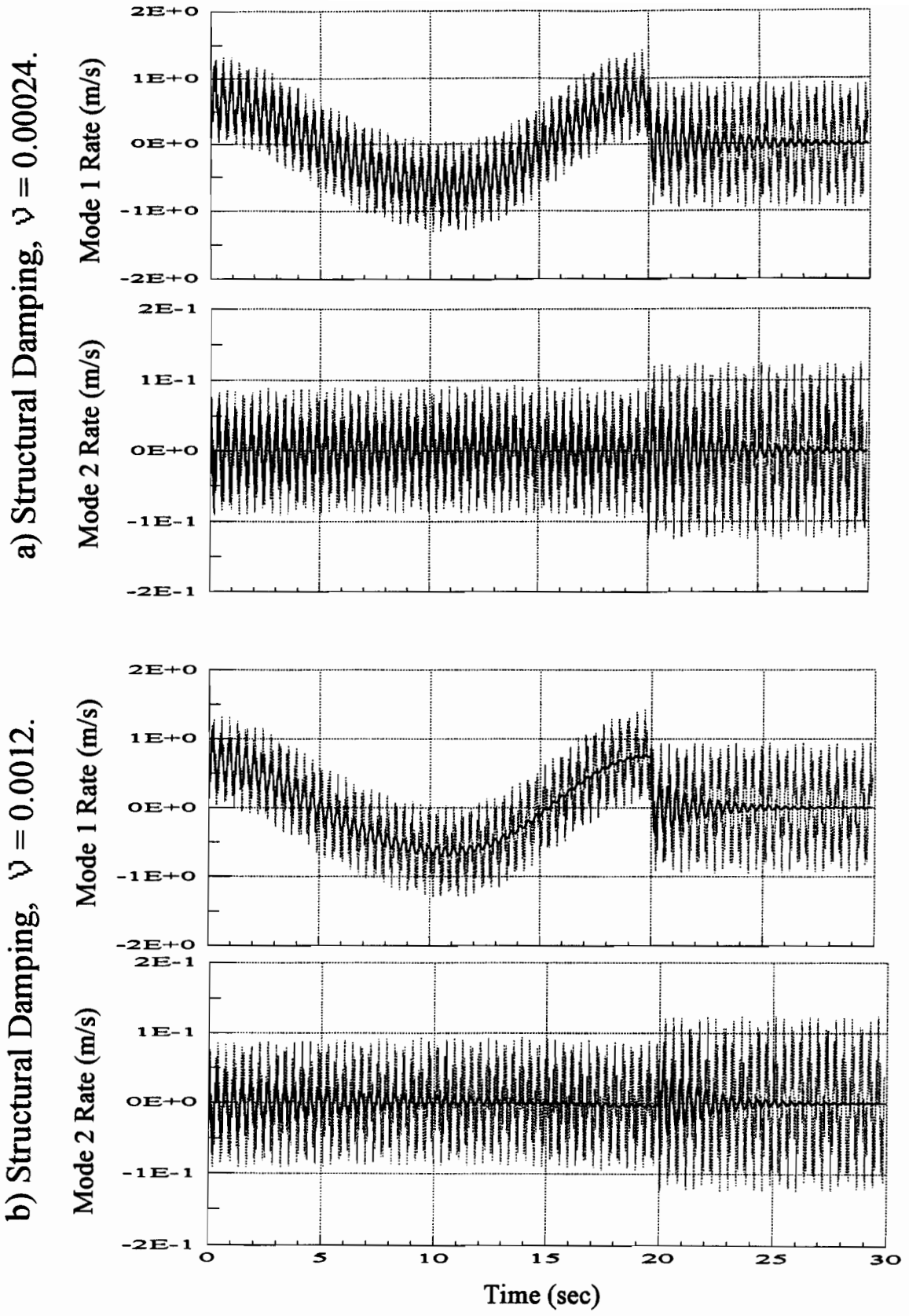

Figure 8.22: Vibration suppression with structural damping.
(——With damping, · · · · · · Without damping.)

Chapter 9

CLOSURE

9.1 Conclusions

The dynamic equations of motion for a specific articulating truss topology, were derived in this thesis. For the link connection, actuator installation, and resulting kinematic arrangement considered, the motion is confined to a plane. The actuator members are modelled as rigid, however, their treatment as individual links by the formulation will accommodate flexibility considerations for future work. Truss flexibility is modelled with linear axial deformation of the elements, and modal discretization of the corresponding nodal deformations was implemented to reduce the order the system. The dynamical formulation consisted of utilizing the modal discretization method along with the Euler-Lagrange equations, from which the equations of motion for an individual link were initially obtained in terms of its twist vector. By applying the natural orthogonal complement to the assembled system, the non-working constraint forces were eliminated to provide the minimum set of dynamical equations in terms of the actuators' (piston-rod) extensions, and the flexible (modal) coordinates of each truss link. If vibration frequencies of the flexible links are considerably greater than that of the rigid body motion, then reduced-order models can be obtained by applying the singular perturbation method, and a composite control strategy can be implemented. In this work, a robotic based computed torque with PD control scheme was selected for the main (quasi-static) maneuver, and the optimal LQR control gains

determined for a specific orientation of the truss crane was employed for the flexible modes. The control schemes were applied in a continuous fashion, hence, a discrete control system has not been considered.

The code GENMAN was developed to contain the simulation algorithm of the dynamical equations of motion for truss cranes. Simulations with planar arrangements of robotic manipulators were used to initially verify the results obtained with GENMAN. For the multi-loop kinematic arrangement associated with truss cranes, manual calculations were performed to verify the kinematic loop computations and the computed actuator forces of the simulated inverse dynamics. To simulate the forward dynamics, the actuator forces are computed off-line, that is, the inverse dynamics are initially performed for a prescribed extension trajectory of the actuators, and the computed actuator forces are saved to an ASCII file. The simulations of the forward dynamics then interpolate from this ASCII file to obtain the corresponding actuator forces.

Based on the simulations and dicussion presented for the truss crane models considered here, the following conclusions are presented,

1. The instabilities observed in simulating the rigid body forward dynamics of the multi-loop truss arrangement in Section 8.2, result when the actuator values computed from the inverse dynamics (which contain a non-zero mean of numerical errors) are integrated in the simulations of the forward dynamics to produce an unbounded response. This argument is made per the following considerations,

   (a) The instability is not an integrator instability since the Gear, Adams, and Runga-Kutta schemes experienced the same behaviour.

   (b) The simulations of the forward dynamics experienced opposite divergence when using ASCII files, of the off-line computed actuator forces, containing different storage rates.

(c) The introduction of the computed torque PD control scheme for the maneuver adequately stabilized the simulations, and the additional actuation was only of the order of 10^{-6} of the original maneuver actuation.

(d) When using prescribed actuator extension trajectories to perform the simulations of the flexible mode dynamics, the instabilities did not occur.

(e) For less complex manipulator arrangements, the numerical instabilities take longer to appear.

2. The introduction of the computed torque PD control scheme intended for the main maneuver, also provides damping of the vibration, as observed in the flexible body simulations.

3. The vibration control simulations performed here with the reduced-order models, did not consider the characteristic of the actuators, and assumed full-state feedback of the vibration modes. Therefore, the observed performance corresponds to ideal actuators with no limitations on their operation or on the feedback loops. (High operation bandwidths of the actuators would actually be required to damp the high frequency flexible modes.) In addition, the control was applied in a continuous fashion. The simulation results of this initial investigation indicate favorable vibration suppression. Although no destabilizing spillover was observed for the unmodelled modes examined, more unmodelled modes should be considered in future work.

4. When performing dynamic simulations of the flexible modes, in which the prescribed actuator extension trajectories are used directly, we do not observe the high vibration frequencies obtained during the simulations of the forward dynamics of the coupled rigid and flexible body motion.

5. Structural damping is most desirable, since it may alleviate the need for complex vibration control.

6. The code GENMAN is a simulation tool for the dynamic analysis of space cranes, confined to planar motion. Its flexibility model is restricted to the linear deformation of truss elements, and the structure arrangement must correspond to that of the actuator and link connection considered. Although GENMAN was executed on 486 PC's, the code is by no means optimal and the formulation it employs is computationally demanding. Therefore, such simulations should be performed on more powerfull platforms, namely with greater memory and processing capacity for large structural systems.

9.2 Recommendations

The following recommendations are made for future investigations regarding the dynamic simulation and vibration control of truss (crane) structures,

1. The link joint and inter-link kinematic details be extended to allow for the simulation of 3D motion.

2. Higher order deformation models be examined for the truss elements, to consider in-plane and out-of-plane bending and deformation of members.

3. Flexibility models of the actuator members be developed, especially since the dimensions of a truss boom are much greater than that of an individual actuator.

4. The reduced-order model is only valid when the vibration frequencies are greater than the frequency content of the rigid body motion trajectory. If this is not the case, then other vibration control schemes should be examined, and the installation of passive damping or active members into the local truss links be addressed.

5. Operation characteristics of typical actuators be considered, and digital control modelled, in order to fully assess the stability and performance of the control system.

Bibliography

[Amirouche'92] Amirouche, F.M.L, *Computational Methods in Multibody Dynamics*, 1992, Prentic Hall.

[Angeles'88] Angeles, J. *Rational Kinematics*, 1988, Springer-Verlag.

[Angeles et al.'88a] Angeles, J., and Lee, K. S., The formulation of dynamical equations of holonomic mechanical systems using natural orthogonal complements, *ASME Journal of Applied Mechanics*, 1988, Vol. 55, No. 1, pp 243-244.

[Angeles et al.'88b] Angeles, J., and Ma, O., Dynamic simulation of n-axis serial robotic manipulators using a natural orthogonal complement, *The International Journal of Robotics Research*, 1988, Vol. 7, No. 5, pp 32-47.

[Aoustin et al.'93] Aoustin, Y., and Chevallereau, C., The singular perturbation control of a two-flexible-link robot, *Proc. IEEE International Conference on Robotics and Automation*, May 2-6, 1993, Vol. 3, pp. 737-742.

[Baruh et al.'92] Baruh, H., and Boka, J., Issues in modal identification of flexible structures, *AIAA Journal*, 1992, Vol. 30, No. 1, pp. 214-225.

[Bathe'82] Bathe, K-J., *Finite Element Procedures in Engineering Analysis*, 1982, Prentice-Hall.

[Baycan et al.'92] Baycan, C.M., Utku, S., Das, S.K., and Wada, B.K., Optimal actuator placement in adaptive precision trusses, *AIAA/ASME/ASCE/AHS/ASC 33rd Structures, Structural Dynamics, and Materials Conference*,Paper 92-2344-CP, April 13-15, 1992, Dallas TX, pp. 418-423.

[Berry et al.'84] Berry, D.T., Yang, T.Y., Skelton, R.E., and Lafayette, W., Dynamics and control of lattice beams using complex and simplified finite element models, AIAA Paper 84-1043, 1984, pp. 422 - 430.

[Birdwell et al.'88] Birdwell, J. D., Bodenheimer, R. E., and Laub, A. J., *The Cascade Final Report: Volume III - Cascade Library Users' Guide*, 1988, Oak Ridge National Laboratory, U.S. Department of Energy, The University of Tennessee.

[Boutaghou et al.'90] Boutaghou, Z., Tamma, K., and Erdman, A., Continuous/ discrete modelling and analysis of elastic planar multi-body systems, *AIAA/ASME/ASCE/AHS/ASC 31st Structures, Structural Dynamics, and Materials Conference*, 1990, pp. 2101-2109.

[Chan et al.'90] Chan, J. K., and Modi, V. J., Dynamics and control of an orbiting flexible mobile manipulator, *Acta Astronautica*, 1990, Vol. 21, No. 11/12, pp. 759-769.

[Chang et al.'91] Chang, G.-S., and Chang, C.-H., Out-of-plane vibrations of plane frames, *Journal of Sound and Vibration*, 1991, Vol. 147, No.1, pp. 137-154.

[Chang et al.'91b] Chang, L.-W., and Hamilton, J. F., Dynamics of robotics manipulators with flexible links, *Transactions of the ASME*, 1991, Vol. 113, pp. 54-59.

[Chedmail et al.'91] Chedmail, P., Aoustin, Y., and Chevallereau, C., Modelling and control of flexible robots, *International Journal for Numerical Methods in Engineering*, 1991, Vol. 32, pp. 1595-1619.

[Chen et al.'90] Chen, G., and Wada, B.K., On an adaptive truss manipulator space crane concept, *First Joint U.S./Japan Conference on Adaptive Structures*, Wada et al.(Ed.'s), Nov. 13-15, 1990, Maui, Hawii, pp. 726-742.

[Chevallereau et al.'92] Chevallereau, C., and Aoustin, Y, Nonlinear control laws for a 2 flexible link robot: comparison of applicability domains, *Proc. 1992 IEEE International Conference on Robotics and Automation*, May 12-16 1992, pp. 748-753.

[Chow et al.'78] Chow, J. H., and Kokotovic, Petar V., Two-time-scale feedback design of a class of nonlinear systems, *IEEE Transactions on Automatic Control*, 1978, Vol. AC-23, No. 3, pp. 438-443.

[Cook'81] Cook, R. D., *Concepts and Applications of Finite Element Analysis*, John Wiley & Sons, New York, 1981.

[Craig'86] Craig, J., *Introduction to Robotics, Mechanics and Control*, Addison-Wesley, 1986.

[Crawley et al.'87] Crawley, E. F., and de Luis, J., Use of piezoelectric actuators as elements of intelligent structures, *AIAA Journal*, 1987, Vol. 25, No. 10, pp. 1373-1385.

[Cyril'88] Cyril, X., *Dynamics of Flexible Link Manipulators*, PhD Thesis, 1988, Department of Mechanical Engineering, McGill University.

[Cyril et al.'91] Cyril, X., Angeles, J., and Misra,A.K., Dynamics of flexible mechanical systems, *Transactions of the Canadian Society of Mechanical Engineering*, 1991, Vol.15, No. 3, pp. 235-256.

[Darcovitch'91] Darcovitch, J., *Dynamics of Single-Loop Mechanical Systems with Flexible Links*, 1991, Masters Thesis, Department of Mechanical Engineering, McGill University.

[Das et al.'89] Das, S. K., Utku, S., and Wada, B.K., Inverse dynamics of adaptive structures used as space cranes, *7th VPI & SU Symposium on Dynamics and Control of Large Structures*, May 1990, Blacksburg VA,.

[Das et al.'90a] Das, S. K., Utku, S., and Wada, B.K., Inverse dynamics of adaptive space cranes with tip point adjustment, *AIAA/ASME/ASCE/AHS/ASC 31st Structures, Structural Dynamics, and Materials Conference*, April 2-4, 1990, Long Beach CA, pp. 2367-2374.

[Das et al.'90b] Das, S. K., Utku, S., Chen, G.-S., and Wada, B.K., A mathematical basis for the design and design optimization of adaptive trusses in precision control, *First Joint U.S./Japan Conference on Adaptive Structures*, Wada et al.(Ed.'s), Nov. 13-15, 1990, Maui, Hawii, pp. 660-688.

[Das et al.'93] Das, S. K., Utku, S., Chen, G.S., and Wada, B.K., Optimal actuator placement in adaptive precision trusses, *Intelligent Structural Systems*, Tzou et al. (Ed.'s), Kluwer Academic Publishers, 1993, pp 325-357.

[Dorsey et al.'92] Dorsey, John T., Sutter, T.R., and Wu, K.C., A structurally adaptive space crane concept fo assembling space systems on orbit, *Third International Conference on Adaptive Structures*, Wada et al. (Ed.'s), Nov. 9-11, 1992, San Diego CA, pp. 352-371.

[Dosch et al.'92] Dosch, J.J., Leo, D.J., and Inman, D.J., Comparison of vibration control schemes for smart antenna, *IEEE Proceedings of the 31st Conference on Decision and Control*, 1992, pp. 1815-1820.

[Dunn'92] Dunn, H.J., Experimental results of active control on a large structure to suppress vibration, *Journal of Guidance, Control, and Dynamics*, 1992, Vol. 15, No. 6, pp. 1334-1341.

[Fattah et al.'94] Fattah, A., Misra, A.K., and Angeles, J., Modelling and simulation of planar mechanical systems with flexible links and multiple kinematic loops, *Machine Vibration*, 1994, Vol. 3, pp. 130-137.

[Friedland'86] Friedland, B., *Control System Design: An Introduction to State-Space Methods*, 1986, McGraw-Hill.

[Hollerbach'80] Hollerbach, M. J., A recursive Lagrangian formulation of manipulator dynamics and a comparative study of formulation complexity, *IEEE Journal of Systems, Man, and Cybernetics*, 1980, Vol. 10, No. 11, pp. 730-736.

[Hughes'79] Hughes, C. P., Dynamics of a chain of flexible bodies, *The Journal of Astronautical Sciences*, 1979, Vol. 27, No. 4, pp. 359-380.

[Hughes et al.'90] Hughes, P.C., Sincarsin, W.G., and Carroll,K.A., "TRUSSARM"-A variable-geometry-truss manipulator, *First Joint U.S./Japan Conference on Adaptive Structures*, Wada et al.(Ed.'s), Nov. 13-15, 1990, Maui, Hawii, pp. 715-725.

[Huston'90] Huston, R. L., Multibody dynamics formulations via Kane's equations, *Mechanics and Control of Large Flexible Structures*, Progress in Astronautics and Aeronautics, Junkins, J. L. (Editor), 1990, Vol. 129, pp. 71-86.

[Jaar'93] Jaar, G.J., *Dynamics and Control of a Spacecraft-Mounted Robot Capturing a Spinning Satellite*, M.Eng. Thesis, 1993, Department of Mechanical Engineering, McGill University.

[Jalihal et al.'92] Jalihal, P., Utku, S., and Wada, B.K., Optimal location of redundants for prestressing adaptive trusses with buckling considerations, *AIAA/ASME/ASCE/AHS/ASC 33rd Structures, Structural Dynamics,and Materials Conference*,Paper 92-2343-CP, April 13-15, 1992, Dallas TX, pp. 412-417.

[Jalihal et al.'93] Jalihal, P., Utku, S., and Wada, B.K., Actuator placement in prestressed adaptive trusses for vibration control, *AIAA/ASME/ASCE/AHS/ASC 34rd Structures, Structural Dynamics, and Materials Conference*, Paper 93-1694-CP, April 19-22, 1993, La Jolla CA, pp. 3312-3318.

[Kane et al.'65] Kane, R. T., and Wang, F. C., On the derivation of equations of motion, *Journal of the Society for Industrial and Applied Mathematics*, 1965, Vol. 13, No. 2, pp. 487-492.

[Karpurapu et al.'93] Karpurapu, R., and Yogendrakumar, M., A kinematic model for dynamic analysis of space frames, *Computers and Structures*, 1993, Vol. 47, No. 6, pp. 945-955.

[Kimball et al.'29] Kimbal, A.L., and Schenectady, N.Y., Vibration damping including the case of solid friction, *Transactions of the ASME*, 1929, Vol. 51, APM-51-21, pp. 227-236.

[Kokotovic'84] Kokotovic, Petar V., Applications of singular perturbation techniques to control problems, *SIAM Review*, 1984, Vol. 26, No. 4, pp. 501-550.

[Kokotovic'85] Kokotovic, Petar V., Recent trends in feedback design: an overview, *International Journal of Automatic Control*, 1985, Vol. 21, No. 3, pp. 225-236.

[Lammering et al.'94] Lammering, R., Jianhu, J.A., and Rogers, C.A., Optimal placement of piezoelectric actuators in adaptive truss structures, *Journal of Sound and Vibration*, 1994, Vol. 171, No. 1, pp. 67-85.

[Lewis et al.'93] Lewis, F. L., and Vandegrift, M., Flexible robot arm control by a feedback linearization/singular perturbation approach, *Proc. IEEE International Conference on Robotics and Automation*, May 2-6 1993, Vol. 3, pp. 729-736.

[Li'92] Li, D., A control design approach for slew maneuver of elastic multibody systems, *Proc. 1992 IEEE International Conference on Robotics and Automation*, May 12-16 1992,pp. 729-734.

[Lin et al.'92] Lin, Ying Jie., Osegueda, R.A., and Nemir, D.C., Dynamic adaptive stiffness motion control response to random excitations, *Third International Conference on Adaptive Structures*, Wada et al. (Ed.'s), 1992, pp. 277-287.

[Lu et al.'90] Lu, Lyan-Ywan, Utku, S., and Wada, B.K., Location selection for vibration controllers in space crane as adaptive structures, *AIAA/ASME/ASCE/AHS/ASC 31st Structures, Structural Dynamics, and Materials Conference*, Paper 90-1167, 1990, pp. 2375-2380.

[Lu et al.'92] Lu, Lyan-Ywan., Utku, S., and Wada, B.K., The control of large adaptive truss structures using direct output feedback, *Third International Conference on Adaptive Structures*, Wada et al. (Ed.'s), 1992, pp. 335-351.

[Luh et al.'80] Luh, J.Y.S, Walker, M.W., and Paul, R.P.C., On-line computational scheme for mechanical manipulators, *Journal of Dynamic Systems, Measurement, and Control* 1980, Vol. 102, pp. 69-76.

[Maghami et al.'93] Maghami, P.G., and Joshi, S.M., Sensor-actuator placement for flexible structures with actuator dynamics, *Journal of Guidance, Control, and Dynamics*, 1993, Vol. 16, No. 2, pp. 301-307.

[Marino et al.'86] Marino,R. and Kokotovic, Petar V., A geometric approach to composite control of two-time-scale systems, *IEEE Proc. of the 25th Conference on Decision and Control*, Dec. 1986, pp. 1397-1399.

[Meirovitch'80] Meirovitch, L., *Computational Methods in Structural Dynamics*, 1980, Sijthoff & Noordhoff.

[Meirovitch et al.'82] Meirovitch, L., and Baruh, H., Control of self-adjoint distributed-parameter systems, *Journal of Guidance, Control, and Dynamics*, 1982, Vol. 5, No. 1, pp. 60-66.

[Meirovitch et al.'85] Meirovitch, L., and Baruh, H., The implementation of modal filters for control of structures, *Journal of Guidance, Control, and Dynamics*, 1985, Vol. 8, No. 6, pp. 707-716.

[Meirovitch'90] Meirovitch, L., *Dynamics and Control of Structures*, 1990, John Wiley & Sons.

[Midha et al.'77] Midha, A., Erdman, A., and Frohrib, D., An approximate method for the dynamic analysis of elastic linkages, *ASME Journal of Engineering for Industry*, 1977, Vol. 99, No. 2, pp. 449-455.

[Midha et al.'79] Midha, A.,Erdman, A., and Frohrib, D., A computationally efficient numerical algorithm for the transient response of high speed elastic linkages, *ASME Journal of Mechanical Design*, 1979, Vol. 101, No. 1, pp. 138-148.

[Mikulas et al.'88a] Mikulas, M.M. Jr., and Dorsey, J.T., An integrated in-space construction facility for the 21st Century, *NASA TM 101515*, 1988.

[Mikulas et al.'88b] Mikulas, M.M. Jr., Davis, R.C., and Green, W.H., A space crane concept; preliminary design and static analysis, *NASA TM 101498*, Nov. 1988.

[Mikulas et al.'92] Mikulas, Martin M., Wada, B.K., Farhat, G.,and Withnell, P., Initially deformed truss geometry for improving the adaptive performance of

truss structures, *Third International Conference on Adaptive Structures*, Wada et al. (Ed.'s), 1992, pp. 305-319.

[Miura et al.'85] Miura, K., Furuya, H., and Suzuki, K., Variable geometry truss and its application to deployable truss and space crane arm, *Acta Astronautica*, 1985, Vol. 12, No. 7/8, pp. 599-607.

[Miura'93] Miura, K, Researches on adaptive structures in Japan, *44th Congress of the International Astronautical Federation*, 1993, October 16-22.

[Naccarato et al.'91] Naccarato, F.,and Hughes, P., Inverse kinematics of variable-geometry truss manipulators, *Journal of Robotic Systems*, 1991, Vol. 8, No. 2, pp. 249-266.

[Nagarajan et al.'90] Nagarajan, S., and Turcic, D.A., Lagrangian formulation of the equations of motion for elastic mechanisms with mutual dependence between rigid body and elastic motions. Part I: Element level equations. *Journal of Dynamic Systems, Measurement, and Control*, June 1990, Vol. 112, pp. 203-213.

[Naidu'88] Naidu, D.S. *Singular Perturbation Methodology in Control Systems*, IEE Control Engineering Series 34, Peter Peregrinus Ltd., 1988.

[Nashif et al.'85] Nashif, A. D., Jones, D.I., and Henderson, J.P, *Vibration Damping*, 1985, John Wiley & Sons.

[Natori et al.'92a] Natori, M. C., Shengyang H., Miura, Koh-ihi., Miura, Koryo., Sakamaki, M., Motion control of a variable geometry truss, *Third International Conference on Adaptive Structures*, Wada et al. (Ed.'s), Nov. 9-11, 1992, San Diego CA, pp. 573-589.

[Natori et al.'92b] Natori, M. C., Park, K. C., Chiou, J. C., and Namba, Haruyuki., Applications of adaptive structure concepts to construction of space systems in orbit: concepts and formulation, *Journal of Intelligent Materials, Systems and Structures*, 1992, Vol. 3, No. 4, pp. 719-734.

[Nayfeh'85] Nayfeh, A.H., Kinematics of foldable discrete space cranes, *NASA CR 176360*, 1985.

[Necib et al.'89] Necib, B., and Sun, C.T., Analysis of truss beams using a high order Timoshenko beam finite element, *Journal of Sound and Vibration*, 1989, Vol.130,No.1, pp. 149-159.

[Newland'89] Newland, D. E. *Mechanical Vibration Analysis and Computation*, 1989, Longman Scientific and Technical.

[Nikravesh'88] Nikravesh, P.E., *Computer-Aided Analysis of Mechanical Systems*, 1988, Prentice-Hall.

[Nikravesh et al.'85] Nikravesh, P.E., Wehage, R.A., and Kwon, O.K., Euler parameters in computational kinematics and dynamics. Part 1, *Transactions of the ASME*, 1985, Vol. 107, pp. 358-365.

[Park et al.'90] Park, K.C., Chiou, J.C., and Downer, J.D., Staggered solution procedures for multibody dynamics simulation, *Mechanics and Control of Large Flexible Structures*, Progress in Astronautics and Aeronautics, Junkins, J. L. (Editor), 1990, Vol. 129, pp. 183-210.

[Paul'81] Paul, R. *Robotic Manipulators*, 1981, MIT Press.

[Preumont et al.'90] Preumont, A., Sparavier, M., and Dufour, J., Application of piezoelectric actuators to the active damping of a truss structure, *AIAA/ASME/ASCE/AHS/ASC 31st Structures, Structural Dynamics, and Materials Conference*, 1990, pp. 1907-1913.

[Preumont et al.'92] Preumont, A., Dufour, J. and Malekin, C., Active damping by a local force feedback with piezoelectric actuators, *Journal of Guidance, Control, and Dynamics*, 1992, Vol. 15, No. 2, pp. 390-395.

[Ramesh et al.'91a] Ramesh,A.V., Utku, S., and Lu, L. Y., DETRANS: Efficient algorithm for static analysis of determinant trusses, *Journal of Aerospace Engineering*, 1991, Vol. 4, No. 3, pp. 274-285.

[Ramesh et al.'91b] Ramesh,A.V., Utku, S., and Wada, B. K., Real-time control of geometry and stiffness in adaptive structures, *Computer Methods in Applied Mechanics and Engineering*, 1991, Vol. 90, No. 1-3, pp. 761-779.

[Reisenauer et al.'92] Reisenauer, B.T., and Balas, M. J., ROM/RMF control of the flexible, articulated-truss space crane, *AIAA/ASME/ASCE/AHS/ASC 33rd Structures, Structural Dynamics, and Materials Conference*, Paper 92-2463-CP, April 13-15, 1992, Dallas TX, pp. 2127-2134.

[Rhodes et al.'85] Rhodes, M.D., and Mikulas, M.M., Jr., Deployable controllable geometry truss beam, *NASA TM 86366*, 1985.

[Sadigh'95] Sadigh, M. J., *Attitude Dynamics and Maneuvering of Flexible Space Systems*, PhD Thesis, 1995, Department of Mechanical Engineering, McGill University.

[Sener et al.'93] Sener, M.,Utku, S., and Wada, B.K., Geometry control in prestressed adaptive space trusses, *AIAA/ASME/ASCE/AHS/ASC 34th Structures, Structural Dynamics, and Materials Conference*, Paper 93-1676-CP, April 19-22, 1993, La Jolla CA, pp. 3172-3180.

[Sherwood'94] Sherwood, B., Fourth-generation Mars vehicle concepts, *Journal of Spacecraft and Rockets*, 1994, Vol. 31, No. 5, pp. 834-841.

[Siciliano et al.'86] Siciliano, B., Calise, A.J., and Jonnalagadda,V.R.P., Optimal output fast feedback in two-time scale control of flexible arms, *IEEE Proc. of the 25th Conference on Decision and Control*, Dec. 1986, pp. 1400-1404.

[Siciliano et al.'88] Siciliano, B.,and Book,W.J., A singular perturbation approach to control of lightweight flexible manipulators, *The International Journal of Robotics Research*, 1988, Vol. 7, No. 4, pp. 79-90.

[Singh et al.'85] Singh, R.P., Vander Voort, R.J., Likins, P.W., Dynamics of flexible bodies in tree topology - a computer-orientated approach. *Journal of Guidance*, 1985, Vol. 8, No. 5, pp. 584-590.

[Smith et al.'74] Smith, B. T., et al., *Matrix Eigensystem Routines - EISPACK Guide*, Lecture Notes in Computer Science, 1974, Springer-Verlag.

[Soucy et al.'84] Soucy, Y., and Vigneron, F. R., Identification of structural properties of a continuous longeron space mast, *AIAA/ASME/ASCE/AHS 25th Structures, Structural Dynamics, and Materials Conference*, Paper 84-0930, 1984, pp. 130-139.

[Sunada et al.'81] Sunada, W., and Dubowsky, S., The application of finite element methods to the dynamic analysis of flexible spatial and co-planar linkage systems, *ASME Journal of Mechanical Design*, 1981, Vol. 103, pp. 643-651.

[Sutter et al.'90] Sutter, T. R., and Bush, H.G., An articulated-truss space crane concept, *AIAA/ASME/ASCE/AHS/ASC 31st Structures, Structural Dynamics, and Materials Conference*, April 2-4, 1990, Long Beach CA, pp. 2117-2125.

[Sutter et al.'92] Sutter, T.R., Wu, C.K.,and Riutort,K.T., Structural characterization of a first-generation articulated-truss joint for space crane applications, *NASA TM 4371*, May 1992.

[Suzuki'81] Suzuki, M., Composite controls for singularly perturbed systems, *IEEE Transactions on Automatic Control*, 1981, Vol. AC-26, No. 2, pp. 505-507. 1988, Vol. 7, No. 4, pp. 79-90.

[Takahashi et al.'70] Takahashi, Y., Rabins, M. J., and Auslander, D. M., *Control and Dynamic Systems*, 1970, Addison-Wesley Publishing Company.

[Tongco et al.'94] Tongco, E., and Meldrum, D., Optimal sensor placement and active vibration suppression of large space structures, *AIAA Guidance, Navigation, and Control Conference*, Paper 94-3638-CP, August 1-3,1994, Scottsdale AZ, pp. 857-866.

[Ueno'92] Ueno, S., Optimal trajectories of a planar space crane as an adaptive structure, *Third International Conference on Adaptive Structures*, Wada et al. (Ed.'s), Nov. 9-11, 1992, San Diego CA, pp. 320-334.

[Umland et al.'92] Umland, J.W., and Chen, G.-S., Active member vibration control for a 4 meter primary reflector support structure, *AIAA/ASME/ASCE/AHS/ASC 33rd Structures, Structural Dynamics, and Materials Conference*, Paper 92-2341-CP, April 13-15, 1992, Dallas TX, pp. 393-401.

[Utku et al.'91a] Utku,S., Norris,C.H.,and Wilbur,J.B., *Elementary Structural Analysis, Fourth Edition*, 1991, McGraw-Hill.

[Utku et al.'91b] Utku, S., Ramesh, A. V., Das, S. K., Wada, B.K., and Chen G. S., Control of a slow-moving space crane as an adaptive structure, *AIAA Journal*, June 1991, Vol. 29, No. 6, pp. 961-967.

[Vail et al.'91] Vail, J. D., and Lake, M.S., Comparison of structural performance of one- and two-bay rotary joints for truss applications, *NASA TM 4282*, August 1991.

[Voth et al.'94] Voth, C.T.,Richards, K.E. Jr., Schmitz, E., Gehling, R.N., and Morgenthaler, D.R., Integrated active and passive control design methodology for the LaRC CSI evolutionary model, *NASA CR 4580*, April 1994.

[Wada'90] Wada, B.K., Adaptive structures: an overview, *Journal of Spacecraft and Rockets* 1990, Vol. 27, No. 3, pp. 330-337.

[Wada et al.'90] Wada, B.K., Fanson,J.,and Crawley, E., Adaptive structures, *Journal of Intelligent Materials, Systems and Structures*, 1990, Vol. 1, pp. 157-174.

[Wada et al.'92] Wada, B.K., and Utku, S., Adaptive structures for deployment / construction of structures in space, *AIAA/ASME/ASCE/AHS/ASC 33rd Structures, Structural Dynamics, and Materials Conference*, Paper 92-2339-CP, April 13-15, 1992, Dallas TX, pp. 379-385.

[Wu et al.'92] Wu, K.-C., and Sutter, T.R., Structural analysis of three space crane articulated-truss joint concepts, *NASA TM 4373*, May 1992.

Appendix A

Vector and Matrix Operations

Several mathematical properties regarding vectors, and the use of their skew symmetric matrices are provided here. The following relations are those presented in [Nikravesh'88].

Given 3D vectors **a** and **b**, which contain the components,

$$\mathbf{a} = \langle a_x \quad a_y \quad a_z \rangle^T \quad , \quad \mathbf{b} = \langle b_x \quad b_y \quad b_z \rangle^T \tag{A.1}$$

Their skew symmetric forms are denoted by $\tilde{\mathbf{a}}$ and $\tilde{\mathbf{b}}$, and constructed as,

$$\tilde{\mathbf{a}} = \begin{bmatrix} 0 & -a_z & a_y \\ a_z & 0 & -a_x \\ -a_y & a_x & 0 \end{bmatrix} \quad , \quad \tilde{\mathbf{b}} = \begin{bmatrix} 0 & -b_z & b_y \\ b_z & 0 & -b_x \\ -b_y & b_x & 0 \end{bmatrix} \tag{A.2}$$

As shown in [Nikravesh'88], the following properties exist,

$$\mathbf{a} \cdot \mathbf{b} = \mathbf{a}^T\mathbf{b} \tag{A.3}$$

$$\mathbf{a} \times \mathbf{b} = \tilde{\mathbf{a}}\mathbf{b} \tag{A.4}$$

$$\tilde{\mathbf{a}}^T = -\tilde{\mathbf{a}} \tag{A.5}$$

$$\frac{d}{dt}(\tilde{\mathbf{a}}\mathbf{b}) = \dot{\tilde{\mathbf{a}}}\mathbf{b} + \tilde{\mathbf{a}}\dot{\mathbf{b}} \tag{A.6}$$

$$\dot{\tilde{\mathbf{a}}} = \widetilde{\dot{\mathbf{a}}} \tag{A.7}$$

$$\widetilde{(\mathbf{a} + \mathbf{b})} = \tilde{\mathbf{a}} + \tilde{\mathbf{b}} \tag{A.8}$$

$$\widetilde{(\tilde{\mathbf{a}}\mathbf{b})} = \tilde{\mathbf{a}}\tilde{\mathbf{b}} - \tilde{\mathbf{b}}\tilde{\mathbf{a}} \tag{A.9}$$

$$\tilde{\mathbf{a}}\tilde{\mathbf{b}} = \mathbf{b}\mathbf{a}^T - \mathbf{a}^T\mathbf{b}\mathbf{1}_{33} \tag{A.10}$$

where $\mathbf{1}_{33}$ is the 3x3 unit matrix.

Appendix B

Link Mass Matrix Details

B.1 Truss Link Elements

The components of the elemental mass matrix from Section 4.1 for eq.(4.26)-(4.33), are evaluated in this section. Firstly, the expansion of the skew symmetric matrix $\tilde{\mathbf{r}}_i$ is considered using the vectors of eq.'s (4.7) and (4.9),

$$\mathbf{a}_o^j = \langle\, \mathbf{a}_{o,1}^{j\,T} \quad \mathbf{a}_{o,2}^{j\,T} \,\rangle^T \qquad , \qquad \mathbf{a}_e^j = \langle\, \mathbf{a}_{e,1}^{j\,T} \quad \mathbf{a}_{e,2}^{j\,T} \,\rangle^T \tag{B.1}$$

where, $\mathbf{a}_{o,1}^j$ and $\mathbf{a}_{o,2}^j$ are defined in eq.(4.8), and $\mathbf{a}_{e,1}^j$ and $\mathbf{a}_{e,2}^j$ are defined in eq.(4.10).

Using the linear shape function matrix of eq.(4.11) and the nodal vectors given above, we can rewrite eq.(4.2) as,

$$\begin{aligned} \mathbf{r}_i &= [\, N_1 \mathbf{1}_{33} \quad N_2 \mathbf{1}_{33} \,] \left(\begin{Bmatrix} \mathbf{a}_{o,1}^j \\ \mathbf{a}_{o,2}^j \end{Bmatrix} + \begin{Bmatrix} \mathbf{a}_{e,1}^j \\ \mathbf{a}_{e,2}^j \end{Bmatrix} \right) \\ &= N_1 \left(\mathbf{a}_{o,1}^j + \mathbf{a}_{e,1}^j \right) + N_2 \left(\mathbf{a}_{o,2}^j + \mathbf{a}_{e,2}^j \right) \end{aligned} \tag{B.2}$$

where $\mathbf{1}_{33}$ is the 3x3 unit matrix. Using the property of eq.(A.8), $\tilde{\mathbf{r}}_i$ is given as,

$$\tilde{\mathbf{r}}_i = \left[N_1 \left(\tilde{\mathbf{a}}_{o,1}^j + \tilde{\mathbf{a}}_{e,1}^j \right) + N_2 \left(\tilde{\mathbf{a}}_{o,2}^j + \tilde{\mathbf{a}}_{e,2}^j \right) \right] \tag{B.3}$$

where the tilda indicates the skew symmetric matrix of the vector, as defined in eq.(A.2). With this result, mass matrix component $\mathbf{M}_{dr}^j$ from eq.(4.26) becomes,

$$\mathbf{M}_{dr}^j = -\rho^j \left[\left(Q_1^j \tilde{\mathbf{a}}_{o,1}^j + Q_2^j \tilde{\mathbf{a}}_{o,2}^j \right) + \left(Q_1^j \tilde{\mathbf{a}}_{e,1}^j + Q_2^j \tilde{\mathbf{a}}_{e,2}^j \right) \right] \tag{B.4}$$

where,

$$\begin{array}{rcccl} Q_1^j & = & \int_{\forall j} N_1 d\forall & = & \int_{\forall j} (1 - x^j/L^j)\, d\forall \\ Q_2^j & = & \int_{\forall j} N_2 d\forall & = & \int_{\forall j} (x^j/L^j)\, d\forall \end{array} \tag{B.5}$$

For mass matrix $\mathbf{M}_{de}^j$, we obtain after expanding the expression of eq.(4.27),

$$\begin{aligned} \mathbf{M}_{de}^j &= \rho^j \int_{\forall j} \mathbf{N}^j d\forall \\ &= \rho^j \int_{\forall j} [\, N_1 \mathbf{1}_{33} \quad N_2 \mathbf{1}_{33}\,]\, d\forall \end{aligned} \tag{B.6}$$

Therefore, substituting the integrals evaluated in eq.(B.5) into the above, yields,

$$\mathbf{M}_{de}^j = \rho^j \,[\, Q_1^j \mathbf{1}_{33} \;\;,\;\; Q_2^j \mathbf{1}_{33}\,] \tag{B.7}$$

To evaluate the terms of $\mathbf{M}_{rr}^j$ in eq.(4.29), it is necessary to expand $\tilde{\mathbf{r}}_i^2$, which is given as,

$$\begin{aligned} \tilde{\mathbf{r}}_i^2 &= (N_1)^2(\tilde{\mathbf{a}}_{o,1}^j + \tilde{\mathbf{a}}_{e,1}^j)^2 + N_1N_2(\tilde{\mathbf{a}}_{o,1}^j + \tilde{\mathbf{a}}_{e,1}^j)(\tilde{\mathbf{a}}_{o,2}^j + \tilde{\mathbf{a}}_{e,2}^j) \\ &\quad + N_1N_2(\tilde{\mathbf{a}}_{o,2}^j + \tilde{\mathbf{a}}_{e,2}^j)(\tilde{\mathbf{a}}_{o,1}^j + \tilde{\mathbf{a}}_{e,1}^j) + (N_2)^2(\tilde{\mathbf{a}}_{o,2}^j + \tilde{\mathbf{a}}_{e,2}^j)^2 \end{aligned} \tag{B.8}$$

Therefore, mass matrix component $\mathbf{M}_{rr}^j$ becomes,

$$\begin{aligned} \mathbf{M}_{rr}^j &= -\rho^j \Big[S_{11}^j (\tilde{\mathbf{a}}_{o,1}^j + \tilde{\mathbf{a}}_{e,1}^j)^2 + S_{12}^j (\tilde{\mathbf{a}}_{o,1}^j + \tilde{\mathbf{a}}_{e,1}^j)(\tilde{\mathbf{a}}_{o,2}^j + \tilde{\mathbf{a}}_{e,2}^j) \\ &\quad + S_{12}^j (\tilde{\mathbf{a}}_{o,2}^j + \tilde{\mathbf{a}}_{e,2}^j)(\tilde{\mathbf{a}}_{o,1}^j + \tilde{\mathbf{a}}_{e,1}^j) + S_{22}^j (\tilde{\mathbf{a}}_{o,2}^j + \tilde{\mathbf{a}}_{e,2}^j)^2 \Big] \end{aligned} \tag{B.9}$$

where the shape function integrals are evaluated as,

$$\begin{array}{rcccl} S_{11}^j & = & \int_{\forall j} (N_1)^2 d\forall & = & \int_{\forall j} (1 - x^j/L^j)^2\, d\forall \\ S_{12}^j & = & \int_{\forall j} N_1 N_2 d\forall & = & \int_{\forall j} (1 - x^j/L^j)\,(x^j/L^j)\, d\forall \\ S_{22}^j & = & \int_{\forall j} (N_2)^2 d\forall & = & \int_{\forall j} (x^j/L^j)^2\, d\forall \end{array} \tag{B.10}$$

Mass matrix component $\mathbf{M}_{re}^j$ from eq.(4.30) will be evaluated by first expanding,

$$\begin{aligned} \tilde{\mathbf{r}}_i \mathbf{N}_e^j &= \left[N_1 \left(\tilde{\mathbf{a}}_{o,1}^j + \tilde{\mathbf{a}}_{e,1}^j \right) + N_2 \left(\tilde{\mathbf{a}}_{o,2}^j + \tilde{\mathbf{a}}_{e,2}^j \right) \right] [\, N_1 \mathbf{1}_{33}, \quad N_2 \mathbf{1}_{33}\,] \\ &= \left[\left((N_1)^2 \tilde{\mathbf{a}}_{o,1}^j + N_1 N_2 \tilde{\mathbf{a}}_{o,2}^j \right), \quad \left(N_1 N_2 \tilde{\mathbf{a}}_{o,1}^j + (N_2)^2 \tilde{\mathbf{a}}_{o,2}^j \right) \right] \\ &+ \left[\left((N_1)^2 \tilde{\mathbf{a}}_{e,1}^j + N_1 N_2 \tilde{\mathbf{a}}_{e,2}^j \right), \quad \left(N_1 N_2 \tilde{\mathbf{a}}_{e,1}^j + (N_2)^2 \tilde{\mathbf{a}}_{e,2}^j \right) \right] \end{aligned} \tag{B.11}$$

Hence, $\mathbf{M}^j_{re}$ becomes,

$$\begin{aligned}\mathbf{M}^j_{re} &= \rho^j \left[\left(S^j_{11}\tilde{\mathbf{a}}^j_{o,1} + S^j_{12}\tilde{\mathbf{a}}^j_{o,2} \right), \quad \left(S^j_{12}\tilde{\mathbf{a}}^j_{o,1} + S^j_{22}\tilde{\mathbf{a}}^j_{o,2} \right) \right] \\ &+ \rho^j \left[\left(S^j_{11}\tilde{\mathbf{a}}^j_{e,1} + S^j_{12}\tilde{\mathbf{a}}^j_{e,2} \right), \quad \left(S^j_{12}\tilde{\mathbf{a}}^j_{e,1} + S^j_{22}\tilde{\mathbf{a}}^j_{e,2} \right) \right] \end{aligned} \tag{B.12}$$

Finally, from the expansion of,

$$\begin{aligned}(\mathbf{N}^j_e)^T\mathbf{N}^j_e &= \begin{bmatrix} N_1\mathbf{1}_{33} \\ N_2\mathbf{1}_{33} \end{bmatrix} [\, N_1\mathbf{1}_{33}, \quad N_2\mathbf{1}_{33} \,] \\ &= \begin{bmatrix} (N_1)^2\mathbf{1}_{33}, & N_1N_2\mathbf{1}_{33} \\ N_1N_2\mathbf{1}_{33}, & (N_2)^2\mathbf{1}_{33} \end{bmatrix} \end{aligned} \tag{B.13}$$

the mass component $\mathbf{M}^j_{ee}$ from eq.(4.33) becomes,

$$\mathbf{M}^j_{ee} = \rho^j \begin{bmatrix} S^j_{11}\mathbf{1}_{33}, & S^j_{12}\mathbf{1}_{33} \\ S^j_{12}\mathbf{1}_{33}, & S^j_{22}\mathbf{1}_{33} \end{bmatrix} \tag{B.14}$$

B.2 Truss Link Node Masses

If there are concentrated masses located at each node, or in order to reduce computation time, the mass of the truss elements may be simply lumped at the nodes. Hence, when considering the expression for the inertial position $\mathbf{s}_i$ of an arbitrary node in eq.(4.1), then, the local nodal vector is required for $\mathbf{r}_i$ eq.(4.2). In this case, vectors $\mathbf{r}_{o,i}$ and $\mathbf{r}_{e,i}$ correspond simply to that of the node k position and deflection vectors, designated respectively as,

$$\mathbf{r}_{o,i} = \mathbf{a}_{o,k} = \langle\, a_{o,k(x)} \quad a_{o,k(y)} \quad a_{o,k(z)} \,\rangle^T \tag{B.15}$$

$$\mathbf{r}_{e,i} = \mathbf{a}_{e,k} = \langle\, a_{e,k(x)} \quad a_{e,k(y)} \quad a_{e,k(z)} \,\rangle^T \tag{B.16}$$

The velocity of the node k is obtained as in eq.(4.18), and can be expressed in the form of eq.(4.20),

$$\dot{\mathbf{s}}_i = \mathbf{E}\mathbf{v}_{i,k} \tag{B.17}$$

where

$$\mathbf{E} = [\, \mathbf{1}_{33} \quad -\tilde{\mathbf{r}}_i \quad \mathbf{1}_{33} \,] \tag{B.18}$$

and the flexible twist vector $\mathbf{v}_{i,k}$ for the node k is given by,

$$\mathbf{v}_{i,k} = \langle \dot{\mathbf{p}}_i^T \quad \boldsymbol{\omega}_i^T \quad \mathring{\mathbf{a}}_{e,k}^T \rangle^T \tag{B.19}$$

Hence, as done with the truss elements in Section 4.1.2, the kinetic energy $\mathrm{T}_{i,k}$ of the concentrated mass $M_{i,k}$ is given by,

$$\mathrm{T}_{i,k} = \frac{1}{2}\dot{\mathbf{s}}_i^T M_{i,k}\dot{\mathbf{s}}_i = \frac{1}{2}\mathbf{v}_{i,k}{}^T\mathbf{M}_{i,k}\mathbf{v}_{i,k} \tag{B.20}$$

where the concentrated nodal mass matrix $\mathbf{M}_{i,k}$ contains components,

$$\mathbf{M}_{dd,k} = M_{i,k}\mathbf{1}_{33} \tag{B.21}$$

$$\mathbf{M}_{dr,k} = -M_{i,k}\tilde{\mathbf{r}}_i \tag{B.22}$$

$$\mathbf{M}_{de,k} = M_{i,k}\mathbf{1}_{33} \tag{B.23}$$

$$\mathbf{M}_{rr,k} = M_{i,k}\tilde{\mathbf{r}}_i^T\tilde{\mathbf{r}}_i = -M_{i,k}\tilde{\mathbf{r}}_i^2 \tag{B.24}$$

$$\mathbf{M}_{re,k} = -M_{i,k}\tilde{\mathbf{r}}_i^T = M_{i,k}\tilde{\mathbf{r}}_i \tag{B.25}$$

$$\mathbf{M}_{ee,k} = M_{i,k}\mathbf{1}_{33} \tag{B.26}$$

The $\tilde{\mathbf{r}}_i$ matrix is obtained by the forming the skew symmetric matrix of vector $\mathbf{r}_i = \mathbf{a}_{o,k} + \mathbf{a}_{e,k}$, the components of which were given previously in eq.'s (B.15) and (B.16).

To assemble the link mass matrix due to all the concentrated nodal masses, the concept of a k^{th} node association matrix $\boldsymbol{\Phi}_{,k}$ is used, such that,

$$\mathbf{a}_{e,k} = \boldsymbol{\Phi}_{,k}\mathbf{a}_e \tag{B.27}$$

where $\mathbf{a}_e$ is the total nodal dof vector as presented previously in eq.(4.41), and the k^{th} node association matrix $\boldsymbol{\Phi}_{,k}$ consists of zeros and ones which properly associate the node k DOF's to that of the total link nodal DOF vector. Hence, $\boldsymbol{\Phi}_{,k}$ is of dimension κ' x κ^* (i.e. the number of DOF per node by the total number of nodal DOF per link). So by substituting eq.(B.27) into eq.(B.19) and reforming the kinetic energy in terms of the link's nodal twist vector $\mathbf{v}_i^*$, given previously in eq.(4.43), the kinetic

energy due to all of the concentrated nodal masses is obtained from the summation of $\mathrm{T}_{i,k}$ for all nodes h^*,

$$\mathrm{T}_{i,c} = \sum_{k=1}^{h^*} \mathrm{T}_{i,k} = \frac{1}{2} \mathbf{v}_i^{*T} \mathbf{M}_{i,c}^* \mathbf{v}_i^* \tag{B.28}$$

where the assembled concentrated node mass matrix $\mathbf{M}_{i,c}^*$ for truss link i is given by,

$$\mathbf{M}_{i,c}^* = \sum_{k=1}^{h^*} \begin{bmatrix} \mathbf{M}_{dd,k} & \mathbf{M}_{dr,k} & \mathbf{M}_{de,k}\boldsymbol{\Phi}_{,k} \\ \mathbf{M}_{dr,k}{}^T & \mathbf{M}_{rr,k} & \mathbf{M}_{re,k}\boldsymbol{\Phi}_{,k} \\ (\mathbf{M}_{de,k}\boldsymbol{\Phi}_{,k})^T & (\mathbf{M}_{re,k}\boldsymbol{\Phi}_{,k})^T & \boldsymbol{\Phi}_{,k}{}^T\mathbf{M}_{ee,k}\boldsymbol{\Phi}_{,k} \end{bmatrix} \tag{B.29}$$

Again, it should be noted that this mass matrix is in terms of the full number of nodal DOF's, which will replace that of eq.(4.45) if the concentrated node masses $M_{i,k}$ represent lumped values of the elements. However, if the node masses $M_{i,k}$ are additional concentrated values such as to account for the node hardware, then matrix $\mathbf{M}_{i,c}^*$ will be added to that of the element mass contribution of eq.(4.45).

B.3 Rigid Cylinder Link

The actuator cylinder cross-sectional dimensions were assumed to be considerably smaller than that of the length (i.e. such as a slender rod), and will be modelled with uniform internal and outer diameters. Hence, the integrals of the mass matrix component $\mathbf{M}_{dr}$ of eq.(4.74) can be evaluated as,

$$\mathbf{M}_{dr} = -\rho_i \int_{\forall_i} x\tilde{\mathbf{x}}_i d\forall = -\rho_i \left(\int_{x=0}^{L_i} A_i x \, dx \right) \tilde{\mathbf{x}}_i = -\left(\frac{M_i L_i}{2} \right) \tilde{\mathbf{x}}_i \tag{B.30}$$

where, M_i is the total mass of the cylinder link, L_i is the length, and $\tilde{\mathbf{x}}_i$ is the unit skew symmetric matrix of the X_i axis,

$$\tilde{\mathbf{x}}_i = \begin{bmatrix} 0 & 0 & 0 \\ 0 & 0 & -1 \\ 0 & 1 & 0 \end{bmatrix} \tag{B.31}$$

Similarly component $\mathbf{M}_{rr}$ of eq.(4.74), becomes,

$$\mathbf{M}_{rr} = -\rho_i \int_{\forall_i} x^2\tilde{\mathbf{x}}_i^2 d\forall = -\rho_i \left(\int_{x=0}^{L_i} A_i x^2 \, dx \right) \tilde{\mathbf{x}}_i^2 = -\left(\frac{M_i L_i^2}{3} \right) \tilde{\mathbf{x}}_i^2 \tag{B.32}$$

If the diameters are not uniform, then the appropriate cross-sectional area A_i variation over the component length should be included in the integrations performed above. However, if their dimensions are again much smaller than the length, then their effect on the rotational inertias above would not be significant.

B.4 Rigid Piston-rod Link

The piston-rod mass matrix is formulated as done previously for the cylinder in equations (B.30) and (B.32), however, the integration must be performed as,

$$\mathbf{M}_{dr} = -\rho_i \int_{\forall_i} x\tilde{\mathbf{x}}_i d\forall = -\rho_i \left(\int_{x=-L_i}^{0} A_i x \, dx \right) \tilde{\mathbf{x}}_i = +\left(\frac{M_i L_i}{2} \right) \tilde{\mathbf{x}}_i \tag{B.33}$$

and,

$$\mathbf{M}_{rr} = -\rho_i \int_{\forall_i} x^2 \tilde{\mathbf{x}}_i^2 d\forall = -\rho_i \left(\int_{x=-L_i}^{0} A_i x^2 \, dx \right) \tilde{\mathbf{x}}_i^2 = -\left(\frac{M_i L_i^2}{3} \right) \tilde{\mathbf{x}}_i^2 \tag{B.34}$$

where, M_i is the total mass of the piston-rod link, L_i is the length, and $\tilde{\mathbf{x}}_i$ is as given in eq.(B.31). The discussion given in the previous section regarding the diameter dimension of the cylinder, is also applicable to the piston-rod.

If a concentrated mass is located at the origin of the frame of the piston-rod, as is the case with inter-link assembly hardware, then its contribution to the mass matrices is considered by evaluating eq.'s (4.66) to (4.75), with the introduction of $x = 0$ and the integral replaced by the concentrated mass, $M_{i,c}$. This correponds to the velocity of the concentrated mass being simply that of the link frame origin. Hence, only a contribution to the displacement components $\mathbf{M}_{dd}$ is obtained, i.e.,

$$\mathbf{M}_{dd} = (M_i + M_{i,c})\, \mathbf{1}_{33} \tag{B.35}$$

Appendix C

Mass Matrix Rates

The mass matrix rates required in eq.'s(5.18) to (5.20), are established in this section. These quantities are derived by performing the absolute time derivatives of the vectorial contents within the original mass matrices. It is first necessary to recall the general expression for the inertial velocity of an arbitary point on a link described by eq.(4.16),

$$\dot{\mathbf{s}}_i = \dot{\mathbf{p}}_i + (\boldsymbol{\omega}_i \times \mathbf{r}_i) + \overset{\circ}{\mathbf{r}}_i \tag{C.1}$$

where as before $\dot{\mathbf{p}}_i$ is the velocity of the origin of the link frame, $\boldsymbol{\omega}_i$ is the angular velocity of the link frame and $\overset{\circ}{\mathbf{r}}_i$ is the local velocity of the point. The local vector $\mathbf{r}_i$ is 3-dimensional and of the form of eq.(3.5),

$$\mathbf{r}_i = \mathbf{r}_{o,i} + \mathbf{r}_{e,i} \tag{C.2}$$

where again $\mathbf{r}_{o,i}$ denotes the rigid body location of the point with respect to the origin of the link frame, and $\mathbf{r}_{e,i}$ is the elastic deformation component. For the derivations to follow, the deformation is expressed in the general discretized form of eq.(3.7),

$$\mathbf{r}_{e,i} = \mathbf{B}_i \mathbf{b}_i \tag{C.3}$$

where $\mathbf{b}_i$ is the m_i dimensional vector of elastic coordinates per eq.(3.6), and $\mathbf{B}_i$ is the shape function matrix of dimension 3 by m_i.

By rearranging eq.(C.1) in a form similar to eq.'s (4.18), we obtain,

$$\dot{\mathbf{s}}_i \;=\; \dot{\mathbf{p}}_i - (\mathbf{r}_i \times \boldsymbol{\omega}_i) + \overset{\circ}{\mathbf{r}}_i$$

$$= \dot{\mathbf{p}}_i - \tilde{\mathbf{r}}_i\boldsymbol{\omega}_i + \mathbf{B}_i\dot{\mathbf{b}}_i \tag{C.4}$$

Now, if we recall the arrangement of eq.(4.20), we can rewrite the above as,

$$\dot{\mathbf{s}}_i = \mathbf{E}\mathbf{v}_i \tag{C.5}$$

where

$$\mathbf{E} = [\,\mathbf{1}_{33} \quad -\tilde{\mathbf{r}}_i \quad \mathbf{B}_i\,] \tag{C.6}$$

and the flexible twist vector $\mathbf{v}_i$ for the link is that given by eq.(3.10), i.e.,

$$\mathbf{v}_i = \langle\, \dot{\mathbf{p}}_i^T \quad \boldsymbol{\omega}_i{}^T \quad \dot{\mathbf{b}}_i^T \,\rangle^T \tag{C.7}$$

The kinetic energy of the link T_i is obtained by evaluating,

$$\mathrm{T}_i = \frac{1}{2}\int_\forall \dot{\mathbf{s}}_i^T\dot{\mathbf{s}}_i\rho d\forall = \frac{1}{2}\mathbf{v}_i{}^T\mathbf{M}_i\mathbf{v}_i \tag{C.8}$$

where the mass matrix $\mathbf{M}_i$ is given by the general form of,

$$\mathbf{M}_i = \int_\forall \mathbf{E}^T\mathbf{E}\rho d\forall = \begin{bmatrix} \mathbf{M}_{dd} & \mathbf{M}_{dr} & \mathbf{M}_{de} \\ \mathbf{M}_{rd} & \mathbf{M}_{rr} & \mathbf{M}_{re} \\ \mathbf{M}_{ed} & \mathbf{M}_{er} & \mathbf{M}_{ee} \end{bmatrix} \tag{C.9}$$

and as before, notation d represents displacement of the origin of link frame i, r represents rotation of the the frame, and e is the elastic deformation. The mass matrix components consist of,

$$\mathbf{M}_{dd} = \rho\int_\forall \mathbf{1}_{33}d\forall = M_i\mathbf{1}_{33} \tag{C.10}$$

$$\mathbf{M}_{dr} = -\rho\int_\forall \tilde{\mathbf{r}}_i d\forall \tag{C.11}$$

$$\mathbf{M}_{de} = \rho\int_\forall \mathbf{B}_i d\forall \tag{C.12}$$

$$\mathbf{M}_{rd} = -\rho\int_\forall \tilde{\mathbf{r}}_i^T d\forall = \mathbf{M}_{dr}^T \tag{C.13}$$

$$\mathbf{M}_{rr} = \rho\int_\forall \tilde{\mathbf{r}}_i^T\tilde{\mathbf{r}}_i d\forall \tag{C.14}$$

$$\mathbf{M}_{re} = -\rho\int_\forall \tilde{\mathbf{r}}_i^T\mathbf{B}_i d\forall \tag{C.15}$$

$$\mathbf{M}_{ed} = \rho\int_\forall \mathbf{B}_i^T d\forall = \mathbf{M}_{de}^T \tag{C.16}$$

$$\mathbf{M}_{er} = -\rho\int_\forall \mathbf{B}_i^T\tilde{\mathbf{r}}_i d\forall = \mathbf{M}_{re}^T \tag{C.17}$$

$$\mathbf{M}_{ee} = \rho\int_\forall \mathbf{B}_i^T\mathbf{B}_i d\forall \tag{C.18}$$

In performing the time differentation upon the above matrices, the properties of skew symmetric matrices presented in Appendix A will be used considerably.

Firstly, it should be noted that there is no scalar mass addition or reduction in the links considered for the truss manipulator. If this was not the case, then the corresponding change in mass associated with each link would have to be included in the following expressions. Therefore, to evaluate $\dot{\mathbf{M}}_{dd}$, we note from eq.(C.10) that its scalar value yields,

$$\dot{\mathbf{M}}_{dd} = \mathbf{0}_{33} \tag{C.19}$$

The time derivative of $\dot{\mathbf{M}}_{dr}$ is obtained by considering the absolute rate of the local vector $\mathbf{r}_i$, given by,

$$\frac{d}{dt}(\mathbf{r}_i) = \dot{\mathbf{r}}_i = \boldsymbol{\omega}_i \times \mathbf{r}_i + \mathring{\mathbf{r}}_i = \tilde{\boldsymbol{\omega}}_i \mathbf{r}_i + \mathring{\mathbf{r}}_i \tag{C.20}$$

According to eq.'s (A.7) and (A.8), we can write,

$$\frac{d}{dt}(\tilde{\mathbf{r}}_i) = (\widetilde{\tilde{\boldsymbol{\omega}}_i \mathbf{r}_i}) + \tilde{\mathring{\mathbf{r}}}_i \tag{C.21}$$

Now applying eq.(A.9) to the first term on the right hand side of the above equation we have,

$$\frac{d}{dt}(\tilde{\mathbf{r}}_i) = (\tilde{\boldsymbol{\omega}}_i \tilde{\mathbf{r}}_i - \tilde{\mathbf{r}}_i \tilde{\boldsymbol{\omega}}_i) + \tilde{\mathring{\mathbf{r}}}_i \tag{C.22}$$

Recalling the integral for evaluating eq.(C.11), we obtain,

$$\begin{aligned} \dot{\mathbf{M}}_{dr} &= -\rho \int_{\forall} (\tilde{\boldsymbol{\omega}}_i \tilde{\mathbf{r}}_i - \tilde{\mathbf{r}}_i \tilde{\boldsymbol{\omega}}_i + \tilde{\mathring{\mathbf{r}}}_i) d\forall \\ &= \tilde{\boldsymbol{\omega}}_i \mathbf{M}_{dr} - \mathbf{M}_{dr} \tilde{\boldsymbol{\omega}}_i + \mathring{\mathbf{M}}_{dr} \end{aligned} \tag{C.23}$$

where,

$$\mathring{\mathbf{M}}_{dr} = -\rho \int_{\forall} \tilde{\mathring{\mathbf{r}}}_i d\forall \tag{C.24}$$

Matrix rate $\dot{\mathbf{M}}_{de}$, is obtained by noting that the rows of the elastic shape function matrix $\mathbf{B}_i$ correspond to the local axes of the link frame, which change with time by virtue of frame rotation. But since $\mathbf{B}_i$ contains only functions of the spacial

coordinates of the link, then we require only the cross product term due to the angular velocity of the frame, to yield,

$$\begin{aligned} \dot{\mathbf{M}}_{de} &= \rho \int_{\forall} \tilde{\boldsymbol{\omega}}_i \mathbf{B}_i d\forall \\ &= \tilde{\boldsymbol{\omega}}_i \mathbf{M}_{de} \end{aligned} \tag{C.25}$$

The derivative of $\tilde{\mathbf{r}}_i^T$ contained in $\mathbf{M}_{rd}$, is obtained by performing the transpose of eq.(C.22), to yield,

$$\begin{aligned} \dot{\mathbf{M}}_{rd} &= -\rho \int_{\forall} (\tilde{\mathbf{r}}_i^T \tilde{\boldsymbol{\omega}}_i^T - \tilde{\boldsymbol{\omega}}_i^T \tilde{\mathbf{r}}_i^T + \tilde{\overset{\circ}{\mathbf{r}}}_i^T) d\forall \\ &= \mathbf{M}_{rd} \tilde{\boldsymbol{\omega}}_i^T - \tilde{\boldsymbol{\omega}}_i^T \mathbf{M}_{rd} + \overset{\circ}{\mathbf{M}}_{rd} \end{aligned} \tag{C.26}$$

where, by recalling the symmetry of $\mathbf{M}_{rd} = \mathbf{M}_{dr}^T$, we can write,

$$\overset{\circ}{\mathbf{M}}_{rd} = -\rho \int_{\forall} \tilde{\overset{\circ}{\mathbf{r}}}_i d\forall = (\overset{\circ}{\mathbf{M}}_{dr})^T \tag{C.27}$$

and,

$$\mathbf{M}_{rd} \tilde{\boldsymbol{\omega}}_i^T = (\tilde{\boldsymbol{\omega}}_i \mathbf{M}_{dr})^T \tag{C.28}$$

Matrix $\dot{\mathbf{M}}_{rr}$ is similarly established by considering the differentiation of,

$$\begin{aligned} \frac{d}{dt}(\tilde{\mathbf{r}}_i^T \tilde{\mathbf{r}}_i) &= \dot{\tilde{\mathbf{r}}}_i^T \tilde{\mathbf{r}}_i + \tilde{\mathbf{r}}_i^T \dot{\tilde{\mathbf{r}}}_i \\ &= (\tilde{\boldsymbol{\omega}}_i \tilde{\mathbf{r}}_i - \tilde{\mathbf{r}}_i \tilde{\boldsymbol{\omega}}_i + \tilde{\overset{\circ}{\mathbf{r}}}_i)^T \tilde{\mathbf{r}}_i + \tilde{\mathbf{r}}_i^T (\tilde{\boldsymbol{\omega}}_i \tilde{\mathbf{r}}_i - \tilde{\mathbf{r}}_i \tilde{\boldsymbol{\omega}}_i + \tilde{\overset{\circ}{\mathbf{r}}}_i) \end{aligned} \tag{C.29}$$

By using the property of eq.(A.5), then the term $\tilde{\mathbf{r}}_i^T \tilde{\boldsymbol{\omega}}_i^T \tilde{\mathbf{r}}_i + \tilde{\mathbf{r}}_i^T \tilde{\boldsymbol{\omega}}_i \tilde{\mathbf{r}}_i = \mathbf{0}_{33}$, and $\dot{\mathbf{M}}_{rr}$ becomes,

$$\begin{aligned} \dot{\mathbf{M}}_{rr} &= \rho \int_{\forall} -(\tilde{\boldsymbol{\omega}}_i^T \tilde{\mathbf{r}}_i^T \tilde{\mathbf{r}}_i + \tilde{\mathbf{r}}_i^T \tilde{\mathbf{r}}_i \tilde{\boldsymbol{\omega}}_i) + (\tilde{\overset{\circ}{\mathbf{r}}}_i^T \tilde{\mathbf{r}}_i + \tilde{\mathbf{r}}_i^T \tilde{\overset{\circ}{\mathbf{r}}}_i) d\forall \\ &= -\tilde{\boldsymbol{\omega}}_i^T \mathbf{M}_{rr} - \mathbf{M}_{rr} \tilde{\boldsymbol{\omega}}_i + \overset{\circ}{\mathbf{M}}_{rr} \\ &= \tilde{\boldsymbol{\omega}}_i \mathbf{M}_{rr} + \mathbf{M}_{rr} \tilde{\boldsymbol{\omega}}_i^T + \overset{\circ}{\mathbf{M}}_{rr} \end{aligned} \tag{C.30}$$

where again the property $\tilde{\boldsymbol{\omega}}_i^T = -\tilde{\boldsymbol{\omega}}_i$ is used, and,

$$\overset{\circ}{\mathbf{M}}_{rr} = \rho \int_{\forall} (\tilde{\overset{\circ}{\mathbf{r}}}_i^T \tilde{\mathbf{r}}_i + \tilde{\mathbf{r}}_i^T \tilde{\overset{\circ}{\mathbf{r}}}_i) d\forall \tag{C.31}$$

The rate of mass matrix $\mathbf{M}_{re}$ is obtained by performing,

$$\begin{aligned}\frac{d}{dt}\left(\tilde{\mathbf{r}}_i^T\mathbf{B}_i\right) &= (\tilde{\boldsymbol{\omega}}_i\tilde{\mathbf{r}}_i - \tilde{\mathbf{r}}_i\tilde{\boldsymbol{\omega}}_i + \tilde{\dot{\mathbf{r}}}_i)^T\mathbf{B}_i + \tilde{\mathbf{r}}_i(\tilde{\boldsymbol{\omega}}_i\mathbf{B}_i) \\ &= \tilde{\mathbf{r}}_i^T\tilde{\boldsymbol{\omega}}_i^T\mathbf{B}_i - \tilde{\boldsymbol{\omega}}_i^T\tilde{\mathbf{r}}_i^T\mathbf{B}_i + \tilde{\dot{\mathbf{r}}}_i^T\mathbf{B}_i + \tilde{\mathbf{r}}_i^T\tilde{\boldsymbol{\omega}}_i\mathbf{B}_i \\ &= \tilde{\boldsymbol{\omega}}_i\tilde{\mathbf{r}}_i^T\mathbf{B}_i + \tilde{\dot{\mathbf{r}}}_i^T\mathbf{B}_i \qquad \text{(C.32)}\end{aligned}$$

where the results of eq.'s (C.22) and (A.5) are used. Hence we obtain for $\dot{\mathbf{M}}_{re}$,

$$\begin{aligned}\dot{\mathbf{M}}_{re} &= -\rho\int_{\forall}(\tilde{\boldsymbol{\omega}}_i\tilde{\mathbf{r}}_i^T\mathbf{B}_i + \tilde{\dot{\mathbf{r}}}_i^T\mathbf{B}_i)d\forall \\ &= \tilde{\boldsymbol{\omega}}_i\mathbf{M}_{re} + \mathring{\mathbf{M}}_{re} \qquad \text{(C.33)}\end{aligned}$$

where,

$$\mathring{\mathbf{M}}_{re} = -\rho\int_{\forall}\tilde{\dot{\mathbf{r}}}_i^T\mathbf{B}_i d\forall \qquad \text{(C.34)}$$

Matrix $\dot{\mathbf{M}}_{ed}$, is evaluated by recalling eq.(C.16) and including the cross product term due to the angular velocity of the frame as done in eq.(C.25),

$$\begin{aligned}\dot{\mathbf{M}}_{ed} &= \rho\int_{\forall}(\tilde{\boldsymbol{\omega}}_i\mathbf{B}_i)^T d\forall \\ &= \mathbf{M}_{ed}\tilde{\boldsymbol{\omega}}_i^T \\ &= (\tilde{\boldsymbol{\omega}}_i\mathbf{M}_{de})^T \\ &= \dot{\mathbf{M}}_{de}^T \qquad \text{(C.35)}\end{aligned}$$

To construct $\dot{\mathbf{M}}_{er}$, we recall the form of eq.(C.17) and the corresponding time differentiation of eq.(C.22), to obtain,

$$\begin{aligned}\frac{d}{dt}\left(\mathbf{B}_i^T\tilde{\mathbf{r}}_i\right) &= (\tilde{\boldsymbol{\omega}}_i\mathbf{B}_i)^T\tilde{\mathbf{r}}_i + \mathbf{B}_i^T(\tilde{\boldsymbol{\omega}}_i\tilde{\mathbf{r}}_i - \tilde{\mathbf{r}}_i\tilde{\boldsymbol{\omega}}_i + \tilde{\dot{\mathbf{r}}}_i) \\ &= \mathbf{B}_i^T\tilde{\boldsymbol{\omega}}_i^T\tilde{\mathbf{r}}_i + \mathbf{B}_i^T\tilde{\boldsymbol{\omega}}_i\tilde{\mathbf{r}}_i - \mathbf{B}_i^T\tilde{\mathbf{r}}_i\tilde{\boldsymbol{\omega}}_i + \mathbf{B}_i^T\tilde{\dot{\mathbf{r}}}_i \\ &= -\mathbf{B}_i^T\tilde{\mathbf{r}}_i\tilde{\boldsymbol{\omega}}_i + \mathbf{B}_i^T\tilde{\dot{\mathbf{r}}}_i^T \qquad \text{(C.36)}\end{aligned}$$

Therefore $\dot{\mathbf{M}}_{er}$ becomes,

$$\begin{aligned}\dot{\mathbf{M}}_{er} &= -\rho\int_{\forall}(-\mathbf{B}_i^T\tilde{\mathbf{r}}_i\tilde{\boldsymbol{\omega}}_i + \mathbf{B}_i^T\tilde{\dot{\mathbf{r}}}_i)d\forall \\ &= -\mathbf{M}_{er}\tilde{\boldsymbol{\omega}}_i + \mathring{\mathbf{M}}_{er} \\ &= (\tilde{\boldsymbol{\omega}}_i\mathbf{M}_{re})^T + \mathring{\mathbf{M}}_{re}^T \qquad \text{(C.37)}\end{aligned}$$

where,

$$\overset{\circ}{\mathbf{M}}_{er} = -\rho \int_{\forall} \mathbf{B}_i^T \tilde{\overset{\circ}{\mathbf{r}}}_i^T d\forall = \overset{\circ}{\mathbf{M}}_{re}^T \tag{C.38}$$

Finally, $\dot{\mathbf{M}}_{ee}$ is obtained from eq.(C.18) and by maintaining the vectorial significance of the matrix $\mathbf{B}_i$ when performing the time differentiation. This results in,

$$\begin{aligned} \frac{d}{dt}\left(\mathbf{B}_i^T \mathbf{B}_i\right) &= (\tilde{\boldsymbol{\omega}}_i \mathbf{B}_i)^T \mathbf{B}_i + \mathbf{B}_i^T (\tilde{\boldsymbol{\omega}}_i \mathbf{B}_i) \\ &= \mathbf{B}_i^T \tilde{\boldsymbol{\omega}}_i^T \mathbf{B}_i + \mathbf{B}_i^T \tilde{\boldsymbol{\omega}}_i \mathbf{B}_i \\ &= \mathbf{0}_{m_i m_i} \end{aligned} \tag{C.39}$$

where the property of eq.(A.5) was employed. Therefore, $\dot{\mathbf{M}}_{ee}$ is simply,

$$\dot{\mathbf{M}}_{ee} = \mathbf{0}_{m_i m_i} \tag{C.40}$$

Appendix D

Kinematic Loop Details

Based on the kinematic loop details illustrated in Fig.D.1, the expressions required to generate the solution of the dependent angles θ_i and θ_j, and the corresponding rates will be derived here. The motion is considered to be planar, hence the positional vectors will be two dimensional and contain only the X and Y components. In addition, the rotation matrices will be expressed in their 2D forms. Therefore, the transformation from link frame i to the frame $i-1$ is denoted per eq.(3.30),

$$\mathbf{R}_i = \mathbf{D}^i_{i-1}\mathbf{C}_i \tag{D.1}$$

where, $\mathbf{D}^i_{i-1}$ is the rotation component due to the deflection of the end of truss link $i-1$, given previously by eq.(3.32). For planar motion with small deflections, this matrix is approximately,

$$\mathbf{D}^i_{i-1} = \begin{bmatrix} 1 & -\delta_{i/i-1(z)} \\ \delta_{i/i-1(z)} & 1 \end{bmatrix} \tag{D.2}$$

where $\delta_{i/i-1(z)}$ is defined in eq.(3.33) and re-presented here for convenience,

$$\delta_{i/i-1(z)} = \mathbf{B}^{i*}_{i-1(y)}\mathbf{b}_{i-1}(t) \tag{D.3}$$

Row matrix $\mathbf{B}^{i*}_{i-1(y)}$ is as defined in eq.(3.34),

$$\mathbf{B}^{i*}_{i-1(y)} = \frac{\mathbf{B}^i_{i-1(y)}}{a_{o,i/i-1}} \tag{D.4}$$

where constant $a_{o,i/i-1}$ represents the rigid body distance of the origin of frame i from $i-1$, given by the magnitude of its rigid body position vector $\mathbf{r}_{o,i/i-1}$,

$$a_{o,i/i-1} = |\mathbf{r}_{o,i/i-1}| \tag{D.5}$$

Matrix $\mathbf{C}_i$ is that given before in eq.(3.31), but here only the components of the XY dimensions are retained,

$$\mathbf{C}_i = \begin{bmatrix} cos(\theta_i) & -sin(\theta_i) \\ sin(\theta_i) & cos(\theta_i) \end{bmatrix} \tag{D.6}$$

And similarly for link frame j we have the rotation relations,

$$\mathbf{R}_j = \mathbf{D}^j_{i-1}\mathbf{C}_j \tag{D.7}$$

where $\mathbf{D}^j_{i-1}$ has the same form of eq.(D.2) but contains the deflection slope of $\delta_{j/i-1(z)}$, corresponding to the node of frame origin j, given by,

$$\delta_{j/i-1(z)} = \mathbf{B}^{j*}_{i-1(y)}\mathbf{b}_{i-1}(t) \tag{D.8}$$

$$\mathbf{B}^{j*}_{i-1(y)} = \frac{\mathbf{B}^j_{i-1(y)}}{a_{o,j/i-1}} \tag{D.9}$$

where, again $\mathbf{B}^j_{i-1(y)}$ represents the Y axis shape function components of link $i-1$ (corresponding with the node at frame origin j), and constant $a_{o,j/i-1}$ represents the rigid body distance of frame origin j from $i-1$, given by the magnitude its rigid body position vector $\mathbf{r}_{o,j/i-1}$,

$$a_{o,j/i-1} = |\mathbf{r}_{o,j/i-1}| \tag{D.10}$$

Matrix $\mathbf{C}_j$ accounts for frame j rotation due to dependent angle θ_j, and is given as,

$$\mathbf{C}_j = \begin{bmatrix} cos(\theta_j) & -sin(\theta_j) \\ sin(\theta_j) & cos(\theta_j) \end{bmatrix} \tag{D.11}$$

The loop equation can be constructed within frame $i-1$, according to the following,

$$\boldsymbol{\zeta} = \mathbf{R}_i(\mathbf{p}_i + \mathbf{r}_{j+1/i}) - \mathbf{R}_j(\mathbf{p}_j + \mathbf{r}_{j+1/j}) = \mathbf{0}_2 \tag{D.12}$$

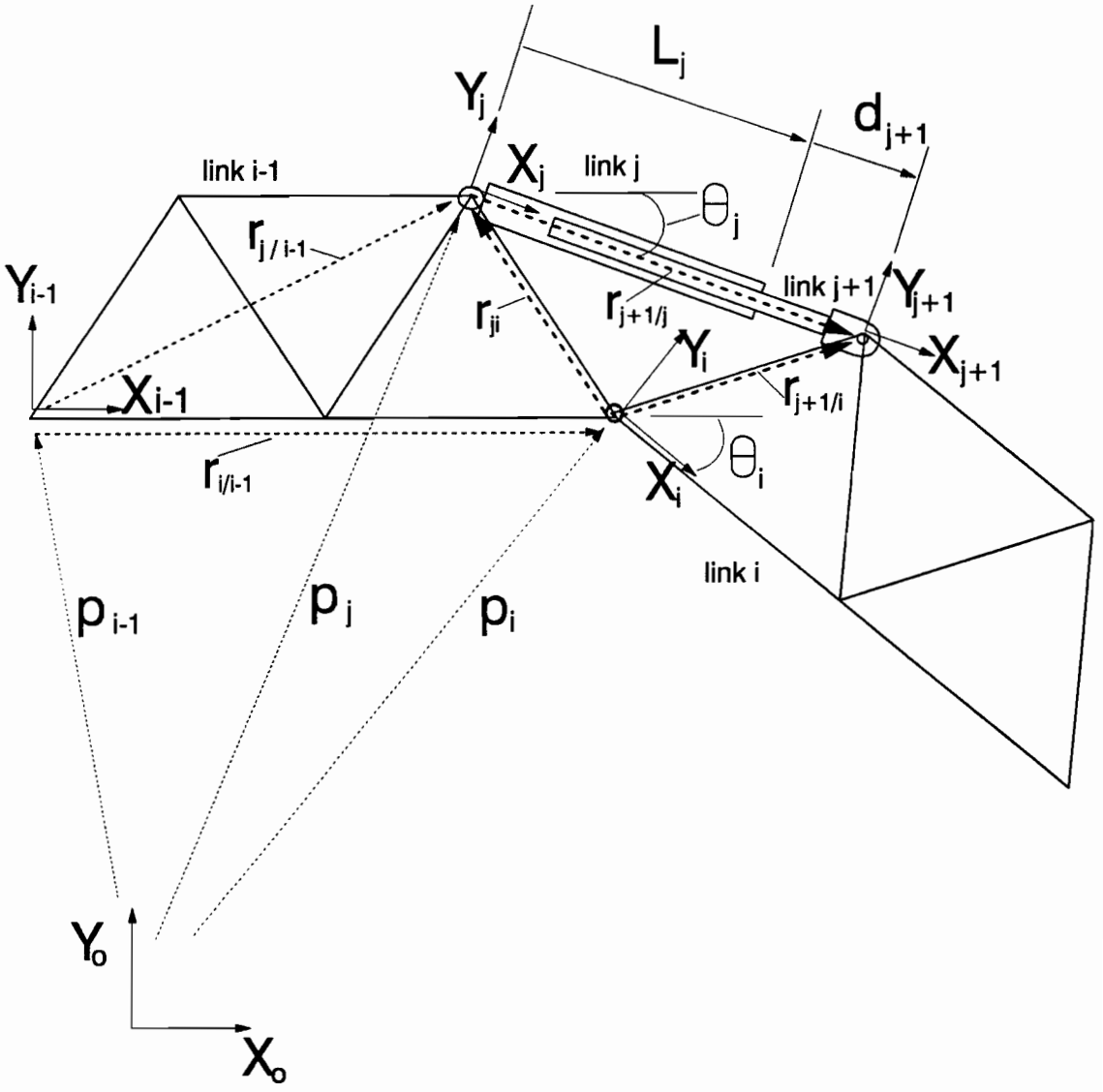

Figure D.1: The kinematic loop details.

where vector $\mathbf{p}_i$ is the inertial vector of the origin of frame i expressed in frame i, and $\mathbf{r}_{j+1/i}$ is the vector of connection point $j+1$ with respect to frame i (and also expressed in frame i). Vectors $\mathbf{p}_j$ and $\mathbf{r}_{j+1/j}$ are similarly defined and correspond to frame j. As well, inertial positions $\mathbf{p}_i$ and $\mathbf{p}_j$ are given as,

$$\mathbf{p}_i = \mathbf{R}_i^T(\mathbf{p}_{i-1} + \mathbf{r}_{i/i-1}) \quad , \quad \mathbf{p}_j = \mathbf{R}_j^T(\mathbf{p}_{i-1} + \mathbf{r}_{j/i-1}) \tag{D.13}$$

where $\mathbf{p}_{i-1}$ is the inertial position vector of the origin of frame $i-1$, $\mathbf{r}_{i/i-1}$ is the position vector of frame origin i with respect to frame origin $i-1$, and $\mathbf{r}_{j/i-1}$ is the position vector of frame origin j with respect to frame origin $i-1$; where all these vectors are expressed within the frame $i-1$. Substituting eq.(D.13) into eq.(D.12), we obtain the loop equation in the form of,

$$\mathbf{R}_i\mathbf{r}_{j+1/i} - \mathbf{R}_j\mathbf{r}_{j+1/j} = \mathbf{r}_{ji/i-1} \tag{D.14}$$

where vector $\mathbf{r}_{ji/i-1}$ is given by,

$$\mathbf{r}_{ji/i-1} = \mathbf{r}_{j/i-1} - \mathbf{r}_{i/i-1} \tag{D.15}$$

Now vector $\mathbf{r}_{i/i-1}$ contains,

$$\mathbf{r}_{i/i-1} = \mathbf{r}_{o,i/i-1} + \mathbf{r}_{e,i/i-1} \tag{D.16}$$

where $\mathbf{r}_{o,i/i-1}$ is the rigid body position vector of frame origin i with respect to $i-1$, and $\mathbf{r}_{e,i/i-1}$ is the elastic deflection given by the components of the shape function matrix for node i,

$$\mathbf{r}_{e,i/i-1} = \mathbf{B}_{i-1}^i\mathbf{b}_{i-1}(t) \tag{D.17}$$

Similarly, vector $\mathbf{r}_{j/i-1}$ is,

$$\mathbf{r}_{j/i-1} = \mathbf{r}_{o,j/i-1} + \mathbf{r}_{e,j/i-1} \tag{D.18}$$

where $\mathbf{r}_{o,j/i-1}$ is the rigid position of frame origin j with respect to $i-1$, and $\mathbf{r}_{e,j/i-1}$ is the elastic deflection given by the components of the shape function matrix for node j,

$$\mathbf{r}_{e,j/i-1} = \mathbf{B}_{i-1}^j\mathbf{b}_{i-1}(t) \tag{D.19}$$

Therefore, vector $\mathbf{r}_{ji/i-1}$ can be written as,

$$\begin{aligned}\mathbf{r}_{ji/i-1} &= \mathbf{r}_{j/i-1} - \mathbf{r}_{i/i-1} \\ &= (\mathbf{r}_{o,j/i-1} - \mathbf{r}_{o,i/i-1}) + (\mathbf{B}^{j}_{i-1} - \mathbf{B}^{i}_{i-1})\mathbf{b}_{i-1}(t) \end{aligned} \tag{D.20}$$

Truss link i vector $\mathbf{r}_{j+1/i}$ is also written using the similar notation,

$$\mathbf{r}_{j+1/i} = \mathbf{r}_{o,j+1/i} + \mathbf{r}_{e,j+1/i} \tag{D.21}$$

where again the flexible deformation $\mathbf{r}_{e,j+1/i}$ of node $j+1$ is modelled using the corresponding truss i shape function components,

$$\mathbf{r}_{e,j+1/i} = \mathbf{B}^{j+1}_{i}\mathbf{b}_{i}(t) \tag{D.22}$$

The actuator vector $\mathbf{r}_{j+1/j}$ consists of the cylinder link j length denoted as L_j, and the extended length d_{j+1} of the piston-rod link $j+1$,

$$\mathbf{r}_{j+1/j} = (L_j + d_{j+1})\mathbf{x} \tag{D.23}$$

where $\mathbf{x}$ signifies the X axis of link j, and is therefore represented vectorially as,

$$\mathbf{x} = \langle 1 \quad 0 \rangle^T \tag{D.24}$$

From these detailed descriptions of the vectors contained in the kinematic constraint eq.(D.14), the Newton-Raphson iterative scheme outlined in [Nikravesh'88], can be applied to obtain the dependent angles θ_i and θ_j of truss i and cylinder j, respectively.

Now differentiating eq.(D.14) with respect to time, we obtain,

$$\mathbf{R}_i\left(\boldsymbol{\omega}_i \times \mathbf{r}_{j+1/i} + \mathring{\mathbf{r}}_{j+1/i}\right) - \mathbf{R}_j\left(\boldsymbol{\omega}_j \times \mathbf{r}_{j+1/j} + \mathring{\mathbf{r}}_{j+1/j}\right) = \boldsymbol{\omega}_{i-1} \times \mathbf{r}_{ji/i-1} + \mathring{\mathbf{r}}_{ji/i-1} \tag{D.25}$$

where, from eq.'s(D.20) to (D.23) we have the following local vector rates,

$$\mathring{\mathbf{r}}_{ji/i-1} = (\mathbf{B}^{j}_{i-1} - \mathbf{B}^{i}_{i-1})\dot{\mathbf{b}}_{i-1} \tag{D.26}$$

$$\mathring{\mathbf{r}}_{j+1/i} = \mathbf{B}^{j+1}_{i}\dot{\mathbf{b}}_{i} \tag{D.27}$$

$$\mathring{\mathbf{r}}_{j+1/j} = \dot{d}_{j+1}\mathbf{x} \tag{D.28}$$

Since only planar motion is examined for the truss structures considered in this work, then the angular velocities of frames $i-1$, i, and j are about a common $\mathbf{z}$ axis, and can be written as,

$$\boldsymbol{\omega}_i = \omega_{i(z)}\mathbf{z} = (\omega_{i-1(z)} + \mathring{\delta}_{i/i-1(z)} + \dot{\theta}_i)\mathbf{z} \tag{D.29}$$

$$\boldsymbol{\omega}_j = \omega_{j(z)}\mathbf{z} = (\omega_{i-1(z)} + \mathring{\delta}_{j/i-1(z)} + \dot{\theta}_j)\mathbf{z} \tag{D.30}$$

The cross product operation for planar motion can be expressed in the form of,

$$\boldsymbol{\omega}_i \,\mathrm{x}\, \mathbf{r}_{j+1/i} = \omega_{i(z)}\mathbf{z} \,\mathrm{x}\, \mathbf{r}_{j+1/i} = \mathbf{G}\mathbf{r}_{j+1/i}\omega_{i(z)} \tag{D.31}$$

where, matrix $\mathbf{G}$ is given by,

$$\mathbf{G} = \begin{bmatrix} 0 & -1 \\ 1 & 0 \end{bmatrix} \tag{D.32}$$

By using this operation, and substituting eq.'s (D.29) and (D.30) into eq.(D.25), yields,

$$\begin{aligned} \mathbf{R}_i\mathbf{G}\mathbf{r}_{j+1/i}\dot{\theta}_i - \mathbf{R}_j\mathbf{G}\mathbf{r}_{j+1/j}\dot{\theta}_j \;=\; & \left(\mathbf{G}\mathbf{r}_{ji/i-1} - \mathbf{R}_i\mathbf{G}\mathbf{r}_{j+1/i} + \mathbf{R}_j\mathbf{G}\mathbf{r}_{j+1/j}\right)\omega_{i-1(z)} \\ & -(\mathbf{R}_i\mathbf{G}\mathbf{r}_{j+1/i})\mathring{\delta}_{i/i-1(z)} + (\mathbf{R}_j\mathbf{G}\mathbf{r}_{j+1/j})\mathring{\delta}_{j/i-1(z)} \\ & + \mathring{\mathbf{r}}_{ji/i-1} - \mathbf{R}_i\mathring{\mathbf{r}}_{j+1/i} + \mathbf{R}_j\mathring{\mathbf{r}}_{j+1/j} \end{aligned} \tag{D.33}$$

From the above, we can construct the coefficent matrix $[\boldsymbol{\zeta}_\theta]$ corresponding to the dependent angles θ_i and θ_j, given as,

$$[\boldsymbol{\zeta}_\theta] = [\,\mathbf{R}_i\mathbf{G}\mathbf{r}_{j+1/i} \quad -\mathbf{R}_j\mathbf{G}\mathbf{r}_{j+1/j}\,] \tag{D.34}$$

Substituting eq.'s(D.26) to (D.28), along with,

$$\mathring{\delta}_{i/i-1(z)} = \mathbf{B}^{i*}_{i-1(y)}\dot{\mathbf{b}}_{i-1} \tag{D.35}$$

$$\mathring{\delta}_{j/i-1(z)} = \mathbf{B}^{j*}_{i-1(y)}\dot{\mathbf{b}}_{i-1} \tag{D.36}$$

into eq.(D.33) and premultiplying the result by the inverse of $\boldsymbol{\zeta}_\theta$, yields,

$$\begin{Bmatrix} \dot{\theta}_i \\ \dot{\theta}_j \end{Bmatrix} = [\boldsymbol{\zeta}_\theta]^{-1}\left[\mathbf{G}\mathbf{r}_{ji/i-1} - \mathbf{R}_i\mathbf{G}\mathbf{r}_{j+1/i} + \mathbf{R}_j\mathbf{G}\mathbf{r}_{j+1/j}\right]\omega_{i-1(z)}$$

$$+[\zeta_\theta]^{-1}\left[(-\mathbf{R}_i\mathbf{G}\mathbf{r}_{j+1/i}\mathbf{B}^{i*}_{i-1(y)}+\mathbf{R}_j\mathbf{G}\mathbf{r}_{j+1/j}\mathbf{B}^{j*}_{i-1(y)})\right.$$
$$\left.+(\mathbf{B}^{j}_{i-1}-\mathbf{B}^{i}_{i-1})\right]\dot{\mathbf{b}}_{i-1}$$
$$-[\zeta_\theta]^{-1}[\mathbf{R}_i\mathbf{B}^{j+1}_i]\dot{\mathbf{b}}_i+[\zeta_\theta]^{-1}[\mathbf{R}_j\mathbf{x}]\dot{d}_{j+1} \qquad (D.37)$$

Note, that this is the form required in eq.(5.53) for the construction of the natural orthogonal complement for the system.

The angular acceleration is obtained in a similar manner by differentiating eq.(D.25) with respect to time, to obtain in full vector notation,

$$\mathbf{R}_i\left(\dot{\boldsymbol{\omega}}_i \mathbf{x}\, \mathbf{r}_{j+1/i}+\boldsymbol{\omega}_i \mathbf{x}\, \boldsymbol{\omega}_i \mathbf{x}\, \mathbf{r}_{j+1/i}+2\boldsymbol{\omega}_i \mathbf{x}\, \mathring{\mathbf{r}}_{j+1/i}+\mathring{\mathbf{r}}^{\circ}_{j+1/i}\right)$$
$$-\mathbf{R}_j\left(\dot{\boldsymbol{\omega}}_j \mathbf{x}\, \mathbf{r}_{j+1/j}+\boldsymbol{\omega}_j \mathbf{x}\, \boldsymbol{\omega}_j \mathbf{x}\, \mathbf{r}_{j+1/j}+2\boldsymbol{\omega}_j \mathbf{x}\, \mathring{\mathbf{r}}_{j+1/j}+\mathring{\mathbf{r}}^{\circ}_{j+1/j}\right)$$
$$=\dot{\boldsymbol{\omega}}_{i-1} \mathbf{x}\, \mathbf{r}_{ji/i-1}+\boldsymbol{\omega}_{i-1} \mathbf{x}\, \boldsymbol{\omega}_{i-1} \mathbf{x}\, \mathbf{r}_{ji/i-1}+2\boldsymbol{\omega}_{i-1} \mathbf{x}\, \mathring{\mathbf{r}}_{ji/i-1}+\mathring{\mathbf{r}}^{\circ}_{ji/i-1} \qquad (D.38)$$

where the local vector accelerations are given by,

$$\mathring{\mathbf{r}}^{\circ}_{ji/i-1} = (\mathbf{B}^{j}_{i-1}-\mathbf{B}^{i}_{i-1})\ddot{\mathbf{b}}_{i-1} \qquad (D.39)$$
$$\mathring{\mathbf{r}}^{\circ}_{j+1/i} = \mathbf{B}^{j+1}_{i}\ddot{\mathbf{b}}_i \qquad (D.40)$$
$$\mathring{\mathbf{r}}^{\circ}_{j+1/j} = \ddot{d}_{j+1}\mathbf{x} \qquad (D.41)$$

Therefore, substituting into eq.(D.38) the forms of frame angular accelerations for planer motion, given by,

$$\dot{\boldsymbol{\omega}}_i=\dot{\omega}_{i(z)}\mathbf{z}=(\dot{\omega}_{i-1(z)}+\mathring{\delta}^{\circ}_{i/i-1(z)}+\ddot{\theta}_i)\mathbf{z} \qquad (D.42)$$
$$\dot{\boldsymbol{\omega}}_j=\dot{\omega}_{j(z)}\mathbf{z}=(\dot{\omega}_{i-1(z)}+\mathring{\delta}^{\circ}_{j/i-1(z)}+\ddot{\theta}_j)\mathbf{z} \qquad (D.43)$$

and using the planar cross product notation of eq.(D.31), yields for the dependent angular acceleration rates,

$$[\zeta_\theta]\begin{Bmatrix}\ddot{\theta}_i\\ \ddot{\theta}_j\end{Bmatrix} = [\mathbf{G}\mathbf{r}_{ji/i-1}-\mathbf{R}_i\mathbf{G}\mathbf{r}_{j+1/i}+\mathbf{R}_j\mathbf{G}\mathbf{r}_{j+1/j}]\dot{\omega}_{i-1(z)}$$
$$+[\mathbf{G}^2\mathbf{r}_{ji/i-1}]\omega_{i-1(z)}{}^2-[\mathbf{R}_i\mathbf{G}^2\mathbf{r}_{j+1/i}]\omega_{i(z)}{}^2+[\mathbf{R}_j\mathbf{G}^2\mathbf{r}_{j+1/j}]\omega_{j(z)}{}^2$$
$$+2[\mathbf{G}\mathring{\mathbf{r}}_{ji/i-1}]\omega_{i-1(z)}-2[\mathbf{R}_i\mathbf{G}\mathring{\mathbf{r}}_{j+1/i}]\omega_{i(z)}+2[\mathbf{R}_j\mathbf{G}\mathring{\mathbf{r}}_{j+1/j}]\omega_{j(z)}$$
$$+\mathring{\mathbf{r}}^{\circ}_{ji/i-1}-\mathbf{R}_i\mathring{\mathbf{r}}^{\circ}_{j+1/i}+\mathbf{R}_j\mathring{\mathbf{r}}^{\circ}_{j+1/j} \qquad (D.44)$$

Note that the above equation is in terms of the angular velocities $\omega_{i(z)}$ and $\omega_{j(z)}$, which are obtained by substituting the solution of eq.(D.37) into eq.'s (D.29) and (D.30).

Appendix E

Truss Model

The truss structure of Figure E.1 originates from the 3D truss crane of [Mikulas et al.'88b]. The joint arrangement is modelled with an intermediate 3 member truss section, mainly for simplification since the joint concepts of the original space crane would require more detailed modelling. The specific truss member designations of longeron, diameter, and batten, and the structure dimensions , are illustrated in Fig. 8.1 of Chapter 8.

The actual members are of a tube geometry with 5.08 cm (2 inch) outer diameter and 0.15 cm (.06 inch) wall thickness. The material is a graphite epoxy with Young's modulus of 275 GPa (40×10^6 psi) and density of 1744 kg/m^3 (0.063 lbm/in^3). To establish an approximate 2D model of the 3D geometry, the material density and Young's modulus were scaled to account for the true number of truss members contained within the structure. The Young's modulus was additionally scaled by 3/4 inorder to examine a more flexible configuration. Hence, the following properties were used for the dynamic simulations presented in this thesis.

The material density presented in the above Table for the end-batten also accounts for the mass distribution of a 300 kg platform mass. The cylinder and piston-rod components of the actuators were modelled with the same density as the diagonal members. The cylinder maintained the original tube outer diameter (5.08 cm) and wall thickness (0.15 cm), and it was assumed that the piston-rod diameter was the

Table E.1: Model properties of the planar truss crane.

Member type	Density (kg/m^3)	Young's modulus (Gpa)	Cross-sect. Area (m^2)
longeron	8000	412.5	2.3592×10^{-4}
diagonal	4000	412.5	2.3592×10^{-4}
batten	12000	618.7	2.3592×10^{-4}
end-batten	8.49×10^6	618.7	2.3592×10^{-4}

corresponding inner diameter of the cylinder. For the flexible link model of Section 8.2.3, actuators 3 to 6 were modelled as static members with a Young's modulus of the longerons (but maintained the same dimensions of the actuator components). The element numbering configuration of Figure E.1b pertains to the FE model presented in Figure 8.8.

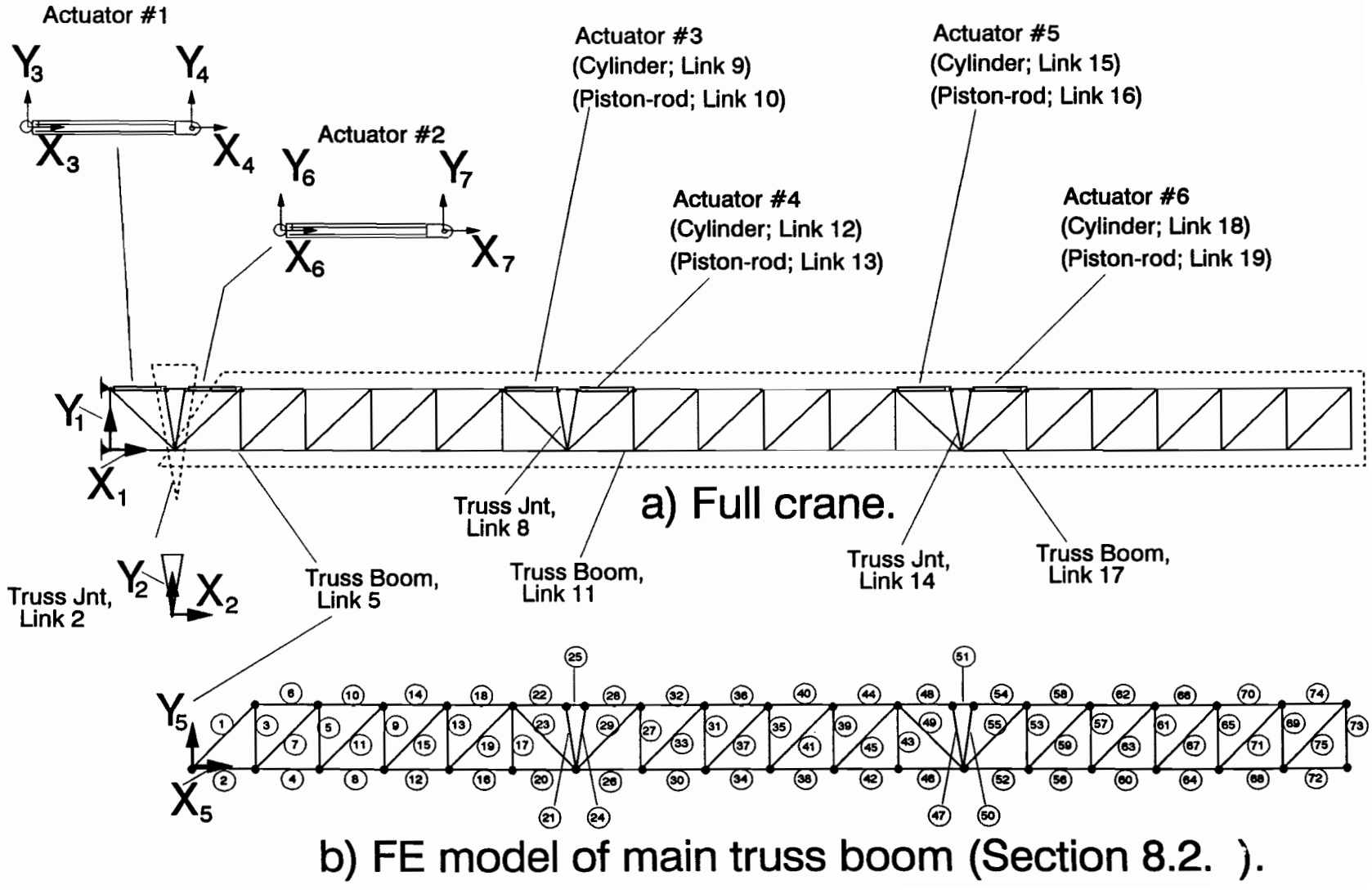

Figure E.1: A truss crane model.
(Refer to Figure 8.1a for dimensional details.)